GENETIC AND EPIGENETIC ANALYSIS OF IMMORTAL AND SENESCENCE ARRESTED LIVER CANCER CELLS

A THESIS SUBMITTED TO
THE DEPARTMENT OF MOLECULAR BIOLOGY AND GENETICS
AND THE INSTITUTE OF ENGINEERING AND SCIENCE
OF
BİLKENT UNIVERSITY
IN PARTIAL FULFILLMENT OF THE REQUIREMENTS
FOR THE DEGREE OF DOCTOR OF PHILOSOPHY

By
G. SEVGİ BAĞIŞLAR
August 2009

I certify that I have read this thesis and that in my opinion it is fully adequate, in scope and in quality, as a thesis for the degree of Doctor of Philosophy.

_____

Prof. Dr. Mehmet Öztürk (Supervisor)

I certify that I have read this thesis and that in my opinion it is fully adequate, in scope and in quality, as a thesis for the degree of Doctor of Philosophy.

_____

Asst. Prof. Dr. Özlen Konu

I certify that I have read this thesis and that in my opinion it is fully adequate, in scope and in quality, as a thesis for the degree of Doctor of Philosophy.

_____

Asst. Prof. Dr. Cengiz Yakıcıer

I certify that I have read this thesis and that in my opinion it is fully adequate, in scope and in quality, as a thesis for the degree of Doctor of Philosophy.

_____

Prof. Dr. Funda Yılmaz-Barbet

I certify that I have read this thesis and that in my opinion it is fully adequate, in scope and in quality, as a thesis for the degree of Doctor of Philosophy.

_____

Doç. Dr. Esra Erdal

Approved for the Institute of Engineering and Science

_____

Prof. Dr. Mehmet Baray

Director of Institute of Engineering and Science

To my mother…..

Anneme…..

ABSTRACT

G. SEVGİ BAĞIŞLAR

PhD in Molecular Biology and Genetics

Supervisor: Prof. Dr. Mehmet Öztürk

August 2009, 123 Pages

Genetic and epigenetic aspects of cellular senescence and immortality in hepatocellular carcinoma (HCC) are poorly elucidated. The aim of our thesis was to characterize senescence and immortality gene network (SIGN) involved in these cancers. We also wished to explore epigenetic changes associated with senescence and immortality of HCC cells. First, we identified differentially expressed genes in immortal, pre-senescent and senesce-arrested Huh7 clones. Our microarray analysis revealed 6390 probesets significantly changing among groups. Moreover, the significant gene signature could successfully discriminate both replicative senescent cells, and oncogene-induced senescent cells from their immortalized counterparts. E2F1 targets, stem-cell related genes, DNA repair, RNA splicing and cell cycle related gene sets were enriched specifically in immortal cells, whereas immune function, stress response, electron transporter activity, protein modification, metabolism, chromatin biogenesis related gene groups were significantly up-regulated in senescent clones. Next, we integrated gene expression data from senescence-programmed and immortal HCC cells with the data from cirrhosis and HCC tissues to generate a SIGN signature. This signature identified several HCC classes, including one “normal-like”, and two with increased expression of immortality genes. Senescence-to-immortality transition was accompanied by hepatic dedifferentiation and increased expression of cell proliferation, chromosome modification and DNA damage response genes. Finally, we identified a large set of upregulated DNA damage checkpoint and DNA repair genes that showed significant associations with some SIGN classes of HCC tumors. As retinoblastoma/E2F pathway plays a key role in cellular senescence, we also analyzed E2F and DP family members in senescent and immortal hepatocellular carcinoma cells. *E2F1, E2F5, E2F7, E2F8* and *DP1* were up-regulated in immortal hepatocellular carcinoma (HCC) cell lines as compared to senescent cells, whereas E2F3a and *DP-2* expressions were downregulated. Upregulation of DP2

expression in senescent cells correlated with increased DP2 protein expression, as tested with TGF-beta induced senescence models. Finally, we demonstrated important epigenetic changes associated with hepatocellular immortality and senescence. Among histone methyltransferases and demethylases, *MLL3, FBXL11, SUV420H1, UTX, SMYD2, SETD2, JMJD2B, JMJD3, JARID1B* and *ASH1L* genes were up-regulated, and *EZH2* was down-regulated in senescent cells. These changes were accompanied with changes in histone methylation patterns. Of particular interest, H3K27me1, H3K27me3, H4K20me3, H3R2me2a and H4R3me2a forms of methylated histones displayed increased expression in both Huh7 and MRC5 senescent cells, as compared to their immortal forms. Finally, H3K27me3, H4K20me3, H3K36me3, H3R17me2a, H4R3me2a also showed decreased expression in some cirrhotic liver and primary HCC tumors. In conclusion, we demonstrated that a large set of senescence and immortailty genes were dysregulated in HCC. This profound change in gene expression was associated with differential expression of histone modifying enzymes, as well as histone methylation status. Thus, the immortalization of hepatocytes during hepatocellular carcinogenesis is accompanied with global gene expression changes probably mediated by a major modification of their epigenetic program via histone demethylation.

ÖZET

İMMORTAL VE HÜCRE YAŞLANMASI PROGRAMLI KARACİĞER KANSER HÜCRELERİNDE GENETİK VE EPİGENETİK ANALİZİ

G. SEVGİ BAĞIŞLAR

Doktora Tezi, Moleküler Biyoloji ve Genetik Bölümü
Danışman: Prof. Dr. Mehmet ÖZTÜRK
Ağustos 2009, 123 Sayfa

Hepatoselüler karsinomda (HCC), hücre yaşlanması ve immortalitesinin genetik ve epigenetik özellikleri henüz zayıf olarak açıklanmıştır. Tezimizin amacı; karaciğer kanserinde rol alan hücre yaşlanması ve immortalite gen ağını karakterize etmektir. Ayrıca, hücre yaşlanması ve immotral HCC hücrelerinin epigenetik değişikliklerini de incelemek istedik. İlk önce, immortal, erken hücre yaşlanması ve hücre yaşlanması Huh7 klonlarında gen ifade farklılıklarını bulduk. Mikroarray çip çalışmamız sonucunda 6390 prob seti, bu gruplar arasında değişiklik gösterdi. Daha fazlası, bu anlamlı gen seti; hem replikatif hücre yaşlanması hem de oncogen indüklenmiş hücre yaşlanması modellerini, bunların immortalize edilmiş karşılıklarından başarı ile ayırdı. Biyolojik fonksiyon gruplama çalışmaları; E2F1 hedef genlerinin, kök hücre ilişikli genlerin, DNA tamir, RNA splicing ve hücre döngüsü ilişik gen gruplarının özellikle immortal hücrelerde ifadesinin arttığını gösterdi. Öte yandan, immün sistem, stres cevabı, elektron taşınımı, protein modifikasyonu, metabolizma ve kromatin biyogenezi ile ilgili grupları yaşlanmış hücre klonlarında ifade gösteriyordu. Ayrıca, immortal ve hücre yaşlanması programlı hücre datasıyla siroz ve HCC doku datasını birleştirerek, ortak değişen "hücre yaşlanması ve immortal gen ağı (SIGN) listesini elde ettik. SIGN gen seti, farklı HCC alt gruplarını birbirinden ayırmayı başardı. SIGN gen setinde hücre yaşlanmasından immortale doğru anlamlı olarak değişen gruplar; hepatic de-differensiye genleri, hücre döngüsü, kromozom modifikasyonu ve DNA hasarına cevap veren gen grupları idi. Ayrıca, geniş bir sayida DNA tamir genlerinin tümor oluşumu ve ilerlemesi ile alakalı olduğunu belirledik.

Retinoblastoma/E2F yolağı hücre yaşlanmasında önemli bir rol oynamaktadır, biz de bu yüzden E2F ve DP protein ailesi üyelerinin yaşlanmış ve immortal programlı hepatoselüler karsinomlarında analiz ettik. *E2F1, E2F5, E2F7, E2F8* ve *DP1* genlerinin

ifadesi immortal hücrelerde artış gösterdi. Öte yandan E2F3a ve *DP2* genlerinin ifadesi azalmıştı. *DP-2* ifadesinin senesens Huh7 hücrelerde artışı; DP2 protein artışı ile ilintilendirildi ve aynı artış TGF-beta indüklenmiş hücre yaşlanmasında da gözlendi.

Son olarak, hepatoselüler immortalite ve yaşlanmış hücrelerinde önemli epigenetik değişiklikler gösterdik. Histone metiltransferaz ve demetilazlar arasında; *MLL3, FBXL11, SUV420H1, UTX, SMYD2, SETD2, JMJD2B, JMJD3, JARID1B* ve *ASH1L* genlerinin hücre yaşlanmasında artış gösterdiğini ve *EZH2* geninin azalış gösterdiğini gözlemledik. Bu değişiklikler eşliğinde, histon metilasyon seviyeleri de değişikliğe uğruyordu. Yaşlanmış Huh7 ve MRC5 hücrelerde immortal eşdeğerlerine göre, H3K27me1- and 3, H4K20me3, H3R2me2a ve H4R3me2a rezidülerinin artış gösterdiğini gözledik. H3K27me3, H4K20me3, H3K36me3, H3R17me2a, ve H4R3me2a rezidüleri bazı sirotik karaciğer ve HCC tümörlerinde azalan bir ifade gösterdi.

Sonuç olarak, geniş sayıda immortal ve hücre yaşlanması genlerinin HCC de de değiştiğini göstermiş olduk. Histon modifiye eden genleri ve histon metilasyon seviyesi de değişikliğe uğruyordu. Yani, hepatositlerin immortalizasyon süreçleri global gen ifade değişikliği ile oluyor ve, büyük ihtimalle, bu değişim epigenetik program tarafından yönlendiriliyor.

ACKNOWLEDGEMENTS

I would like to express my gratitude to Prof. Mehmet Öztürk for his supervision, endless support and valuable suggestions throughout the course of my studies. It has always been a privilege for me to be accepted in his team, work with him and being educated by him.

I would like to thank to the jury members for evaluating my thesis.

I would like to express my special thanks to Assist. Prof. Özlen Konu for sharing her excellent experiences on bioinformatics, her support, her patience, and being such a kind person all the time.

I would like to attend my very special thanks to Assist. Prof. Tamer Yağcı for his support, for scientific discussions and for paying attention to my scientific ideas, even if they were foolish. I would like to thank to Assist. Prof. Cengiz Yakıcıer for his support, his friendship, his kindness. I would like to thank to Assist. Prof. Uygar Tazebay for his kindness and patience. For three of you, thank you for being there.

I would like to thank to Prof. Dr. Funda Yılmaz-Barbet and Prof. Dr. Hakan Bozkaya for their supports in my projects.

I would like to thank to my previous supervisor Prof. Dr. Tayfun Özçelik for teaching me, and all PI's in MBG for educating me and being patient to me. I would like to thank to Prof. Dr. Stéfan Dimitrov for his very kind supports.

I would like to thank to my project partners Ayça Arslan-Ergül and Haluk Yüzügüllü for working and being with me, and all current and past group friends Şerif Şentürk, Mine Mumcuoğlu, Nuri Öztürk for teaching me a lot, and Nilgün Taşdemir, Pelin Gülay, Eylül and Gökhan.

I would like to express all my gratitude to my friends Bàlà Gür-Dedeoğlu, Elif Uz, Ceren Çıracı and Elif Yaman for the happy days and being with me. I thank to Tolga Acun, Hani Al-Otaibi, Ender Avcı and Emin BeyAbi for being there with smiley faces when I need anything. I would like to thank other MBG graduate students that I can not list here for making the PhD life easier.

I would like to thank to "ma p'tite" Sophie Barral for being her, being my friend or more than a friend. I would like to thank to Angeline Eymery for being very lovely to me everytime. Thanks god, I came to France and I met you. I would like to express my

deepest feelings to my dear friends Nicolas Reynoird, Sébastien Cadau, Leila Todeschini, Aurelia Vavasseur, Faycal Boussouar, Hong Lien and Xavier Camous. I feel lucky to know you. Thank you for being my friends.

I would like to thank to Mrs. Sevim Baran, Mrs. Füsun Elvan, Mr. Abdullah Ünnü, Mr. Turan Daştandır, Mrs. Bilge Özbayoğlu, Miss. Tülay Arayıcı for their very kind helps to make my life easier. This thesis could not be completed without your helps. I would like to thank to Mrs. Denise Leardini, Mrs. Sanie Claraz, Mr. Michail Gidopoulos and Mrs. Dalenda Benmedjahed for helping me and for loving me like a family.

Lastly, I wish to thank to my parents and my sister, Betül, and brother, Ümit, for their endless support during my life and loving me in every condition. I dedicate this thesis to my mother, my endless love source, who believed in me, trusted in me, who is absolutely unique and a perfect mother.

TABLE OF CONTENTS

SIGNATURE PAGE	ii
ABSTRACT	iv
ÖZET	vi
ACKNOWLEDGEMENTS	viii
TABLE OF CONTENTS	x
LIST OF FIGURES	xvii
LIST OF TABLES	xix
ABBREVIATIONS	xx

CHAPTER 1. INTRODUCTION 1
1.1 Hepatocellular malignancy 1
1.2 Pathogenesis of hepatocellular carcinoma 2
1.2.1 Viral induced hepatocarcinogenesis 2
1.2.2 Alcohol-induced hepatocarcinogenesis 4
1.2.3 Aflatoxin-B1-induced hepatocarcinogenesis 5
1.3 Genetic and epigenetic events in HCC 5
1.3.1 The *p53* tumor suppressor 5
1.3.2 β-Catenin and *AXIN1* 6
1.3.3 ErbB receptor family 6
1.3.4 MET ad HGF 7
1.3.5 Methylation of cancer-relevant genes 7
1.3.6 c-myc 7
1.4 Liver cirrhosis and senescence 8
1.4.1 Cellular senescence 8
1.4.1.1 Replicative senescence 9
1.4.1.2 Oncogene and ROS-induced senescence 10
1.4.2 Senescence as an anti-tumor mechanism in hepatocellular carcinoma 10
1.4.3 Cyclin-dependent inhibitors 11
1.5 Expression profiling using Affymetrix GeneChip Microarrays 12
1.6 Rb/E2F pathway 13
1.6.1 DP-2 14
1.7 Chromatin midifications and hepatocellular carcinoma 15
1.7.1 DNA methylation 15
1.7.1.1 DNA methylation and cancer 16
1.7.2 Histone modifications 18
1.7.2.1 Histone modifying enzymes 19
1.7.2.2 Histone methylation and cancer 21
1.7.2.2.1 H3K27 methylation 22
1.7.2.2.1.1 EZH2 22
1.7.2.2.1.2 BMI1 23

1.7.2.2.2 H3K9 methylation 23
1.7.2.2.2.1 HP1-a H3K9 methylation “reader” 23
1.7.2.2.2.2 SUV39H-RIZ1-H3K9 methylation “writers” 23
1.7.2.2.2.3 JMJD2C- H3K9 methylation “eraser” 24
1.7.2.2.3 H3K4 methylation 24
1.7.2.2.3.1 MLL-SMYD3- H3K4 methylation “writers” 24
1.7.2.2.3.2 ING proteins- H3K9 methylation “readers” 25
1.7.2.2.4 H3K36, H4K20 and H3K79 methylation 25
1.7.2.2.4.1 H3K36, H4K20, H3K79methylation‘writers’ 25
1.7.2.3 Histone lysine acetylation and cancer 25
1.7.2.4 Histone methylation and senescence 26
1.7.2.5 Histone variants 27
CHAPTER 2. OBJECTIVES AND RATIONALE 28
CHAPTER 3. MATERIALS AND METHODS 30
3.1 Materials 30
3.1.1 Reagents 30
3.1.2 Nucleic acids and proteins 30
3.1.3 Oligonucleotides 30
3.1.4 Enzymes 30
3.1.5 Electrophoresis 30
3.1.6 Protein transfer materials 31
3.1.7 Tissue culture reagents and cell lines 31
3.1.8 Antibodies and chemiluminescence 31
3.1.9 Kits 32
3.2 Solutions and media 32
3.2.1 General solutions 32
3.2.2 Tissue culture solutions 32
3.2.3 RNA solutions 33
3.2.4 Protein extraction and western blotting solutions 34
3.2.5 Immunofluoroscence and immunoperoxidase solutions 35
3.2.6 SABG solutions 35

3.2.7 Immunohistochemistry solutions 36
3.3 Methods 36
3.3.1 Tissue culture techniques 36
3.3.1.1 Cell lines 36
3.3.1.2 Cell lines for microarray study 37
3.3.1.3 Thawing cell lines 37
3.3.1.4 Cryopreservation of cell lines 37
3.3.1.5 TGF-β and LiCL treatment 38
3.3.2 RNA extraction 38
3.3.2.1 Extraction of total RNA from tissue culture cells 38
3.3.2.2 Extraction of total RNA from tissue samples 38
3.3.3 Expression microarray analysis 39
3.3.3.1 Microarray experiments 39
3.3.3.2 Data processing and quality controls 40
3.3.3.3 Determination of differentially expressed gene sets 40
3.3.3.4 Visualization of dataset 42
3.3.3.5 Data integration 42
3.3.3.6 Functional gene annotation cluster analysis 42
3.3.3.6.1 DAVID 42
3.3.3.6.2 GSEA 43
3.3.3.6.3 Onto express 43
3.3.3.6.4 Ingenuity Pathway Analysis 43
3.3.3.7 Meta Data 43
3.3.3.7.1 HPEC replicative senescence data 43
3.3.3.7.2 IMR90 Oncogene-induced senescence data 44
3.3.3.7.3 HCC molecular classification data 44
3.3.3.8 BRB Array Tools 44
3.3.4 Quantification of nucleic acids 44
3.3.4.1 Horizantal agarose gels of DNA samples 44
3.3.4.2 Gel electrophoresis of of total RNA 45
3.3.5 First strand cDNA synthesis 45

3.3.6 Polymerase chain reaction (PCR) 45
3.3.6.1 Primer design for expression analysis for SQ and Q PCR 46
3.3.6.2 Expression analysis of a gene by semi-quantitative PCR 49
3.3.6.2.1 Determination of optimal cycle of a gene for semi-quantitative PCR 49
3.3.6.2.2 GAPDH normalization 49
3.3.6.2.3 PCR amplification of target region 49
3.3.6.3 Quantitative real-time PCR 50
3.3.6.3.1 Amplification efficiency calculations 50
3.3.7 Total protein isolation 51
3.3.7.1 Protein isolation from tissue culture cells 51
3.3.7.2 Protein isolation tissue samples 51
3.3.7.3 Histone extraction 51
3.3.8 Quantification of proteins 52
3.3.9 Western blotting 52
3.3.10 Immunofluorescence 53
3.3.11 Immunoperoxidase 53
3.3.12 Immunohistochemistry on paraffin-embedded tissue sections 54
3.3.13 SABG assay 55

CHAPTER 4. RESUTS 56
4.1 Identification of senescence and immortality gene network and its role in hepatocellular carcinoma 56
4.1.1 Expression analysis of immortal and reprogrammed senescent cells of hepatocellular carcinoma 56
4.1.2 Differentially expressed gene set between immortal, pre- and senescent clones 57
4.1.3 Confirmation of microarray data 59
4.1.4 Analysis of significant gene set on other senescence microarray data 61
4.1.5 Functional classification of senescence and immortality genes 63
4.1.6 Identification of the role of senescence and immortality genes in HCC 68
4.1.6.1 Molecular classification of HCC by the SIGN signature 69

4.1.6.2 DNA damage response genes as potential therapeutic targets 76

4.2 Expression analysis of E2F/DP family in senesence and immortality,senescence association of DP-2 78

4.2.1 Differential expression of E2F/DP family genes in senescent/immortal hepatocellular carcinoma cells 78

4.2.2 Expression analysis of differentially regulated E2F/DP genes in HCC cell lines 80

4.2.3 DP2 protein is abundant in senescent clone but lost in immortal clone 81

4.2.4 Examination of the DP-2 isoforms in different cell cycle conditions and upon TGF-β treatment 83

4.3 Epigenetic changes in immortality and senescence of liver *in vitro* and *in vivo* 86

4.3.1 Differential expression of histone modifying enzyme genes in senescent and immortal hepatocellular carcinoma cells 86

4.3.2 Histone methylation changes between immortal and senescent Huh7 clones 87

4.3.3 Does histone methylation levels differ *in-vivo*? 93

4.3.4 Histone variant differences in immortal and senescent Huh7 cells 96

CHAPTER 5. DISCUSSION 98

5.1 Global expression analysis of immortality and senescence in liver cancer 98

5.1.1 Identification of differentially expressed genes between immortal, pre- and senescent Huh7 clones 98

5.1.2 Establishing a senescence and immortality gene network signature for cirrhosis and hepatocellular carcinoma 99

5.2 DP-2 is associated with senescence 101

5.3 Histone methylation levels of some H3 and H4 residues change in immortality and senescence of liver *in vitro* and *in vivo* 102

CHAPTER 6. FUTURE PERSPECTIVES 105

REFERENCES 107

APPENDIX A 116

APPENDIX B 116

APPENDIX C 122
APPENDIX D 127

LIST OF FIGURES

Figure 1.1	Multistage process of hepatocarcinogenesis	2
Figure 1.2	Mechanisms of hepatocarcinogenesis	5
Figure 1.3	Senescence controlled by the p53 and p16-Rb pathways	9
Figure 1.4	Senescence pathways	10
Figure 1.5	E2F/DP family	15
Figure 1.6	Epigenetic alterations in tumor progression	16
Figure 1.7	DNA methylation differences in some cancers	17
Figure 1.8	Histone modifications	19
Figure 1.9	Histone modifying enzymes	20
Figure 4.1.1	Senescence associated B-galactosidase (SABG) staining of immortal and senescent cells	56
Figure 4.1.2	Quality assesment of microarray data	57
Figure 4.1.3	Plots of microarray data before and after normalization	58
Figure 4.1.4	Huh7 isogenic clones significant gene list unsupervised hierarchical cluster analysis	58
Figure 4.1.5	Confirmation of microarray data	61
Figure 4.1.6	Meta-analysis with previously published senescence data	63
Figure 4.1.7	Enrichement plots and cluster dendograms of 3 enriched gene sets	66
Figure 4.1.8	Biological functions	67
Figure 4.1.9	Venn diagram	68
Figure 4.1.10	Hierarchical clustering of senescence-programmed and immortal cell lines, and cirrhosis and hepatocellular carcinoma (HCC) tissues	70
Figure 4.1.11	The SIGN signature separates hepatocellular carcinomas (HCCs) into distinct subclusters	71
Figure 4.1.12	Binary analysis and senescence-immortality associated gene rate of Boyault groups	72
Figure 4.1.13	The protein networks generated through the use of Ingenuity Pathway Analysis	74
Figure 4.2.1	Differential expression of E2F and DP family members in immortal,	79

presenescent and senescent cells
Figure 4.2.2 mRNA expression levels of differentially regulated *E2F/DP* genes in HCC cell lines 80
Figure 4.2.3 DP-2 immunostaining 82
Figure 4.2.4 Expression analysis of DP-2 protein 83
Figure 4.2.5 Western blot analysis of DP-2 in LiCl and TGF- β treated cells 84
Figure 4.3.1 Expression analysis of histone methyltransferases and de-methylases in immortal and senescence Huh7 clones 86
Figure 4.3.2 Histone methylation status of H3 and H4 tail modifications in immortal, pre- and senescent cells 88
Figure 4.3.3 Immunoperoxidase analysis of histone methylation residues in replicative senescence model of MRC5 92
Figure 4.3.4 Histone mehtylation in *in-vivo* 95
Figure 4.3.5 Histone variant levels of immortal, pre- and senescent cells 96

LIST OF TABLES

Table 3.1	Antibodies	31
Table 3.2	Required R packages	40
Table 3.3	Experiment file of *in-vitro* data	41
Table 3.4	Primers and their sequences	46
Table 3.5	A standard curve preparation with BSA dilution	52
Table 3.6	Protein sample preparation for Bradford assay	52
Table 4.1.1	The numerical report of significant probes and genes	59
Table 4.1.2	Examples of significantly upregulated GSEA gene sets	64
Table 4.1.3	Biological pathways affected in hepatocellular carcinoma classes ccording to SIGN signature	76
Table 4.1.4	Upregulation of DNA damage response genes	77

ABBREVIATIONS

APC	Adeno poliposis coli
APS	Ammonium persulphate
bp	Base Pairs
BSA	Bovine serum albumin
cDNA	Complementary DNA
CDKI	Cycline dependent kinase inhibitor
Ct	Cycle Threshold
ddH2O	Double distilled water
DMEM	Dulbecco's Modified Eagle's Medium
DMSO	Dimethyl Sulfoxide
DNA	Deoxyribonucleic Acid
dNTP	Deoxyribonucleotide triphosphate
DNMT	DNA methyltransferase
DP	Dimerization partner
ds	Double strand
EGFR	Epidermal growth factor receptor
EtBr	Ethidium Bromide
ER	Endoplasmic reticulum
FBS	Fetal Bovine Serum
H	Histone
HAT	Histone acetyl transferase
HCC	Hepatocellular carcinoma
HB	Hepatoblastoma
HBcAg	Hepatitis B core antigen
HBV	Hepatitis B virus
HBx	Hepatitis B protein x
HCV	Hepatitis C virus
HDAC	Histone deacetylase
HGF	Hepatocyte growth factor
HRP	Horseradish peroxidase
LCD	Large cell dysplasia
µg	Microgram
mg	Miligram
min	Minute
µl	Microliter
ml	Mililiter
µm	Micrometer
µM	Micromolar
mM	Milimolar
mRNA	Messenger RNA
Oligo(dT)	Oligodeoxythymidylic acid
PBS	Phosphate Buffered Saline
PCR	Polymerase Chain Reaction

PDL	Population doubling
pRB	Retinoblastoma protein
pmol	Picomole
q-PCR	Quantitative real time RT-PCR
Rpm	Revolutions Per Minute
RMA	Robust multichip average
RT PCR	Reverse Transcription PCR
ROS	Reactive oxygen species
SABG	senescence-associated b-galactosidase
SAHF	Senescence associated heterochromatin loci
SCD	Small cell dysplasia
Sec	Second
TAE	Tris-Acetate-EDTA buffer
TBS	Tris buffered saline
TERC	Telomerase RNA
TERT	Telomerase reverse transcriptase
Tm	Melting Temperature
Tris	Tris (Hydroxymethyl)- Methylamine
UV	Ultraviolet
v/v	volume/volume
w/v	weight/volume

CHAPTER 1. INTRODUCTION

1.1 Hepatocellular malignancy

The **liver** is a vital organ present in vertebrates and some other animals; it has a wide range of functions, a few of which are detoxification, protein synthesis, and production of biochemicals necessary for digestion. The liver plays a major role in metabolism and has a number of functions in the body, including glycogen storage, decomposition of red blood cells, plasma protein synthesis, hormone production, and detoxification. It lies below the diaphragm in the thoracic region of the abdomen. It produces bile, an alkaline compound which aids in digestion, via the emulsification of lipids. It also performs and regulates a wide variety of high-volume biochemical reactions requiring highly specialized tissues, including the synthesis and breakdown of small and complex molecules, many of which are necessary for normal vital functions (Anthea et al, 1993).

Primary cancer of the liver is the fourth most common cause of death from cancer (estimated mortality is more than 600,000 deaths per year) and the third most common malignancy in human (Ferlay et al, 2001), (1). The lethality of liver cancer stems in part from its resistance to existing anticancer agents, a lack of biomarkers that can detect surgically resectable incipient disease, and underlying liver disease that limits the use of chemotherapeutic drugs (2). There are two main kinds of primary liver cancer, hepatoma and cholangiocarcinoma. Hepatoma is cancer of the hepatocytes, the main functioning liver cells. Cholangiocarcinoma originates in the bile ducts. Hepatoblastoma (HB) is the most common pediatric liver malignancy, comprising approximately 1% of all pediatric cancers (3). Liver angiosarcoma is a very rare type of primary liver cancer developing from the cells of blood vessels within the liver. Hepatocellular carcinoma (HCC) is one of the most common malignant liver tumors (83% of all cases) in the world with a high prevalence in Asia and sub-Saharan Africa (4). Recent studies have shown that the incidence of HCC has substantially increased in the USA as well as in other areas including Japan and Europe (El-Serag and Mason, 1999), (Taylor-Robinsonet al., 1997). HCC is one of the few human cancers in which an underlying etiology can often be identified in most cases. Hepatocarcinogenesis nearly always develops in the setting of chronic hepatitis or cirrhosis; conditions in which many hepatocytes are killed, inflammatory cells invade the liver and connective tissue (5). Development of HCC is a multistep process and slow. The sequential events leading to HCC may be summarized in five steps: chronic liver injury that produces inflammation, cell death, cirrhosis and regeneration, DNA damage, dysplasia, and finally HCC (Figure 1.1) (6), (2).

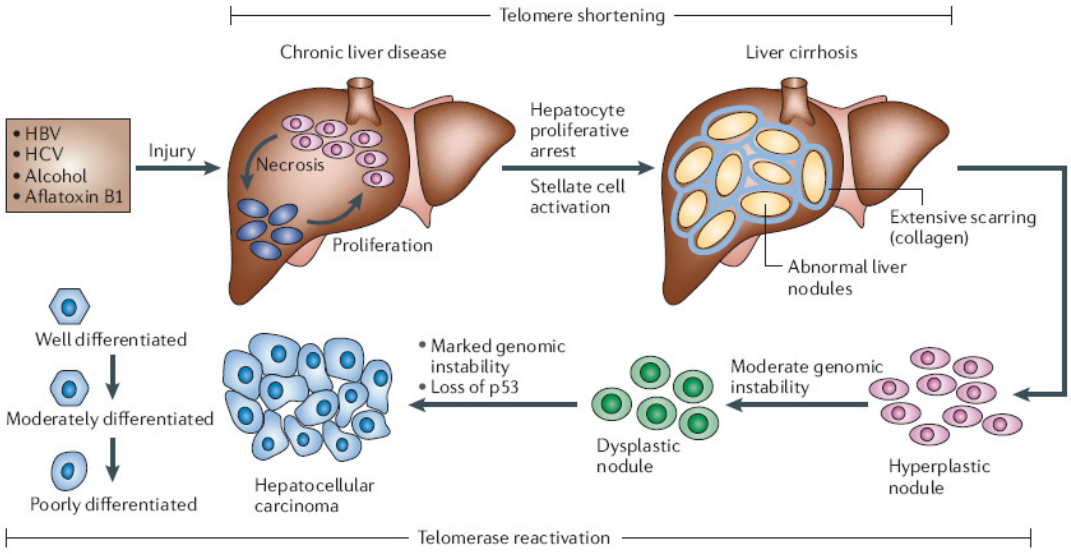

Figure 1.1: **Multistage process of hepatocarcinogenesis** (2).

1.2 Pathogenesis of hepatocellular carcinoma

HCC affects all segments of the world population, although significant differences in HCC incidence in various countries reflect the regional differences in the prevalence of specific etiological factors as well as ethnicity (American Cancer Society. Cancer Facts and FIGS 2005. American Cancer Society [online], http://www.cancer.org/docroot/home/index.asp (2005)). The most prominent factors associated with HCC include chronic hepatitis B and C viral infection, chronic alcohol consumption, aflatoxin-B1-contaminated food and virtually all cirrhosis-inducing conditions (Figure 1.2) (7). Other etiological factors have also been proposed to lead to HCC, albeit at a lower frequency; such as certain metabolic disorders, diabetes, non-alcoholic fatty liver disorders. In addition, gender can also influence the risk and behavior of HCC, with males accounting for a larger fraction of cases (8).

1.2.1 Viral-induced hepatocarcinogenesis

Hepatitis B virus (HBV) infects approximately 2 billion individuals worldwide and causes an estimated 320,000 deaths annually. Approximately 30–50% of HBV-related deaths are attributable to HCC (9). The impact of HBV infection on HCC development is reflected by the correlation between increased incidences of HCC in patients with increasing levels of HBV DNA in serum (10). Hepatitis C virus (HCV) infects approximately 170 million individuals worldwide (11). Approximately 20% of chronic HCV cases develop liver

cirrhosis, and 2.5% develop HCC (12). The viral-associated mechanisms driving hepatocarcinogenesis are complex and involve both host and viral factors.

HBV is a non-cytopathic, partially double-stranded hepatotropic DNA virus classified as a member of the *hepadnaviridae* family. The HBV genome encodes several viral proteins essential to its life cycle, including a reverse transcriptase/DNA polymerase (pol), the capsid protein known as hepatitis B core antigen (HBcAg), and the L, M and S envelope proteins that associate with the endoplasmic reticulum (ER) membrane as part of their replication process. HBV also encodes a number of proteins whose functions are not fully understood, such as protein x (HBx) (13).

Several lines of evidence support the direct involvement of HBV in the transformation process. First, HBV genome integration has been associated with host DNA microdeletions (14) that can target cancer-relevant genes including telomerase reverse transcriptase (*TERT*), platelet-derived-growth-factor receptor-β (*PDGFR*β), *PDGF*β and mitogen activated protein kinase 1 (*MAPK1*), among others (15). Second, HBx transcriptional activation activity can alter the expression of growth-control genes, such as *SRC* tyrosine kinases, Ras, Raf, MAPK, *ERK*, *JNK* and others (16), (17). Finally, HBx can bind and inactivate the tumor suppressor p53 *in vitro*, therefore increasing cellular proliferation and survival and compromising DNA-damage checkpoints (18), (19). The hepatocarcinogenic potential of HBx has been genetically validated in HBx transgenic mice, of which 90% develop HCC (20).

Host–viral interactions seem to contribute to hepatocarcinogenesis in several ways. A robust T-cell immune response is presumably elicited to combat viral infection, however, this response contributes to hepatocyte necrosis, inflammation and consequently regeneration, leading to carcinogenesis (13). Such continuous replication of hepatocytes might enable the propagation of oncogenic lesions and telomere erosion with consequent genomic instability. Another proposed mechanism of HBV-induced hepatocarcinogenesis might stem from viral–ER physical interactions, that provoke ER stress and ultimately the induction of oxidative stress (21), which can stimulate growth- and survival-signaling pathways, cause mutations through the generation of free radicals and activate stellate cells (22).

HCV is a non-cytopathic virus of the *flaviviridae* family. The HCV positive-stranded RNA genome encodes non-structural proteins (NS2, NS3, NS4A, NS5A and NS5B), which associate with the ER membrane to form the viral replicase and viral envelope proteins (E1 and E2). An important recent advance has been the establishment of a cell-culture model supporting efficient HCV replication and infectious particle production (23) (24), enabling the molecular dissection of these processes for the first time. 5–10% of HCV-infected patients

develop liver cirrhosis after 10 years of infection, a frequency that is approximately 10–20-fold higher than HBV, a highly relevant association as cirrhosis is a significant correlate of HCC development (25).

Both viral and host factors are thought to contribute to HCC development in the setting of HCV infection, analogous to HBV (13). One theory for HCV-induced hepatocarcinogenesis posits that the continuous cycles of hepatocyte death caused by the immune response to the virus and subsequent regeneration provide a context for the accumulation and propagation of mutations. HCV RNA and/or core proteins have been suggested to impair dendritic cell functions that are important for T-cell activation (26). In addition, HCV core proteins have been shown to interact with components of the MAPK signaling pathway (such as ERK, MEK and Raf) and therefore modulate cell proliferation (27). NS5A has also been shown to interact with and inactivate p53 by sequestration to the perinuclear membrane, thereby affecting the p53-regulated pathways that control cell-cycle progression, cellular survival, response to hypoxic and genotypic stresses, and tumor angiogenesis (28).

1.2.2 Alcohol-induced hepatocarcinogenesis

Chronic alcohol intake has been implicated in causing the production of proinflammatory cytokines through monocyte activation and provoking increased concentrations of circulating endotoxin, activating Küpffer cells which release many chemokines and cytokines (including TNFα, interleukin-1β (IL1β), IL6 and prostaglandin E2) with adverse effects on hepatocyte survival (29). In the setting of chronic ethanol exposure, hepatocytes show increased sensitivity to the cytotoxic effects of TNFα, which sets the stage for chronic hepatocyte destruction–regeneration, stellate cell activation, cirrhosis and ultimately HCC (29).

Alcohol also damages the liver through oxidative stress mechanisms. Alcoholic hepatitis shows increased isoprostane, a marker of lipid peroxidation (30). Oxidative stress might contribute to hepatocarcinogenesis in several ways; promoting fibrosis and cirrhosis via activation of stellate cells, actin on HCC-relevant signalling pathways, such as the documented reduction in tyrosine phosphorylation of STAT1, and causing accumulation of oncogenic mutations.

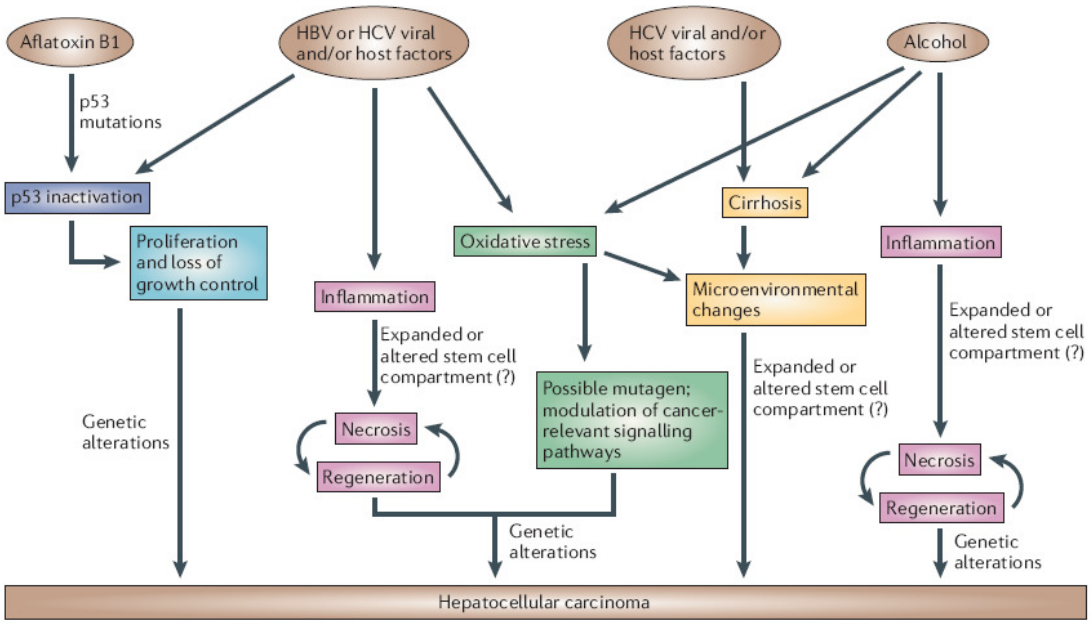

Figure 1.2 Mechanisms of hepatocarcinogenesis (2).

1.2.3 Aflatoxin-B1-induced hepatocarcinogenesis

Ingestion of the fungal toxin, aflatoxin B1, also poses an increased risk for the development of HCC. Aflatoxin B1 seems to function as a mutagen, and is associated with a specific p53 mutation (codon 249, G to T mutation) (31).

1.3 Genetic and epigenetic events in HCC

The neoplastic evolution of HCC proceeds through a multi-step histological process that is less well defined than that of other cancer types (Figure 1.2). The molecular analysis of human HCC has shown many genetic and epigenetic alterations that result in the deregulation of key oncogenes and tumor-suppressor genes including *TP53*, β-catenin, ErbB receptor family members, *MET* and its ligand hepatocyte growth factor (*HGF*), *p16(INK4a)*, E-cadherin and cyclooxygenase 2 (*COX2*).

1.3.1 The *p53* tumour suppressor

Although it is widely accepted that p53 deficiency participates in the development of HCC, whether p53 mutation contributes to cancer initiation, progression or both remains an area of active investigation. In humans, analyses of HBV- and HCV-related HCCs have shown a greater frequency of p53 mutations in advanced malignancies (43%) than in regenerative nodules (~7%) (32). In the context of aflatoxin B1, regions of high aflatoxin B1 exposure

show frequent p53 mutations in early-stage HCC lesions, whereas regions of low aflatoxin B1 exposure show p53 mutations in much later stages of HCC (33).

1.3.2 *β-catenin* and *AXIN1*

β-catenin is a crucial downstream component of the Wnt signalling pathway. When Wnt signalling is engaged, the adenomatosis polyposis coli (APC) and Axin proteins no longer bind β-catenin, with consequent β-catenin stabilization and translocation to the nucleus where it associates with the Tcf family of transcription factors. This transcription factor complex trans-activates a host of target genes governing cancer-relevant processes, including *MYC*, cyclin D1, *COX2*, and matrix metalloproteinase 7 (*MMP7*) (34).

β-catenin mutations and increased nuclear expression have been detected in human HCC (35). In some reports, β-catenin over-expression and mutations have been related to early-stage HCCs (5) and in others to HCC progression (36). Over-expression and mutations of β-catenin occur more frequently in HCV-related HCCs compared with HBV-related HCCs (37).

Aberrant accumulation of beta-catenin is observed at high frequency in many cancers (38). This accumulation correlates with either mutational activation of *CTNNB1* (beta-catenin) or mutational inactivation of *APC* and *Axin1* genes in some tumors. In addition to mutations in the beta-catenin gene, mutations in the Axin1 and Axin2 genes may alter the Wnt signaling pathway, resulting in accumulation of beta-catenin in HCC. In literature; there are studies indicating that Axin1 mutation is observed in a specific portion of HCC cases (10%-25% in different studies) (39), (40). Somatic mutations of exon 3-5 of *AXIN1* have been observed in 25% of HCC patients. Moreover, reduced or absent expression of axin was seen in 66.7% HCCs tested. The abnormal expression of beta-catenin and axin proteins was closely correlated with mutations of *AXIN1* and beta-catenin ($P < 0.0001$ and $P = 0.008$, respectively). The researchers suggest that mutation of *AXIN1* gene is a frequent and late event for HCC, associated with cirrhosis, and is correlated significantly with abnormal expression of axin and beta-catenin. Transduction of the wild-type Axin gene (*AXIN1*) induces apoptosis in HCC cells as well as in colon cancer cells.

1.3.3 ErbB receptor family

The examination of these receptor tyrosine kinases has documented the overexpression of ERBB1 (also known as epidermal growth factor receptor (EGFR)) in 68% of HCC cases,

ERBB3 in 84%, ERBB2 (also known as HER2) in 21% and ERBB4 in 61% (but at a lower level) (41).

1.3.4 MET and HGF

Overexpression of the MET receptor has been reported in advanced human HCCs (42). The role of MET signalling in HCC development has been confirmed in mouse models, whereby mice transgenic for the MET ligand HGF, one of the most potent hepatocyte mitogens, develop HCCs by 1.5 years of age (43).

1.3.5 Methylation of cancer-relevant genes

Aberrant DNA methylation patterns have been reported in human HCC (44). Methylation has been detected in the earliest stages of hepatocarcinogenesis, and to a greater extent in tumor progression (45). Specific hypermethylation events in HCC have targeted *p16(INK4a)*, E-cadherin, *COX2*, apoptosis-associated speck-like protein (*ASC*) and deleted in liver cancer 1 (*DLC1*), among others (18).

Studies have reported methylation at p15, SOCS1, RIZ1 and *CASP8* in HCC (46). Methylation status of *RASSF1A*, *SOCS1* and *CASP8* in 97 tumors found to be hypermethylated in 30.9, 33.0 and 15.5%, respectively. Moreover, methylation status of RASSF1A but not the other 2 genes predicted the outcome of HCC (47). In an other study, Okochi et. al. detected that aberrant methylation of the SOCS-1 gene in 30 of 50 (60%) HCC specimens. No corresponding nontumorous liver tissues have showed SOCS-1 methylation. Subsequent Northern analysis proved that methylation of the SOCS-1 promoter inactivated translation and diminished expression of SOCS-1 mRNA. They analyzed the correlation between the clinicopathological data and SOCS-1 aberrant methylation and found that HCC derived from liver cirrhosis had a significant relationship with SOCS-1 methylation ($P = 0.0207$) (48).

1.3.6 c-Myc

Recently, Kaposi-Novak et. al. identified that the MYC oncogene as a plausible driver gene for malignant conversion of the dysplastic nodules. They showed that induction of MYC target genes occurred ubiquitously during malignant conversion (49).

1.4 Liver cirrhosis and senescence

Liver cirrhosis, the irreversible terminal stage of chronic liver disease, characterized by widespread fibrous scarring, serious complications of liver cirrhosis includes those: accumulation of fluid in the abdomen (ascites), bleeding disorders (coagulopathy), increased pressure in the blood vessels (portal hypertension), and confusion or a change in the level of consciousness (hepatic encephalopathy). Regenerative nodules are characteristic lesions of the cirrhotic liver. Dysplastic foci, which are smaller than 1 mm, can be found in regenerative nodules. There are two types of dysplastic foci in cirrhotic livers, small cell-dysplasia (SCD) and the large cell-dysplasia (LCD), according to the nuclear/cytoplasmic ratio.

Hepatocyte telomere shortening and senescence are general markers of human liver cirrhosis, and correlates with progression of fibrosis in cirrhosis samples (Wiemann SU.et al., 2002). Additionally, Paradis V et al. observed an increasing percentage of replicative senescent liver cells from normal liver to chronic hepatitis and HCC (Paradis V. et al., 2002).

1.4.1 Cellular senescence

The term ‘‘cellular senescence” was initially used by Hayflick and colleagues to define cells that ceased to divide in culture (50). Today, cellular senescence is recognized as a response of proliferating somatic cells to stress and damage from exogenous and endogenous sources. It is characterized by permanent cell cycle arrest. Senescent cells also display altered morphology and an altered pattern of gene expression, and can be recognized by the presence of senescence markers such as senescence-associated b-galactosidase (SABG), p16INK4A, senescence-associated DNA-damage foci and senescence-associated heterochromatin foci (51). This cellular response has both beneficial (anti-cancer) and probably deleterious (such as tissue aging) effects on the organism.

Upstream checkpoint kinases, such as ATM or ATR are activated in response to DNA damage in the form of double-stand breaks. These kinases phosphorylate downstream factors including CHK1 and CHK2 that in turn phosphorylate p53. Phosphorylation of p53 results in its activation by the displacement of the MDM2 protein. Critical involvement of this p53 activating pathway has been reported for both telomere-dependent, and oncogene-induced senescence (52). Most cells senesce owing to engagement of the p53 pathway, p16–pRB pathway, or both (Figure 1.3).

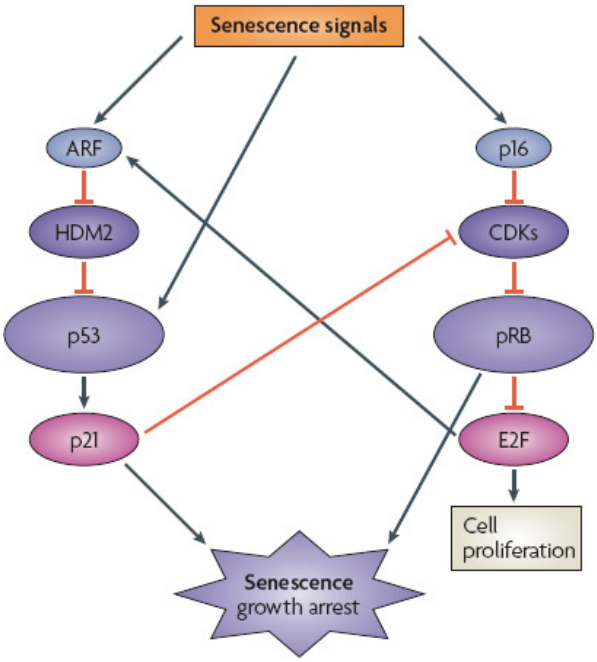

Figure 1.3 Senescence controlled by the p53 and p16–pRB pathways (51).

1.4.1.1 Replicative senescence

Human chromosome telomere ends which are composed of TTAGGG repeats (5–20 kb) in a DNA-protein complex formed by six telomere-specific proteins, called ‘‘shelterin” (53) prevent genomic instability and the loss of essential genetic information by ‘‘capping” chromosome ends. They are also indispensable for proper recombination and chromosomal segregation during cell division. Telomeres become shorter with every cell division in somatic cells, because of replication complex’s inability to copy the ends of linear DNA, which also makes them a ‘‘cell cycle counter” for the cell (54). Telomeres are added to the end of chromosomes with a complex containing the RNA template TERC and the reverse transcriptase TERT (55). Most somatic cells lack telomerase activity because the expression of TERT is repressed, in contrast to TERC expression. It is now well known that telomere-dependent senescence is induced by a change in the protected status of shortened telomeres, whereby the loss of telomere DNA contributes to this change (56). At least two other forms of telomere-independent senescence are presently known: (1) oncogene-induced senescence; and (2) reactive oxygen species (ROS)-induced senescence (Figure 1.4).

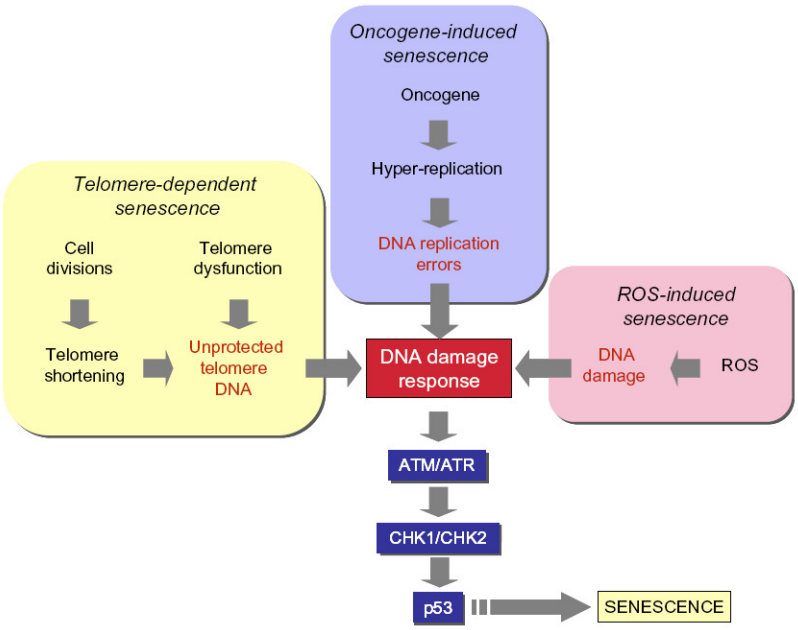

Figure 1.4 Senescence pathways (52).

1.4.1.2 Oncogene and ROS-induced senescence

Oncogene-induced senescence had initially been identified as a response to expression of Ras oncogene in normal cells, accompanied by accumulation of p53 and p16INK4a. In addition to Ras, other oncogenes including Raf, Mos, Mek, Myc and Cyclin E also induce senescence (57). Similar to telomere-dependent senescence, oncogene-induced senescence is also primarily a DNA damage response (Figure 1.3).

ROS-induced senescence, the other telomere-independent senescence pathway is gaining importance, also. Experimental induction of ROS accumulation in cells (for example by mild H2O2 treatment or glutathione depletion) induces senescence-like growth arrest in different cell types, whereas anti-oxidant treatment can inhibit senescence (58). More importantly, ROS have been identified as critical mediators of both telomere-dependent and oncogene-induced senescence (52).

1.4.2 Senescence as an anti-tumor mechanism in hepatocellular carcinoma

Recent findings indicate that senescence induction is a powerful mechanism of HCC regression. Xue et al. expressed H-ras oncogene and suppressed endogenous p53 expression in mouse hepatoblasts which produced massive HCCs upon implantation into livers of athymic mice (59). However, these tumors regressed rapidly upon restoration of p53 expression. Tumor regression was due to differentiation and massive senescence induction,

followed by immune-mediated clearance of senescent cells. These observations may indicate that oncogene-induced senescence is also involved in HCC. On the other hand, HCCs induced by tet-regulated c-Myc activation in mouse liver cells differentiate into mature hepatocytes and biliary cells or undergo senescence (60). Thus, senescence induction may also be relevant to oncogene inactivation in HCC. So far, all the reported examples of senescence induction in HCC cells are in the form of a telomere-independent permanent cell cycle arrest. Until recently, it was unknown whether replicative senescence could also be induced in immortal cancer cells. Our group reported recently that immortal HCC cells can revert spontaneously to a replicative senescence phenotype (61). HCC cells generated progeny that behaved, in vitro, similar to normal somatic cells. Such senescence-programmed progeny (C3 and G12 clones) lacked telomerase activity due to TERT repression (probably mediated by SIP1 gene), and displayed progressive telomere shortening in cell culture, resulting in senescence arrest. On the other hand, immortal clones (C1 and G11) had indefinite proliferation capacity with high tumorigenic capacity.

1.4.3 Cyclin-dependent inhibitors as common mediators of senescence arrest

Most if not all senescence pathways result in the activation of cyclin-dependent kinase inhibitors (CDKIs) in order to induce permanent cell cycle arrest. Senescent cells accumulate at G1 phase of the cell cycle due to an inability to enter into S phase in order to initiate DNA synthesis. The transition of proliferating cells from G1 to S phase requires the release of E2F factors from their inhibitory partner retinoblastoma protein (pRb) following phosphorylation by cyclin-dependent kinases (CDKs), in particular by CDK4/CDK6 and CDK2 at this stage of the cycle (62). The senescence arrest is mediated by inhibition of pRb phosphorylation by CDK4 and CDK2. The activities of these enzymes are controlled by different mechanisms, but the major proteins involved in the control of senescence arrest are CDKIs. Almost all known CDKIs have been reported to be implicated in senescence arrest, but three of them are best characterized: p16INK4a and p15INK4b which inhibit CDK4/CDK6, and p21Cip1 which inhibits CDK2 (Fig. 2). p21Cip1 is one of the main targets of p53 for the induction of cell cycle arrest following DNA damage (63). Pathways that generate DNA damage response and p53 activation use p21Cip1 as a major mediator of cellular senescence to control pRb protein (64). Exceptionally, p21Cip1 can be activated by p53-independent pathways to induce senescence (65).

1.5 Expression Profiling Using Affymetrix GeneChip Microarrays

The approximately 25,000 genes in mammalian genomes can be transcribed at different levels. Measurements of gene expression for ten thousands of genes in parallel give the most comprehensive picture of steady-state levels of transcripts and is used in basic and applied research. Microarrays are the most frequently used technology for genome-wide expression profiling; from the various available microarray platforms, Affymetrix GeneChips are most frequently used for expression profiling and over 3,000 scientific publications describe results of this technology. In medical research, expression profiling by microarrays holds great promises for better understanding of diseases, identification of new therapeutic targets, and subclassification of diseases to identify individualized treatment strategies (66). Microarray studies provide evidence that a large set of growth control genes is deregulated in HCC (1).

A typical microarray experiment involves the hybridization of an mRNA molecule to the DNA template from which it is originated. Many DNA samples are used to construct an array. The amount of mRNA bound to each site on the array indicates the expression level of the various genes. This number may run in thousands. All the data is collected and a profile is generated for gene expression in the cell (67).

Affymetrix microarray technology uses oligonucleotides consisting of 25 bases. A special technique called photolithographical array production is applied to sequence or synthesize the oligonucleotides on a glass support. Each gene (or transcript) is represented by 22 different oligonucleotide fragments that are attached to a tiny section of the chip (density of up to 500 000 sections per 1.6 cm^2). Each section carries 22 different oligonucleotide sequences (11 matches and 11 mismatches). Thus, the expression of a gene is given by 11 signal intensities (compared to 1 signal for cDNA microarrays). The 11 mismatch strands serve to determine the specificity of measured signal. The production of target DNS includes some further steps. After the isolation of mRNA and the reverse transcription to cDNA, the cDNA strands are converted to double stranded DNA molecules. After this step, the DNA is converted to cRNA molecules using a special polymerase (T7 polymerase) and fluorescently labelled. This cRNA is hybridised to the microarray. Unbound cRNA are washed away and signal intensities are scanned. The Affymetrix GeneChip Human Genome U133 set is made up of over 1,000,000 unique oligonucleotide features covering over 39,000 transcript variants which represent 33,000 of the best characterized human genes. Sequences used in the design of array were selected from GeneBank, dbEST, and RefSeq.

1.6 Rb/E2F pathway

The Rb-E2F pathway links growth-regulatory pathways to a transcription program involved in DNA synthesis, cell-cycle progression, cell division, apoptosis, DNA repair, differentiation and senescence (68). This transcription program is repressed when hypophosphorylated pRb is bound to E2F proteins or recruit co-repressors to the proteins, and active when pRb is phosphorylated by CDK4/6, which frees E2F proteins to function as transcription factors via forming heterodimers with DP proteins. Eight E2F genes encode nine major proteins that share a related DNA-binding domain and are classified as either 'activating' or 'repressor' E2Fs (69). E2F1, E2F2 and E2F3a localize to the promoters of target genes in the G_1/S phase and activate transcription of these genes; whereas E2F4, E2F5 and, most probably, E2F3b bind their target promoters in association with Rb family members in the G_0/G_1 phase coincident with their repression (70). E2Fs 1-5 have pocket-protein binding domains that enable them to interact with pRb and its homologs p107 and p130. E2Fs 6-8 lack this domain, and repress transcription via other mechanisms; for example, E2F6 exerts its effect by binding to the Polycomb group's transcriptional repressors. The E2F proteins, except E2F7 and 8, form heterodimers with DP (or TFDP), which enhances their DNA binding, transactivation and pRb-binding activities DP1 and DP2 (which is the human equivalent to murine DP3) proteins are 70% homologous and each form functional dimers with any E2F protein (71). The other DP family protein, DP4, which has been recently characterized, shares 90% homology with DP1 and heterodimerizes with E2F (72). DP proteins have a DNA-binding domain that shares sequence homology with the E2F DNA-binding domain (73). As pRb protein is the key player in cell-cycle progression, it is not surprising that it and its upstream regulators, such as Cyclin D1, cyclin-dependent kinase 4 and $p16^{INK4a}$ are frequently mutated in numerous types of human tumours (73). And thus, attention has focused on the involvement of downstream regulators of pRb in tumourigenesis, of which E2F/DP transcription factors are the best characterized set. Increased levels of E2F1 have been associated with tumorigenesis and a poorer outcome of melanoma, small-cell lung carcinoma, breast and pancreas carcinomas both *in vitro* and *in vivo*, whereas decreased E2F1 expression has resulted in more aggressive disease progression in colon cancer, bladder cancer and diffuse large B-cell lymphoma (74), (75), (76), (77).

It is becoming apparent that the function of any given E2F/DP family protein in regulating cell proliferation, apoptosis, quiescence or senescence is more complex than previously thought and most probably dependent on cell type and context (78). The Rb pathway is among the pathways most frequently disrupted in HCC. RB1 is inactivated by

direct mutation or loss of the *RB1* gene, and phosphorylation of the pRb protein is deregulated through aberrant cdk activity (via loss of $p16^{INK4a}$ expression or cyclin-D1 amplification) (5). Up-regulation of pRb-free E2F1-DP1 and E2F2-DP1 heterodimers is found to be a major cause of aberrant G_1-S transition in c-myc/TGF-β-dependent HCC models (79). Also, Hepatitis B viral core protein (HBc) has been found to interact with E2F1 and reduce the DNA-binding ability of E2F1 to the p53 promoter (80). Mutations of E2F4 have been detected in HCC (81). Yasui *et al.* showed that the DP1 gene was located at 13q34, a frequent amplification site in HCC, and that over-expression of this gene was correlated with large tumour size (82). Nonetheless, the involvement of different DP subunits (including splice variants) and different E2F-DP heterodimers in the oncogenic and tumor suppressor mechanisms (such as immortality and senescence) in HCC are not completely understood.

1.6.1 DP-2 (TFDP2)

Human cells express at least three DP2 isoforms (of 55, 48 and 43 kDa) (83). Despite being identified more than 13 years ago (84), the DP2 gene remains underexplored, particularly in terms of its role in tumorigenesis.

An increase in *DP2*expression has been reported in a smal set of HCC tissues by RT-PCR (85).

It has been reported that the expression of *DP2* is controlled during tissue development (86), (87) and cell cycle (88). Moreover, the expression of *DP2* in adult tissues is highly variable, detected in some tissues - including liver - but not in others. Differential expression of *DP2* was also observed in cancer cell lines (71).

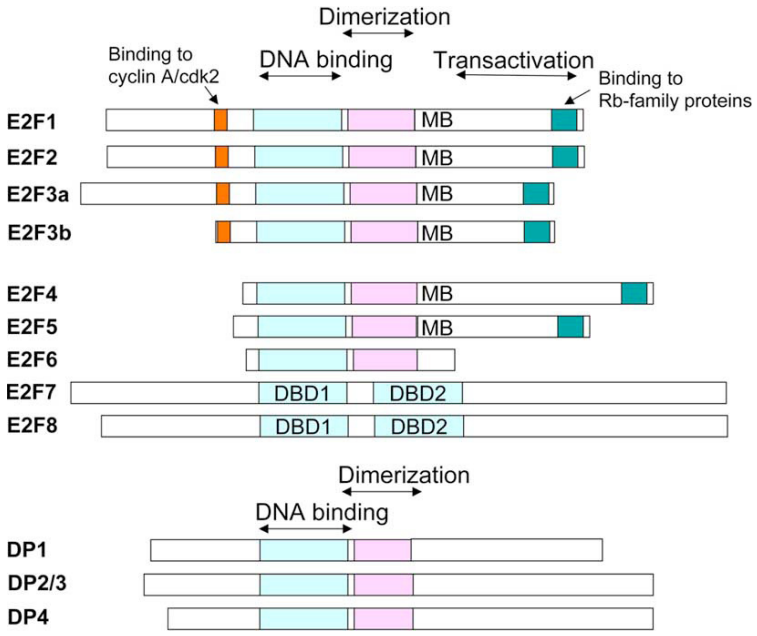

Figure 1.5 E2F/DP family (89).

1.7 Chromatin modifications and hepatocellular carcinoma

The term **epigenetics** refers to changes in gene expression or phenotype caused by mechanisms other than changes in the underlying DNA sequence, hence the name *epi-* (Greek: over; above) *-genetics*. These changes may remain through cell divisions for the remainder of the cell's life and may also last for multiple generations.

1.7.1 DNA methylation

The 5' cytosine of CpG dinucleotides within mammalian genomes can be methylated by *denovo* DNA methyltransferases such as DNMT3A and DNMT3B. Maintenance of DNA methylation is performed by DNMT1, utilizing hemimethylated DNA as a substrate. This provides a mechanism to propagate the epigenetic mark following DNA replication. The methyl groups serve as docking sites for gene silencing proteins. In general, DNA methylation correlates with increased chromatin condensation and gene silencing (90).

There are several ways in which altered patterns of DNA methylation lead to disease. Alterations in methylation patterns are responsible for several congenital diseases that affect growth through the misregulation of imprinted genes. In addition to alterations in the patterns of DNA methylation, loss of DNA methyl transferase also leads to disease. Given that mutations within DNA methyltransferase genes are associated with disease, it follows that mutations within genes encoding proteins that bind to methylated cytosines also result in

disease. MeCP2 (methyl-CpG-binding protein 2) is a member of a class of DNA methyl binding proteins (MBDs) that specifically recognize methylated cytosine residues. These binding proteins function by recruiting histone deacetylases (HDACs) to silencetarget genes. Mutations in the X-linked gene encoding MeCP2 are responsible for approximately 95% of classic Rett syndrome cases (RTT, OMIM 312750) (91).

1.7.1.1 DNA methylation and cancer

CpG dinucleotides are generally methylated in normal cells, with the exception of hypomethylation at CpG "islands" located upstream of many active genes. In contrast, cancer cells exhibit a global hypomethylation and CpG island hypermethylation (92) (Fig. 1.6 and 1.7). This shift in the pattern of DNA methylation frequently results in inappropriate silencing of genes. Global DNA hypomethylation (also known as demethylation) is associated with activation of protooncogenes, such as c-JUN, c-MYC, and c-Ha-Ras, and generation of genomic instability. Hypermethylation on CpG islands located in the promoter regions of tumor suppressor genes results in transcriptional silencing and genomic instability. For example, expression of the serine protease inhibitor family member *maspin* is reduced due to methylation of promoter sequences in many advanced forms of cancer (93).

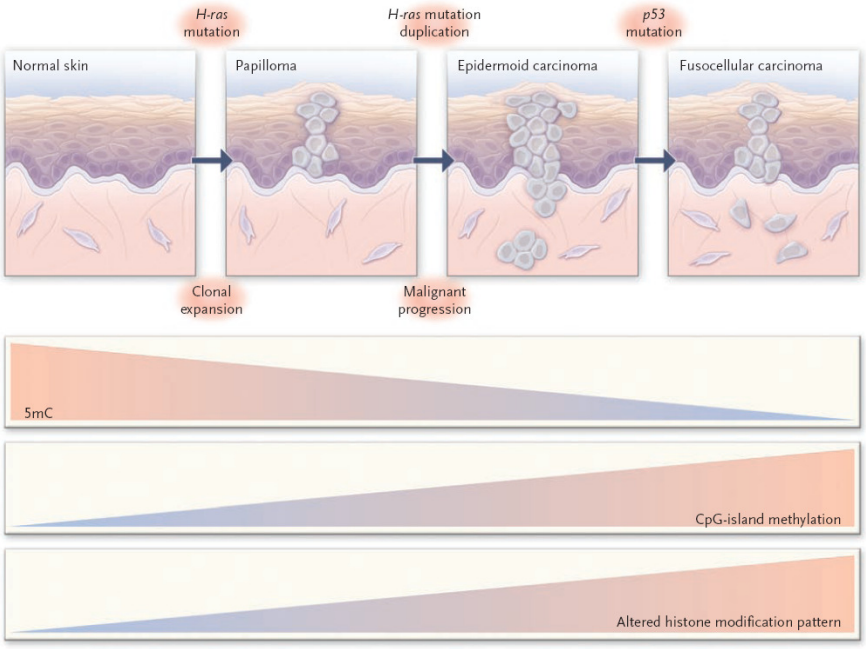

Figure 1.6 Epigenetic Alterations in Tumor Progression, skin tumor as a model (94).

A growing number of genes undergoing aberrant CpG island hypermethylation in HCC have been discovered, suggesting that de novo methylation is an important mechanism underlying malignant transformation in the liver. Epigenetic silenced genes are involved in

important molecular pathways of carcinogenesis e.g., cell cycle regulation, apoptosis, DNA repair or cell adhesion (45). The genes frequently found to be methylated in HCC are APC, GSTP1, RASSF1A, p16, COX-2, CCND2, SPINT2, RUNX3, CFTR, HINT1, RIZ1 and E-cadherin (45). Furthermore, a combination of RASSF1A, CCND2 and SPINT2 showed 89-95% sensitivity, 91-100% specificity and 89-97% accuracy in discriminating between HCC and non-HCC tissues, and correctly diagnosed all early HCCs (95). Also, it was shown that one of the regulation mechanisms of hTERT promoter was DNA methylation (96). Some miRNA's were also shown to be silenced by DNA methylation and play a role in hepatocellular carcinogenesis, for example micro-RNA 1 (97). Also, methylation of Tip30 promoter was associated with poor prognosis in human hepatocellular carcinoma (98). Yan et. al. associated the promoter methylation and reduced T-cadherin expression (40% HCC) with the development and progression of hepatocellular carcinoma.

Calvisi et. al. showed that the extent of global DNA hypomethylation and CpG hypermethylation correlates with biologic features and clinical outcomes of HCC. They suggested that aberrant methylation is a major event in both early and late stages of liver malignant transformation and might constitute a critical target for cancer risk assessment, treatment, and chemoprevention of HCC (99).

Type of Cancer	Epigenetic Disruption
Colon cancer	CpG-island hypermethylation (*hMLH1*, *p16^{INK4a}*, *p14^{ARF}*, *RARB2*, *SFRP1*, and *WRN*), hypermethylation of miRNAs (*miR-124a*), global genomic hypomethylation, loss of imprinting of *IGF2*, mutations of histone modifiers (*EP300* and *HDAC2*), diminished monoacetylated and trimethylated forms of histone H4
Breast cancer	CpG-island hypermethylation (*BRCA1*, E-cadherin, *TMS1*, and estrogen receptor), global genomic hypomethylation
Lung cancer	CpG-island hypermethylation (*p16^{INK4a}*, *DAPK*, and *RASSF1A*), global genomic hypomethylation, genomic deletions of *CBP* and the chromatin-remodeling factor *BRG1*
Glioma	CpG-island hypermethylation (DNA-repair enzyme *MGMT*, *EMP3*, and *THBS1*)
Leukemia	CpG-island hypermethylation (*p15^{INK4b}*, *EXT1*, and *ID4*), translocations of histone modifiers (*CBP*, *MOZ*, *MORF*, *MLL1*, *MLL3*, and *NSD1*)
Lymphoma	CpG-island hypermethylation (*p16^{INK4a}*, *p73*, and DNA-repair enzyme *MGMT*), diminished monoacetylated and trimethylated forms of histone H4
Bladder cancer	CpG-island hypermethylation (*p16^{INK4a}* and *TPEF/HPP1*), hypermethylation of miRNAs (*miR-127*), global genomic hypomethylation
Kidney cancer	CpG-island hypermethylation (*VHL*), loss of imprinting of *IGF2*, global genomic hypomethylation
Prostate cancer	CpG-island hypermethylation (*GSTP1*), gene amplification of polycomb histone methyltransferase *EZH2*, aberrant modification pattern of histones H3 and H4
Esophageal cancer	CpG-island hypermethylation (*p16^{INK4b}* and *p14^{ARF}*), gene amplification of histone demethylase *JMJD2C/GASC1*
Stomach cancer	CpG-island hypermethylation (*hMLH1* and *p14^{ARF}*)
Liver cancer	CpG-island hypermethylation (*SOCS1* and *GSTP1*), global genomic hypomethylation
Ovarian cancer	CpG-island hypermethylation (*BRCA1*)

Figure 1.7 DNA methylation differences in some cancers (Esteller M, Epigenetics in cancer, NEJM, 2008).

1.7.2 Histone modifications

The nucleosome is the fundamental unit of chromatin and it is composed of an octamer of the four core histones (H3, H4, H2A, H2B) around which 147 base pairs of DNA are wrapped. The core histones are predominantly globular except for their N-terminal ‘‘tails,’’ which are unstructured. A striking feature of histones, and particularly of their tails, is the large number and type of modified residues they possess. These modifications serve to alter charge interactions of the histone tails with DNA, thereby influencing chromatin packaging. In addition, these modifications serve as binding sites for specific factors that “read” a proposed histone code. In most cases, specific modifications correlate with biological functions such as chromatin condensation, transcriptional regulation and DNA replication. Generally speaking, two kinds of enzymatic activities impinge on chromatin structure. One family involves mainly ATP hydrolysing enzymes that can re-model chromatin by ‘shuffling’ nucleosomes. Another family includes a set of enzymes that are able to modify histones covalently, at specific residues, located most commonly at the histone tails (100). There are at least eight distinct types of modifications found on histones. We have the most information regarding the modifications include acetylation, phosphorylation, methylation and ubiquination. Although these modifications have been known for many years to occur on histones, their function is only recently being recognised. There are over 60 different residues on histones where modifications have been detected either by specific antibodies or by mass spectrometry. However, this represents a huge underestimate of the number of modifications that can take place on histones. Extra complexity comes partly from the fact that methylation at lysines or arginines may be one of three different forms: mono-, di-, or trimethyl for lysines and mono- or di- (asymmetric or symmetric) for arginines (101). The timing of the appearance of a modification will depend on the signaling conditions within the cell.

Whereas lysine acetylation almost always correlates with chromatin accessibility and transcriptional activity, lysine methylation can have different effects depending on which residue is modified. Methylation of histone H3 lysine 4 (H3K4) and H3 lysine 36 is associated with transcribed chromatin. In contrast, methylation of H3 lysine 9 (H3K9), H3 lysine 27 (H3K27), and H4 lysine 20 (H4K20) generally correlate with repression. Distinct histone modifications can influence each other and may also interact with DNA methylation,

in part through the activities of protein complexes that bind modified histones or methylated cytosines (102). (Fig. 1.8).

1.7.2.1 Histone modifying enzymes

Most modifications have been found to be dynamic, and enzymes that remove the modification have been identified (Fig. 1.9).

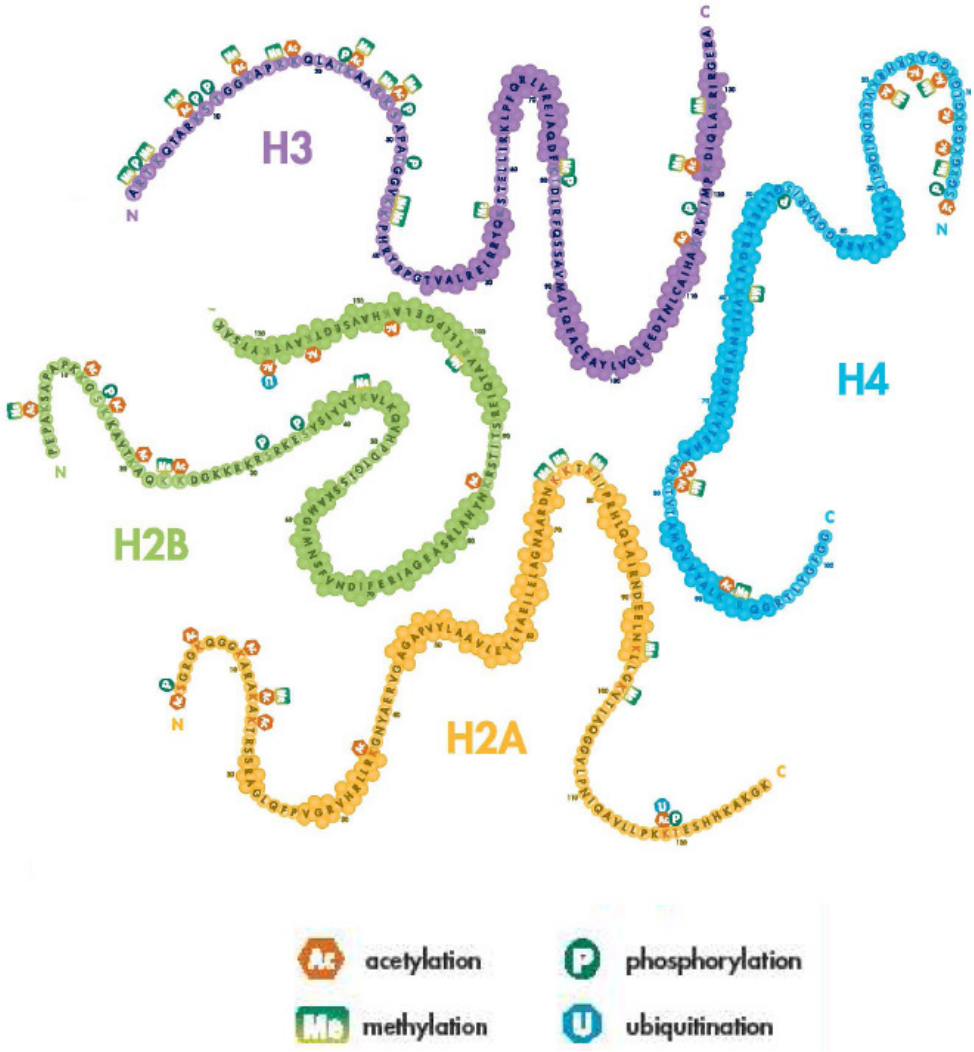

Figure 1.8 Histone modifications (Upstate)

Of all the enzymes that modify histones, the methyltransferases and kinases are the most specific. This is perhaps the reason why methylation is the most characterized modification to date. In some cases, the specificity of enzymes that modify histones can be influenced by other factors: complexes in which enzymes are found (103); proteins that associate with the enzyme may affect its selection of residue to modify (104), or the degree of methylation (mono-, di-, or tri-) at a specific site (105). Proteins are recruited to modifications

and bind via specific domains. Methylation is recognized by chromo-like domains of the Royal family (chromo, tudor, MBT) and nonrelated PHD domains, acetylation is recognized by bromodomains, and phosphorylation is recognized by a domain within 14-3-3 proteins.

Enzymes that Modify Histones	Residues Modified
Acetyltransferase	
HAT1	H4 (K5, K12)
CBP/P300	H3 (K14, K18) H4 (K5, K8) H2A (K5) H2B (K12, K15)
PCAF/GCN5	H3 (K9, K14, K18)
TIP60	H4 (K5, K8, K12, K16) H3 K14
HB01 (ScESA1, SpMST1)	H4 (K5, K8, K12)
ScSAS3	H3 (K14, K23)
ScSAS2 (SpMST2)	H4 K16
ScRTT109	H3 K56
Deacetylases	
SirT2 (ScSir2)	H4 K16
Lysine Methyltransferase	
SUV39H1	H3K9
SUV39H2	H3K9
G9a	H3K9
ESET/SETDB1	H3K9
EuHMTase/GLP	H3K9
CLL8	H3K9
SpClr4	H3K9
MLL1	H3K4
MLL2	H3K4
MLL3	H3K4
MLL4	H3K4
MLL5	H3K4
SET1A	H3K4
SET1B	H3K4
ASH1	H3K4
Sc/Sp SET1	H3K4
SET2 (Sc/Sp SET2)	H3K36
NSD1	H3K36
SYMD2	H3K36
DOT1	H3K79
Sc/Sp DOT1	H3K79
Pr-SET 7/8	H4K20
SUV4 20H1	H4K20
SUV420H2	H4K20
SpSet 9	H4K20
EZH2	H3K27
RIZ1	H3K9

Enzymes that Modify Histones	Residues Modified
Lysine Demethylases	
LSD1/BHC110	H3K4
JHDM1a	H3K36
JHDM1b	H3K36
JHDM2a	H3K9
JHDM2b	H3K9
JMJD2A/JHDM3A	H3K9, H3K36
JMJD2B	H3K9
JMJD2C/GASC1	H3K9, H3K36
JMJD2D	H3K9
Arginine Methlytransferases	
CARM1	H3 (R2, R17, R26)
PRMT4	H4R3
PRMT5	H3R8, H4R3
Serine/Thrionine Kinases	
Haspin	H3T3
MSK1	H3S28
MSK2	H3S28
CKII	H4S1
Mst1	H2BS14
Ubiquitilases	
Bmi/Ring1A	H2AK119
RNF20/RNF40	H2BK120
Proline Isomerases	
ScFPR4	H3P30, H3P38

Figure 1.9 Histone modifying enzymes (101).

Also, recently Chang et. al. identified that the Jumonji domain-containing 6 protein (JMJD6) was a JmjC-containing iron- and 2-oxoglutarate-dependent dioxygenase that demethylates histone H3 at arginine 2 (H3R2) and histone H4 at arginine 3 (H4R3) in both biochemical and cell-based assays (106).

The abundance of modifications on the histone tail makes ‘‘crosstalk’’ between modifications very likely. Mechanistically such communication between modifications may occur at several different levels. Firstly, many different types of modification occur on lysine residues. This will undoubtedly result in some form of antagonism since distinct types of modifications on lysines are mutually exclusive. Secondly, the binding of a protein could be disrupted by an adjacent modification. The best example of this is that of phosphorylation of H3S10 affecting the binding of HP1 to methylated H3K9 (107). Thirdly, the catalytic activity of an enzyme could be compromised by modification of its substrate recognition site; for example, isomerization of H3P38 affects methylation of H3K36 by Set2 (108). Fourthly, an enzyme could recognize its substrate more effectively in the context of a second modification; the example here is the GCN5 acetyltransferase, which may recognize H3 more effectively when it is phosphorylated at H3S10 (109).

1.7.2.2 Histone methylation and cancer

Hypermethylation of the CpG islands in the promoter regions of tumor-suppressor genes in cancer cells is associated with a particular combination of histone markers: deacetylation of histones H3 and H4, loss of H3K4 trimethylation, and gain of H3K9 methylation and H3K27 trimethylation. The presence of the hypo-acetylated and hypermethylated histones H3 and H465 silences certain genes with tumor-suppressor–like properties, such as *p21WAF1,* despite the absence of hypermethylation of the CpG island (94). In human tumors generally, modifications of histone H4 entail a loss of monoacetylated and trimethylated forms (110). These changes appear early and accumulate during the development of the tumor. The losses occur predominantly at the monoacetylated Lys16 and trimethylated Lys20 residues of histone H4 in association with hypomethylated repetitive DNA sequences. They have been found in breast and liver cancer (111); (112). In prostate cancer, weak immunohistochemical staining of two histone modifications (the dimethylation of lysine 4 and the acetylation of lysine 18 of histone H3) has been proposed as a marker of a high risk of recurrence. Expression patterns of histone modifying enzymes distinguish cancer tissues from their normal counterparts, and they differ according to tumor type. In leukemias and sarcomas, chromosomal translocations that involve histone-modifier genes, such as histone

acetyltransferases (e.g., cyclic AMP response-element-binding protein [CREB]–binding protein–monocytic leukemia zinc finger [*CBP-MOZ*]) and histone methyltransferases (e.g., mixed-lineage leukemia 1 [*MLL1*], nuclear-receptor binding SETdomain protein 1 [*NSD1*], and nuclear-receptor binding SET-domain protein 3 [*NSD3*]), create aberrant fusion proteins (113). In solid tumors, there is amplification of genes for histone methyltransferases such as *EZH2,* mixed-lineage leukemia 2 (*MLL2*), or *NSD3*58,69 or a demethylase (e.g., Jumonji domain-containing protein 2C [*JMJD2C/GASC1*]).

1.7.2.2.1 H3K27 methylation

The H3K27 methylation mark is primarily governed by the polycomb group (PcG) proteins that are initially genetically defined in Drosophila melanoganster. Two polycomb repressor complexes (PRC1 and PRC2) have been characterized. PRC1, comprising core components of BMI-1, Ring-1, HPH and HPC, recognizes trimethylated H3K27 and mediates the maintenance of the silent state. PRC2, comprising of enhancer of zeste homologue 2 (EZH2), suppressor of zeste 12 (SUV12) and embryonic ectoderm development (EED), mediates the initiation of gene repression via association with HDACs and DNA methyltransferases (DNMTs) (114).

1.7.2.2.1.1 EZH2

EZH2, a SET domain methyltransferase for H3K27, plays essential roles in embryonic development and stem cell renewal (114). Overexpression of EZH2 has been observed and positively correlates with the progression of multiple malignancies, including prostate cancer, breast cancer, lymphoma, myeloma, colorectal cancer, endometrial cancer, bladder cancer and melanoma and liver (90). Ectopic overexpression of EZH2 leads to increased cell proliferation and transformation independent of growth factors in multiple myeloma, whereas decreased expression of EZH2 by RNAi leads to growth arrest in prostate cancer cells. The methyltransferase activities of both EZH2 and HDAC recruited by EED are required for cell proliferation and invasion mediated by EZH2. The fact that the PRC2 complex recruits DNMTs to the promoters of EZH2 target genes and induces their silencing in tumor cells suggests that EZH2 might selectively induce the silencing of tumor-suppressor genes during cancer cell evolution (115). However, direct evidence supporting EZH2-mediated silencing of tumor-suppressor genes remains to be established. Alternative mechanisms of oncogenesis have been proposed. For example, cytoplasmic EZH2 controls actin polymerization and cell signaling upstream of the small GTPase CDC42 (116).

1.7.2.2.1.2 BMI1

BMI1 is recruited to trimethylated H3K27 (H3K27me3) as part of the PRC1 complex via the interaction between HPC and H3K27me3. It was originally identified as a protooncogene that cooperates with Myc to promote B-cell lymphoma development in mouse models (117). It is also overexpressed in lymphoma, leukemia, medulloblastoma, neuroblastoma and non-small-cell lung cancer (NSCLC). BMI1 inhibits Myc-induced apoptosis through repression of the CDKN2A locus (118). In addition, BMI1 harbors crucial activities in maintaining proliferative capacities of both normal stem cells and leukemic stem cells, suggesting that BMI1 might promote tumorigenesis by misdirecting tumor cells toward a stem cell fate (118).

1.7.2.2.2 H3K9 methylation

1.7.2.2.2.1 HP1 – an H3K9 methylation 'reader'

HP1 proteins (HP1a, HP1b, HP1g) bind to methyl-H3K9 and are crucial for the formation of heterochromatin and gene silencing. Decreased HP1a and HP1b expression has been observed in metastatic breast tumors, melanoma and other metastatic tumors. Ectopic expression of HP1a reduces invasion of breast cancer cells, whereas inhibition of HP1a leads to increased invasion without affecting cell growth, implicating its role in tumor metastasis suppression. However, either an increase or reduction in HP1 levels can lead to chromosome instability and aneuploidy (90); (119).

1.7.2.2.2.2 SUV39H and RIZ1 – H3K9 methylation 'writers'

SUV39H1 and SUV39H2, mammalian homologues of Drosophila SU(VAR)3–9, are SET domain HMTs for H3K9. Whereas SUV39H1-/- and SUV39H2 -/- mice are viable with no clear phenotype, SUV39H1-/-/SUV39H2-/- mice exhibit severely compromised viability, increased chromosomal instability and increased risk of B-cell lymphoma. These phenotypes were associated with chromosomal mis-segregation, abnormally long telomeres and significant reduction of di- and tri-methylation of H3K9 and loss of HP1 binding at pericentric heterochromatin and telomeres (120). Biochemically, SUV39H1 and HP1 interact with pRb and mediate gene silencing of –pRb targets. SUV39H1 also prevents Ras-induced tumorigenesis by promoting senescence. Despite these observations, the role of SUV39H1inhuman cancer is not defined because there have not been any SUV39H1 mutations or losses reported in human cancers. RIZ1/PRDM2, another family of SET domain

H3K9 methyltransferase, was originally identified as a pRb-binding protein. Inactivation of RIZ1 by mutations and silencing via promoter hypermethylation are observed in many human cancers, including hepatocellular, colon, breast and gastric cancers, suggesting a tumorsuppressive role. Furthermore, missense mutations that abolish the HMT activity of RIZ1 are found in human cancers (121), (122).

1.7.2.2.2.3 JMJD2C – an H3K9 methylation 'eraser'

Jumonji-domain-containing proteins (JMJD) have recently been characterized as histone lysine demethylases. JMJD2C, initially identified as gene amplified in squamous cell carcinoma 1 (GASC1), is also frequently amplified and overexpressed in esophageal squamous cell carcinoma, lung sarcomatoid carcinoma and desmoplastic medulloblastoma. It removes the methyl group from tri- and di-methylated H3K9. Overexpression of JMJD2C/GASC1 induces reduction of global H3K9 triand di-methylation levels and delocalization of HP1, which might contribute to tumorigenesis (123), (124).

1.7.2.2.3 H3K4 methylation

Initial genetic analysis in D. melanoganster defines the functional roles of the trithorax group (Trx-G), the 'writers' for the H3K4 methylation mark, during development. Conserved from flies to mammals, Trx-G proteins maintain the epigenetic activation of homeodomain genes, whereas PcG proteins mediate their silencing. These two antagonistic groups of proteins control important aspects of differentiation and proliferation during embryogenesis (124).

1.7.2.2.3.1 MLL and SMYD3 – H3K4 methylation 'writers'

The mixed lineage leukemia (MLL) protein, a mammalian Trx-G protein, is a SET domain H3K4 methyltransferase and maintains activation of Hox gene expression during development. In several leukemia subtypes, several genetic events have been observed to involve the MLL gene. Indeed, AF10, an MLL fusion partner, binds the H3K79 HMT hDOT1L, linking H3K79 methylation to leukemogenesis and persistent activation of Hox-A protooncogenes. However, the mechanism of MLL fusion involving other partners remains to be elucidated. SET- and MYND-domain-containing protein 3 (SMYD3), another methyltransferase for H3K4, is found to be frequently upregulated in colorectal and hepatocellular carcinoma cell lines. SMYD3 interacts with RNA helicase HELZ and RNA polymerase II and mediates transcriptional activation of targets, including oncogenes, homeobox genes and cell-cycle regulatory genes. Overexpression of SMYD3 enhances cell

growth and promotes transformation, whereas inhibition of SMYD3 expression represses cell growth in cancer cell lines (125).

1.7.2.2.3.2 ING proteins – H3K4 methylation 'readers'

Mammalian ING family proteins, INGs 1–5, are putative tumor suppressors and have been observed to cooperate with p53 to mediate growth arrest, cellular senescence and apoptosis. Reduced expression, somatic mutations and allelic loss of ING proteins (especially ING1, ING3 and ING4) are observed in breast cancer, gastric cancer, melanoma, glioma and head and neck squamous cell carcinoma (HNSCC) (126).

1.7.2.2.4 H3K36, H4K20 and H3K79 methylation

1.7.2.2.4.1 H3K36, H4K20 and H3K79 methylation 'writers'

The nuclear-receptor-binding SET-domain-containing protein 1 (NSD1), initially identified as a fusion partner of nucleoporin 98 (NUP98) in t(5;11)(q35;p15.5)-containing pediatric AML, is a methyltransferase for H3K36, and to a lesser degree for H4K20. NSD1 mediates cellular context-dependent gene silencing and activation. NUP98-NSD1 translocation leads to hematopoietic transformation and leukemia, at least partly as a result of the activation of Hox-A genes via the H3K36 methyltransferase activity of NSD1. Heterozygous mutation or loss of heterozygosity (LOH) of NSD1 causes Sotos syndrome, a childhood overgrowth syndrome exhibiting increased risk (2%–7%) for hepatocellular carcinoma, leukemia and neuroblastoma. hDOT1L is a human non-SET-domain methyltransferase for H3K79. hDOT1L has been shown to interact with AF10, one of the MLL fusion partners in AML. In leukemias caused by MLL-AF10 and clathrin-assembly protein-like lymphoid-myeloid (CALM)-AF10 fusion proteins, hDOTL is mistargeted to the Hox-A9 and Hox-A5 loci, respectively; subsequent H3K79 hypermethylation at these loci and upregulation of Hox-A genes are thought to be responsible for leukemogenesis (127).

1.7.2.3 Histone lysine acetylation and cancer

Several lines of evidence support the connection between HAT dysregulation and oncogenesis. The viral oncoproteins E1A (adenovirus) and large T-antigen (SV40) primarily target p300, CBP and PCAF (p300/CBP-associated factor) and inhibit their function (128). Bi-allelic mutations of p300 and CBP have been observed in colorectal, gastric, hepatocellular and breast cancers. Chromosomal translocations resulting in fusion proteins of HATs,

including MLL-CBP, MLL-p300, MOZ-CBP, MOZ-p300 and MOZ-TIF2 (transcriptional intermediary factor 2), have been identified in leukemia and myelodysplastic syndrome, and the leukemogenic potential has been confirmed in murine models in the case of MLL-CBP.

In cell lines and murine models of colon cancer, HDAC2 is upregulated upon loss of adenomatosis polyposis coli (APC), and the expression of HDAC2 is required for tumorigenesis, presumably via its aberrant repressive activities. Recently, HDAC inhibitors (HDACis) have been shown to be a class of promising anti-cancer agents, exhibiting a range of observed cellular effects, including growth arrest, differentiation and apoptosis in a variety of cancers in clinical trials. Similarly, overexpression of HDAC1–3 and 6 has also been observed in prostate, gastric, breast and cervical cancer (129).

1.7.2.4 Histone methylation and senescence

Certain types of cells exhibit senescent arrest that is accompanied by senescence-associated heterochromatic focis (SAHFs), a new type of facultative heterochromatin (130). Such drastic chromatin rearrangement can also be observed during some types of cellular differentiation, another state of stable cell cycle arrest (Francastel et al, 2000). Very little is known about the effector mechanism of cellular senescence, but the global chromatin reorganisation may not simply be a senescence marker, but rather play a key role in the senescence mechanism. In fact, there is a strong correlation between SAHF formation and the irreversibility of the senescence phenotype (131), (130), (132).

The kinetics of the accumulation of SAHF-positive cells after triggering senescence by ras is well correlated with that of other indicators of senescence, such as SA-b-gal activity, p16 induction, Rb hypo-phosphorylation and cell cycle arrest; and SAHFs and DNA synthesis are mutually exclusive events (130). Senescence-associated heterochromatic focis are enriched for markers of heterochromatin, such as heterochromatin protein 1 (HP1) and Lys9 tri-methyl (K9me3) of histone H3 (which confers a docking site to HP1), and exclude euchromatic markers, such as histone H3 K9 acetyl and K4me3 (130). Interestingly, SAHF formation is largely dependent on the p16/Rb pathway in ras-induced senescence, although the impact of p53 on SAHF is marginal (130). The experiments revealed that high-mobility group A (HMGA) proteins are senescence-associated chromatin binding proteins and that HMGA proteins are essential structural components of SAHFs. Furthermore, HMGA-dependent SAHF formation contributes to the stable senescence arrest (130), (132).

1.7.2.5 Histone variants

In higher organisms each histone subtype, with the possible exception of histone H4, is represented by a family of genes encoding multiple non-allelic primary-sequence variants. The presence of replacement variants that, unlike most other histones, are expressed throughout the cell cycle and serve as a source of chromatin components needed during repair or recombination of DNA or to replace histones lost through turnover in quiescent cells. Because different histone variants can contribute to a distinct or unique nucleosomal architecture, this heterogeneity can be exploited to regulate a wide range of nuclear functions, and evidence is accumulating that histone variants do indeed have distinct functions (133).

CHAPTER 2. OBJECTIVES AND RATIONALE

The molecular pathogenesis of HCC largely remains unsolved. Genetic mutations are apparently limited to a few genes such as *TP53* and *CTNNB1* occurring in distinct subsets of HCC. In contrast, expression changes such as induced expression of telomerase reverse transcriptase (*TERT*) and epigenetic silencing of *CDKN2A* gene, affecting >80% and >50% of HCCs respectively, are quite common (134). Inactivation of *TP53* and CDKN2A and reactivation of *TERT* provide strong evidence for the bypass of cellular senescence as a key event involved in HCC (52). Adult hepatocytes, like other somatic cells, are programmed for senescence, a mechanism that blocks excessive cell proliferation by a telomere-dependent mechanism. Telomere-independent forms, such as oncogene-induced and DNA damageinduced senescence are also observed, both in normal and cancer cells. p16INK4a- and p21Cip1-dependent pathways leading to retinoblastoma protein (pRb) activation and permanent G1 arrest are involved as mediators in the senescence arrest (135). Cellular senescence appears to play a major role in liver diseases. Chronic liver diseases are associated with progressive telomere shortening leading to the cellular senescence that is observed frequently in cirrhosis, but also in some HCCs (136). But, there was no experimental evidence for spontaneous reprogramming of replicative senescence in immortalized cancer cells. Using hepatocellular carcinoma (HCC)-derived Huh7 cells as a model system, our group have shown that cancer cells with replicative immortality are able to spontaneously generate progeny with replicative senescence (61). To investigate the mechanism of spontaneous senescence in HCC-derived cells, we performed whole genome expression microarray analysis in immortal, senescent committed and pre-senescence stage clones. We tested our significant gene set on previously published senescence models. We obtained differentially expressed gene sets and biological pathways that can play a major role in reprogramming-senescence and immortality.

Experimental animal models also provide strong evidence for a critical role of cellular senescence in HCC (59). However, the role of cellular senescence and immortality in human HCC remains elusive. We integrated immortal and senescence-programmed Huh7 data and malignant and non-malignant human liver tissue data to define a senescence and immortality gene network (SIGN) to predict and classify the progressive steps of human hepatocellular carcinogenesis and molecular subtypes of HCC.

The Rb pathway is among the pathways most frequently disrupted in HCC (137). The Rb-E2F pathway links growth-regulatory pathways to a transcription program involved in DNA synthesis, cell-cycle progression, cell division, apoptosis, DNA repair, differentiation

and senescence (138). We performed unsupervised hierarchical cluster analysis of E2F/DP family genes using our immortal and senescence-programmed Huh7 microarray data. We studied expression profiles of E2F/DP family members in immortal and senescence-arrested HCC cells. Our results prompted us to further investigate DP-2 gene and protein in HCC.

Classical genetics alone is not able to explain all the changes of a tumor cell. It is apparent that cancer is also a disease that is driven by 'epigenetic changes' — patterns of altered gene expression that are mediated by mechanisms that do not affect the primary DNA sequence. These epigenetic alterations occur within a larger context of extensive alterations to chromatin in neoplastic cells in comparison with the normal cells from which they are derived. These involve both losses and gains of DNA methylation as well as altered patterns of histone modifications (139). Recent studies indicate that epigenetic alterations might initiate the expansion of pre-malignant cells during the early stages of tumorigenesis. During the earliest steps of development of principal tumour types, a subset of these pre-malignant cells undergo genetic alterations that allow them to mediate tumour progression and growth. The early epigenetic changes that occur in these cells
might determine the subsequent genetic changes and thereby foster progression of these clones. In the search of most significantly changing gene sets between senescence and immortal clones of Huh7, we identified that chromatin binding proteins, especially chromatin modifying enzymes are changing between these groups. We grouped the significant chromatin modifying enzymes with unsupervised hierarchial cluster analysis. We hypothesized that spontaneous induction of senescence could be an epigenetic re-programming event. We decided to investigate the expression levels of histone methyltransferases and demethylases, and examine the levels of histone residue modifications in immortal, pre-senescent and senescence programmed clones. We also hypothesized that the abberantly regulated histone residues in senescence and immortal clones may also regulated in cirrhosis and HCC. Therefore, we decided to screen normal, cirrhotic and tumor liver samples for spesific histone residues.

CHAPTER 3. MATERIALS AND METHODS

3.1 MATERIALS

3.1.1 Reagents

The general laboratory chemicals were supplied from Sigma Chemical Co. (St.Louis, USA), Merck (Darmstadt, Germany), Stratagene (Heidelberg, Germany) and AppliChem (Darmstadt, Germany). Ethanol was from Delta Kim Sanayi ve Ticaret A.S (Turkey). TGF-beta and lithium chloride was supplied from (R&D Systems, Minneapolis, USA). Mayer's heamatoxylene was supplied from Sigma (Missouri, USA).

3.1.2 Nucleic acids and Proteins

DNA molecular weight standard and ultrapure deoxyribonucleotides were purchased from MBI Fermentas GmbH (Germany). Protein size markers were from MBI Fermentas GmbH (Germany) and Euromedex (Soufferweyelsheim, France).

3.1.3 Oligonucleotides

The oligonucleotides used in polymerase chain reactions were synthesized and supplied from Iontek Inc. (Istanbul, Turkey) and Eurofins MWG (Ebersberg, Germany).

3.1.4 Enzymes

Taq DNA polymerases (EP0405) and SYBR Green Supermix (K0231, F-400, 600825) were supplied from MBI Fermentas, Finzymes (Finland) and Stratagene (La Jolla, USA). Reverse Transcriptase was supplied from MBI Fermentas (K1621) (Ontario, Canada).

3.1.5 Electrophoresis

Electrophoresis grade agarose was obtained from Sigma Biosciences Chemical Company Ltd. (St. Louis, MO, USA). Horizontal electrophoresis apparatuses were from Stratagene (Heidelberg, Germany) and E-C Apparatus Corporation (Florida, USA). Vertical electrophoresis apparatuses were from Invitrogen (California, USA) or BioRad (Hercules, USA). The power supply Power-PAC300 and Power-PAC200 was from Bio Rad Laboratories (CA, USA). The Molecular Analyst software used in agarose gel profile visualizing was from BioRad Laboratories (Hercules, CA, USA).

3.1.6 Protein transfer materials

Immobilen P transfer (PVDF) membrane was from Roche (Germany) and nitrocellose membrane was supplied from Amersham& GE Healthcare (Buckinghamshire, UK). 3MM filter paper was from Whatman International Ltd. (Madison, USA).

3.1.7 Tissue culture reagents and cell lines

Dulbecco's modified Eagle's medium (DMEM), fetal calf serum and magnesium-free phosphate buffered saline (PBS) was obtained from GIBCO (BRL Company; Grand Island, USA) and Biochrom (Berlin, Germany). L-glutamine, calcium, and Penicillin/Streptomycin mixture was from Biochrom (Berlin, Germany). Tissue culture flasks, petri dishes, 15 ml polycarbonate centrifuge tubes with lids and cryotubes were purchased from Costar Corp. (Cambridge, England). Geneticin-G418 sulfate was purchased from GibcoBRL, Life tech. (USA), Puromycin was purchased from Sigma (St. Louis, MO, USA).

3.1.8 Antibodies and chemiluminescence

The antibodies used in immunoblotting (western blotting) and immunostaining were obtained from different sources, and their working dilutions are given in Table 3.1. Anti-mouse (A-4789) and anti-rabbit HRP (P0399) conjugated secondary antibodies were obtained from Sigma (Missouri, USA) and Dako (Glostrup, Denmark). Green fluoroscent secondary antibodies (A10680) (44-1100A1) (Alexa Flour 488) against mouse or rabbit were obtained from Invitrogen (California, USA). ECL Western Blotting detection kit (RPN2132) was purchased from Amersham Pharmacia Biotech Ltd. (Buckinghamshire, UK).

Table 3.1 Antibodies

Company	Antibody	Cat No	Dilution for Western 1 in Xul	Dilution for Immunperoxidase 1 in Xul
Abcam	H3 K4 Me3 - Rabbit- Pol	**ab8580**	5000	1200
Abcam	H3 K9 Me1 - Rabbit - Pol	**ab9045**	2000	600
Upstate	H3 K9 Me3 - Rabbit Antiserum	**Ups 07-523**	5000	1200
Upstate	H3 K27 Me1 - Rabbit -Pol -IgG	**Ups 07-448**	5000	1200
Upstate	H3 K27 Me3 - Rabbit - Pol- IgG	**Ups 07-449**	5000	1200
Abcam	H3 K36 Me1 - Rabbit- Pol	**ab 9048**	2000	600
Abcam	H3 K36 Me3	**ab 9050**	2000	1200
Abcam	H3 K79 Me3 - Rabbit- Pol	**ab2621**	2000	300
Upstate	H4 K20 Me3	**Ups 07-463**	2000	600
Upstate	H3 Pab - Rabbit - Pol IgG	**Ups 06-755**	500	500
Upstate	H4 Pab - Rabbit - Pol IgG	**Ups 07-108**	1000	500

Abcam	H3 Monoclonal - Mouse	**ab 31827**	2000	500
Abcam	H4 Monoclonal - Mouse	**ab 24834**	2000	500
Abcam	5-Methyl Cytidine - Mouse	**ab 10805**	2000	-
Upstate	H3 R2 Me2 - Rabbit Antiserum	**Ups 07-585**	2000	600
Abcam	H3 R17 Me2 - Rabbit -Pol	**Ab8284**	5000	900
Upstate	H4 R3 Me2 - Rabbit IgG Purif.	**Ups 07-213**	2000	600
Upstate **Abcam**	H4 K Ac Pab TFDP2	**Ups 06-598** **Ab26260**	1000 1000	250 250

3.1.9 Kits

Trireagent was from AppliChem (Darmstadt, Germany) and the RNA isolation kit was from Macharel Nagel, (Duren, Germany). RevertAid first strand cDNA synthesis kit was from MBI Fermentas. DAB+ substrate kit was supplied from Dako (Glostrup, Denmark). One cycle cDNA synthesis kit for affymetrix experiments were supplied from Affymetrix (U.S.A).

3.2 SOLUTIONS AND MEDIA

3.2.1 General Solutions

50X Tris-acetic acid-EDTA (TAE):	2 M Tris-acetate, 50 mM EDTA pH 8.5 Diluted to 1X for working solution.
Ethidium bromide:	10 mg/ml in water (stock solution), 30 ng/ml (working solution)
1X Gel loading buffer:	0.25% bromophenol blue, 0.25% xylene cyanol**,** 50% glycerol, 1mM EDTA

3.2.2 Tissue culture solutions

DMEM/RPMI working medium	10% FBS, 1% penicillin/streptomycin, 1% Non-Essential Amino Acid were added and stored at 4^{o}C.
10X Phosphate-buffered saline (PBS)	*Per liter:* 80 g NaCl, 2 g KCl, 14.4 g Na2HPO4, 2.4 g KH2PO4, pH 7.4 or 1XPBS was obtained commercially from GIBCO
Freezing solution	10% DMSO and 90% FCS were mixed freshly.

Antibiotics

Geneticin (G418 Sulfate)	500 mg/ml solution in double-distilled water. Sterilized by filtration and stored at

	-20°C (stock solution). 500 µg/ml (working solution for stable cell line selection), and 250 µg/ml(working solution for maintenance of stable cell lines).
Puromycin	2 mg/ml solution in double-distilled water, sterilized by filtration (0.2 um pores) and stored at -20°C (stock solution). 2 µg/ml (working solution for stable cell line selection), and 1 µg/ml (working solution for maintenance of stable cell lines). 20°C (stock solution). 2 µg/ml (working solution).

3.2.3 RNA solutions

DEPC-Treated Water	1ml DEPC was added to 1lt ddH2O and stirred under hood overnight. DEPC was inactivated by autoclaving.
FA Gel Buffer	Stock solution (10XFA Gel Buffer) was prepared by dissolving 20.927g MOPS, 3.40g NaAc and 1.86g EDTA in 500ml ddH2O. pH of the stock solution was adjusted to 7.0. Working solution was prepared by diluting the stock solution to 1X with ddH2O.
5x RNA Loading Buffer	Bromophenol blue solution 16 µl, 500 mM EDTA, pH 8.0. 80 µl, 37% formaldehyde 720 µl, 100% glcerol 2 ml, Formamide 3084 µl, 10x FA gel buffer 4 ml, RNase free (DEP-C treated) water to 10 ml.

3.2.4 Protein extraction and western blotting solutions

RIPA Buffer	50 mM Tris pH: 8.0, 150 mM NaCl, 1% NP-40, 1% NP-40, 0.5% SodiumDeoxycalate, 0.1% SDS and 1X protease inhibitor mix were mixed in ddH2O.
Bradford Stock Solution	17.5 mg Coomassie brilliant blue was dissolved in 4.75 ml ethanol and 10 ml phosphoric acid and completed to 25 ml final volume with ddH2O.
Bradford Working Solution	1.5 ml Bradford stock solution was mixed with 0.75 ml 95% Ethanol and 1.5 ml phosphoric acid and completed to final volume up to 25 ml with ddH2O.

Or commercial Bradford Solution was obtained from Sigma.

30% Acrylamide mix (1:29)	*Per 100 ml*: 29 g acrylamide, 1 g bisacrylamide in double-distilled water, filtered, degassed, and stored at 4°C (stock solution).
5X SDS gel-loading buffer	3.8 ml double-distilled water, 1 ml of 0.5 M Tris-HCl, 0.8 ml glycerol, 1.6 ml of 10% SDS, o.4 ml of 0.05% bromophenol-blue. Before use, β-mercaptoethanol was added to 5% to reach 1% when mixed with samples.
5X SDS-electrophoresis buffer	*Per liter:* 15.1 g Tris base, 95 g Glycine, 5 g SDS. Diluted to 1 X for working solution. Stored up to 1 month at 4°C.
10% Ammonium persulfate (APS)	0.1 g/ml solution in double distilled water (Prepared freshly).

1.5 M Tris-HCl, pH 8.8	54.45 g Tris base (18.15 g/100 ml) ~150 ml distilled water Adjust to pH 8.8 with 1 N HCl. Completed to 300 ml with distilled water and stored at 4° C. 1 M Tris-HCl, pH 6.8 12.14 g Tris base ~ 60 ml distilled water, adjust to pH 6.8 with 1 N HCl. Completed to 100 ml with distilled water and store at 4° C.
Wet Transfer Buffer	6 g tris and 28.8g glycine was mixed with 1ml 10% SDS and 20% methanol and completed to final volume of 1 liter.
10XTBS	*Per liter:* 100 mM Tris-base, 1.5 M NaCl, pH 7.6 in double distilled water.
TBS-T	0.3% Tween 20 was added into 1X TBS solution.
Blocking Solution	3% milk powder in 0.3% TBS-Tween 20 solution

3.2.5 Immunofluorescence and immuoperoxidase solutions

DAPI (4', 6-diamidino-2-phenylindole)	0.1-1 µg/ml (working solution in PBS).
4% paraformaldehyde	4 g paraformaldehyde in 100 ml. PBS, pH 7.4. Stable at 4°C for a week.
PBS-TritonX-100 (PBS-T)	0.1 TritonX-100 in PBS
DAB + substrate	1 drop solution A in 1 ml solution B.
Blocking Solution	10%FBS, 0.3% Triton-X in 1xPBS
Dilution Solution	2%FBS, 0.3% Triton-X in 1xPBS.

3.2.6 SABG solutions

SABG solution pH 6.0	200 µl 200nM citric acid, 50 µl 100mM potasium ferrocyanide, 50 µl 100mM potasium ferricyanide, 75 µl 2 M NaCl, 20 µl 100 mM$MgCl_2$, 200 µl sodium buffer, 380 µl distilled H_2O for 1ml SABG solution.

Na buffer pH 6.0	420 µl 1M Na_2HPO_4, 180 µl NaH_2PO_4

3.2.7 Immunohistochemistry solutions

Citrate buffer 10 mM pH 6	Citric acid solution 0.1 M (anhydrous) (solution A), Sodium Citrate solution 0.1 M (solution B), 9 ml solution A+41 ml solution B+450 ml H2O (adjust pH with NaOH)
Blocking Solution	5% milk in 1XPBS
Dilution Solution	1% BSA 1xPBS
Washing Solution	0.5% milk in 1xPBS

3.3 METHODS

3.3.1 Tissue culture techniques

3.3.1.1 Cell Lines

14 HCC derived cell lines (Huh7, FOCUS, Mahlavu, Hep40, Hep3B, HepG2, PLC/PRF/5, SK-Hep1, Snu182, Snu387, Snu398, Snu423, Snu449 and Snu475) used in this study were cultured as described in previously (38). Briefly, cell lines were maintained in Dulbecco's Modified Eagle's Medium (DMEM, Biochrom, UK) supplemented with 10% fetal calf serum, 50 mg/ml penicillin/streptomycin, and 1% non-essential aminoacid.

Huh7- derived isogenic clones were obtained by either G-418 (200 µg/ml) selection after transfection with neomycin- resistance pcDNA3.1 (Invitrogen) or pEGFP-N2 (Clontech) plasmids, or by low-density cloning. Huh7-derived isogenic clones C1 and C3 were obtained with pCDNA3.1 and G11 and G12 with pEGFP-N2 (61). For low-density cloning, cells were plated at 30 cells per cm^2 and single-cell derived colonies were expanded in 24-well plates. Culture medium was refreshed in every three days. The cells were incubated at a 37^oC incubator with an atmosphere of 5% CO2 in air. The cells were passaged before reaching confluence. The growth medium was aspirated and the cells were washed with 1X PBS. Trypsin solution (Biochrom, UK) was added to the flasks to detach the monolayer cells from the surface. Cells were dispersed by pipetting the cells with fresh medium. The cells were transferred to new flasks using different dilutions depending on requirements.

Primary human liver cells (NHEP) were supplied from Lonza (Basel, Switzerland) as a cryopreserved vial (CC-2591), with its special medium HCM (hepatocyte culture medium, phenol red free) (CC-3198). Before culturing supplement kit (CC-4192) obtained from Lonza was added into medium. Instructions for culturing the NHEP were sitrictly followed that were obtained from manufacturer. While thawing cells, the tube containing the cell suspension was centrifuged at 50 x g in a refrigerated centrifuge (2-8ºC) for three minutes. The recommended seeding density for attachment is approximately 150,000 cells/cm^2. on plates or flasks coated with 60 µg/cm^2 Type 1 Collagen.

DMEM and PBS were kept at 4^{o}C, trypsin was kept at -20^{o}C. All the solutions were warmed to 37^{o}C before use.

3.3.1.2 Cell lines for microarray study

In vitro microarray experiments were performed with senescenceprogrammed (C3, G12), and immortal (C1I, G11I) clones. Senescence-programmed clones were tested at proliferating presenescent (C3P, G12P) and senescent (C3S, G12S) states. Immortal clones were tested after PD 150. Proliferating pre-senescent cells were tested at PD 20-30 before senescence-arrest. Presenescent cels were >85% BrdU-positive upon labeling for 24h. Senescent cells were <5% BrdU-positive and displayed >50% senescence-associated β-galactosidase (SABG) activity.

3.3.1.3 Thawing cell lines

One vial of the frozen cell line from the liquid nitrogen tank was taken and immediately put into ice. The vial was then placed into 37oC water bath until the external part of the cell solution was thawed (takes approximately 1-2 minutes). The cells were resuspended gently using a pipette and transferred immediately into a 15 ml. sterile tube containing 10 ml cold fresh medium. The cells were centrifuged at 1500 rpm at 4oC for 5 minutes. Supernatant was discarded and the pellet was resuspended in 10 ml 37oC culture medium to be plated into 100 mm dish. After overnight incubation in a humidified incubator at 37°C supplied with 5% CO2, culture mediums were replenished.

3.3.1.4 Cryopreservation of cell lines

Exponentially growing cells were harvested by trypsinization and neutralized with growth medium. The cells were counted and precipitated at 1500 rpm for 5 min. The pellet was

suspended in a freezing solution (10% DMSO, 90% FCS) at a concentration of 4x106cells/ml. 1 ml of this solution was placed into 1 ml screw capped-cryotubes. The tubes were left at -70°C overnight. The next day, the tubes were transferred into the liquid nitrogen storage tank.

3.3.1.5 TGF-β and LiCl treatment

Cells were seeded into 6 cm plates 24 before the treatment. At the time of treatment cells were at 30% confluency. 5 μg TGF-β was added into fresh medium which was then applied onto plates. DMEM without TGF-β was added to some other plates that will be used as negative control. After four days of treatment cells were washed with 1xPBS and pelletted. Fresh medium containing 20 nM LiCl was used for LiCl treatment. As the negative control of LiCl, 20 nM NaCl containing medium was used. After three days, NaCl treated and one LiCl treated plate was washed and pelletted to be used as time zero. Other plates were cultured with fresh DMEM, and stopped and pelletted at hours of 6, 12, 24, 30, 36 and 48.

3.3.2 RNA extraction

3.3.2.1 Extraction of total RNA from tissue culture cells

Exponentially growing monolayer cultures were washed twice with ice-cold PBS, tyripsinized, pelleted and snap frozen in liquid nitrogen and stored at -70^{o}C until needed for RNA preparation. The total RNA isolation from cell line pellets was performed directly by use of NucleoSpin RNA II kit (740955) (MN Macherey-Nagel, Duren, Germany) according to the manufacturer's instructions. The RNAs were eluted in a total volume of 30-50 μl. DNAse digestion was performed according to the kit protocol.The concentration of the isolated RNA and the ratio of absorbance at 260 nm to 280 nm were measured with the NanoDrop ND-1000 spectrophotometer (NanoDrop Technologies, Montchanin, DE, USA) in triplicate. Isolated RNAs were stored at -80^{o}C.

For *in-vitro* microarray study, immortal, presenescent and senescent cells (described above) were plated in triplicate and subjected to RNA extraction. RNA quality was evaluated by the ratio of 18S to 28S RNAs by Agilent 2100 Bioanalyzer (Agilent Technologies, USA); all samples passed this quality control test.

3.3.2.2 Extraction of total RNA from tissue samples

The isolation of RNA requires pure reagents and care in preparation due to the sensitivity of RNA to chemical breakdown and cleavage by nucleases. Therefore all the solutions and

materials were treated with DEPC (AppliChem, Darmstadt, Germany) in order to avoid RNase contamination and hence degradation of RNA.

Total RNA of tumor tissues was isolated with TRI reagent (AppliChem, Darmstadt, Germany). The frozen tumor and cirrhosis tissue samples were cut into 5-µm-thick sections and used for RNA isolation (4-5 slices for each sample). Tissue samples were lysed in 1ml TRI reagent with a homogenizer and passed through a 21-gauge needle several times. After 5 min incubation at room temperature, 0.2 ml chloroform was added per ml of TRI reagent. Tubes were shaken vigorously by hand for 15 seconds and incubated at room temperature for 2-3 min. After incubation the mixture was centrifuged at 12000xg for 15 min at 4^{o}C and then aqueous phase was collected into a new tube. 0.5 ml isopropanol was added onto aqueous phase per 1ml of TRI reagent used. The mixture was incubated at room temperature for 10 min and then centrifuged at 12000xg for 15 min at 4^{o}C to recover RNA. The supernatant was removed and the pellet was washed with 75% ethanol twice, centrifuged at 7500xg for 5 min at 4^{o}C. The pellet was air-dried and dissolved in ddH2O. The isolated RNA solution was subjected to a second round of isolation by using NucleoSpin RNA II kit (Macharel Nagel, Duren, Germany) to remove any remaining contaminants of DNA.

3.3.3 Expression Microarray Analysis

3.3.3.1 Microarray experiments

In-vitro microarray experiments were performed at Ankara University Biothecnology Institute by Dr. Hilal Ozdağ. GeneChip Human Genome U133 Plus 2 arrays were used on Affymetrix platform. Protocols supplied by the manufacturer were strictly followed (One-Cycle cDNA Synthesis Kit, Affymetrix). Briefly, 2 µg of RNA from cell line samples was converted to double-stranded cDNA (One-Cycle cDNA Synthesis Kit, Affymetrix). The cDNA samples then served as a template in an invitro transcription (IVT) reaction to obtain biotinylated and amplified cRNA (GeneChip IVT Labeling Kit, Affymetrix). 20 µg of labeled cRNA was fragmented, and 15 µg of fragmented RNA was hybridized to GeneChips for 16 hours. Immediately following hybridization, the GeneChip arrays were washed and stained with streptavidin phycoerythrin conjugate using an automated protocol on a GeneChip Fluidics Station 450, followed by scanning on a GeneArray Scanner.

3.3.3.2 Data processing and quality control

GeneChip Operating Software (GCOS, Affymetrix) was used to collect and store the data. CEL files were uploaded to RMAExpress program to assess the quality of the arrays at the image level (2009, http://rmaexpress.bmbolstad.com/). Quality assessment of the Affymetrix datasets was performed using affyPLM (affyPLM; http://www.bioconductor.org/packages/2.4/bioc/html/affyPLM.html) on R suite of programme (R 2.4.0 or later). AffyPLM was used to detect artifacts on arrays that could pose potential quality problems and also for assessment of homogeneity of expression signal across arrays (Appendix A).

3.3.3.3 Determination of differentially expressed gene sets

The raw Affymetrix intensity measurements of all probe sets were background corrected, normalized and summarized into gene expression level measurements by applying the RMA (Robust Multichip Average) algorithm of the 'affy' package and log transformed (log 2 base) in Bioconductor suite of array analysis tools running in R version 2.4.0 (140). Please see required R packages for this analysis in Table 3.2.

Table 3.2 Required R packages

Package	URL
affy	http://www.bioconductor.org/repository/release1.4/package/html/affy.html
Biobase	http://www.bioconductor.org/repository/release1.4/package/html/Biobase.html
hgu95av2cdf	http://www.bioconductor.org/data/metaData.html
affyPLM	http://www.bioconductor.org/repository/release1.4/package/html/affyPLM.html
affydata	http://www.bioconductor.org/repository/release1.4/package/html/affydata.html
gcrma	http://www.bioconductor.org/repository/release1.4/package/html/gcrma.html
matchprobes	http://www.bioconductor.org/repository/release1.4/package/html/matchprobes.html
hgu95av2probes	http://www.bioconductor.org/data/metaData.html
siggenes	http://www.bioconductor.org/packages/2.3/bioc/html/siggenes.html
multtest	http://www.bioconductor.org/packages/2.3/bioc/html/multtest.html
genefilter	http://www.bioconductor.org/packages/2.5/bioc/html/genefilter.html

The code used for loading the affy package, reading the targets file and the CEL files into R and image plots is given in Appendix B1.

Differentially expressed probesets in the in vitro dataset derived from immortal, presenescent, and senescent Huh7 clones were identified between any two classes (i.e., immortal vs. senescent, immortal vs. presenescent, and presenescent vs. senescent) using a two-tailed, unpaired, unequal variance Welch's t-test using R statistical package (www.bioconductor.com). The significance test code is given in Appendix B2.

Probesets were considered significantly differentially expressed if the raw p value was less than 0.05 for a given probeset in both sets of clones (e.g., for determining probesets modulated between immortality and senescence conditions, C11I versus C3S clones, as well as G11I versus G12S clones were compared). Moreover, only those probesets showing expression modulation in the same direction in both the C and G clones were used for future analysis. The resulting probeset list containing differentially altered genes as described above was further filtered by discarding probesets with annotations stated as unknown or those with ambiguous annotations based on HGU133 plus2 version release 21, November 2006.

Confirmatory and further analyses with in vitro dataset were performed using BRB-ArrayTools developed by Dr. Richard Simon and BRB-ArrayTools Development Team (2009, BRB Array Tools; http://linus.nci.nih.gov/BRB-ArrayTools.html). Annotations for the differentially expressed probesets were done using release 28, version 2.2.5, also. Experiment set used is in Table 3.3.

Table 3.3 Experiment file of *in-vitro* data

EXP	Patient Id	Group
05-09-2006_g12_X3-1.CEL	G12P	P
29-08-2006_g12_X3-2.CEL	G12P	P
29-08-2006_g12_X3-3.CEL	G12P	P
g11_X6-1_07-12-2005.CEL	G11	I
g11_X6-2_07-12-2005.CEL	G11	I
g11_X6-3_07-12-2005.CEL	G11	I
g12-L1_16-12-2005.CEL	G12L	S
g12-L2_16-12-2005.CEL	G12L	S
g12-L3_16-12-2005.CEL	G12L	S
L1_ 15-12-2005.CEL	C3L	S

L2_ 15-12-2005.CEL	C3L	S
L3_ 15-12-2005.CEL	C3L	S
pC1_X29-2_06-01-2006.CEL	C1	I
pC1-X29-1_21-12-2005.CEL	C1	I
pC1-X29-3_21-12-2005.CEL	C1	I
X4-1_14-12-2005.CEL	C3P	P
X4-2_14-12-2005.CEL	C3P	P
X4-3_14-12-2005.CEL	C3P	P

3.3.3.4 Visualization of datasets

For all cluster analyses, Cluster 3.0 program (http://bonsai.ims.utokyo.ac.jp/~mdehoon/software/cluster/) was used to perform hierarchical clustering (141), (142). First data was adjusted by centering genes and arrays separately based on mean values, then average linkage was applied to genes and arrays using correlation (uncentered) similarity metric. Cluster files were visualized by Java Treeview (143) (http://jtreeview.sourceforge.net/).

3.3.3.5 Data integration

Common probesets between the any two gene lists obtained from in vitro and in vivo datasets, CROPPER (http://katiska.uku.fi/jmpaanan/cgi-bin/cropper/multi.pl) and custom perl-codes (CIF, by Ahmet Rasit Ozturk) developed in Bilkent University were used.

3.3.3.6 Functional gene annotation cluster analysis

DAVID (144), GSEA (Gene Set Enrichment Analysis, (145), OntoTools (http://vortex.cs.wayne.edu/projects.htm, (146) and Ingenuity pathway analysis (Ingenuity® Systems, www.ingenuity.com) were used to annotate the functions of gene lists.

3.3.3.6.1 DAVID

DAVID was used from the link: http://david.abcc.ncifcrf.gov/tools.jsp. Probe set lists were downloaded to Functional Annotation tool of DAVID. As the cutoff for significance; we selected biological groups with >1.3 enrichment score, <0.001 p-value, and <5% FDR multiple test corrected values.

3.3.3.6.2 GSEA (Gene Set Enrichment Analysis)

Version 2 of GSEA was downloaded from http://www.broad.mit.edu/gsea/. Gene sets were downloaded from MsigDB database. The file extentions used in the analysis were *.gct for expression data, *.cls for phenotype file, *.gmt for gene sets, and *.chip for chip annotations. Phenotypes were permutted 1000 times. Gene sets which had <20% FDR were selected for evaluation. Data was collapsed with the collapse parametre of the software. “Weighted” was used as enrichment statistic. Signal2noise was selected for metric for ranking genes. Gene sets which were >500 and <15 genes were excluded from the analysis. “Meandiv” was used as normalization mode. “149” option was selected as seed for permutation.

3.3.3.6.3 Onto Express

A data set containing gene identifiers and corresponding expression values was uploaded into in the application. Binomial distribution was used as the statistic method in onto-express analysis. <0.05 was used as the cut-off value.

3.3.3.6.4 Ingenuity Pathway Analysis

The trial version of ingenuity pathway analysis software was used. A data set containing gene identifiers and corresponding expression values was uploaded into in the application. Each gene identifier was mapped to its corresponding gene object in the Ingenuity Pathways Knowledge Base. Fischer’s exact test ($p<0.05$) was used to calculate a p-value determining the probability that each biological function and/or disease assigned to that data set.

3.3.3.7 Meta data

3.3.3.7.1 HPEC replicative senescence data

Gene expression dataset (two –channel array) reported by Schwarze et al (147) from proliferating (HPEC-P), replicative early senescent (growth arrest, but SABG-negative; HPEC-ES), replicative senescent (SABGpositive; HPEC-S), and human papillomavirus E7 oncogene-immortalized (HPEC-I) HPEC was downloaded from SMD (release 1.11, 2006, July), Stranford Microarray Database (http://smd.stanford.edu). Log(2) base of R/G normalized median ratio, with >0.6 regression correlation, was retrieved. More than 50% good data according to SMD criteria was filtered and quantile normalized in R (9597 probe sets (6927 genes) and 9 samples). SMD uses the external sources of biological annotation:NCBI, SwissProt, dbEST, Locuslink, RHdb, Unigene, GeneCards, Genemap99. The merge of HPEC data and our data was made using gene symbols by CIF. CIF took the

mean value for redundant gene symbols. Resulting data was "median center"-normalized and subjected to cluster analysis, as described previously.

3.3.3.7.2 IMR90 Oncogene-induced senescence data

.CEL files of 10 affy chips (Affymetrix HGU-133A; 22283 probes) generated by Collado *et. al.* (148) was downloaded from GEO (Gene Expression Omnibus, http://www.ncbi.nlm.nih.gov/geo/) with the GEO accession number of GSE2487. Data was normalized using RMA method and then median centered, as described previously. Merge of IMR90 data and our data was made using gene symbols by CIF. CIF took the mean value for redundant gene symbols. Resulting data was "quantile" and "median center"-normalized and subjected to cluster analysis, as described previously.

3.3.3.7.3 HCC molecular classification data

HCC molecular classification dataset reported by Boyault et al (57 HCC, three hepatocellular adenoma, five non-tumor liver pool), obtained through special permission (149), was using BRB-ArrayTools.

3.3.3.8 BRB array tools

Further analyses with combined in vitro dataset were performed using BRB-ArrayTools developed by Dr. Richard Simon and BRB-ArrayTools Development Team (2009, BRB Array Tools; http://linus.nci.nih.gov/BRB-ArrayTools.html). We performed binary tree classification to predict the class of samples provided by the Boyault datasets using BRB array tools. The individual binary classifiers were based on the "Compound Covariate Predictor" incorporating genes that were differentially expressed among genes at the 0.001 significance level as assessed by the random variance t-test.

3.3.4 Quantification of nucleic acids

3.3.4.1 Horizontal agarose gels of DNA samples

DNA fragments were fractionated by horizontal electrophoresis by using standard buffers and solutions. DNA fragments less than 1 kb were generally separated on 1.0% or 2.0 % agarose gel, those greater than 1 kb (up to 11 kb) were separated on 0.8 % agarose gels. Agarose gels were completely dissolved in 1x TAE electrophoresis buffer to required percentage in microwave and ethidium bromide was added to final concentration of 30 µg/ml. The DNA

samples were mixed with one volume loading buffer and loaded onto gels. The gel was run in 1x TAE at different voltage and time depending on the size of the fragments at room temperature.

3.3.4.2 Gel electrophoresis of total RNA

RNA was fractionated through 1% (w/v) agarose gels containing formaldehyde which disrupts hydrogen bonds. 0.5 g agarose was melted in 1X formaldehyde gel running buffer, allowed to cool, and 10 ml of 37% formaldehyde was added. The gel was immediately poured in a laminar hood. 5µl of RNA sample was mixed with 15 µl of RNA loading buffer and heated at 70 °C for 5 minutes. Samples were quenched on ice and loaded onto gel. Electrophoresis was performed at a constant voltage (85 V) for 4 hr at 4 °C in 1X formaldehyde gel running buffer. Following electrophoresis, gel was soaked for 5 min in 5 volumes water to remove formaldehyde. This step was repeated for 3 times. The gel was stained in 30ug/ml ethidium bromide solution for 5 min, and destained overnight in double-distilled water.

Nucleic acids were visualized under ultraviolet light (long wave, 340 nm) and GeneRuler (MBI Fermentas) DNA size markers was used to estimate the fragment sizes.1 kb DNA ladder for horizontal agarose gels and 100 bp ladder for vertical agarose gels.

3.3.5 First strand cDNA synthesis

First strand cDNA synthesis from total RNA was performed using RevertAid First Strand cDNA synthesis kit (MBI Fermantas, Germany). The RevertAid kit relies on genetically engineered version of Moloney Murine Leukemia Virus reverse transcriptase (RevertAid M-MuLV RT) with low RNase H activity. This allows the synthesis of full length cDNA from long templates. The first strand reactions were primed with oligo(dT)18 primer to specifically amplified mRNA population with 3'-poly(A) tails. As the reaction conditions and components of this kit and those of conventional PCR are compatible, first strand synthesized with this system can be used as a template for PCR.

1 to 5 µg total RNA was used to synthesize the first stand cDNA following the manufacturer's instruction. After 1:1 dilution of total reaction products in DEPC-treated water, 2 µl of diluted first strand cDNA was used for PCR. The rest is stored in -20 °C.

3.3.6 Polymerase chain reaction (PCR)

3.3.6.1 Primer design for expression analysis by semi-quantitative and quantitative PCR

The primer pairs that have been used in expression profile analyses were designed carefully using "Primer exe" or "Primer 3.0" (http://frodo.wi.mit.edu/cgibin/primer3/primer3_www.cgi) programmes. Forward and reverse primer were positioned on different exons of the gene of interest, so that the primer pair was either be able to produce a longer amplicon from genomic DNA or not be able to amplify from the covered genomic DNA region in a given PCR condition (critical parameter was extension time). Therefore the amplicon, which was amplified from cDNA, was not be longer than 1500 bp for semi-quantitative PCR and 200 bp for quantitative PCR. The sequences of the gene-specific primers were put into the blast search to determine their specificities. None of the primer pairs showed significant homology to other sequences in the genome but their own.Primers used for expression analysis have been designed strictly considering these criteria, and listed in Table 3.4. For real-time PCR analysis, all primers were subjected to the "primer efficiency" analysis with serialy diluting (2 fold-dilutions) the parental Huh7 cDNA. The Ct values were obtained in 1, 1:2, 1:4, 1:8, 1:16, 1:32 and 1:64 fold dilutions and primer efficiencies were calculated by using the formula; $E=2^{[-1/slope]}$. The primer efficiency values of the primers which were used in Q-PCR analysis were listed in Table 3.4, also.

Table 3.4 Primers, and their sequences. Primer efficiencies were given only for primers used in Q-PCR.

Name	Sequence	Primer efficiency (if used in Q-PCR)
E2F1-F	5'-CATCAGTACCTGGCCGAGAG-3'	
E2F1-R	5'-CCAGTTCAGGTCGACGACAC-3'	2.06
E2F2-F	5'-GCCAAGAACAACATCCAGTG-3'	
E2F2-R	5'-TCAGGTGCTTGAAGCTCAGA-3'	1.7
E2F3-F	5'-CAAGACTTGAAGTGCCTGAC-3'	
E2F3-R	5'-GCTATGTCCTGAGTTGGTTG-3'	1.8
E2F4-F	5'-CAGCAGCAGCAGCAACAGTA-3'	
E2F4-R	5'-ACATCAACTCCTCCAGCAGC-3'	2.1
E2F5-F	5'-AGGCACCTTCTGGTACACAA-3'	
E2F5-R	5'-AAGCAGCACATGGATAGGTC-3'	2
E2F6-F	5'-CAGGCCTTCCATGAACAGAT-3'	
E2F6-R	5'-ACATCGATAGGTCCGTTGGT-3'	2.1
E2F7-F	5'-CAAGGATCAGGTGGCTACTC-3'	
E2F7-R	5'-GGAGGCACCACTCTCTTACT-3'	2.1
E2F8-F	5'-GCATGCTCGAGGACAGTGGT-3'	
E2F8-R	5'-GATGAGCACTGCGTGAGAGG-3'	1.7
DP1-F	5'-AGAAGTCTGGTCCCCAAGG-3'	
DP1-R	5'-AAGTCATCGTCCTCCTCGTC-3'	1.9

DP2-F	5'-GGAGTCAGGCAAATGCTCTC-3'	
DP2-R	5'-GCTAAGGCCACTTCTGCATC-3'	2
ACTB-F	5'-CCAACCGCGAGAAGATGACC-3'	
ACTB-R	5'-GGAGTCCATCACGATGCCAG-3'	2
ACE2-F	5'-AGGATGTGCGAGTGGCTAAT-3'	
ACE2-R	5'-AGGCTGTTGTCATTCAGACG-3'	-
EHF-F	5'-GATCTCCATGACAACCACCA-3'	
EHF-R	5'-AGAGGATGTCGCGGATGAAT-3'	-
HEPH-F	5'-CCTCTCACCGTCATCACCAA-3'	
HEPH-R	5'-CAGAGGCCAGCATCTCAACA-3'	-
KRT19-F	5'-GATGAGCAGGTCCGAGGTTA-3'	
KRT19-R	5'-GTGTGTCTTCCAAGGCAGCT-3'	-
MAGEB2-F	5'-TGAATTCTCAGGACTGGTCG-3'	
MAGEB2-R	5'-GCTTCAGTGACCTGAGGAAC-3'	-
PRDM1-F	5'-TCCACCTGAGAGTGCACAGT-3'	
PRDM1-R	5'-ATCTCTTGTGGCAGACCTGG-3'	-
NOX1-F	5'-TCCTTGCACCGGTCATTCTT-3'	
NOX1-R	5'-CCACGCTTGTTCATCTGCAA-3'	-
TIMP2-F	5'-GTCAGTGAGAAGGAAGTGGA-3'	
TIMP2-R	5'-CTCTATATCCTTCTCAGGCC-3'	-
GIPC2-F	5'-CCACAATGTTTGAAGCTGGA-3'	
GIPC2-F	5'-ATCACCAATGACTCCCCAAA-3'	-
CAPN2-F	5'-CAAGTCAGATGGCTTCAGCA-3'	
CAPN2-R	5'-AACTCCTTCAGCCCCAGCTT-3'	-
CCNG2-F	5'-GCCTTGTGCCTTCTCAATTT-3'	
CCNG2-R	5'-AGCTGTTGTGGAGGTTCTGG-3'	-
NGFRAP1L1-F	5'-CAGCCGATTTCAAGGCTAAG-3'	
NGFRAP1L1-R	5'-TCCAGGCTCCTGGTATTCAC-3'	-
REEP1-F	5'-GCACTTTTCACCACAGCAGA-3'	
REEP1-R	5'-TTTTGAAGATAGCGTGGGATG-3'	-
MAF-F	5'-TGGAGTCGGAGAAGAACCAG-3'	
MAF-R	5'-GCTTCCAAAATGTGGCGTAT-3'	-
MAP3K5-F	5'-CGTGAGCACGCTCAGTTCTA-3'	
MAP3K5-R	5'-TTCCGAACCAATTCTTCCAG-3'	-
SSTR1-F	5'-TAACAGACCGCACATGCACT-3'	
SSTR1-R	5'-CGGCTCTGGACTGGTAAATG-3'	-
PPARGC1A-F	5'-GATACACTTTGCGCAGGTCA-3'	
PPARGC1A-R	5'-GTGGAAGCAGGGTCAAAGTC-3'	-
IL17D-F	5'-TCAGTGCCTTCCACCACAC-3'	
IL17D-R	5'-CACAGGCAGTAGGCTTCAGG-3'	-
KLF4-F	5'-GTTCCCATCTCAAGGCACAC-3'	
KLF4-R	5'-CCCCGTGTGTTTACGGTAGT-3'	-
MAPK13-F	5'-GGAGCTAGACGTGGACAAGC-3'	
MAPK13-R	5'-AATGGGGCTGAAGTTCACAA-3'	-
RASGEF1B-F	5'-CTGGCCAAACAAGTGAGTGA-3'	
RASGEF1B-R	5'-TGAAGACTGGTACTGTGAGCAGA-3'	-
TFEC-F	5'-AACAACAGAGAGCCCGAGAA-3'	
TFEC-R	5'-TGGCAGACCATGAGTACGAG-3'	-

TMEFF1-F	5'-CTGCATCCATGGAAAATGTG-3'	
TMEFF1-R	5'-GCTTTTGCCTACTTGGCACT-3'	-
TP53INP1-F	5'-GGGGCAGCATATTCATTGTT-3'	
TP53INP1-R	5'-TAAGATTTTGGCGACGAAGG-3'	-
ZNF177-F	5'-CAATTGCTATGCAGAACATTCC-3'	
ZNF177-R	5'-GAAGGCTTTCCCACAGTCAC-3'	-
ZNF304-F	5'-ACTCCTTGAGGAGGCACAGA-3'	
ZNF304-R	5'-TGCCTCATGTTCTGCTTCAC-3'	-
ZNF419-F	5'-TTGTGACTTCAGCCATACCG-3'	
ZNF419-R	5'-CACAGTGCTGCTTCTGGTGT-3'	-
ZNF585A-F	5'-CCTGAAGCAGAGGTGGTCAT-3'	
ZNF585A-R	5'-TCAAATTTGGCGCATTCATA-3'	-
C18ORF22-F	5'-GCGGCCGCATGTGGGCTGCGGCGGGC-3'	
C18ORF22-R	5'-GGATCCCTCCCTGCTTGCTCCGCA-3'	-
TGIF-F	5'-GCGGCCGCATGAAAGGCAAGAAAGGT-3'	
TGIF-R	5'-GGATCCAGCTGTAAGTTTTGCCTG-3'	-
THOC4-F	5'-AGATCTATGGCCGACAAAATGGAC-3'	
THOC4-R	5'-GGATCCACTGGTGTCCATTCTCGC-3'	-
ZNF232-F	5'-GCGGCCGCATGGAACCTCCTGGTCCT-3'	
ZNF232-R	5'-GGATCCATGGGAAGGCTCTTTTCT-3'	-
FBXL11-F	5'-ACTGCATAACCAACCGTTCC-3'	
FBXL11-R	5'-TTCTCGATCCACTGCTTCCT-3'	2.2
CARM1-F	5'-GGCTCCATAATGACCGTGTG-3'	
CARM1-R	5'-GCGAACAGTGGTGACTGGAA-3'	1.9
PRMT1-F	5'-CACCAACGCCTGCCTCATAA-3'	
PRMT1-R	5'-TGGCAGCGTGTGAACTCGAT-3'	2.2
ASH1L-F	5'-GTCTCATGATCCAGTGTGAC-3'	
ASH1L-R	5'-GATGAAGTAGACACAGCCAG-3'	2.2
MLL3-F	5'-CATCCTACAGCTGCTGAGAA-3'	
MLL3-R	5'-GACATCTGGAGCACTGCTAA-3'	2.1
EZH2-F	5'-AGCCTTGTGACAGTTCGTGC-3'	
EZH2-R	5'-CAGCGGCTCCACAAGTAAGA-3'	2
SUV420H1-F	5'-CCGCCAAGGAACTCTGTGAA-3'	
SUV420H1-R	5'-AATGCCTTGAGCTCCTCGAA-3'	2.2
PCAF-F	5'-GAATTAGAGAGACAGGCTGG-3'	
PCAF-R	5'-GGAGCTTCTGTTCTCTTCAC-3'	-
JARID1B-F	5'-AAGAACCGTGAACTGGCAGC-3'	
JARID1B-R	5'-TGTTGTGCCAGGAGGTTGAG-3'	2.1
UTX-F	5'-GGAAGTTGCAGCTACATGAG-3'	
UTX-R	5'-TCCTGATGACCTGGTGTTCT-3'	1.9
JMJD2B-F	5'-TTCCTGCGGCATAAGATGAC-3'	
JMJD2B-R	5'-GGTGGCGAAGTTGGTAGATT-3'	2.3
JMJD3-F	5'-TCTGCAGGAGGAGAAGGAGA-3'	
JMJD3-R	5'-TCCACCGCTTAGCATCAGAC-3'	2.1
SMYD2-F	5'-GACATGGTCAGATATGCACG-3'	
SMYD2-R	5'-CCTGGTACATCATGTGCAAC-3'	2.2

SETD2-F	5'-TGATCACAAGGCAGACTCAG-3'	
SETD2-R	5'-CAGGTCCATCTCAGCTTCAT-3'	2

3.3.6.2 Expression analysis of a gene by semi-quantitative PCR

3.3.6.2.1 Determination of optimal cycle of a gene for semi-quantitative PCR

Using equal amount of templates for PCR amplifications of a gene of interest give comparable results at a certain number of PCR cycles. The number of optimal PCR cycle was determined by an initial study for each gene by performing 35-cycle PCR during which PCR amplicon samples were collected by 3-cycle intervals. Agarose gel analysis of samples from 20th, 23rd, 26th, 29th, 32nd, 35th, cycles of PCR with an equal load defined the minimum number of cycle to visualize the product on agarose gel and the saturation cycle. Agarose gels were analyzed by Densitometric Fluorescence-Chemiluminescence image analyzer and The Molecular Analyst software (BioRad). The determined cycle number was used for amplification of the gene of interest.

3.3.6.2.2 GAPDH normalization

Equal volume (2µl) of all first strand cDNA samples was used for cold-PCR amplification of *GAPDH* transcript using the pre-determined optimal cycle number for GAPDH (18 cycles). Then an equal volume of each sample was loaded onto agarose gel and intensity of each band was analyzed by Densitometric Fluorescence-Chemiluminescence image analyzer and The Molecular Analyst software. After intensities were determined, intensity of sample with the highest densitometric reading and 2 µl loading volume were used as reference points for normalization of input loading volume of other samples for expression analysis of both *GAPDH* and gene of interest by cold PCR amplification. Amplification products were analyzed in computer.

3.3.6.2.3 PCR amplification of target region

A reaction mixture of 2.5µl 10X reaction buffer, 1.5µl MgCl2 (25mM), 0.5 µl dNTP (10µM), 1µl of each primer (10 pmol), and 0.2 µl Taq DNA polymerase (5u/µL) was prepared per 2µl cDNA and total volume was adjusted to 25µl with ddH2O. The optimized PCR condition for all primer pairs used in this study was as follows:

Initial denaturation 95.0^{o}C 5 min

Denaturation	95.0°C	30 sec	30 cycles
Annealing	60.0oC	30 sec	
Extension	72.0oC	30 sec	
Final extension	72.0oC	10 min	

3.3.6.3 Quantitative real time RT-PCR

Real-time qRT-PCR was performed on BioRad iCycler (Bio-Rad, California, USA) using the BioRad iQTM SYBR Green Supermix or Stratagene MX3005P (Stratagene, U.S.A.) using Stratagene SYBR green supermix. The amplification mixtures contained 2.0 µl of 1:1-diluted cDNA template, 12.5 µl SYBR Green PCR Master Mix Buffer (2X), and 10 pmol of forward and reverse primers in a total volume of 25 µl. The cycling conditions were as follows: an initial incubation of 95°C for 5 min and then 45 cycles of 95°C for 30 s, 60°C for 30 s and 72°C for 30 s during which the fluorescence data were collected. To verify that the used primer pair produced only a single product, a dissociation protocol was added after thermocycling, determining dissociation of the PCR products from 55°C to 95°C in 80 cycles. The amplification reactions were performed in 96 well-PCR plates and the plates were sealed with optical sealing tapes (Bio-Rad, California, USA). All PCR reactions were studied in duplicate or triplicate. Tumor and matched normal samples were always analyzed in the same run to exclude between-run variations and each sample was studied in duplicate. A no-template control of nuclease-free water was included in each run. Following amplification, a reaction product melt curve was obtained to provide evidence for a single reaction product. The iCycler iQ Optical System Software (version 3, BioRad Laboratories) or Stratagene MxPro Software (Strategene laboratories) were used to determine the melting temperatures of the products. The threshold cycle (Ct) value was calculated as the cycle where the fluorescence of the sample exceeded a threshold level.

3.3.6.3.1 Amplification efficiency calculations

The PCR amplification efficiencies (E) were evaluated by 2-fold dilution series of cDNAs (1-1:256 dilution) for each pair of primers used in this study by using Huh7 cDNA. A graph of threshold cycle (Ct) was produced and the reaction efficiency was determined for each primer set by using the slope of this graph ($E=2^{(-1/slope)}$) and presented at Table (La Jolla, USA). For the evaluation of the real-time RT-PCR results 2-ΔΔCt method was corrected according to efficiency method (150) as: [(*E*target) ΔCtTarget (*control-sample*)/ (*E*ref) ΔCtReference

(*control-sample*)] using normal pair samples as control. In this formula, in the place of "reference" the Ct values of three reference genes, ACTB was used.

3.3.7 Total Protein isolation

3.3.7.1 Protein isolation from tissue culture cells

Adherent monolayer cells (both stable and parental cells) were grown to 70% confluency in growth medium lacking selective antibiotic. After removal of growth medium, cells were washed twice with ice-cold PBS to remove any serum residue. 400 µl of RIPA lysis-buffer (150 mM NaCl, 50 mM Tris-HCl pH 8.0, 0.5% sodium deoxycholate, 1 % NP-40, 0.1% SDS and 1X Complete Protein Inhibitor mix (Roche)) was added into tissue culture petri dish (6 cm or 10 cm), and cells were scraped with rubber scrapper. Complete lysis was achieved by pipetting of crude cell lysates several times and by incubating the lysates on ice for 30 min with vortexing every 6 minutes, and then centrifuged at 13.000 XG for 30 minutes. Total cell protein was collected as supernatant.

3.3.7.2 Protein isolation from tissue samples

The 5 µm thick tissue sections were cut with cryostat and collected in an eppendorf tubes. Tissues were freezed in liquid nitrogen after excision. Some nitrogen was added onto tissues in a mortar, and they were powdered with a mortar and pestle. 500 ul RIPA buffer was added onto powdered tissue. The collected samples were vortexed for 60 s and incubated on ice for 1 hour. After they were homogenized with a polytron during 15 secods 2 times. They were centrifuged a 14.000 XG for 30 minutes at 4 °C. The supernatant were stored at -80 °C.

3.3.7.3 Histone extraction

Cells were harvested and washed twice with ice-cold PBS. PBS and subsequent buffers were supplemented with 5 mM sodium butyrate to retain levels of histone acetylation. Cells were resuspended in Triton Extraction Buffer (TEB: PBS containing 0.5% Triton X 100 (v/v), 2 mM phenylmethylsulfonyl fluoride (PMSF), 0.02% (w/v) NaN_3) at a cell density of 10^7 cells per ml. Cells were lysed on ice for 10 minutes with gentle stirring, and centrifuged at 6,500 x g for 10 minutes at 4°C to spin down the nuclei. Supernatant were removed and discarded. The nuclei was washed in half the volume of TEB and centrifuged as before. The pellet was re-suspended in 0.2 N HCl at a density of $4x10^7$ nuclei per ml. The histones were acid extracted over night at 4°C. Then, samples were centrifuged at 6,500 x g for 10 minutes at

4°C to pellet debris. the supernatant, which contains the histone protein, was saved and protein content was determined using the Bradford assay. Aliquots were store at -20°C.

3.3.8 Quantification of proteins

After the cell lysates were prepared, their concentrations were detected by Bradford assay. As described in Table 3.5. 2 µl of the samples were diluted with 98 µl deionised water and then 900 µl of Bradford working solution was added to the samples and mixed well. After 5 minutes of incubation, the protein amounts of the samples were measured at OD595 nm versus blank reagent. Known concentrations of BSA were prepared according to Table 3.6 as a standard. After reading at OD595, samples and standard values were plotted; unknown concentrations were calculated from the standard curve.

Table 3.5 A standard curve preparation with BSA dilution.

Tubes	1	2	3	4	5	6	7	8
BSA (µl)	0	2.5	5	7.5	10	12.5	15	20
ddH_2O (µl)	100	97.5	95	92.5	90	87.5	85	80
Bradford (µl)	900	900	900	900	900	900	900	900
Total (ml)	1	1	1	1	1	1	1	1

Table 3.6 Protein sample preparation for Bradford assay

Tubes	1	2	3	4	5
Sample (µl)	0	2	2	2	2
ddH_2O (µl)	100	98	98	98	98
Bradford (µl)	900	900	900	900	900
Lysis buffer (µl)	2	0	0	0	0

3.3.9 Western Blotting

10% Bis-tris gel (invitrogen) was used for western blot assays. Invitrogen vertical gel system was set up according to manufacturer's instructions. For 10% Bis-tris gel (invitrogen), MOPS-SDS running buffer and Nu-PAGE Transfere buffer (Invitrogen) were used. Equal amounts of cell lysates were solubilized in 1X LDS sample buffer with 1X sample reducing agent (Invitrogen), denatured at 70°C for 10 min and incubated on ice for 2 min. After a quick spin, samples were loaded onto polyacrylamide gel. After electrophoresis at 120 V for 1-2 hours, proteins were transferred onto PVDF western blotting membrane (Roche) by using

wet-tramsfere technique in Invitrogen electroblotting apparatus according to the manufacturer's instructions at 25V for 2 or 4 hours (depending on the size of the target ptorein). Membrane was immediately treated for an hour in blocking solution at room temperature and probed with primary antibody either for an hour at room temperature or overnight at 4°C. After washing 3 times for 10 min. in TBS-T solution at room temperature, the membrane was incubated with appropriate HRP conjugated secondary antibody for 1 hr. The membrane was washed 3 times for 10 min in TBS-T solution at room temperature. After final wash, the blot was exposed to ECL western blot detection kit (Amersham) according to manufacturer's instructions. The chemiluminescence emitted was captured on X-ray film within 30 sec. to 25 min. exposure times.

3.3.10 Immunofluorescence

Autoclaved-sterilized coverslips were placed into the well of 24-multiwell plates. $5x10^4$ cells were seeded onto each coverslip and grown overnight in 0.5 ml growth medium. Cells were washed with PBS and fixed in 0.5 ml of 4% formaldehyde for 5 min.

After fixation cells were permeabilized with 0.5% TritonX-100/0.5% Saponin in PBS for 5 min 3 times and blocked in 0.5 ml blocking solution for 1 hour at room temperature. Coverslips were probed with primary antibody in appropriate dilution for 1 hr at room temperature or overnight at 4°C. After 3 times washing for 5 min each with dilution solution, appropriate FITC-conjugated secondary antibody was applied for 45 min at room temperature. Cells were washed 3 times for 5 min with dilution solution and DNA counter staining was performed by with Hoechst 33258 or DAPI for 3 min. Hoechst 33258 or DAPI was aspirated and destaining was done in double-distilled water for 15 min. immediately after coverslips were taken out from the well and excess water removed by tissue paper, coverslips were mounted onto slides containing 10 µl 80% glycerol, or mounting medium. All steps after the addition of FITC-conjugated secondary antibody were performed in the dark.

Stained cells were examined under fluorescence microscope (ZEISS or Olympus) and pictures were captured in a digital Kodak Camera (DC290, Eastman Kodak Co., Rochester, NY), using Adobe Photo Deluxe (Adobe Systems Inc.) software. The pictures were edited using Adobe Photoshop 5.0 (Adobe Systems Inc.) software. Digital images were magnified when needed during picture editing.

3.3.11 Immunoperoxidase

Autoclaved-sterilized coverslips were placed into the well of 24-multiwell plates. $5x10^4$ cells were seeded onto each coverslip and grown overnight in 0.5 ml growth medium. Cells were washed with PBS and fixed in 0.5 ml of 4% formaldehyde for 5 min. After fixation cells were permeabilized with 0.5% TritonX-100/0.5% Saponin in PBS for 5 min 3 times and blocked in 0.5 ml blocking solution for 1 hour at room temperature. Coverslips were probed with primary antibody in appropriate dilution for 1 hr at room temperature or overnight at 4°C. After 3 times washing for 5 min each with dilution solution, appropriate HRP-conjugated secondary antibody was applied for 45 min at room temperature. Cells were washed 3 times for 5 min with dilution solution. As the substrate of HRP, DAB plus was prepared freshly. Cells were incubated with DAB+ within 30 seconds to 3 minutes, and washed with tab water for 3 minutes. DNA counter staining was performed by with Mayer's Heamatoxylene (Sigma) for 3 min. Deastaining was done with distilled water during 5 minutes. Coverslips were taken out from the well and excess water removed by tissue paper, coverslips were mounted onto slides containing 10 µl 80% glycerol, or mounting medium. Stained cells were examined and counted under light microscope (ZEISS or Olympus) and pictures were captured in a digital Kodak Camera (DC290, Eastman Kodak Co., Rochester, NY).

3.3.12 Immunohistochemistry on paraffin-embedded tissue sections

Slides were washed with dH2O in the glass container briefly. Parrafin removal was successed by incubationg the slides in an owen at 70°C for 60 min.s, and then incubated with toluene 3X10 min.s. Endogenous peroxidase was inhibitted by incubating slides in 100% ethanol for 2 min.s and 3% H_2O_2, prepared in methanol, for30 min.s. Samples were treated with 100% ethanol, 90% ethanol and than 70% ethanol for 2 min.s interval for rehydradion step, and washed with dH2O for 5 min.s. Antigen retrievel was successed by boiling the slides in citrate buffer for 20 min.s and washed two times with dH_20. The slides were blocked in blocking solution for 30 min.s. Slides were incubated with primary antibody solution in appropriate dilutions overnight at 4°C. After washing with wash solution three times for five min.s, Envision Dual Link (Dako) was applied on slides during 1 hour. Secondary antibody was washed and the slides were treated with DAB+ substrate for 30 sec.s to 10 min.s. Counter staining was performed with Mayer's heamatoxylene for 2:30 min.s. The tissue slides were mounted with mounting medium and coverslipts and examined under light microscope (Olympus). The cells were counted under the light microscope by an experienced pathologist.

3.3.13 SABG assay

SABG activity was detected by using a described protocol (151). SABG positive and negative cells were identified and counted under the light microscope.

CHAPTER 4. RESULTS

4.1 Identification of senescence and immortality gene network and its role in hepatocellular carcinoma

4.1.1 Expression analysis of immortal and reprogrammed senescent cells of hepatocellular carcinoma

Recently, our group has observed that some single cell clones of cancer cell lines changed morphology and ceased proliferation at late passages with features reminiscent of cellular senescence. Different Huh7-derived clones were expanded in long-term culture and their potential was examined to undergo replicative senescence by a recent group member, Nuri Ozturk. It has been observed that some clones performed more than 100 PD in culture with stable proliferation rates and heterogeneous SABG staining, while others sustained a limited number of PD, then entered a growth arrest phase with full SABG staining patterns. For example, Huh7 derived C3 clone performed only 80 PD, whereas Huh7 derived C1 clone replicated over 150 PD. Permanently arrested C3 cells (PD 80) displayed enlarged size, flattened shape, and fully positive SABG staining, whereas early passage C3 (PD 57) and C1 (PD 179) cells displayed normal morphology with heterogeneous SABG staining (Figure 4.1.1).

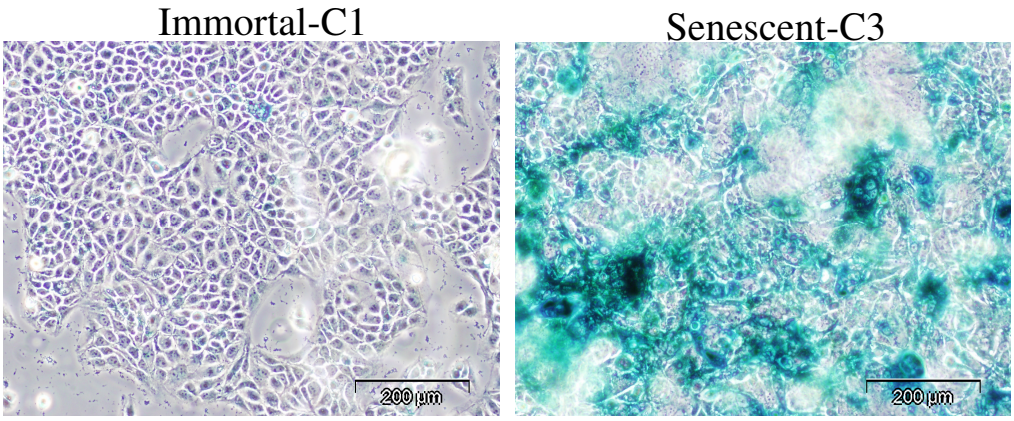

Figure 4.1.1 Senescence associated B-galactosidase (SABG) staining of immortal and senescent cells.

To generate the expression data, we generated the genome wide expression profiling in immortal, pre-senescent and senescent clones. Two immortal clones, namely C1 and G11, were tested after 150 PD following clone isolation. Two senescenceprogrammed clones, namely C3 and G12, were analyzed at both presenescent (20-30 PD before senescence arrest) and senescent (~80 PD) states. Three biological replicates were used for RNA extraction from each clonal cell with a total of 18 cell line samples. Preparation of labelled nucleic acids from

mRNAs, the Affymetrix HG-U133 plus2 hybridization and raw data retrievel were performed in Ankara University Biotechnology Institute with the colloboration of Dr. Hilal Ozdag. RNA quality was evaluated by the ratio of 18S to 28S RNAs by Agilent Bioanalyzer; all samples passed this quality control test (integrity number >4) (data not shown). The quality of every single Affymetrix data was assessed using AffyPLM software in R. Chip pseudo-images (not shown) and NUSE and RLE plots retrieved from the AffyPLM revealed that all 18 Affy data were with high quality (Figure 4.1.2).

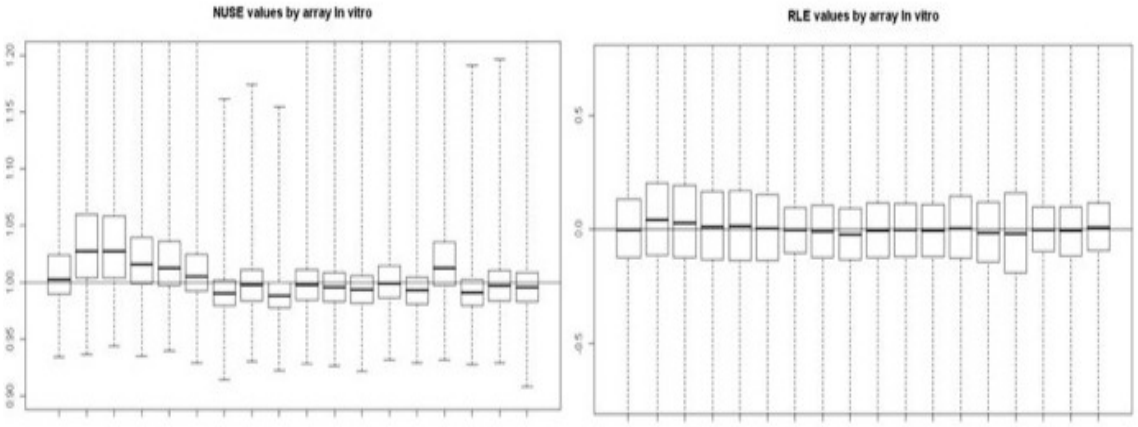

Figure 4.1.2 Quality assessment of microarray data. NUSE and RLE plots of 18 Affy-chips retrieved from affyPLM software showed that all chips were with high quality.

4.1.2 Differentially expressed gene set between immortal, pre- and senescent clones

Then, the raw data were background corrected, normalized (Figure 4.1.3) and summarized into gene expression level measurements by applying the RMA (Robust Multichip Average) algorithm of the 'affy' package and log transformed (log 2 base) in Bioconductor in R (Appendix A and B1). Differentially expressed probesets derived from immortal, presenescent, and senescent Huh7 clones were identified between any two classes (immortal vs. senescent, immortal vs. presenescent, and presenescent vs. senescent) using a two-tailed, unpaired, unequal variance Welch's t-test using R statistical package (Appendix B2). Probesets were considered significantly differentially expressed if the raw p value was less than 0.05 for a given probeset in both sets of clones (e.g., for determining probesets modulated between immortality and senescence conditions, C11I versus C3S clones, as well as G11I versus G12S clones were compared). We identified 6390 probesets showing expression modulation in the same direction in both the C and G clones. This gene set

discriminated the groups from each other with high accuracy (Figure 4.1.4). Gene and probe numbers differentially expressing between any two groups were given in Table 4.1.

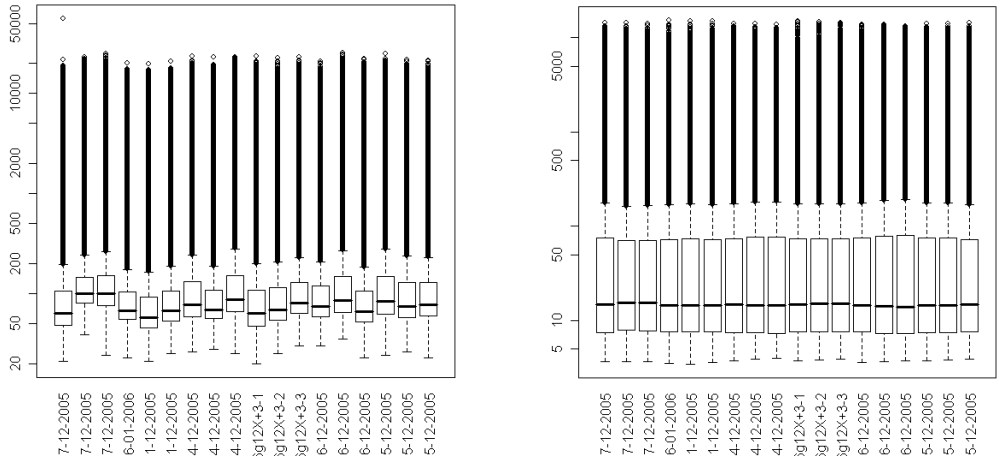

Figure 4.1.3 Plots of microarray data before (*left*) and after (*right*) normalization. The plots were generated in R, using AMDA package. We observe that any bias coming from technology is eliminated after normalization.

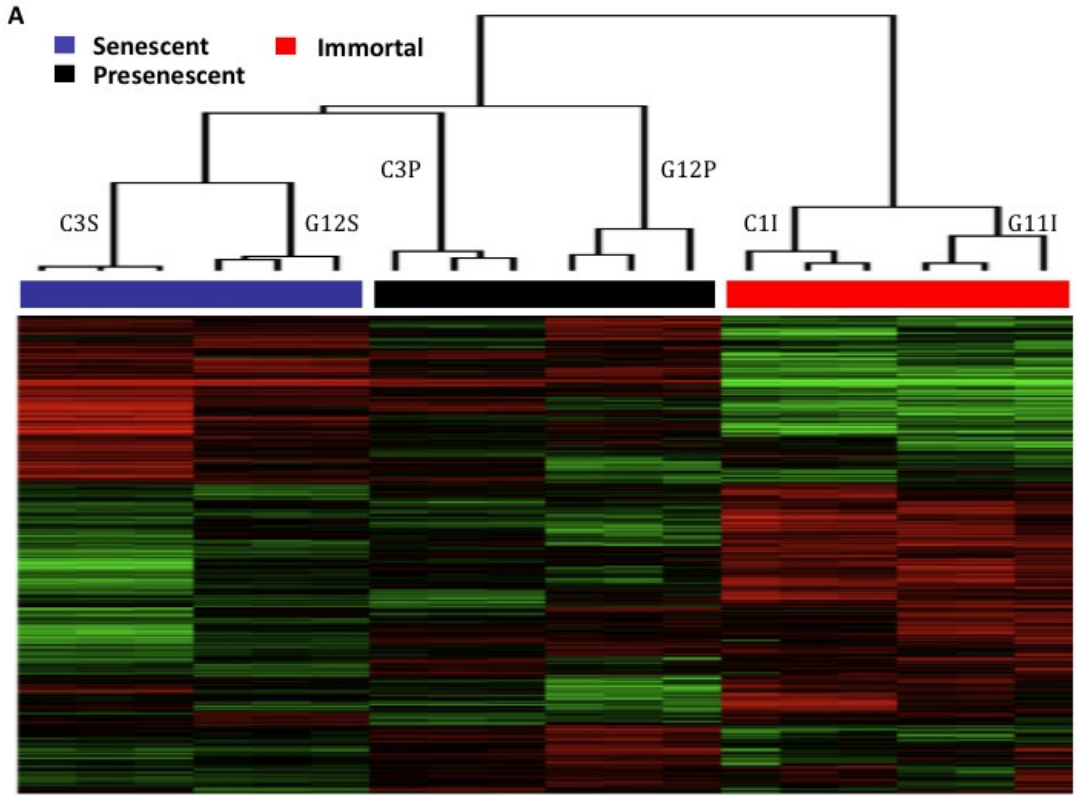

Figure 4.1.4 Huh7 isogenic clones significant gene list (6390 probe sets) unsupervised hierarchical cluster analysis (p<0.05) (I: immortal, P: pre-senescent, S: senescent) Red: up-

regulation, green: down-regulation and black: no change. The grouping of different phenotypes with high accuracy was observed.

Table 4.1.1 The numerical report of significant probes and genes

	I->PS	PS->S	I->S
Gene			
up	1054	1029	1665
down	1095	994	1408
total	2149	2023	3073
Probe			
up	1202	1224	2086
down	1350	1164	1786
total	2552	2388	3872

4.1.3 Confirmation of the microarray data

After obtaining significant gene set, we wanted to test the accuracy of our microarray data by RT-PCR. Sixteen senescence upregulated genes and nine immortal upregulated genes were selected randomly, and primers were designed. We applied semi-quantitative RT-PCR using the mRNA material prepared from an independent (from the mRNA samples used in microarray study) set of immortal, pre-senescent and senescent clones. *GADPH* gene was used as the internal control. All of the amplifications gave the same results as the microarray data, most of them changing more dramatically in RT-PCR than microarray value (Figure 4.1.5 A and B). From the set of senescence up-regulated genes; the genes tested were ACE2 (angiotensin I converting enzyme 2), NOX1 (NADPH oxidase 1), TIMP2 (Tissue inhibitor of metalloproteinases 2), HEPH (Hephestine), PRDM1 (B-lymphocyte-induced maturation protein 1), EHF (ETS domain-containing transcription factor), MAGEB2 (cancer/testis antigen family 3, member 2), CAPN2 (Calcium-activated neutral proteinase 2), TM7SF1 (Transmembrane 7 superfamily member 1 protein), NGFRAP1L1 (Nerve growth factor receptor-associated protein 2), GPR74 (G protein-coupled receptor 74), REEP1 (receptor expression enhancing protein 1), MAP3K5 (MAP/ERK kinase kinase 5), PPARGC (peroxisome proliferator activated receptor gamma, coactivator 1 alpha), and MAP7 (microtubule-associated protein 7). Tested immortality related genes were; RAD50 (RAD50 (S. cerevisiae) homolog), NBN (Cell cycle regulatory protein p95), MND1 (meiotic nuclear divisions 1 homolog (S. cerevisiae)), MRE11A (DNA recombination and repair protein), SLC7A5 (Solute carrier family 7 member 5), TMCO6 (transmembrane and coiled-coil domains 6), DKK1 (dickkopf (Xenopus laevis) homolog 1), GLUD1 (glutamate dehydrogenase (NAD(P)+)), and ROBO2 (roundabout (axon guidance receptor, Drosophila)

homolog 2). The correlation of microarray data and RT-PCR data was 1 (100% correlation) for both senescence and immortality related genes.

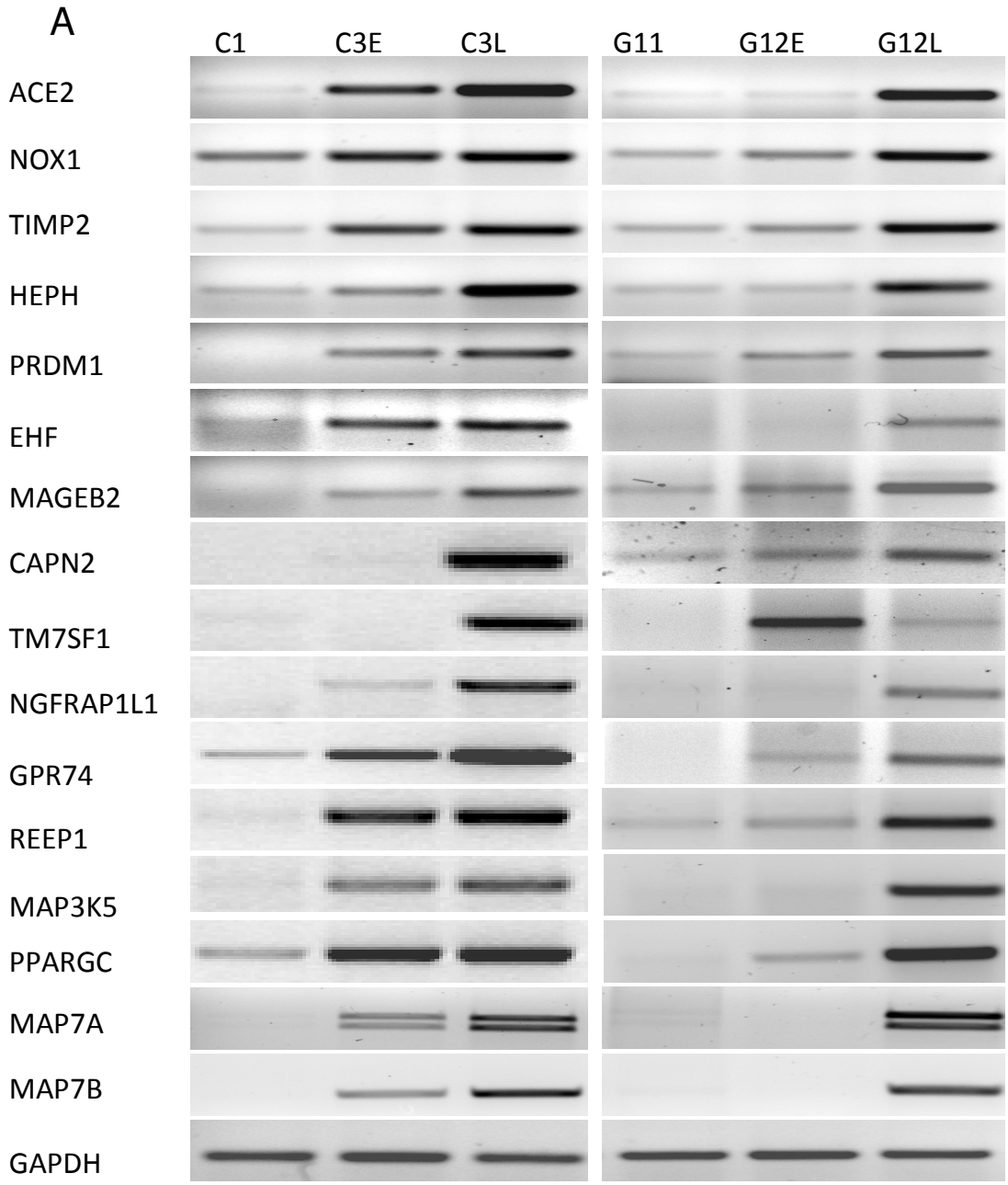

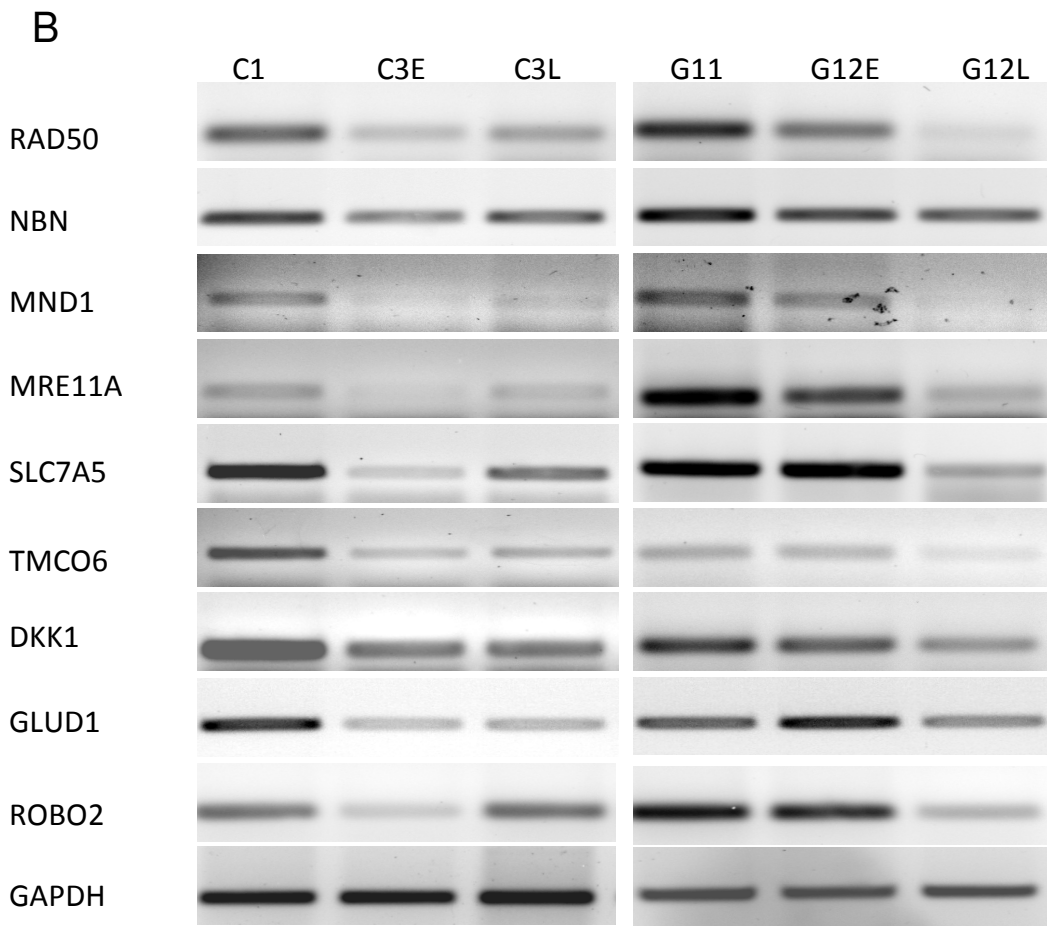

Figure 4.1.5 Confirmation of the microarray data. A) RT-PCR analysis of senescence and, **B)** immortal up-regulated genes. C1 and G11 cells are two immortal clones, C3E and G12E cells are pre-senescent clones and C3L and G12L are senescent cell clones. The mRNA samples used for the analysis were from the different cell vials from the mRNA samples used in microarray study. The correlation efficient between microarray data and RT-PCR data were found to be 1 (http://www.easycalculation.com/statistics/correlation.php).

4.1.4 Analysis of significant gene set on other senescence microarray data

As our senescence model was a unique model; we, then, wanted to see whether the gene expression profile of our senescence model resembles to other senescence models. We screened the literature for the publicly available microarray data performed with different senescence and immortalized cell models. We selected 2 studies and analyzed them, as summarized in material-methods. Schwarze and his colleagues profiled the global gene expression of replicative senescence in HPECs (Human prostate epithelial cells) (147). They

have analyzed expression analysis of proliferating HPECs, serially passaged early-senescent and late-senescent HPECs and hTERT-immortalized HPEC cells. Collado and his friends studied with Mek:Erk induced OIS (oncogene-induced senescence) using IMR90 (human fetal lung) cells (148). They have compared the expression profiles of Mek:Erk transfected senescent, both Mek:Erk and small t-antigen induced senescent, and Mek:Erk, E6 and E7, and small t-antigen induced immortal IMR90 cells. We merged 6390-gene set with downloaded and normalized data, and performed non-supervised hierarchical cluster analysis. We observed that our significant gene signature could succesfuly discriminate both replicative senescent cells and oncogene-induced senescent cells from their immortalized counterparts (Figure 4.1.6 A and B). For the Schwarze data-set, we observed that early- and late-senescent HPEC cells were grouped together with C3S and G12S senescent clones; proliferating HPEC cells clustered in the same branch with C3P and G12P pre-senescent clones, and hTERT immortalized HPECs grouped together with C1 and G11 immortal cells. Mek:Erk and Mek:Erk-Small t-antigen induced senescent IMR90 cells were clustered together with C3S, G12S and C3P, G12P clones, respectively. On the other hand, Mek:Erk-E67-Small t-antigen transfected immortal IMR90 cells were grouped together with C1 and G11 immortal clones.

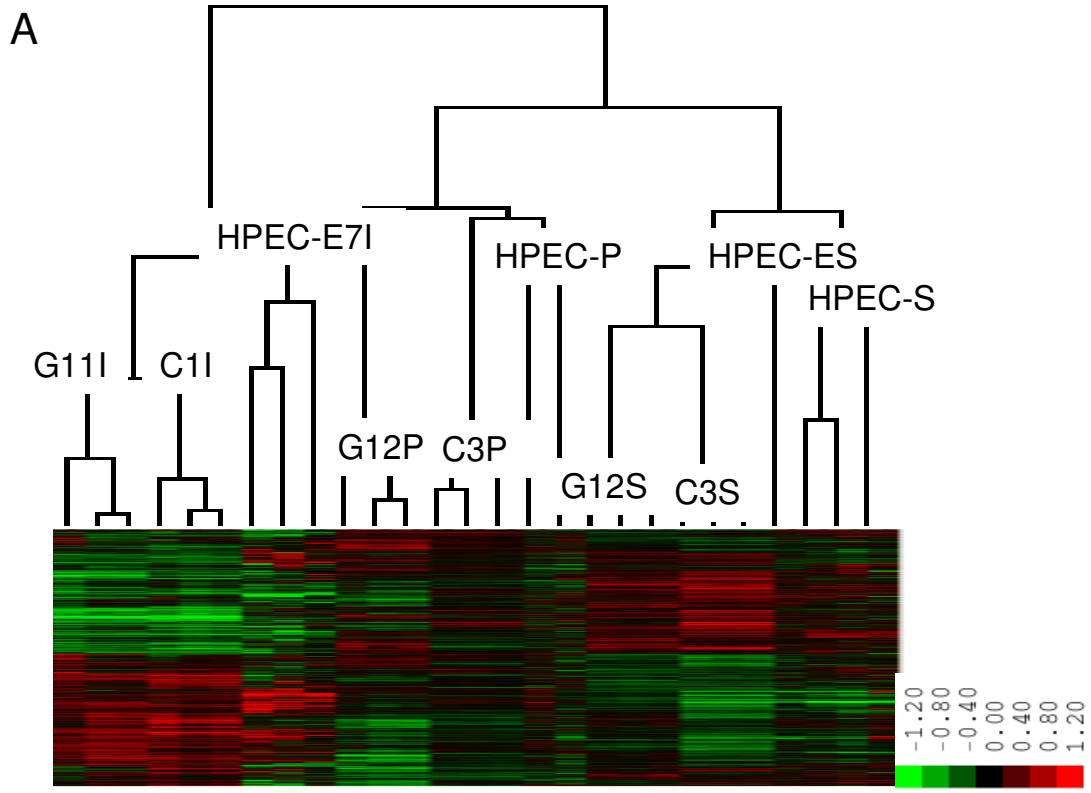

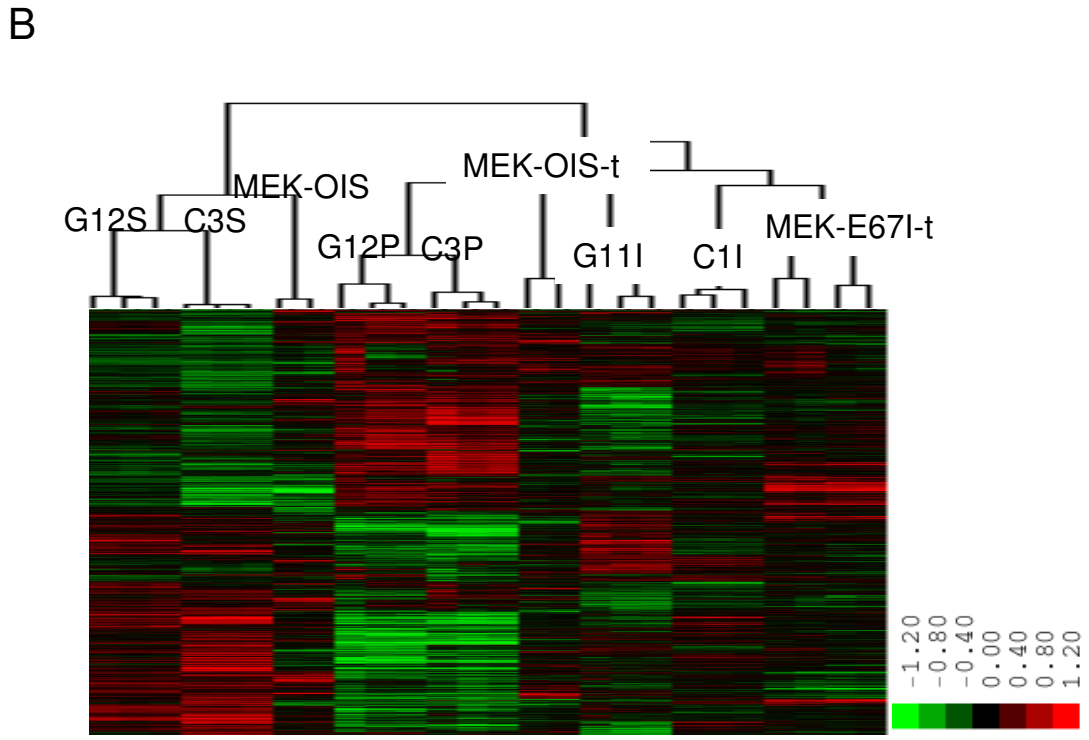

Figure 4.1.6 Meta-analysis with previously published senescence data. A) Unsupervised cluster analysis with Schwarze et. al. data, 2682 genes were common between 9597 probes and 6390 probes (HPEC E7I: E7 immortalized HPECs, HPEC-P: proliferating HPEC cells, HPEC-ES: early senescent HPECs, HPEC-S: late senescent HPECs). **B)** Unsupervised cluster analysis with Collado et. al. data, 3654 genes were common between 22283 probes and 6390 probes (MEK-OIS: Mek:Erk induced senescent IMR90 cells, MEK-OIS-t: Mek:Erk and Small t-antigen induced senescent IMR90 cells, MEK-E67I-t: Mek:Erk, E6 and E7 and small t-antigen transfected immortal IMR90 cells).

4.1.5 Functional classification of senescence and immortality genes

To identify significant biological processes and pathways regulated differentially between immortal, pre- and senescent clones, we have used some bioinformatic tools, such as GSEA (Gene Set Enrichment Analysis), and Onto-tools as summarized in Materials and Methods. The most significant gene sets upregulated in groups that was obtained from GSEA software were listed in Table 4.1.2. “Enrichment plots” and “Blue-pink dendograms” of the most significant gene-sets enriched in groups were given in Figure 4.1.7 (complete lists were given in Appendix C). The genes that are upregulated in immortal group enriched in E2F1 targets, stem-cell related genes, DNA repair and cell cycle related gene sets. Stress response, HOX and TNF-α induced gene sets were clustered in pre-senescent up-regulated genes. Senescence

up-regulated gene sets were immune function related, stress response, electron transporter activity, protein modification, HDAC inhibitor responsive and HOX gene groups.

Table 4.1.2 Examples of significantly upregulated GSEA gene sets

IMM vs SEN: IMMORTAL ENRICHED GENE SETS n=13*

NAME	SIZE	ES**	FDR*** q-val	RANK AT MAX
E2F1_TARGETS_CHIP	38	0.580218	0.051051	2847
CANCER_UNDIFFERENTIATED_META_UP	65	0.487906	0.113817	2000
BRENTANI_REPAIR	36	0.621496	0.117194	1989
MANALO_HYPOXIA_DOWN	80	0.563608	0.127927	1777
NF90_DN	29	0.61834	0.132696	1179
CMV_IE86_UP	37	0.720344	0.139809	1827
SERUM_FIBROBLAST_CELLCYCLE	114	0.581189	0.140873	2000
PEART_HISTONE_DOWN	73	0.408196	0.144511	1732
DOX_RESIST_GASTRIC_UP	47	0.614502	0.147354	2000
SERUM_FIBROBLAST_CORE_UP	173	0.376459	0.154137	2678
P21_ALL_DN	30	0.634628	0.160947	2646
BRCA_PROGNOSIS_NEG	88	0.439633	0.16169	1681
CROONQUIST_IL6_STARVE_UP	29	0.762213	0.176304	2131

PRE-SEN vs IMM: PRE-SENESCENCE ENRICHED GENE SETS n=127*

NAME	SIZE	ES**	FDR*** q-val	RANK AT MAX
IFNG_5ENDOTHELIAL_DOWN	68	0.44511	0.106698	4692
HYPOXIA_REVIEW	80	0.527992	0.107922	3379
TESTIS_EXPRESSED_GENES	61	0.402888	0.108234	375
H2O2_CSBDIFF_C2	26	0.546498	0.109624	3482
HDACI_COLON_BUT12HRS_UP	34	0.476826	0.111217	4478
TNFALPHA_30MIN_UP	38	0.388466	0.111307	2836
TNFALPHA_4HRS_UP	39	0.507071	0.111435	4462
CHIARETTI_T_ALL	238	0.469172	0.1137	2905
OXSTRESS_BREASTCA_UP	27	0.519261	0.114023	411
UV_UNIQUE_FIBRO_DN	28	0.613834	0.114061	4349
CMV_24HRS_UP	58	0.521695	0.116577	3018
CROONQUIST_IL6_STROMA_UP	36	0.591776	0.11798	2096
TNFA_5ENDOTHELIAL_DOWN	71	0.539296	0.118261	1445
UVB_NHEK1_UP	140	0.488482	0.118437	5081
TNFA_5ENDOTHELIAL_UP	70	0.636198	0.119345	2220
HOX_GENES	52	0.626138	0.11986	3451
TSA_HEPATOMA_CANCER_UP	30	0.667311	0.122257	2067
SMITH_HTERT_DOWN	61	0.45944	0.160955	2179

SEN vs IMM: SENESCENCE ENRICHED GENE SETS n=247*

NAME	SIZE	ES**	FDR*** q-val	RANK AT MAX
JECHLINGER_EMT_DOWN	40	0.567248	0.066461	4702
ANDROGEN_GENES	52	0.674071	0.066919	1840
WERNERONLY_FIBRO_UP	30	0.609646	0.069974	2586

BRENTANI_IMMUNE_FUNCTION	50	0.527649	0.070526	4456
ROSS_MLL_FUSION	77	0.548274	0.07101	2989
SMITH_HTERT_DOWN	61	0.530096	0.071046	1680
VEGF_MMMEC_12HRS_UP	25	0.675701	0.071742	3150
IFN_BETA_GLIOMA_UP	50	0.418442	0.072413	5049
TESTIS_EXPRESSED_GENES	61	0.420126	0.073636	279
STRESS_TPA_SPECIFIC_UP	49	0.38809	0.075366	3829
HDACI_COLON_BUT12HRS_UP	34	0.581869	0.075561	3484
H2O2_CSBDIFF_C2	26	0.520755	0.075762	2201
BRCA1_OVEREXP_UP	128	0.535055	0.076798	2340
ELECTRON_TRANSPORTER_ACTIVITY	113	0.555891	0.080027	1595
PENG_RAPAMYCIN_UP	155	0.415837	0.080085	3642
BRENTANI_PROTEIN_MODIFICATION	144	0.482071	0.083533	4586
BRENTANI_DEATH	70	0.499667	0.086309	2388
JISON_STRESS	30	0.519862	0.087565	4518
HOX_GENES	52	0.524791	0.088914	2947
HYPOXIA_REVIEW	80	0.550173	0.090366	3959

*FDR<0.2

**ES:Enrichment score

***FDR: False discovery rate

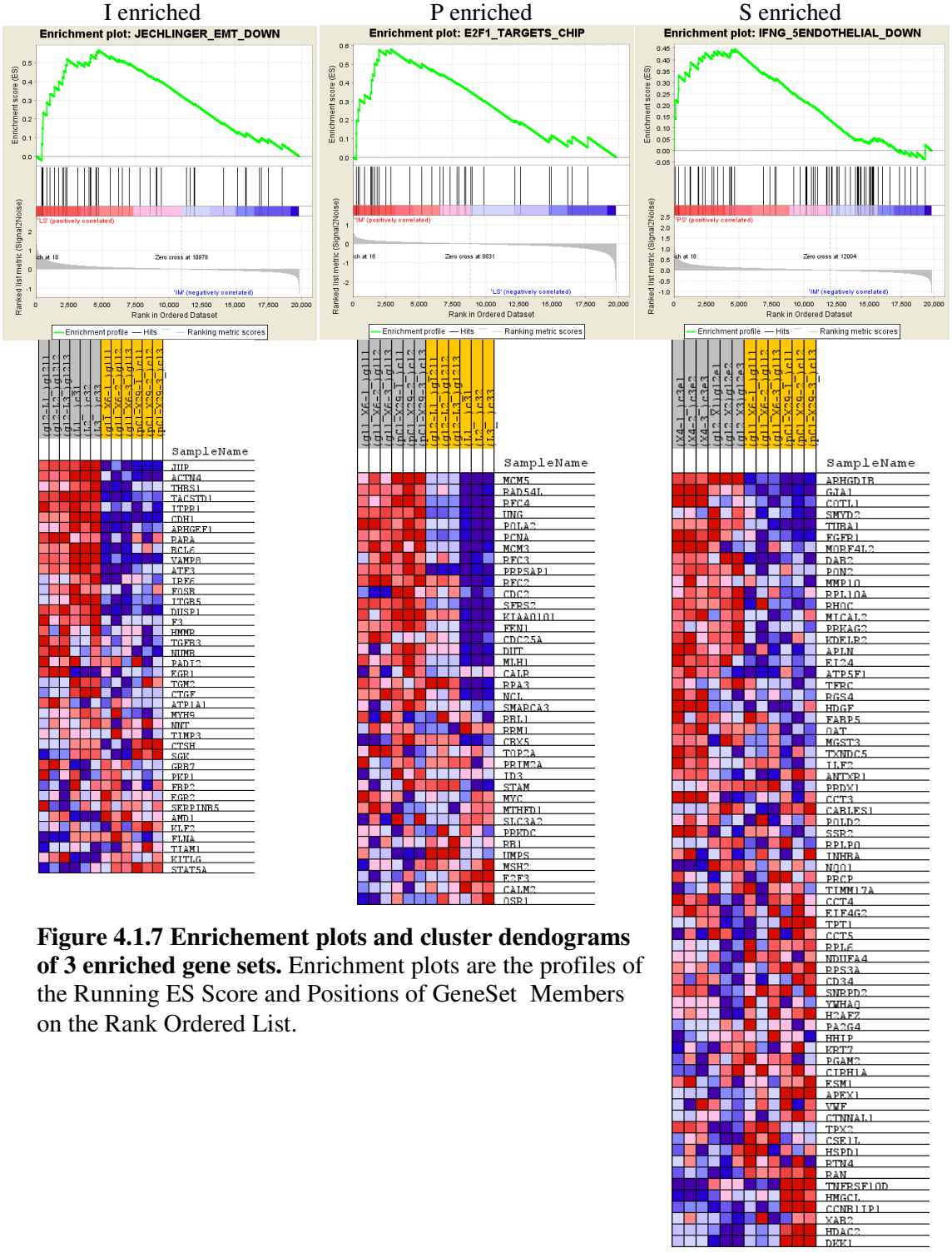

Figure 4.1.7 Enrichement plots and cluster dendograms of 3 enriched gene sets. Enrichment plots are the profiles of the Running ES Score and Positions of GeneSet Members on the Rank Ordered List.

Gene Ontology (GO) annotation of differentiating genes were performed using Onto-Express software (Figure 4.1.8 A, B and C). Immortal upregulated genes (>1 fold, compared to senescence) grouped in protein biosynthesis, DNA replication and repair, nucleic acid

metabolism, and RNA splicing processes. Senescence and pre-senescence enriched groups were chromosome organization and biogenesis, epidermis development, mesodermal cell fate determination, metabolism and immune response (corrected p<0.05).

A

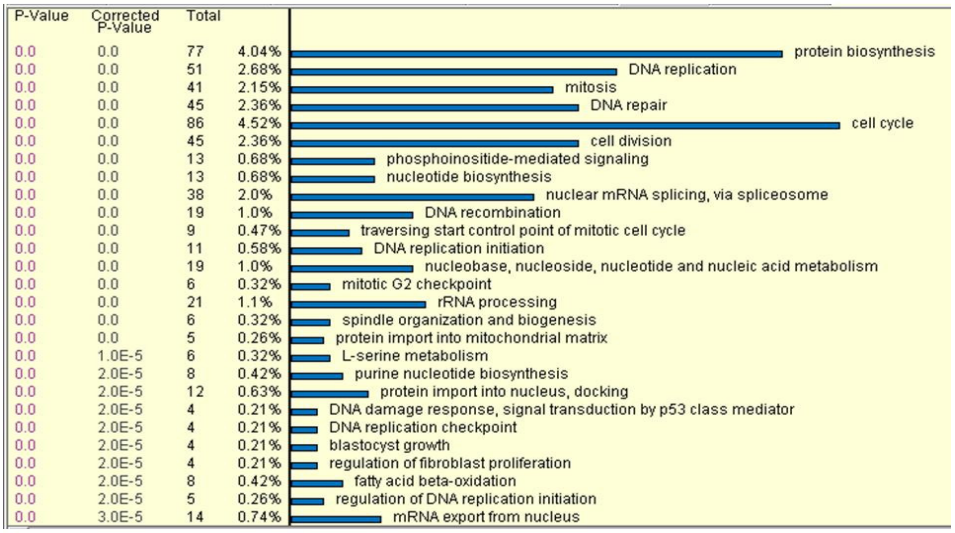

P-Value	Corrected P-Value	Total		
0.0	0.0	77	4.04%	protein biosynthesis
0.0	0.0	51	2.68%	DNA replication
0.0	0.0	41	2.15%	mitosis
0.0	0.0	45	2.36%	DNA repair
0.0	0.0	86	4.52%	cell cycle
0.0	0.0	45	2.36%	cell division
0.0	0.0	13	0.68%	phosphoinositide-mediated signaling
0.0	0.0	13	0.68%	nucleotide biosynthesis
0.0	0.0	38	2.0%	nuclear mRNA splicing, via spliceosome
0.0	0.0	19	1.0%	DNA recombination
0.0	0.0	9	0.47%	traversing start control point of mitotic cell cycle
0.0	0.0	11	0.58%	DNA replication initiation
0.0	0.0	19	1.0%	nucleobase, nucleoside, nucleotide and nucleic acid metabolism
0.0	0.0	6	0.32%	mitotic G2 checkpoint
0.0	0.0	21	1.1%	rRNA processing
0.0	0.0	6	0.32%	spindle organization and biogenesis
0.0	0.0	5	0.26%	protein import into mitochondrial matrix
0.0	1.0E-5	6	0.32%	L-serine metabolism
0.0	2.0E-5	8	0.42%	purine nucleotide biosynthesis
0.0	2.0E-5	12	0.63%	protein import into nucleus, docking
0.0	2.0E-5	4	0.21%	DNA damage response, signal transduction by p53 class mediator
0.0	2.0E-5	4	0.21%	DNA replication checkpoint
0.0	2.0E-5	4	0.21%	blastocyst growth
0.0	2.0E-5	4	0.21%	regulation of fibroblast proliferation
0.0	2.0E-5	8	0.42%	fatty acid beta-oxidation
0.0	2.0E-5	5	0.26%	regulation of DNA replication initiation
0.0	3.0E-5	14	0.74%	mRNA export from nucleus

B

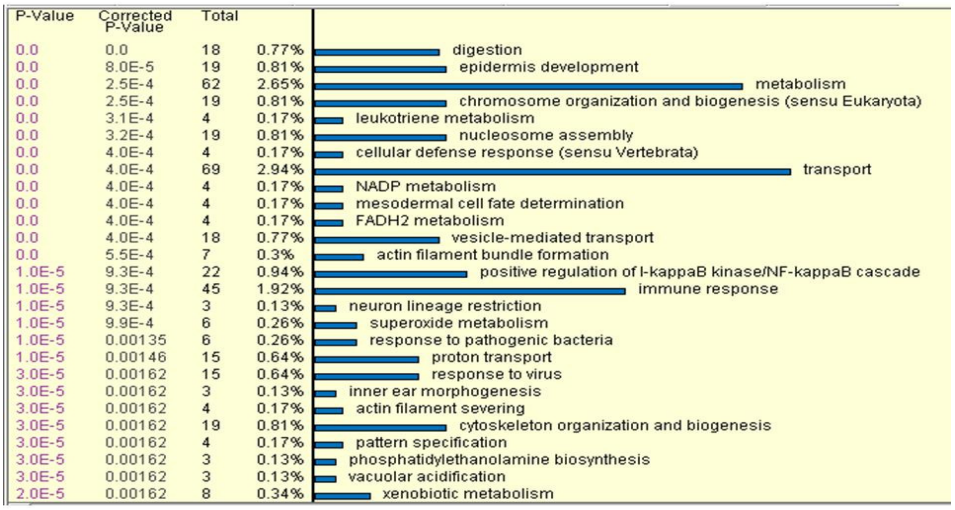

P-Value	Corrected P-Value	Total		
0.0	0.0	18	0.77%	digestion
0.0	8.0E-5	19	0.81%	epidermis development
0.0	2.5E-4	62	2.65%	metabolism
0.0	2.5E-4	19	0.81%	chromosome organization and biogenesis (sensu Eukaryota)
0.0	3.1E-4	4	0.17%	leukotriene metabolism
0.0	3.2E-4	19	0.81%	nucleosome assembly
0.0	4.0E-4	4	0.17%	cellular defense response (sensu Vertebrata)
0.0	4.0E-4	69	2.94%	transport
0.0	4.0E-4	4	0.17%	NADP metabolism
0.0	4.0E-4	4	0.17%	mesodermal cell fate determination
0.0	4.0E-4	4	0.17%	FADH2 metabolism
0.0	4.0E-4	18	0.77%	vesicle-mediated transport
0.0	5.5E-4	7	0.3%	actin filament bundle formation
1.0E-5	9.3E-4	22	0.94%	positive regulation of I-kappaB kinase/NF-kappaB cascade
1.0E-5	9.3E-4	45	1.92%	immune response
1.0E-5	9.3E-4	3	0.13%	neuron lineage restriction
1.0E-5	9.9E-4	6	0.26%	superoxide metabolism
1.0E-5	0.00135	6	0.26%	response to pathogenic bacteria
1.0E-5	0.00146	15	0.64%	proton transport
3.0E-5	0.00162	15	0.64%	response to virus
3.0E-5	0.00162	3	0.13%	inner ear morphogenesis
3.0E-5	0.00162	4	0.17%	actin filament severing
3.0E-5	0.00162	19	0.81%	cytoskeleton organization and biogenesis
3.0E-5	0.00162	4	0.17%	pattern specification
3.0E-5	0.00162	3	0.13%	phosphatidylethanolamine biosynthesis
3.0E-5	0.00162	3	0.13%	vacuolar acidification
2.0E-5	0.00162	8	0.34%	xenobiotic metabolism

C

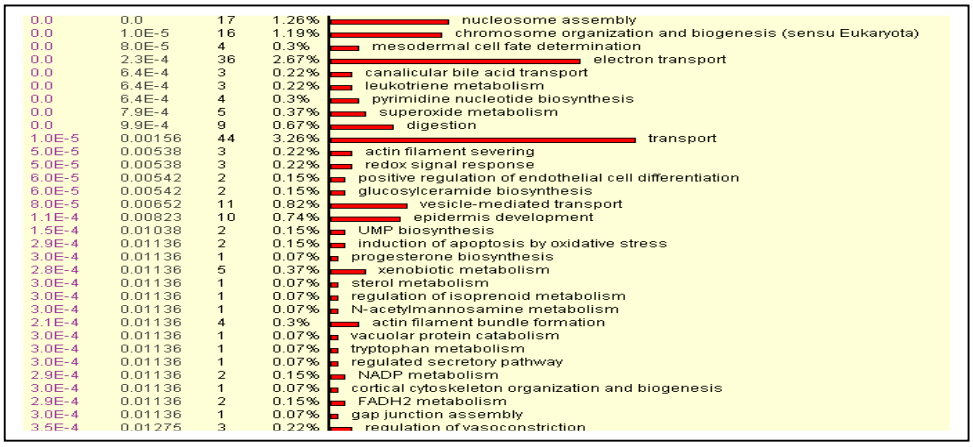

0.0	0.0	17	1.26%	nucleosome assembly
0.0	1.0E-5	16	1.19%	chromosome organization and biogenesis (sensu Eukaryota)
0.0	8.0E-5	4	0.3%	mesodermal cell fate determination
0.0	2.3E-4	36	2.67%	electron transport
0.0	6.4E-4	3	0.22%	canalicular bile acid transport
0.0	6.4E-4	3	0.22%	leukotriene metabolism
0.0	6.4E-4	4	0.3%	pyrimidine nucleotide biosynthesis
0.0	7.9E-4	5	0.37%	superoxide metabolism
0.0	9.9E-4	9	0.67%	digestion
1.0E-5	0.00156	44	3.26%	transport
5.0E-5	0.00538	3	0.22%	actin filament severing
5.0E-5	0.00538	3	0.22%	redox signal response
6.0E-5	0.00542	2	0.15%	positive regulation of endothelial cell differentiation
6.0E-5	0.00542	2	0.15%	glucosylceramide biosynthesis
8.0E-5	0.00652	11	0.82%	vesicle-mediated transport
1.1E-4	0.00823	10	0.74%	epidermis development
1.5E-4	0.01038	2	0.15%	UMP biosynthesis
2.9E-4	0.01136	2	0.15%	induction of apoptosis by oxidative stress
3.0E-4	0.01136	1	0.07%	progesterone biosynthesis
2.8E-4	0.01136	5	0.37%	xenobiotic metabolism
3.0E-4	0.01136	1	0.07%	sterol metabolism
3.0E-4	0.01136	1	0.07%	regulation of isoprenoid metabolism
3.0E-4	0.01136	1	0.07%	N-acetylmannosamine metabolism
2.1E-4	0.01136	4	0.3%	actin filament bundle formation
3.0E-4	0.01136	1	0.07%	vacuolar protein catabolism
3.0E-4	0.01136	1	0.07%	tryptophan metabolism
3.0E-4	0.01136	1	0.07%	regulated secretory pathway
2.9E-4	0.01136	2	0.15%	NADP metabolism
3.0E-4	0.01136	1	0.07%	cortical cytoskeleton organization and biogenesis
2.9E-4	0.01136	2	0.15%	FADH2 metabolism
3.0E-4	0.01136	1	0.07%	gap junction assembly
3.5E-4	0.01275	3	0.22%	regulation of vasoconstriction

Figure 4.1.8 Biological functions of **A)** immortal clone upregulated (>1 fold), **B)** senescence clone upregulating (>1 fold) **C)** pre-senescence clone upregulated (>1 fold) gene lists. Biological processes with a corrected p<0.05 were considered as significant.

4.1.6 Identification of the role of senescence and immortality genes in HCC

In order to understand the role of senescence and immortality related genes in HCC development and molecular heterogeneity; we integrated the senescence/immortal Huh7 microarray data and liver tissue microarray data. A member of our group, Ayca Arslan-Ergul, has generated *in vivo* microarray data using 37 freshly frozen cirrhosis and HCC samples (20 cirrhosis, 17 HCC). Affymetrix GeneChip HG-U133 plus2 chip was used for global expression analysis. The raw data was analyzed using BRB Array Tools, and significant gene list were obtained using t-test (p<0.05). We identified 10185 probesets that displayed differential expression between cirrhosis and tumor samples. Next, we integrated significant probesets generated from *in vitro* cell line and *in vivo* clinical samples (Figure 4.1.9). 1909 probesets were found to be common (**senescence and immortality gene network:SIGN**).

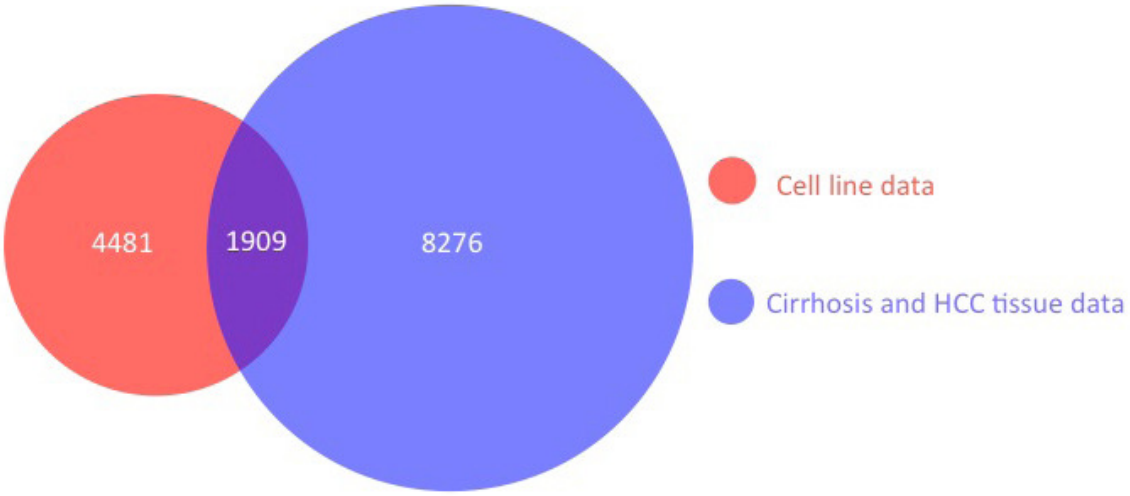

Figure 4.1.9 Venn diagram of probesets selected by two-tailed unpaired Welch's t test and class comparison test in BRB array tools from in vitro cell line and in vivo tissue analysis data, respectively. Red circle represents number of probesets differentially expressed between pre-senescent, senescent and immortal cells (P < 0.05). Blue circle represents number of probesets differentially expressed between cirrhosis and HCC tissue samples (P < 0.05). A total of 1909 probesets that display differential expression in both cell lines and tissues was selected as SIGN probesets.

To test whether our cancer cell-derived probeset can discriminate between normal cell replicative senescence and immortality, we compared our Huh7 clone data with data reported

for human prostate epithelial cells (HPEC; Schwarze et al. 2002). Two major clusters were formed. Senescent Huh7 clones (C3S, G12S) clustered together with senescent and early senescent (growth-arrested, but not yet positive for SABG activity) HPEC (HPEC-ES/S). Immortal Huh7 clones (C1I and G11I) clustered together with HPEC immortalized by Human Papilloma Virus E7 oncoprotein (HPEC-I). Proliferating presenescent Huh7 clones (C3P, G12P) were clustered next to senescent cells, whereas proliferating HPEC (HPEC-P) were positioned next to immortal cells (Figure 4.1.10 A). The SIGN signature could successfully discriminate our immortal, pre- and senescent Huh7 clones, as well as senescent, early senescent and immortalized HPECs. The SIGN signature also separated cirrhosis and HCC samples into two major clusters. One cluster included 85% (17/20) of cirrhosis, and the other 71% (14/17) of HCC samples (data generated by Ayca Arslan-Ergul) (Figure 4.1.10 B). Cirrhosis and HCC have been considered as *in vivo* states of hepatocellular senescence and immortality, respectively. Hence, our *in vitro* and *in vivo* combined data identified a signature that could serve for classification of different hepatic lesions with respect to the states of senescence and immortality.

4.1.6.1 Molecular classification of HCC by the SIGN signature

Genomics and gene expression studies revealed that HCC is a heterogeneous disease that can be classified into different molecular subtypes (152). Recently, Boyault et al., (149) integrated genomic and gene expression data and classified HCCs into six distinct groups (G1 to G6). *TP53* and *CDKN2A* inactivation and chromosomal instability (immortality-associated events) were observed in G1-G3, but not in G4-G6 groups, strongly suggesting that senescence and immortality events may contribute to HCC heterogeneity. Therefore, we subjected this independent cohort of tumors to the SIGN signature analysis (65 samples, 1292 probe set). Unsupervised clustering with the SIGN signature generated two major clusters, each divided into two smaller clusters that we named as 1A, 1B, and 2A, 2B (Figure 4.1.11). Each SIGN signature cluster was highly enriched in a specific group of tumors. Cluster 1A (n=11 HCCs, three adenomas, and five non-tumor samples) was composed of G4 (78.9%), and G5 group (21.1%) of tumors. Non-tumor sample pools and adenoma samples of the G4 group formed two close sub-clusters under 1A. Cluster 1B (n=15 tumors) was composed of mainly G6 (53.3%) and G5 (40.0%) tumors. Cluster 2A (n=23) was composed of mainly G3 (30.4%), G1 (26.5%) and G2 (21.7%) tumors. Cluster 2B (n=8), similar to cluster 1A, was composed mostly (87.5%) of G4 tumors. Based on the major component tumor group(s) of each cluster, we concluded that clusters 1A and 2B were enriched G4 tumors. Class 1B in G6 and a G5,

and cluster 2A in G1-G3 tumors, respectively. The latter three groups were sub-clustered as G1, G2 and G3 tumors in sub-clusters 2A1, 2A2, and 2A3, respectively.

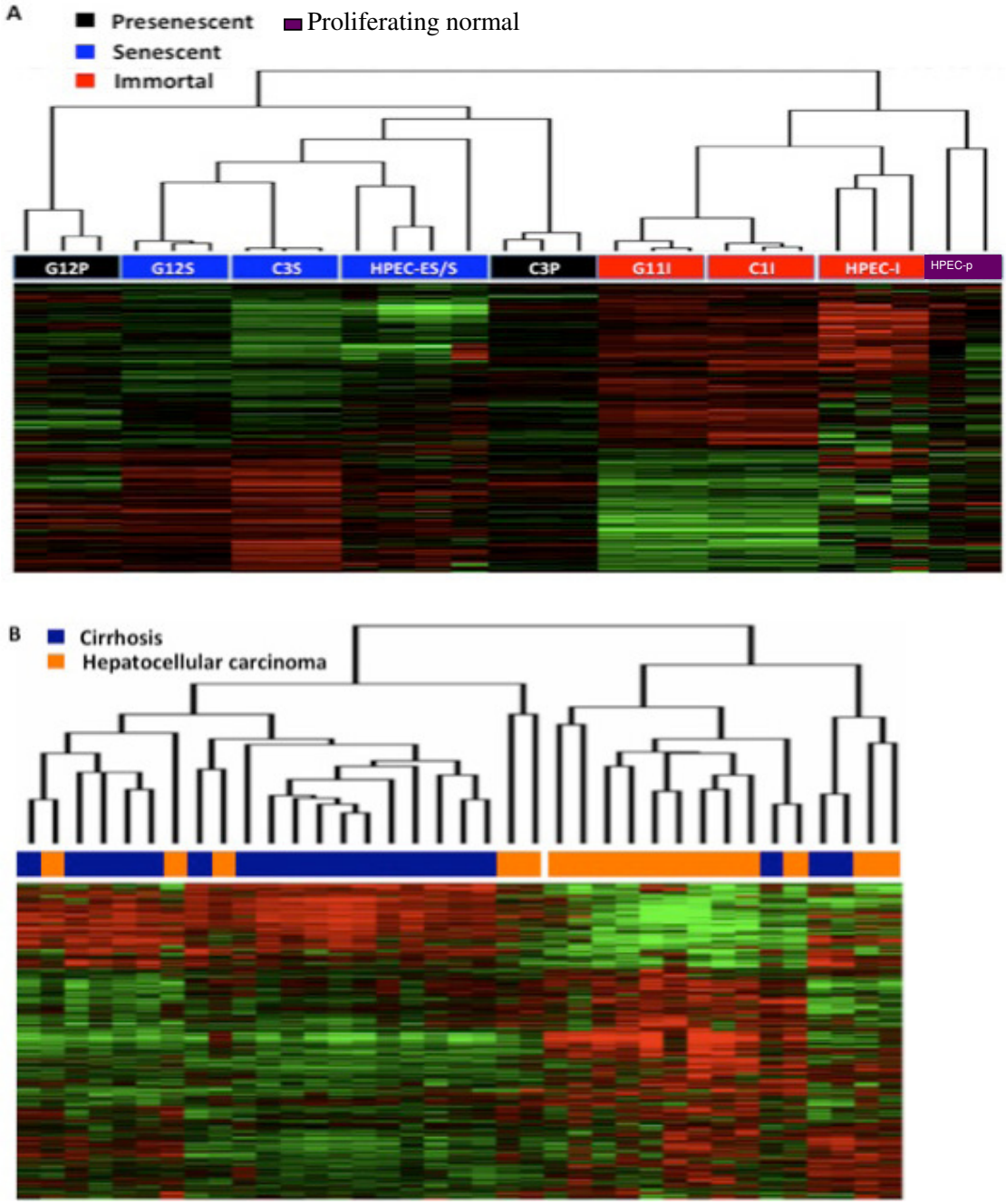

Figure 4.1.10 Hierarchical clustering of senescence-programmed and immortal cell lines, and cirrhosis and hepatocellular carcinoma (HCC) tissues, using the Senescence and Immortality Gene Network (SIGN) probeset. (A) Experimental dendrogram showing the clustering of Huh7-derived clones and human prostate epithelial cells (HPEC) into immortal, presenescent and senescent clusters (top). (B) Experimental dendrogram showing the clustering of tissue samples into cirrhosis and HCC subgroups (top).

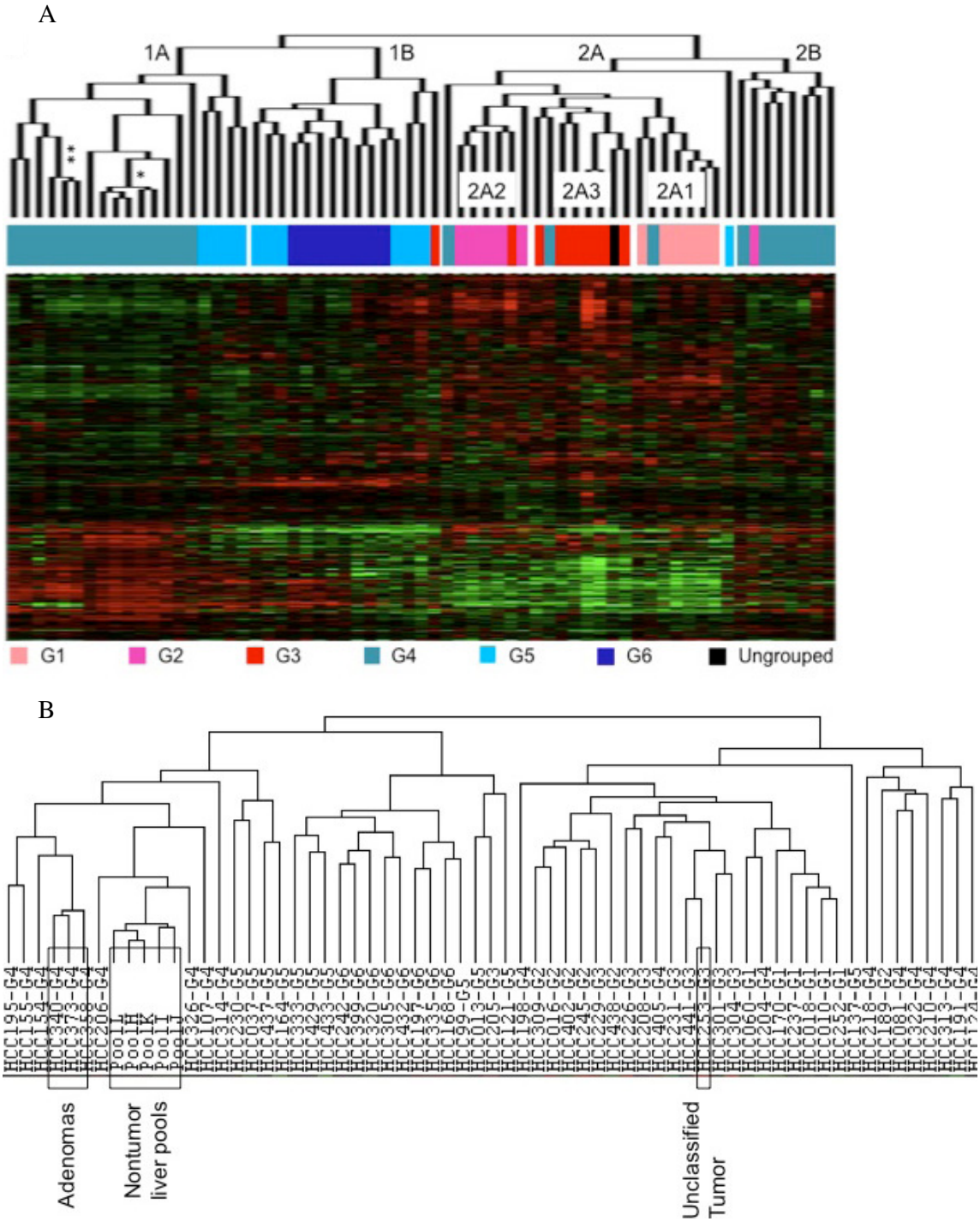

Figure 4.1.11 The SIGN signature separates hepatocellular carcinomas (HCCs) into distinct sub-clusters with differential expression of senescence- and immortality-associated genes. (A) Hierarchical clustering of gene expression data from Boyault et al. (2007). Experimental dendrogram showing the clustering of hepatocellular carcinoma (HCC) tissues into four major clusters, identified as 1A, 1B, 2A and 2B, respectively, and three

minor clusters, identified as 2A1, 2A2 and 2A3, respectively. The correlation with SIGN clusters and previously identified HCC groups (G1 to G6) was also shown. *non-tumor liver tissue pools; **adenoma samples (top). (1292 gene probesets and 65 tissue samples).

The reclassification of molecular groups of HCC according to the SIGN signature provided us with preliminary evidence that senescence- and immortality-associated genes may play an important role in HCC heterogeneity. To test this hypothesis, we first compared the newly described HCC SIGN classes according to relative contributions of senescence- and immortality associated genes. We used the classifier probesets generated by the binary tree analysis (Figure 4.1.12 A and Appendix D) to select genes that displayed a >1.5-fold change between senescent and immortal cells (p value cut-off for binary tree analysis was 0.001). The ratios of the number of senescence- and immortality-associated genes between HCC classes were compared (Figure 4.1.12 B). A comparison of "normal-like" class 1A tumors with class 2B tumors did not show any significant difference ($P = 1$), indicating that these two classes of tumors share the same or a similar SIGN signature. In contrast, class 1B tumors displayed a significant enrichment of immortality-associated genes in comparison with class 1A and 2B tumors ($P < 0.0004$). The class 2A tumors, containing the most advanced HCC samples, which formed a distant class from the other three groups, were also highly enriched in immortality-associated genes ($P < 2X10^{-7}$). Taken together, these findings strongly suggest that hepatocellular immortality plays a major role in HCC heterogeneity. Tumors of class 1A and 2B were the least enriched, and class 2A tumors the most enriched in immortality associated gene expression, with class 1B tumors in an intermediate position.

A

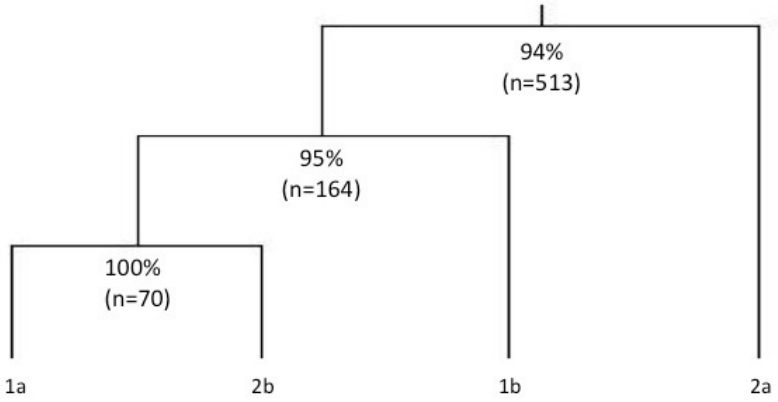

B

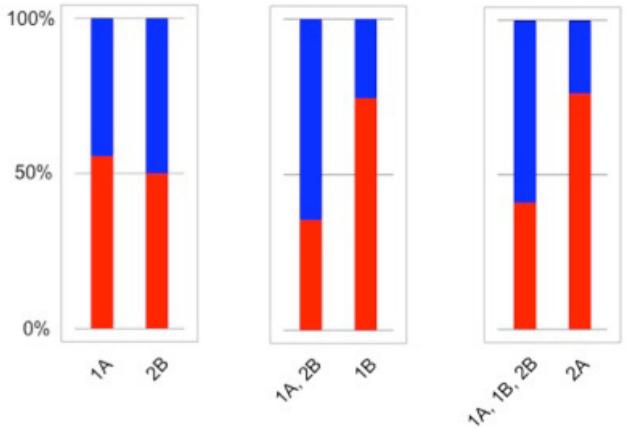

Figure 4.1.12 Binary analysis and senescence-immortality associated gene rate of Boyault groups A) Classification of 65 HCC, 3 adenoma, and 5 non-tumor samples obtained from Boyault et. al, by binary tree analysis using SIGN probe sets. 513 probe sets discriminated the 2a from 1a, 2b, and 1b with 94% accuracy, 164 probe sets discriminated the 1b from 1a, 2b with 95% accuracy, and 70 probe sets discriminated the 1a from 2b with 100% accuracy (Appendix D) **B)** Differential expression of senescence- and immortality-associated genes between different SIGN classes of HCC. Genes with more than 1.5-fold expression change between senescence arrested and immortal cells were identified by binary tree comparison of different tumors, and data were presented as % ratios of senescence-up-regulated (blue) and immortality-up-regulated (red) genes.

The integration of senescence- and immortality-associated gene expression data with in vivo tissue data provided us a unique opportunity to address the contribution of senescence- and immortality-related biological processes to HCC. First of all, the SIGN signature was overlaid onto a global molecular network developed from information contained in the Ingenuity Pathways Knowledge Base. Networks of these focus genes were then algorithmically generated based on their connectivity. The most significant network was a protein network which is called "DNA Replication, Recombination, Repair, Gene Expression, Cancer that includes 33 proteins. The second network was "Cancer, Gastrointestinal Disease, Cell Cycle" network again containing 33 proteins (Figure 4.1.13 A and B).

For identifying the biological processes characterizing different SIGN classes of HCC, we first performed a pair-wise class comparison analysis at two different significance levels ($P < 0.001$ and $P < 0.01$). Next we used these datasets to perform a DAVID Functional Gene Cluster Analysis. Normal-like class 1A tumors were used as a reference. As summarized in Table 4.1.3, class 2B tumors down-regulated monocarboxylic acid metabolism genes. Compared to class 2B, class 1B tumors up-regulated chromosome organization, DNA

metabolism and cell cycle genes. These tumors showed also down-regulation of genes involved in wounding response and carboxylic acid metabolism. Compared to class 1B, class 2A tumors displayed a generalized down-regulation of intermediary metabolism genes (genes involved in beta-oxydation, fatty acid, sulfure amino acid, amino acid derivative metabolism/catabolism, amine metabolism/catabolism, and xenobiotic metabolism). Major up-regulated processes in these tumors were cell proliferation (cell cycle, checkpoint, mitosis, DNA replication), RNA metabolism (splicing and transcription), chromosome organization, and DNA damage response.

A

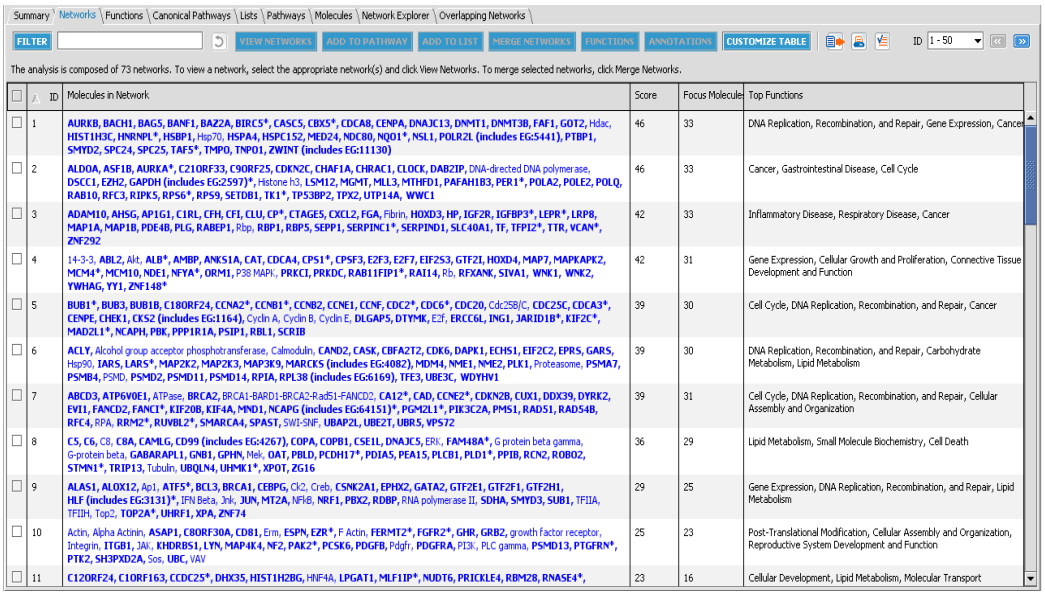

Summary | Networks | Functions | Canonical Pathways | Lists | Pathways | Molecules | Network Explorer | Overlapping Networks

FILTER | VIEW NETWORKS | ADD TO PATHWAY | ADD TO LIST | MERGE NETWORKS | FUNCTIONS | ANNOTATIONS | CUSTOMIZE TABLE | ID 1 - 50

The analysis is composed of 73 networks. To view a network, select the appropriate network(s) and click View Networks. To merge selected networks, click Merge Networks.

ID	Molecules in Network	Score	Focus Molecules	Top Functions
1	**AURKB, BACH1, BAG5, BANF1, BAZ2A, BIRC5*, CASC5, CBX5*, CDCA8, CENPA, DNAJC13, DNMT1, DNMT3B, FAF1, GOT2,** Hdac, **HIST1H3C, HNRNPL*, HSBP1,** Hsp70, **HSPA4, HSPC152, MED24, NDC80, NQO1*, NSL1, POLR2L (includes EG:5441), PTBP1, SMYD2, SPC24, SPC25, TAF5*, TMPO, TNPO1, ZWINT (includes EG:11130)**	46	33	DNA Replication, Recombination, and Repair, Gene Expression, Cancer
2	**ALDOA, ASF1B, AURKA*, C21ORF33, C9ORF25, CDKN2C, CHAF1A, CHRAC1, CLOCK, DAB2IP,** DNA-directed DNA polymerase, **DSCC1, EZH2, GAPDH (includes EG:2597)*,** Histone h3, **LSM12, MGMT, MLL3, MTHFD1, PAFAH1B3, PER1*, POLA2, POLE2, POLQ, RAB10, RFC3, RIPK5, RPS6*, RPS9, SETDB1, TK1*, TP53BP2, TPX2, UTP14A, WWC1**	46	33	Cancer, Gastrointestinal Disease, Cell Cycle
3	**ADAM10, AHSG, AP1G1, C1RL, CFH, CFI, CLU, CP*, CTAGE5, CXCL2, FGA,** Fibrin, **HOXD3, HP, IGF2R, IGFBP3*, LEPR*, LRP8, MAP1A, MAP1B, PDE4B, PLG, RABEP1,** Rbp, **RBP1, RBP5, SEPP1, SERPINC1*, SERPIND1, SLC40A1, TF, TFPI2*, TTR, VCAN*, ZNF292**	42	33	Inflammatory Disease, Respiratory Disease, Cancer
4	14-3-3, **ABL2,** Akt, **ALB*, AMBP, ANKS1A, CAT, CDCA4, CPS1*, CPSF3, E2F3, E2F7, EIF2S3, GTF2I, HOXD4, MAP7, MAPKAPK2, MCM4*, MCM10, NDE1, NFYA*, ORM1,** P38 MAPK, **PRKCI, PRKDC, RAB11FIP1*, RAI14,** Rb, **RFXANK, SIVA1, WNK1, WNK2, YWHAG, YY1, ZNF148***	42	31	Gene Expression, Cellular Growth and Proliferation, Connective Tissue Development and Function
5	**BUB1*, BUB3, BUB1B, C18ORF24, CCNA2*, CCNB1*, CCNB2, CCNE1, CCNF, CDC2*, CDC6*, CDC20,** Cdc25B/C, **CDC25C, CDCA3*, CENPE, CHEK1, CKS2 (includes EG:1164),** Cyclin A, Cyclin B, Cyclin E, **DLGAP5, DTYMK,** E2f, **ERCC6L, ING1, JARID1B*, KIF2C*, MAD2L1*, NCAPH, PBK, PPP1R1A, PSIP1, RBL1, SCRIB**	39	30	Cell Cycle, DNA Replication, Recombination, and Repair, Cancer
6	**ACLY,** Alcohol group acceptor phosphotransferase, Calmodulin, **CAND2, CASK, CBFA2T2, CDK6, DAPK1, ECHS1, EIF2C2, EPRS, GARS,** Hsp90, **IARS, LARS*, MAP2K2, MAP2K3, MAP3K9, MARCKS (includes EG:4082), MDM4, NME1, NME2, PLK1,** Proteasome, **PSMA7, PSMB4,** PSMD, **PSMD2, PSMD11, PSMD14, RPIA, RPL38 (includes EG:6169), TFE3, UBE3C, WDYHV1**	39	30	DNA Replication, Recombination, and Repair, Carbohydrate Metabolism, Lipid Metabolism
7	**ABCD3, ATP6V0E1,** ATPase, **BRCA2,** BRCA1-BARD1-BRCA2-Rad51-FANCD2, **CA12*, CAD, CCNE2*, CDKN2B, CUX1, DDX39, DYRK2, EVI1, FANCD2, FANCI*, KIF20B, KIF4A, MND1, NCAPG (includes EG:64151)*, PGM2L1*, PIK3C2A, PMS1, RAD51, RAD54B, RFC4,** RPA, **RRM2*, RUVBL2*, SMARCA4, SPAST,** SWI-SNF, **UBAP2L, UBE2T, UBR5, VPS72**	39	31	Cell Cycle, DNA Replication, Recombination, and Repair, Cellular Assembly and Organization
8	**C5, C6,** C8, **C8A, CAMLG, CD99 (includes EG:4267), COPA, COPB1, CSE1L, DNAJC5,** ERK, **FAM48A*,** G protein beta gamma, G-protein beta, **GABARAPL1, GNB1, GPHN,** Mek, **OAT, PBLD, PCDH17*, PDIA5, PEA15, PLCB1, PLD1*, PPIB, RCN2, ROBO2, STMN1*, TRIP13,** Tubulin, **UBQLN4, UHMK1*, XPOT, ZG16**	36	29	Lipid Metabolism, Small Molecule Biochemistry, Cell Death
9	**ALAS1, ALOX12,** Ap1, **ATF5*, BCL3, BRCA1, CEBPG,** Ck2, Creb, **CSNK2A1, EPHX2, GATA2, GTF2E1, GTF2F1, GTF2H1, HLF (includes EG:3131)*,** IFN Beta, Jnk, **JUN, MT2A,** NFkB, **NRF1, PBX2, RDBP,** RNA polymerase II, **SDHA, SMYD3, SUB1,** TFIIA, TFIIH, Top2, **TOP2A*, UHRF1, XPA, ZNF74**	29	25	Gene Expression, DNA Replication, Recombination, and Repair, Lipid Metabolism
10	Actin, Alpha Actinin, **ASAP1, C80RF30A, CD81,** Erm, **ESPN, EZR*,** F Actin, **FERMT2*, FGFR2*, GHR, GRB2,** growth factor receptor, Integrin, **ITGB1,** JAK, **KHDRBS1, LYN, MAP4K4, NF2, PAK2*, PCSK6, PDGFB,** Pdgfr, **PDGFRA,** PI3K, PLC gamma, **PSMD13, PTGFRN*, PTK2, SH3PXD2A,** Sos, **UBC,** VAV	25	23	Post-Translational Modification, Cellular Assembly and Organization, Reproductive System Development and Function
11	**C12ORF24, C1ORF163, CCDC25*, DHX35, HIST1H2BG,** HNF4A, **LPGAT1, MLF1IP*, NUDT6, PRICKLE4, RBM28, RNASE4*,**	23	16	Cellular Development, Lipid Metabolism, Molecular Transport

B

Network 1

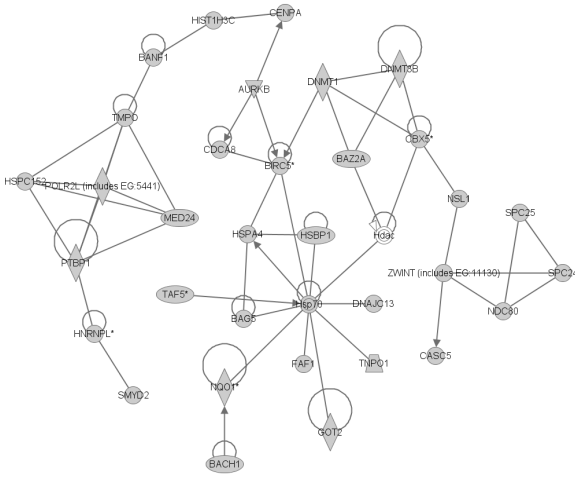

Network 2

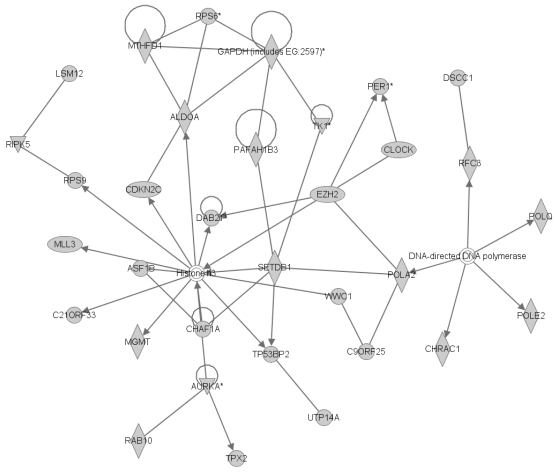

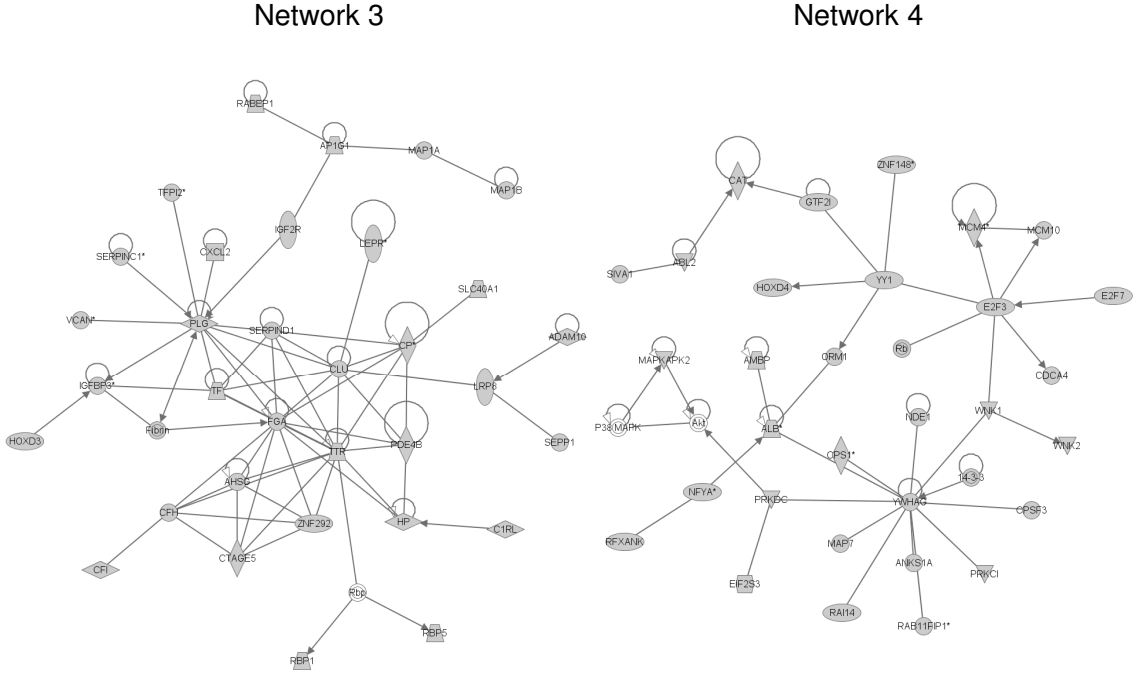

Figure 4.1.13 The protein networks generated through the use of Ingenuity Pathway Analysis. A) This is the list of networks. The SIGN data set containing gene identifiers was uploaded into in the application. Each gene identifier was mapped to its corresponding gene object in the Ingenuity Pathways Knowledge Base. B) First 4 networks generated by SIGN signature. Networks of these focus genes were algorithmically generated based on their connectivity.

Table 4.1.3 Biological pathways affected in hepatocellular carcinoma classes according to SIGN

SIGN Classes	1A Normal-like	2B	1B		2A		
					2A1	2A2	2A3
SIGN Pathways		⇓ Carboxylic acid metabolism	⇑ Chromosome organization ⇑ DNA metabolism ⇑ Cell cycle ⇓ Wounding response ⇓ Carboxylic acid metabolism		⇑ Cell proliferation (cell cycle, checkpoint, mitosis, DNA replication) ⇑ RNA metabolism (splicing and transcription) ⇑ Response to DNA damage ⇑ Chromosome organization ⇓ Lpid metabolism (fatty acid, beta-oxydation) ⇓ Amino acid metabolism and catabolism ⇓ Amine metabolism and catabolism ⇓ Xenobiotic metabolism		
Boyault Groups (Ref. 27)	G4		G5	G6	G1	G2	G3
Genetic & Epigenetic Changes	*TCF1* mut. Chromosomal stability		*CTTNB1* mut. Chromosomal stability *CDH1* methylation	*CTTNB1* mut. Chromosomal stability *CDH1* methylation	*AXIN1* mut. LOH 4q, 16p, 16q Chromosomal instability	*TP53*, *AXIN1* mut. *PIK3CA* mut. LOH 4q, 13q, 16p, 17p Chromosomal instability	*TP53* mut. LOH 4q, 5q, 16p, 17p, 21q 22q Chromosomal instability *CDKN2A* methylation
Biological Pathways			⇑ Wnt-β-catenin ⇓ Stress & immune response	⇑ Wnt-β-catenin ⇑Amino acid metabolism ⇓ E-cadherin	⇑Developmental & imprinting genes, ⇑ IGF2 ⇑Mitotic cycle	⇑ Akt ⇑Mitotic cycle	⇑ Cell cycle ⇑ Nuclear pore ⇑Mitotic cycle

4.1.6.2 DNA damage response genes as potential therapeutic targets

We repeatedly observed the upregulation of DNA damage response genes in different steps and classes of HCC. Although some genes such as TOP2A have been already associated to HCC (153), the role of these genes in HCC remains elusive. Therefore, we further analyzed the expression changes of DNA damage response genes (154). We compared two major classes of SIGN classes of HCC; normal-like 1A tumors versus chromosome instable 2A tumors. We identified 31 genes up-regulated in 2A class tumors, 14 of which were involved in DNA damage checkpoint. These tumors also over-expressed nine base-excision, seven nucleotide-excision, six double-strand break and five mismatch repair genes (Table 4.1.4).

Table 4.1.4 Up-regulation of DNA damage response genes

Genes	Checkpoint	DSBR	BER	NER	MMR	Other	HCC vs. Cirrhosis	SIGN 2A vs. SIGN 1A
BARD1	(+)						(+)	(+)
BAX	(+)						(+)	(+)
CCNA2	(+)						(+)	(+)
CDC2	(+)						(+)	(+)
CHEK1	(+)						(+)	(+)
CHEK2	(+)						(+)	
DTL	(+)						(+)	
DYRK2	(+)						(+)	(+)
GTSE1	(+)						(+)	
H2AFX	(+)						(+)	(+)
RAD1	(+)						(+)	
KIN	(+)						(+)	(+)
POLE2	(+)		(+)	(+)			(+)	(+)
SFN	(+)						(+)	(+)
SMC3	(+)						(+)	(+)
BRCA1	(+)	(+)					(+)	
BRCA2	(+)	(+)					(+)	
DCLRE1A	(+)	(+)					(+)	
MRE11A	(+)	(+)					(+)	(+)
RAD50	(+)	(+)					(+)	
PRKDC	(+)	(+)					(+)	(+)
EME1	(+)	(+)					(+)	
SUPT16H	(+)	(+)					(+)	(+)
FANCD2	(+)	(+)					(+)	
FANCA		(+)					(+)	
FANCG		(+)					(+)	(+)
FANCI		(+)					(+)	(+)
NSMCE2		(+)					(+)	
PRPF19		(+)					(+)	(+)
RAD51		(+)					(+)	
RAD54B		(+)					(+)	
RAD54L		(+)					(+)	
SMC6		(+)					(+)	
BRIP1		(+)					(+)	
HMGB1		(+)	(+)	(+)	(+)		(+)	
NEIL3			(+)				(+)	
PARP1			(+)				(+)	(+)
PARP2			(+)				(+)	(+)
LIG1			(+)	(+)			(+)	(+)
PCNA			(+)	(+)			(+)	(+)
POLD3			(+)	(+)	(+)		(+)	(+)
RFC3			(+)	(+)			(+)	(+)
RFC4			(+)	(+)			(+)	(+)
RUVBL2			(+)				(+)	
FEN1			(+)				(+)	(+)
CUL4A				(+)			(+)	
GTF2H1				(+)			(+)	(+)
MCM7					(+)		(+)	(+)
MSH2					(+)		(+)	(+)
MSH6					(+)		(+)	
PMS1					(+)		(+)	
TIMELESS					(+)		(+)	(+)
UBR5					(+)		(+)	(+)
EXO1					(+)		(+)	
ALKBH2						(+)[1]	(+)	
CEBPG						(+)[2]	(+)	
CHAF1A						(+)[3]	(+)	
ESCO1						(+)[4]	(+)	
NUDT1						(+)[5]	(+)	
POLQ						(+)[6]	(+)	
TDP1						(+)[7]	(+)	
TOP2A						(+)[8]	(+)	(+)
UHRF1						(+)[9]	(+)	
UPF1						(+)[10]	(+)	

DSBR: Double-strand break repair; BER: base-excision repair; NER: nucleotide-excision repair; MMR: DNA mismatch repair.

[1]Direct repair, [2]Repair gene expression, [3]Chromatin assembly, [4]Acetyl transferase-sistercohesion, [5]Hydrolyzes oxidized purine nucleoside triphosphate, [6]Translesion synthesis, [7]SSB repair, [8]DNA breakage & rejoining, [9]AcHvates TOP2A expression, [10]DNA and RNA helicase

4.2 Expression analysis of E2F/DP family in senescence and immortality, and senescence association of DP-2

4.2.1 Differential expression of E2F/DP family genes in senescent and immortal hepatocellular carcinoma cells

To understand the involvement of E2F/DP family members in senescence and immortality of liver; we, first, performed unsupervised hierarchical cluster analysis of E2F/DP family genes using our microarray data of immortal, pre- and senescent Huh7 clones. As shown in figure 4.2.1 A, pair-wise complete-linking hierarchical raw-cluster classified family members in two groups. The first group of genes composed of *E2F1, E2F2, E2F7, E2F6, E2F5, E2F8*, and *DP1* displayed increased expression in immortal clones. The second group of genes composed of *E2F3a, E2F4* and *DP2* displayed increased expression in pre-senescent and/or senescent cells.

In order to confirm differential expression of E2F/DP family genes in immortal and senescent cells, we quantified their relative expression levels by real-time PCR assay. Triplicate samples from immortal C1 and G11 clones, and senescence-arrested C3 and G12 clones were tested in parallel experiments. These studies confirmed the up-regulation of *E2F1, E2F5, E2F7, E2F8* and *DP1* in immortal clones and the up-regulation of *E2F3a* and *DP2* in senescent clones (>2 fold changes; Figure 4.2.1 B). The correlation efficiency of Q-PCR data with microarray data was 80%.

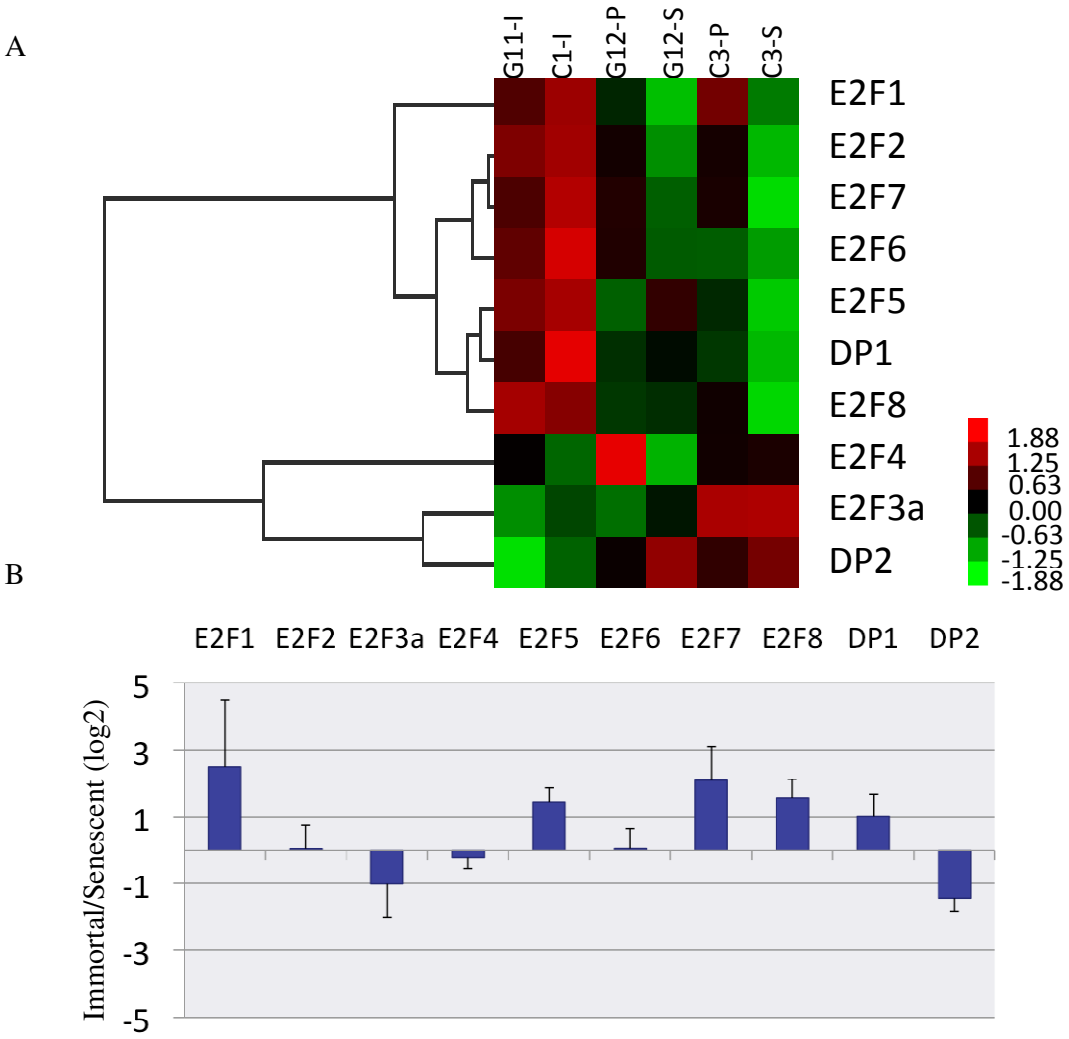

Figure 4.2.1 Differential expression of E2F and DP family members in immortal, presenescent and senescent cells derived from Huh7 cell line. A) Treeview image of hierarchical cluster analysis of *E2F1-8* and *DP1,2* probe sets extracted from the Affymetrix HG-U133 plus expression microarray experiment of immortal (G11-I and PC1-I), pre-senescent (G12-P and PC3-P) and senescent (G12-S and PC3-S) clones. Red: up-regulation, green: down-regulation and black: no change B) Quantitative RT-PCR analysis of *E2F1-8* and *DP1/DP2* transcripts in immortal (G11-I and PC1-I) and senescent (G12-S and PC3-S) clones. Immortal/senescent ratio refers to fold changes, expressed as log (2) transformed. The G and C clones were analyzed separately. Error bars represent the standard deviations of 3 independent experiments with 2 groups of immortal (G11-I and PC1-I) and senescent (G12-S and PC3-S) clones. The mRNA samples used for the Q-PCR analysis were from the different cell vials from the mRNA samples used in microarray study. Primer efficiencies were given in Table 3.4.

4.2.2 Expression analysis of differentially regulated E2F/DP genes in HCC cell lines

Next, we quantified the expression of differentially regulated E2F/DP genes in a set of 13 HCC cell lines. Relative expression levels were represented as fold changes from the expression levels observed in senescent C3 cells, and immortal C1 cells were used as positive control (Figure 4.2.2). As shown in figure 4.2.2, *E2F1, E2F5, E2F7, E2F8* and *DP1* genes that displayed increased expression in immortal cells showed highly variable expression in HCC cell lines. *E2F1, E2F7* and *DP1* genes were up-regulated in the majority (>8/13) of cell lines. But the expressions of *E2F5* and *E2F8* showed a decrease rather than an increase in the same set of cell lines. *E2F3a* and *DP2* genes that displayed a loss of expression in immortal cells were also studied in HCC cell lines. The expression of *E2F3a* showed an increase rather than a decrease in almost all cell lines tested. The observations with *DP2* were the most striking, as they indicated a consistent deficit in expression in all 13 HCC cell lines tested. This suggested that loss of *DP2* expression was strongly associated with immortal phenotype of HCC cells.

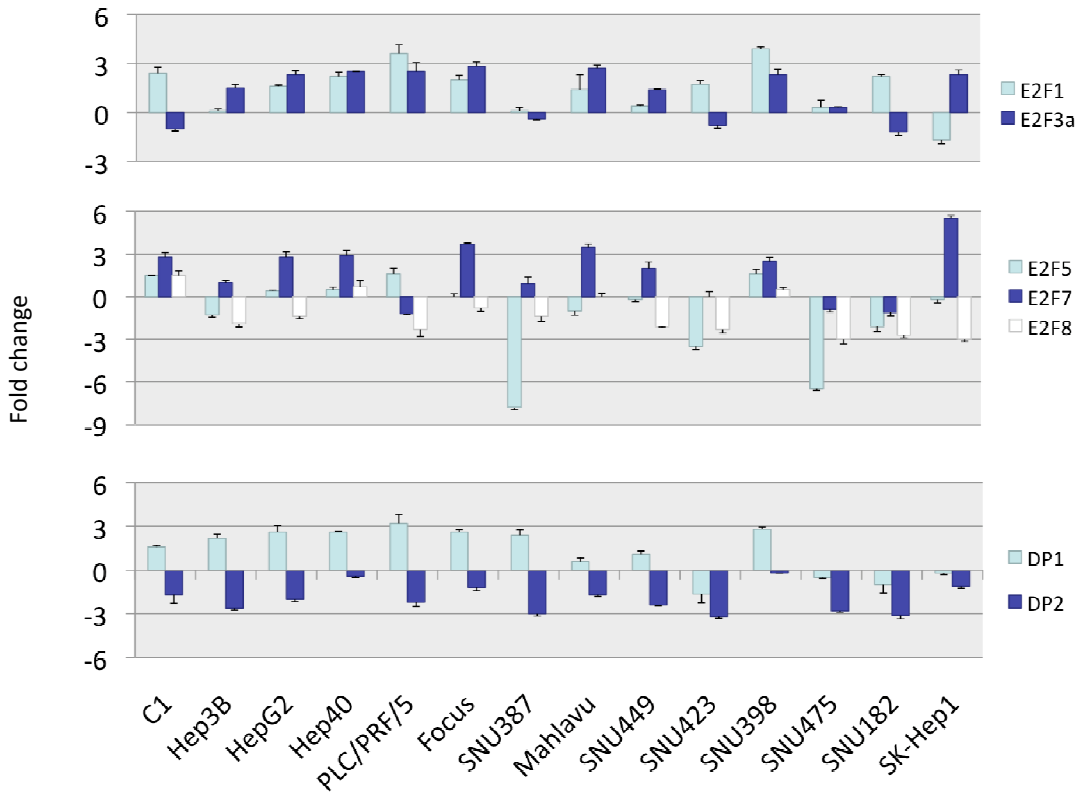

Figure 4.2.2 mRNA expression levels of differentially regulated *E2F/DP* genes in HCC cell lines compared to senescent cells, as tested by quantitative RT-PCR. Fold change refers

to log (2) transformed values of each cell line, as normalized to expression level of C3 senescent cells. Error bars represent the standard deviations of 3 independent experiments.

4.2.3 DP2 protein is abundant in senescent clone but lost in immortal clone

Based on transcript expression data, we decided to further explore the expression status of *DP-2* gene in HCC. We first performed DP2 analysis by immuocytochemistry. Strong nuclear staining was observed in C3 cells at both pre-senescent (C3-P) and senescent (C3-S) states, whereas immortal C1 cells (C1-I) displayed only weak nuclear staining with the exception of mitotic cells (Figure 4.2.3 A). In order to confirm the association of DP-2 positivity with senescence, we also performed double staining. Immortal C1 (C1-I) and senescent C3 (C3-S) cells were first subjected to senescence-associated β-galactosidase (SABG) staining, followed by immunostaining with anti-DP-2 antibody. Immortal cells were negative for both SABG and nuclear DP-2 staining, but senescent cells were positive for both staining (Figure 4.2.3 B). We also performed DP-2 immunostaining on NHEPs (primary human hepatocytes) at culture days 1 and 5, and observed very strong nuclear positivity (Figure 4.2.3 C). Immunoperoxidase staining results of the HCC cell lines were compatible with Q-PCR results. For example, Hep3B and SNU387 cells did not display significant staining, but Hep40 and SNU398 cells displayed weakly positive heterogeneous staining (Figure 4.2.3 D).

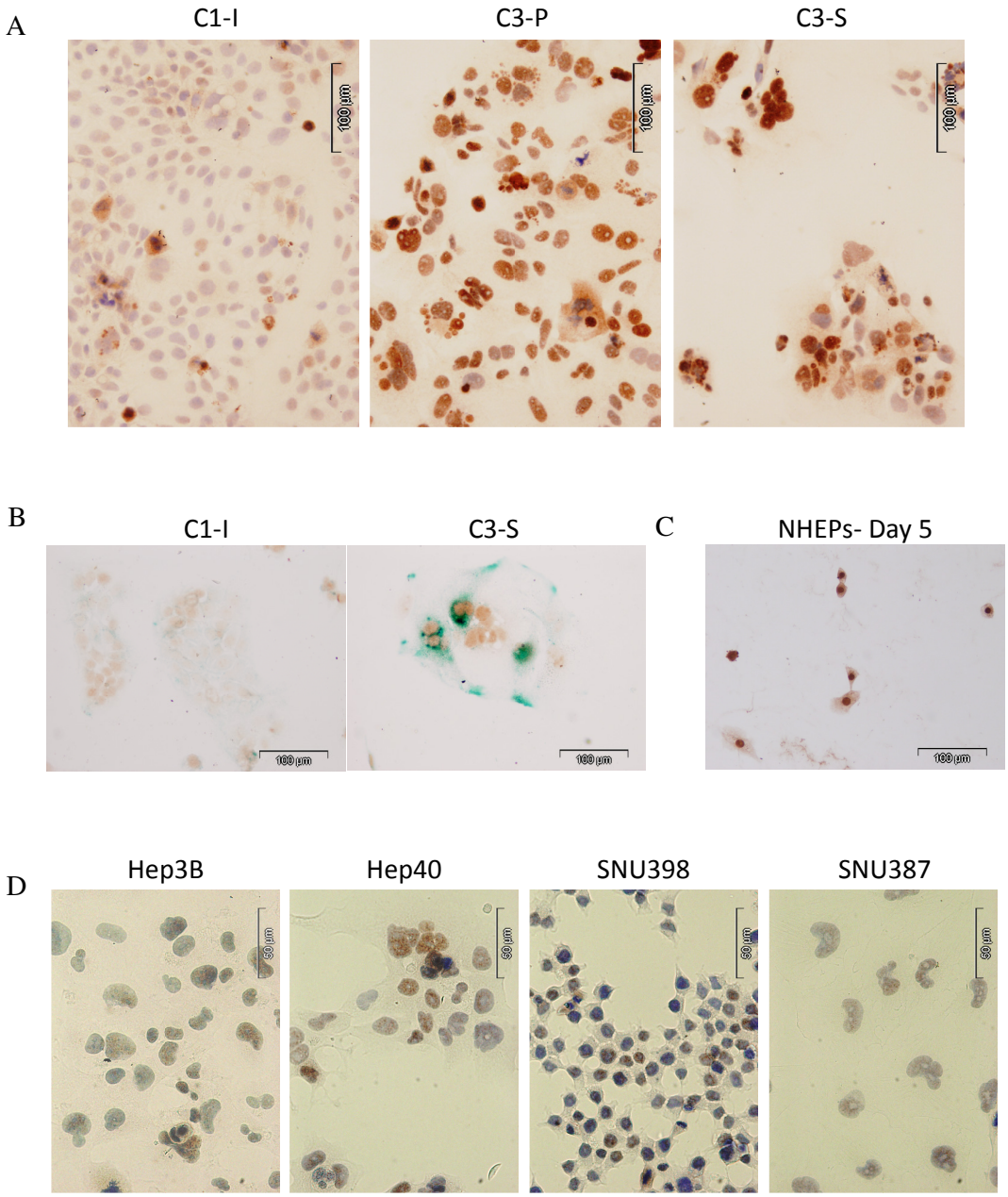

Figure 4.2.3 DP-2 immunostaining; shows increased expression in pre-senescent (C3-P) and senescent (C3-S) cells, as compared to immortal (C1-I) cells. A) Immunoperoxidase staining with anti-DP2 antibody (brown); counter-staining with hematoxylene. B) Senescence-associated β-galactosidase (blue) and anti-DP-2 antibody (brown) co-staining assay indicates that nuclear DP-2 staining is associated with senescence. C) Nuclear DP-2 staining using four different HCC cell lines.

Next, we performed western blot analysis to identify DP2 isoforms expressed in immortal, senescent and NHEPs (normal human hepatocyte cells). Human cells express at least three DP2 isoforms (55, 49 and 43 kDa, respectively), as reported previously (83).

Senescent C3 cells (C3-S) expressed 49 kDa and 43 kDa isoforms, but dominantly 43 kDa isoform. Immortal C1 cells (C1-I) showed decreased expression in total protein level. They decreased the expression of 43 kDa isoform dramatically and displayed a rather increased expression of 49 kDa isoform (Figure 4.2.4 A). NHEPs expressed the 49 kDa isoform and 43 kDa isoform very weakly, however we observed unidentified bands around 60-65 kDa in NHEPs. Moreover, we saw the same bands in some cirrhosis and HCC samples (Figure 4.2.4 B). We concluded that the 49 and 43 kDa isoforms of DP-2 protein may be associated with immortality and senescence respectively. This isoforms may be regulated differentially in different phases of cell cycle also.

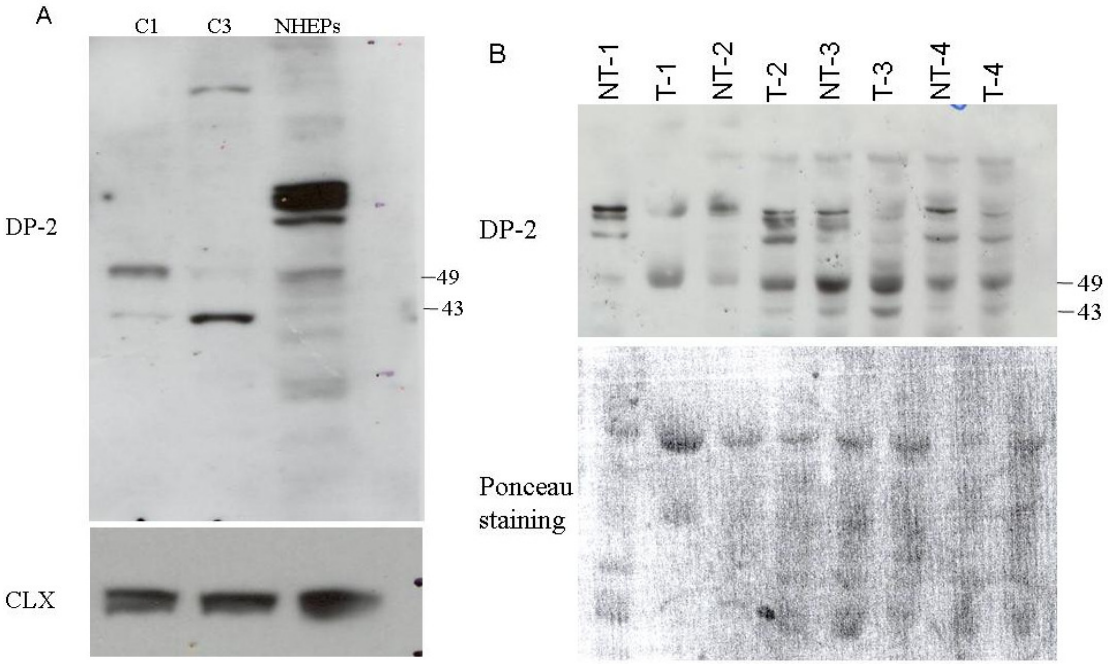

Figure 4.2.4 Expression analysis of DP-2 protein A) western blot analysis with whole cell extracts identified 49 kDa and 43 kDa DP-2 isoforms in C1, C3 and NHEPs cells. Previously un-identified bands were detected in NHEPs (normal human hepatocyte cells). Calnexin (Clnx) was used as a loading control. **B)** western blot analysis of DP-2 in 4 pairs of cirrhosis-HCC tissue samples. Extra bands were detected in tissue samples also.

4.2.4 Examination of the DP-2 isoforms in different cell cycle conditions and upon TGF-β treatment

Based on western blot data indicating that 43 kDa isoform is the major form expressed in senescence cells, and 49 kDa protein become dominant in immortal cells, we hypothesized

that different DP-2 isoforms may be regulated differentially during cell cycle. In order to test this hypothesis, we used LiCl (lithium chloride) which is known to stop cell cycle in G1 phase. When LiCl containing medium is replaced with fresh medium, cells continue to progress through the cell cycle (155). We treated the C1-I (immortal) cells with LiCl-containing medium for 4 days, as well as with NaCl as a control. At the end of 4th day, we stopped the NaCl treated plate and one LiCl-treated plate, which we called time 0. We have supplied the other plates with fresh medium and stopped one vial at 6th, 12th, 24th, and 30th hours. We observed that the levels of 49- and 43 kDa protein changes in different hours of cell cycle (Figure 4.2.5 A). We, then, wanted to examine the levels of the two isoforms in a different type of senescence model. In our group, it has been, recently, identified that most of the liver cancer cell lines enter into senescence upon TGF-β treatment (Serif Senturk, unpublished data). TGF-β treated and non-treated C1-I and parental Huh7 cell lysates were subjected to DP-2 immunoblot analysis. As shown in 4.2.5 B, the small isoform was expressed very strongly in TGF- β treated Huh7 cells, whereas long isoform couldn't be detected. On the other hand, non-treated control cells were observed to express long isoform, and very weakly small isoform. In C1-I cells, again, short isoform became strongly dominant when the cells were treated with TGF- β, just like C3-S (senescent) clone. We concluded that upon senescence arrest, the 43 kda DP-2 protein is dominantly expressed and may have potential role in senescence arrest.

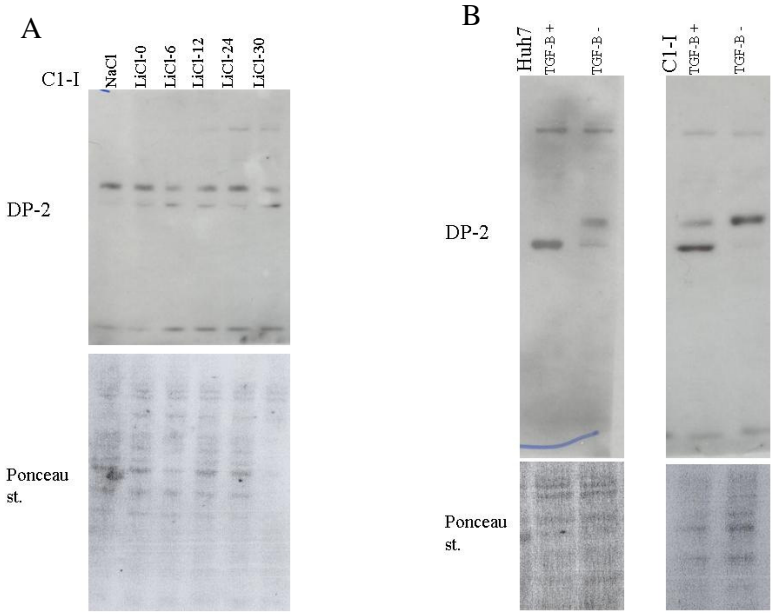

Figure 4.2.5 Western blot analysis of DP-2 in LiCl and TGF- β treated cells. A) Cell cycle synchronization of C1I cells with LiCl identified that the 43- and 49 kDa proteins are

regulated differentially in different time-points. LiCl: lithium chloride, NaCl: sodium chloride. Equal loading was indicated as ponceau staining of the same membrane before blotting. **B)** TGF-β treatment differentiates the dominantly expressed DP-2 protein in Huh7 and C1I cells.

4.3 Epigenetic changes in immortality and senescence of liver *in vitro* and *in vivo*

4.3.1 Differential expression of histone modifying enzyme genes in senescent and immortal hepatocellular carcinoma cells

Based on our observation indicating that expression of epigenetic related gene groups are changing between senescent and immortal Huh7 clones, we hypothesized that epigenetic changes may play an important role in this cell fate determination. We, first, searched for significant histone methylating and de-methylating enzymes in our *in-vitro* microarray data. We, then, grouped these genes according to their expression values (Figure 4.3.1 A). Raw cluster analysis revealed two distinct groups; up-regulated enzymes in immortal and pre- and late senescence. *JMJD4-3-* and *2B, MLL3, JARID1B, FBXL11, ASH1L, SUV420H1, SMYD2, HSPBAP1, SETD5, PRDM1* and *SETD2* were grouped together as senescence associated genes. On the other hand, immortality associated enzymes were *JMJD1C, KIAA1718, MINA, EZH2, CARM1, PRMT1, PRDM16, UTX,* and *WHSC1*. For Q-PCR validation was performed for the enzymes that have known histone residue targets. Microarray results were confirmed for all tested enzymes, except *UTX* (Figure 4.3.1.B). The correlation efficiency of Q-PCR data with microarray data was 92%.

A

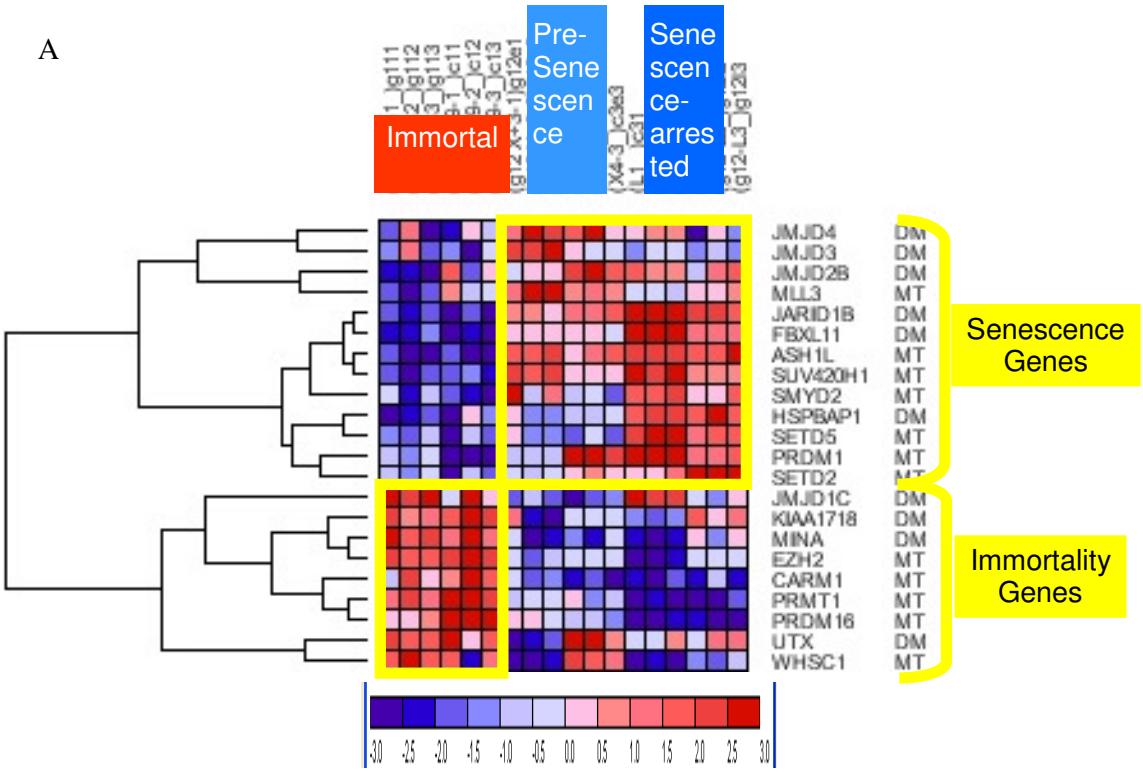

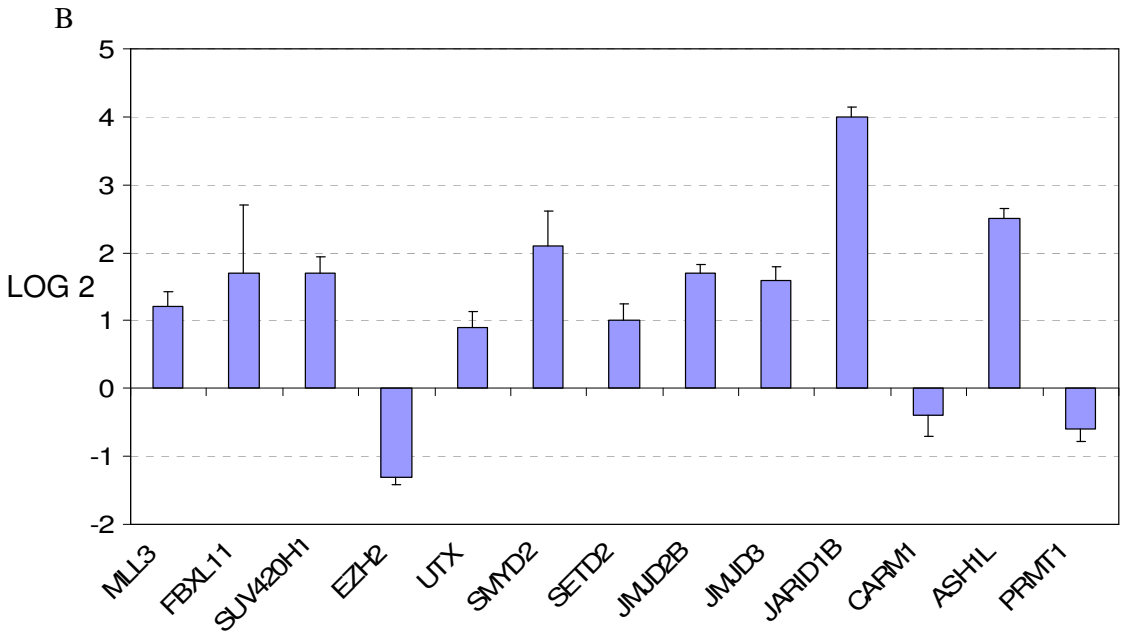

Figure 4.3.1 **Expression analysis of histone methyltransferases and de-methylases in immortal and senescence Huh7 clones. A)** gene-based clustering of enzymes generated two groups. Image has been performed using GenePattern software. Red: up-regulation, blue: down-regulation. Scaled-bar was shown below. **B)** Selected histone methyltransferases and de-methylases in senescent cells compared to immortal cells, as tested by quantitative RT-PCR. Fold change refers to log (2) transformed values. Error bars represent the standard deviations of 3 independent experiments. The mRNA samples used for the Q-PCR analysis were from the different cell vials from the mRNA samples used in microarray study. Primer efficiencies were given in Table 3.4.

4.3.2 Histone methylation changes between immortal and senescent Huh7 clones

We, then, compared histone modification patterns of N-terminal tails of histone 3 and 4 in immortal, pre- and late-senescent Huh7 clones. We used antibodies against specific methylation residues of lysine (K) and arginine (R) aminoacids of H3 and H4. We, first, used immunocytochemistry to asses methylation levels of H3K4me3, H3K9me1- and 3, H3K27me1- and 3, H3K36me1- and 3, H3K79me3, H4K20me3, H3R2me2a (asymmetric), H3R17me2a, H4R3me2a in clones. We obtained positive signal for all the residues tested, except H3K79me3. In pre- and late-senescent Huh7 clones, H3K27me1, H3K36me3, and H4K20me3 were observed to be increased compared to immortal clone (Figure 4.3.2 A). Late-senescent clones had substantially more methylated status of H3K27me3, H3R4me2a,

and H4R3me2a compared to other clones (Figure 4.3.2 B). Moreover, H3K27me3 and H3R2me2a residues increased gradually from immortal to late-senescent cells. The staining intensity of H4R3me2a was very weak. We could observe no marked differences in the methylation levels of H3K4me3, H3K9me1- and 3, H3K36me1, H3R17me2a (Figure 4.3.2 C).

A

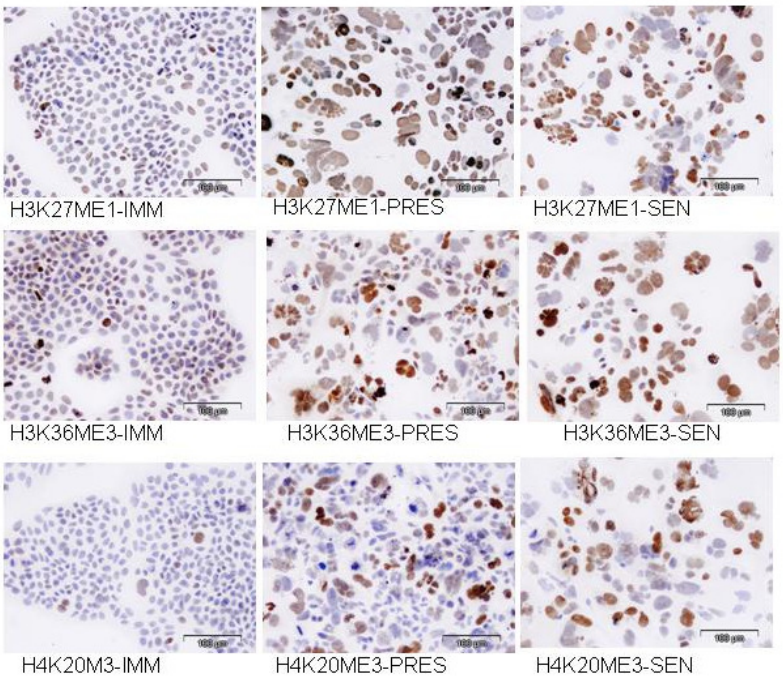

B

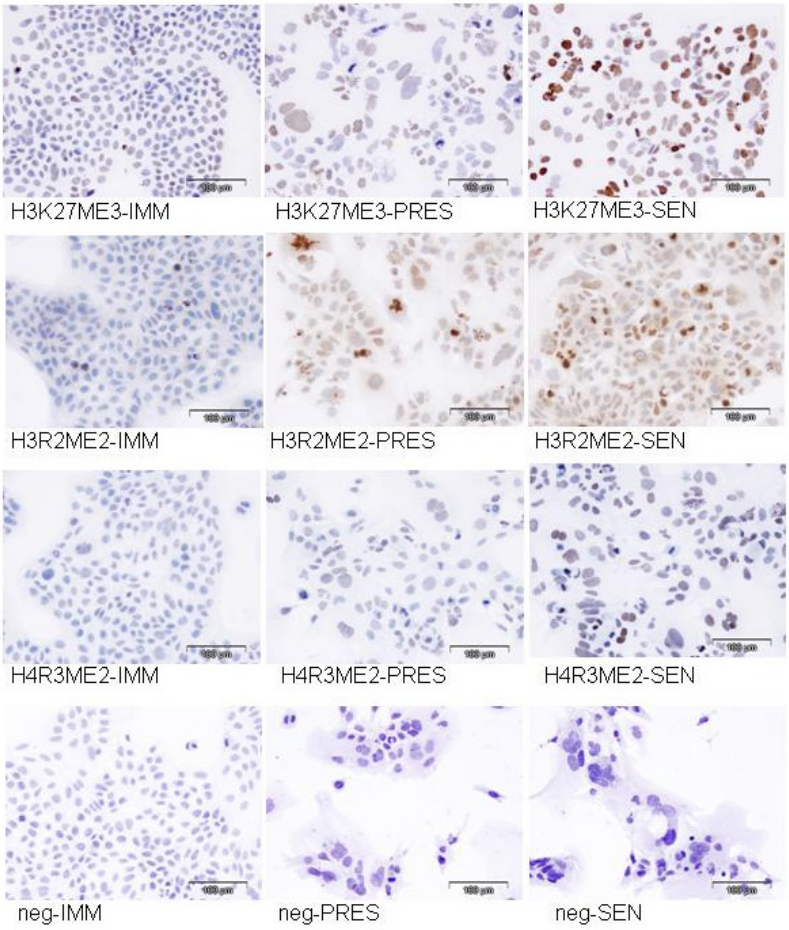
H3K27ME3-IMM
H3K27ME3-PRES
H3K27ME3-SEN
H3R2ME2-IMM
H3R2ME2-PRES
H3R2ME2-SEN
H4R3ME2-IMM
H4R3ME2-PRES
H4R3ME2-SEN
neg-IMM
neg-PRES
neg-SEN

C

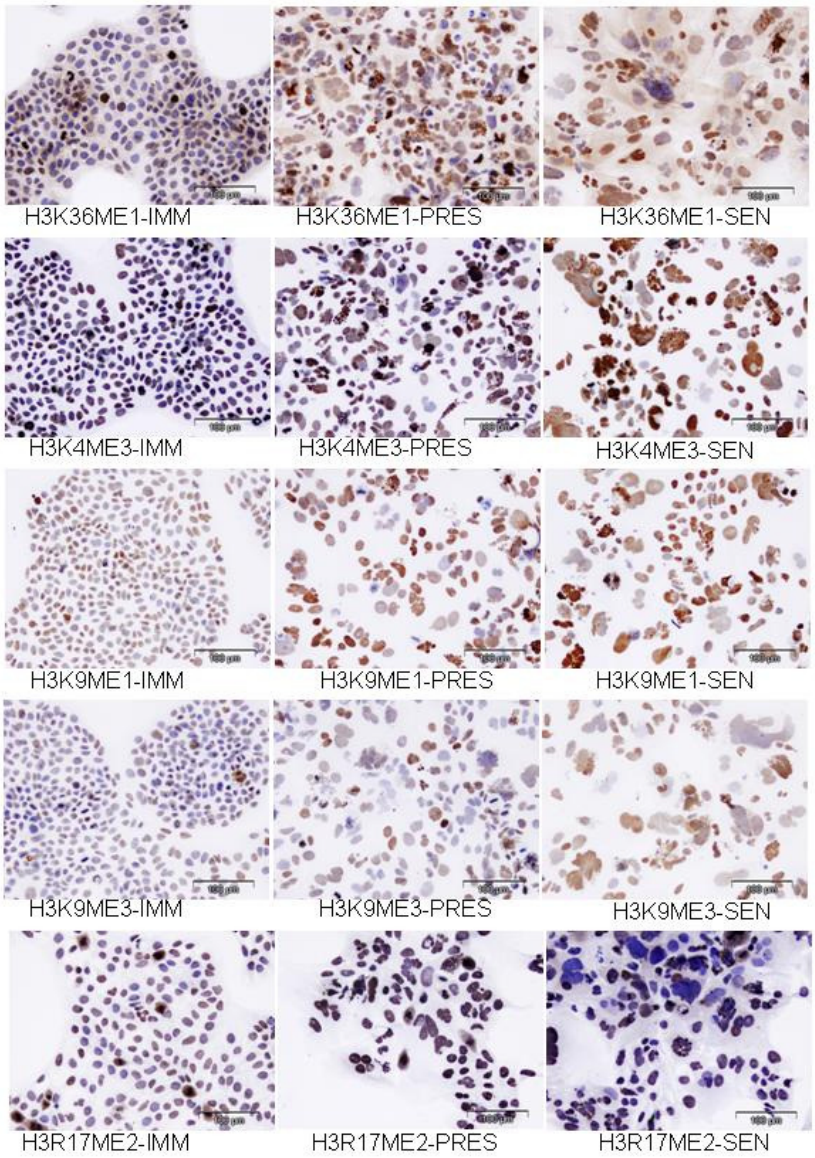

Figure 4.3.2 Histone methylation status of H3 and H4 tail modifications in immortal, pre- and senescent cells. A) Immonoperoxidase images of histone methyl residues over-representing in senescent clone (brown) **B)** in both pre- and senescent clones (brown). **C)** The histone methylation statuses that do not show any marked change. Counter staining was performed with Mayer's heamotoxylene (blue). H: histone, K: lysine, R: arginine, me: methyl.

We, also, carried out the same analysis in an other senescence model. We tested the same histone residues on hTERT immortalized, proliferating (PDL 45), and replicative senescent (PDL 65) MRC5, a human fibroblast cell line. We observed marked increase of H3K27me1- and 3, H4K20me3, H3R2me2a and H4R3me2a in replicative-senescent arrested fibroblasts compared to hTERT immortalized and proliferating normal fibroblasts (Figure 4.3.3). On the other hand, senescent MRC5 cells showed enhanced H3K9me1- and 3 levels when we compared the staining intensity just with proliferating MRC5. We concluded that H3K27me1- and 3, H4K20me3, H3R2me2a and H4R3me2a residue changes may discriminate immortal cells from senescence-arrested cells. Histone 3 lysine 9 methylation changes were only observed between replicative senescent and its normal proliferating counterpart, indicating that this residue may be regulated specifically in replicative senescence.

A

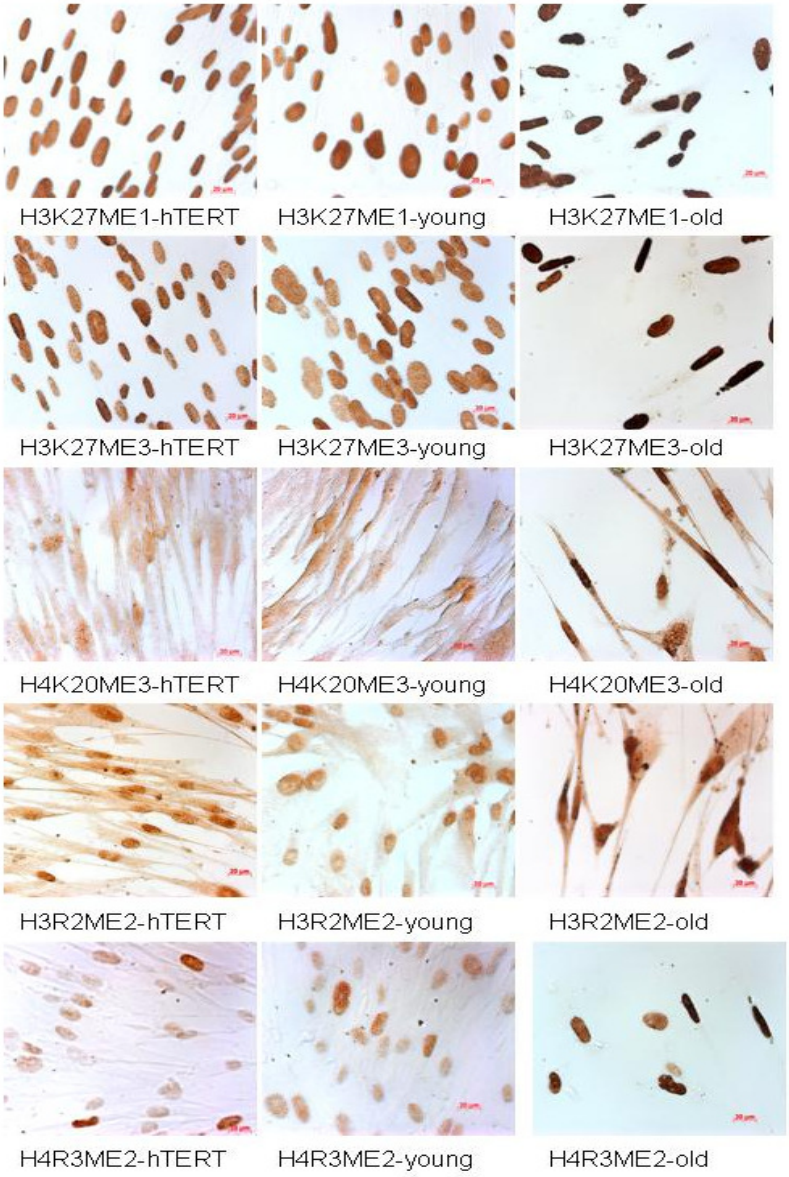
H3K27ME1-hTERT
H3K27ME1-young
H3K27ME1-old
H3K27ME3-hTERT
H3K27ME3-young
H3K27ME3-old
H4K20ME3-hTERT
H4K20ME3-young
H4K20ME3-old
H3R2ME2-hTERT
H3R2ME2-young
H3R2ME2-old
H4R3ME2-hTERT
H4R3ME2-young
H4R3ME2-old

B

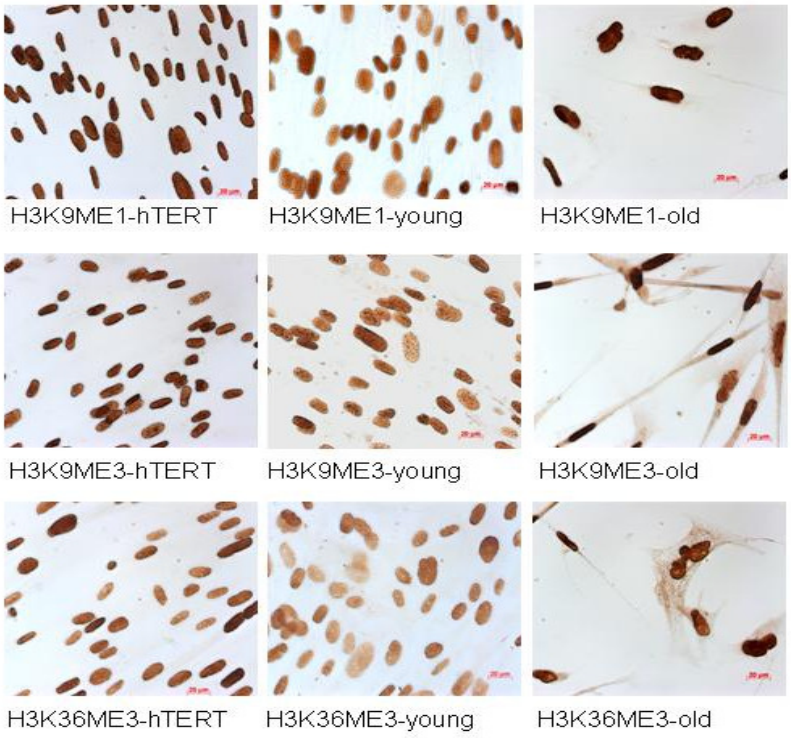

Figure 4.3.3 Immunoperoxidase analysis of histone methylation residues in replicative senescence model of MRC5. A) Immunoperoxidase images of residues which show clear over-representation in late replicative senescence compared to both proliferating normal and hTERT immortalized MRC5s. **B)** Images of residues which show change between proliferating normal and late senescent cells. (brown: positive signal). Young: MRC5 PDL (population doubling) 45, old: MRC5 PDL65.

4.3.3 Does histone methylation levels differ *in-vivo*?

As we indicated before, immortal and senescent cells may represent tumor and cirrhosis stages of liver cancer. We hypothesized that histone methylation may be amended in the tumorigenesis process of liver. To test this hypothesis, we performed immunohistochemistry analysis with the antibodies of residues which were observed to change *in-vitro*. We have collaborated with Dr. Funda Yılmaz in Ege University Department of Pathology for the staining of selected histone residues on formalin fixed paraffin-embedded normal liver, cirrhosis, and HCC tissue samples. All five histone methylation residues tested (H3K27me3, H4K20me3, H3K36me3, H3R17me2a, H4R3me2a) showed homogenous and ubiquitous nuclear positivity in all normal livers (n=10). This kind of staining was called as pattern 1 (Figure 4.3.4 A). Whereas, more heterogeneous pattern with local or dispersed loss of nuclear positivity (pattern 2) has been obtained HCC for all residues tested, and in cirrhosis for

H4K20me3 and H3R17me2 (Figure 4.3.4 B). H3K36me3 and H3R17me2, also, showed apparent decrease in macro-regenerative nodules compared to micro-regenerative nodules. 10% of cirrhosis samples (n=13) lost the homogenous H3K27me3 positivity, whereas 33% of HCC (n=10) is observed to have decreased H3K27me3. Ubiquitous H4K20me3 nuclear staining was lost in 33% of cirrhosis samples, and 75% of HCC. H3K36me3 stained homogenously and ubiquitously in all cirrhosis samples, but this pattern was lost in 33% of HCC samples. Partial loss was observed in 25% and 66% of cirrhosis and HCC samples, respectively. 12% of cirrhosis samples lost their H4R3me2a, and 66% of HCC samples had decreased staining of this residue. The partial loss of H3K27me3, H4K20me3, H3K36me3 and H4R3me2a in HCC perfectly correlated with in-vitro findings performed with immortal and senescent Huh7 clones. These residues may be involved in aberrant regulation of oncogenes and tumor suppressors in HCC.

A

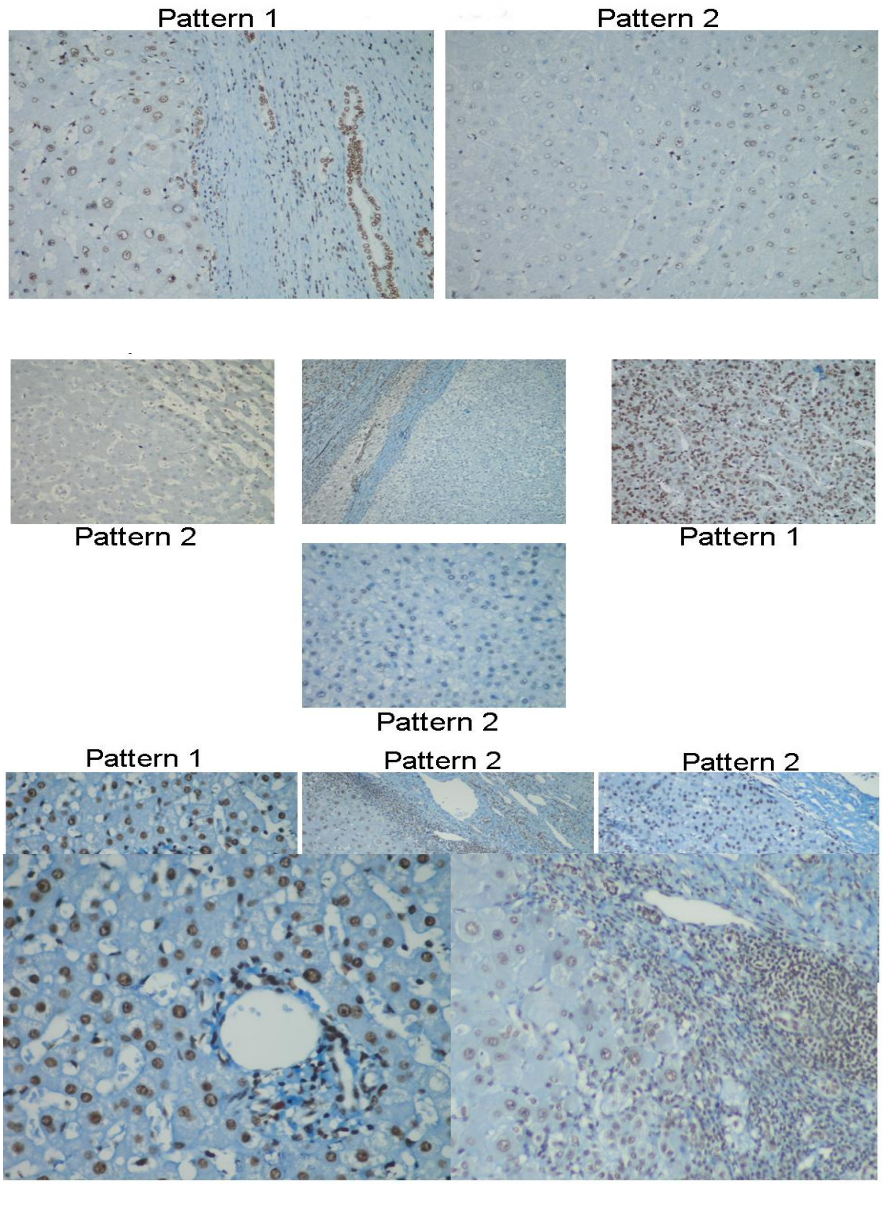
Pattern 1
Pattern 2
Pattern 2
Pattern 1
Pattern 2
Pattern 1
Pattern 2
Pattern 2

B

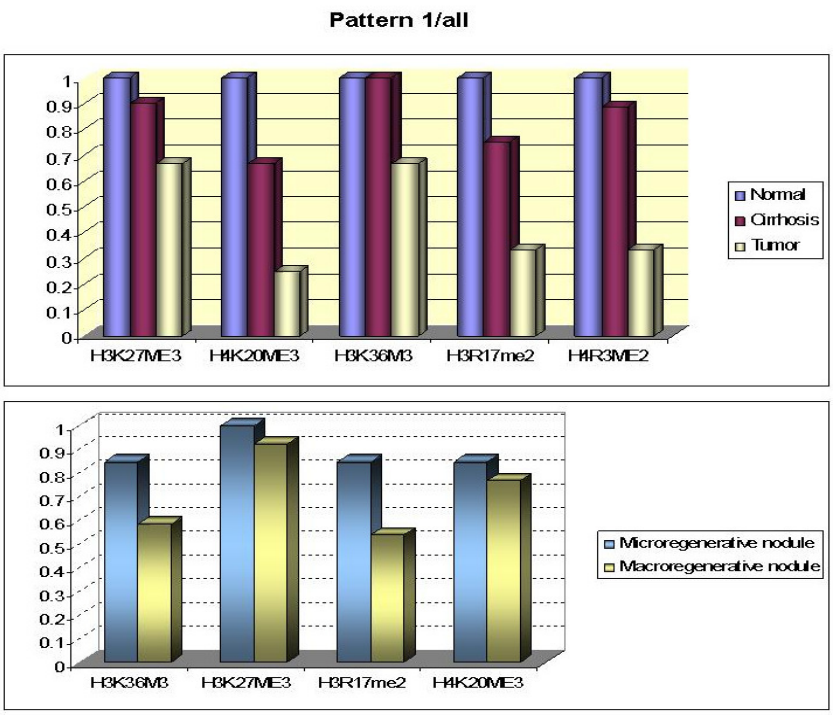

Figure 4.3.4 Histone mehtylation in *in-vivo* A) Example images of Pattern 1 and 2 staining. While analyzing the histone residue staining of tissue samples, we have used a nomenclature. Homogenously and strongly stained areas were named as "Pattern 1", on the other hand heterogeneous and weak staining, partial or local loss of nuclear positivity was called "Pattern 2". Top, and middle panel images were examples of H3K36me3 staining, bottom panel from H3R17me2a straining. **B)** Bar-chart representations of the results of immunohistochemistry counts of indicated histone residues. Y-axis values were calculated by dividing the number of pattern 1tissue samples to number of all tissue samples for a given histone residue and tissue type. A partial loss of the 5 residues tested in HCC samples was observed. Bottom chart represents the same counts comparing macro- and micro-regenerative nodules. H3K36me3 and H3R17me2a residues were observed to loss ubiquitous staining pattern in macro-regenerative nodules compared to micro-regenerative nodules.

4.3.4 Histone variant differences in immortal and senescent Huh7 cells

In order to test, whether the levels histone 2 variants differ between senescence and immortality; we carried out immunoperoxidase analysis of H2AX, H2AZ, macroH2A, and H2B variants in immortal, pre- and late-senescent Huh7 cells. The monoclonal antibodies were obtained from Dr. Stephan Dimitrov Lab in Institute Albert Bonniot in Grenoble.

Interestingly, H2AX and H2AZ were observed to increase dramatically in pre-senescence stage, and remain abundant in senescence (Figure 4.3.5A). mH2A variant, increased gradually from immortal to senescence cells. No marked difference was observed for H2B (Figure 4.3.5A). The three H2 variants, H2AX, H2AZ and mH2A, may be characteristic variants for our senescence model, and they may have functional roles in senescence arrest.

A

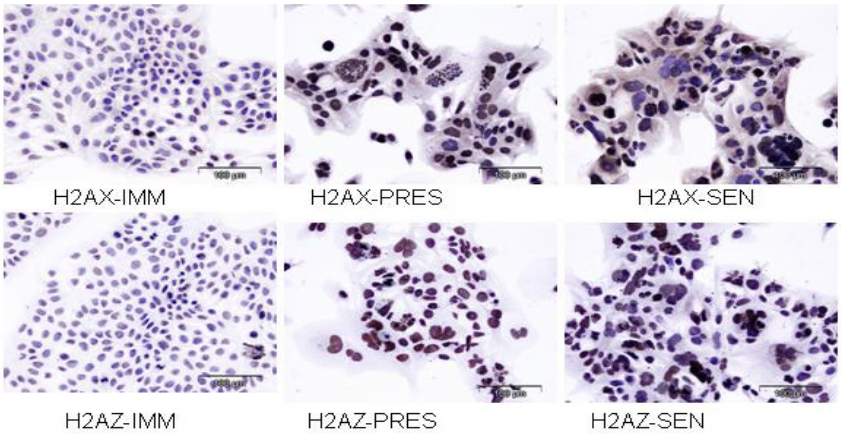

B

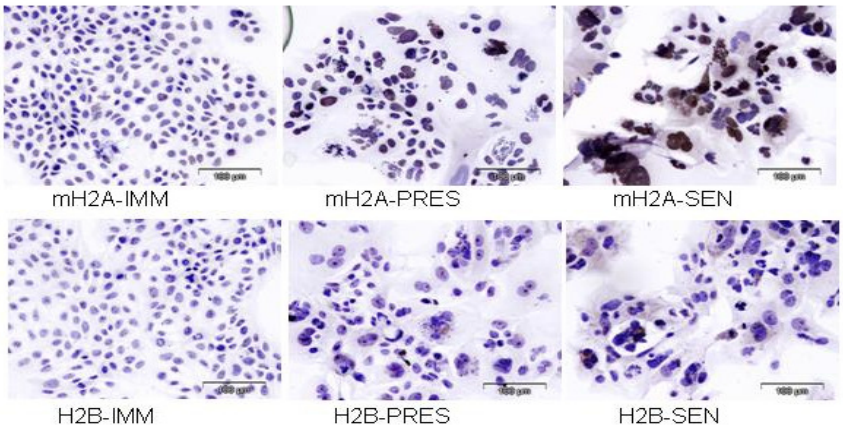

Figure 4.3.5 Histone variant levels of immortal, pre- and senescent cells. A) The histone 2 variants, H2AX and H2AZ, increased in pre-senescence level. B) mH2A increased in pre- and senescent cells gradually. H2B did not change significantly. Positive signal:brown, counter staining: Mayer's heamatoxylene.

CHAPTER 5. DISCUSSION

5.1 Global expression analysis of immortality and senescence in liver cancer

5.1.1 Identification of differentially expressed genes between immortal, pre- and senescent Huh7 clones

Hepatocellular carcinoma development is a multi-step process which takes more than 20 years. Hepatocellular senescence is a process gaining growing interest in the physiopathology field of chronic liver diseases (52), yet the observations are fragmented and somewhat contradictory. Telomere shortening and senescence have been observed in hepatocytes of cirrhotic liver, and replicative senescence was proposed as a key mechanism that contributes to cirrhosis development (136). Our previous observations provided experimental evidence for the generation of senescence-arrested clones from immortal HCC cell lines. Clonal C3 cells have displayed telomerase repression, progressive telomere shortening, and permanent growth arrest after ~80 PD with senescence associated morphological changes and positive SABG staining. Similar changes have also been observed with G12, another independently derived clone. Thus, we have concluded that immortal cancer cells have the intrinsic ability to reprogram the replicative senescence. As expected, this shift in cell fate resulted in a complete loss of tumorigenicity (61).

A complete set of genes associated with hepatocyte senescence and immortality was lacking. To better understand the molecular mechanisms of senescence switch from immortal cells, we, first, determined differentially expressed genes in presenescent, senescent and immortal clones derived from a well-differentiated HCC cell line; Huh7. Our analysis revealed large number of differentially expressed genes between groups, especially between immortal and pre-senescence, and immortal and senescence. This was suprising for the clones derived from the same cell line. We concluded that a genetic and phenotypic switch may be taking place from immortal cells. We, then, determined senescence and immortality-related biological processes and pathways. We observed a gradual increase in immune function and cellular stress related gene groups in pre- and late-senescence. Also, metabolism, nucleosome assembly and chromatin biogenesis and electron transport related genes were specifically enriched in pre- and late senescent cells. One of the most interesting finding was very significant upregulation of DNA repair genes in immortality. We hypothesized that over-expressed DNA repair genes may give a survival advantage to immortal clones that have high division rate. As expected, cell cycle, mitosis related and cell division gene groups were most

significantly up-regulated groups in immortal cells. We, also, observed up-regulation of E2F1 target genes. E2F1 is known to be a mediate proliferation and cell cycle progression. RNA splicing related genes was also up-regulated specifically in immortal cells. The implication and role of these gene groups in the immortal and senescence phases, as well as in cirrhosis and HCC remain to be elucidated.

We, also, examined the resemblance of the established senescence and immortality expression profiles of liver with expression profiles of senescence models in different cellular systems. Meta-analysis was performed with replicative senescence model in HPECs and an oncogene induced senescence model in IMR90 cells. The significant probe set of immortality and senescence could discriminate both replicative and oncogene-induced senescent cells from their immortalized counterparts. Replication induced early and late senescent HPEC cells were grouped together with C3S and G12S senescent Huh7 isogenic clones. Proliferating HPECs were enriched with pre-senescent C3P and G12P cells. On the other hand, C1 and G11 immortal Huh7 clones were grouped together with hTERT-immortalized HPECs. Furthermore; C3S, G12S and C3P, G12P Huh7 isogenic clones were clustered together with Mek:Erk and Mek:Erk-Small t-antigen induced senescent IMR90 cells, respectively. Mek:Erk-Small t-antigen-E6/7 transfected immortal cells were enriched with C1 and G11 immortal cells. These findings indicate that spontaneous induction of senescence in liver cancer cells share common genetic features with both replicative and oncogene induced senescence. These results may give us clue about existence of a common gene signature differentiating in all types and cellular models of senescent cells.

5.1.2 Establishing a senescence and immortality gene network signature for cirrhosis and hepatocellular carcinoma

To better understand the role of cellular senescence in hepatocellular carcinogenesis, we explored the expression of senescence- and immortality-associated genes in HCC and its preneoplastic lesions, including cirrhosis. Along with gene expression levels of pre-senescent, senescent and immortal clones, we also determined differentially expressed genes between liver cirrhosis and HCC (Ayca-Arslan Ergul). Then, we obtained a set of genes by integrating the cell line and tissue data to generate a “SIGN signature”. This signature was tested against independent clinical datasets to analyze the role of senescence and immortality genes in hepatocellular carcinogenesis and tumor heterogeneity. This novel approach allowed us to show that cellular senescence and immortality mechanisms are deeply involved in HCC.

The SIGN signature alone was able to classify a cirrhosis and HCC with high accuracy. The cirrhosis was significantly enriched in senescence genes in confirmation of previous observations describing cirrhosis as a state of cellular senescence (156). Hepatocellular carcinogenesis from cirrhotic lesions was associated with a significant increase in the ratio of upregulated immortality genes in HCC. This finding indicates that the transition from senescence to immortality is a progressive event in HCC.

The availability of large-scale genomic analysis and gene expression profiling methods contributed significantly to a better understanding of tumor heterogeneity and molecular classification of tumors (157). Here, we show that senescence and immortality genes play a major role in the molecular heterogeneity of HCC. We reclassified a recently described HCC cohort using SIGN signature. This cohort was initially classified into six groups (G1-G6) and is composed of tumors with well-characterized clinical and genetic characteristics (149). The SIGN signature identified four major (1A, 1B, 2A, 2B) and three minor (2B1, 2B2, 2B3) classes. The 1A class, which grouped nontumor and some HCC samples together, was a "normal-like" group. Class 2B did not differ significantly from 1A in terms of senescence and immortality gene balance, suggesting that class 2B tumors also may display normal-like, or minimally deviant phenotypes. These two classes were composed mostly from G4 tumors, which are characterized by chromosomal stability and lack of frequent gene mutations. In contrast, class 1B tumors, which differed from 1A and 2B by a significant increase of immortality-associated genes, included G5 and G6 tumors with chromosomal stability and high rates of *CTNNB1* mutations. Class 2A tumors displayed the highest rate of immortality-associated genes. G1, G2 and G3 tumors formed three subclasses within this class. These three groups have in common chromosomal instability, and they display *TP53* and *AXIN1* mutation at different frequencies. In addition, G3 tumors display *CDKN2A* promoter methylation. These genetic aberrations correlate with senescence bypass by checkpoint gene inactivation (*TP53* mutation, *CDKN2A* promoter methylation). Chromosome instability observed in these tumors strongly suggests that tumor cells have survived a "crisis" stage with telomere fusions giving rise to chromosomal aberrations. The upregulation of a large set of DDR genes in HCC, and the association of this process with tumor progression indicate that liver malignancy is associated with acquired ability to deal with DNA damage. This finding correlates with well-known resistance of HCCs to currently available therapies. Thus, although DNA repair deficiency increases tumor susceptibility in normal cells, increased repair capacity may be beneficial for tumor cells. It will be interesting to investigate whether DNA damage response genes that are upregulated in HCC may serve

as novel targets for combined therapies using DNA damaging agents together with DNA repair inhibitors. In summary, our findings demonstrate that senescence and its bypass (i.e. immortality) play a central role in human hepatocellular carcinogenesis as well as in the molecular classification of HCC. These findings may serve in designing new prognostic and therapeutic approaches.

5.2 DP-2 is associated with senescence

In this study, we first identified the member of E2F and DP families that are differentially expressed in senescent and immortal cells. Then, we showed that DP2 were consistently over-expressed in senescent cells. The availability of Huh7-derived isogenic clones with different cell fates allowed us to characterize differential expression of E2F/DP members in senescent and immortal cells. Potential implications of E2F and DP family members in senescence and immortality were addressed by comparative analysis of immortal and senescence-arrested Huh7 clones. Other HCC cell lines, immortal by definition were also analyzed for confirmation. Among 'activating' E2Fs required for S-phase entry, *E2F1* showed an almost consistent up-regulation in both immortal C1 cells and HCC cell lines. *E2F3a* also showed up-regulation in most HCC cell lines, although its expression was slightly higher in senescent clones compared to senescence-arrested cells. Over-expression of *E2F1* in HCC has already been reported (82), but the status of *E2F3a* in these cells was not known. Among 'repressive' E2F members that function in G0/G1 phase, *E2F5* was slightly up-regulated in immortal cells, but its expression was strongly inhibited in poorly differentiated SNU387, SNU423 and SNU475 cell lines with 3-8 fold decrease when compared to senescent cells. Thus, *E2F5* might be involved in growth repression in a subset of HCCs. A third group of *E2F* genes (*E2F6-8*) is believed to play also a 'repressive' effect, but their cellular functions are poorly known (69). *E2F7* and *E2F8* were slightly up-regulated in immortal cells, but only *E2F7* displayed increased expression in many, but not in all HCC cell lines, whereas the expression of *E2F8* was decreased in most HCC cell lines. Thus, loss of *E2F8* in HCC cells correlates with its known functions, but the over-expression of *E2F7* remains to be further explored.

DP family of DNA-binding genes encodes proteins interacting with both 'activating' E2F1-3a and 'repressive' E2F3b-6 proteins (69). In this study we observed opposite patterns of *DP1* and *DP2* expressions. *DP1* was up-regulated in immortal cells, and in most HCC cell lines, whereas *DP2* was consistently down-regulated in immortal and HCC cell lines. The respective roles of these proteins in E2F functions are poorly known. However, over-expression of *DP1* in HCC has been previously reported, and this correlates with its

hyperproliferative effects (158). Studies on the expression of *DP2* in cancer or immortal cells are limited. Based on our observations showing consistent decrease of *DP2* transcripts in immortal HCC cell lines, we decided to further explore this gene as a potential marker for liver malignancy. Our in vitro studies at the protein level showed strong nuclear expression in pre-senescent and senescent cells, as compared to weak expression in immortal cells. The Q-PCR and immunoperoxidase results were confirmed by western blot; total protein level of DP-2 protein was always observed to be higher in senescent cells compared to immortal cells. Western blot analysis showed that senescent cells express dominantly 43 kDa isoforms, which displayed decreased levels in immortal cells. On the other hand, 49 kDa isoform was observed to be very weakly expressed in senescent cells, but more abundant in immortal cells. The same shift was observed in TGF-β induced senescence model. We concluded that these two isoforms of DP-2 may be regulated differentially in senescence and immortality and play important roles in progression and/or maintenance of these phases. We, also, observed change in the amount of isoforms during different time periods of cell cycle. Previously, Van Der Sman *et. al*. observed that in G0, the anti-DP2 monoclonal antibody recognized 3 isoforms of apparent molecular masses of approximately 55, 48, and 43 kDa, and the faster migrating forms of each proteins predominated as cells entered G1 in B lymphocyte cells which supports our findings (159). In a study searching E2F and retinoblastoma protein in neuronal differentiation, total DP-2 protein was observed to increase dramatically in adult brain compared to embryos; the most interesting thing for our study was to see that small isoform was expressed in adult brain, and just big isoform was seen in embryonic neurons (87). It will be noteworthy to search whether small isoform is specific to terminally differentiated cells, whereas big isoform is expressed in stem cells. The pathways regulating different isoforms in immortal and senescence cells, and the molecuar functions of these proteins must be extensively studied. We have, also, observed slowly migrating bands in primary hepatocytes and tissue samples which we have not seen in cell line data. Whether these proteins are previously unidentified isoforms of DP-2 or not must be further elucidated.

5.3 Histone methylation levels of some H3 and H4 residues change in immortality and senescence of liver *in vitro* and *in vivo*

It has long been known that the way genes are packaged inside the nucleus of a cell can determine their expression (transcription). Molecular tags on histones have crucial roles in controlling the activity of associated genes; such tags include acetyl, methyl and phosphate groups. Of the various types of histone modification, methylation is the most stable (160). It

is tightly regulated by specific enzymes that add or remove a methyl group. Although, great effort has been devoted to elucidate the implication of DNA methylation in cancer, including HCC; our knowledge of the involvement of histone methylation changes was rather poor. Especially, in liver cancer there was no study examining the histone methylation changes. There were some encouring reports showing that long-term administration of diets deficient in choline and methionine caused hepatocellular carcinoma in mice. Moreover, treatments with various methionine metabolites in experimental animal models of liver disease showed hepatoprotective properties (161). In this study, we, first, showed that a significant group of histone methyltransferases and demethylases were differentially regulated in immortal and senescent Huh7 clones. The two H3K4 methyltransferases, *MLL3* and *ASH1L*, and the demethylase *JARID1B* were upregulated in senescent cells. We have observed the over-expression of H3K27 methyltransferase, *EZH2*, and down regulation of the demethylases *JMJD3*, and *UTX* in immortal cells. *JMJD2B*, an H3K9 demethylase, was upregulated in senescence cells. Both of the two H3K36 methyltransferases, *SETD2* and *SMYD2*, and two demethylase of the same residue, *FBXL11* and *JMJD2B*, were upregulated in senescence cells. *SUV420H1*, the H4K20 methyltransferase, was upregulated in senescence cells. The histone arginine methyltransferases, *CARM1* and *PRMT1*, did not show a specific change (<1 fold change). Some of these enzymes have been releted to various cancer types (see introduction), the role of these enzymes in the liver cancer development must be intensively studied.

We, than, wanted to compare the global levels of the H3 and H4 methylated residues in these cells. In order to observe and compare the nuclear positivity and cellular heterogeneity, we have choosen to perform immunocytochemistry experiment. Five of the residues did not show any change in the global levels. Interestingly, all of the other residues were observed to increase and become more homogenous in senescent cells. The decrease in the level of H4K20me3 was expected, because it has been previously shown that this residue was regulated by Rb protein and hypomethylated in cancer cells of various tumor models (162). We observed the decrease of this residue, along with, H3K27me3, H3K36me3, H3R2me2, H3R17me2, in HCC compared to non-tumor liver. The function, the up-stream regulators and targets of these residues in HCC must be studied extensively. Also, the factors mediating these changes must be elucidated. We couldn't observe a perfect correlation of histone residue changes with enzyme expression levels, except the upregulation of SUV420H1 and H4K20me3 in senescent cells. The global histone hypomethylation may be caused from

altered methylation methabolism in liver cancer. It has been showed that S-adenosyl-L-methionine/S-adenosylhomocysteine ratio and liver-specific methionine adenosyltransferase (MatI/III) progressively decreased in dysplastic and neoplastic liver lesions developed in c-Myc transgenic mice and in human HCC with better (HCCB) and poorer (HCCP) prognosis (based on patient's survival length), which caused extended DNA hypomethylation and genomic instability (163). It shoud be searched whether the global lypomethylation of histone residues is a consequence of methionine metabolism aberations.

We have also showed global increase in the levels of H2AZ, H2AX, and mH2A histone variants in senescence committed liver cancer cells. They may serve as markers of senescence, and may have important functions in immortality and senescence, as well as in HCC development. The mechanism and consequences of this histone variant replacement must be searched.

Our results show that histone methylation regulators may be very important to serve as new diagnostic, prognostic and therapeutic approaches.

CHAPTER 6. FUTURE PERSPECTIVES

Immortal and senescence associated network and its implication in HCC

We identified that many biological processes were differentially regulated in immortal and senescence arrested liver cancer cells. Among our significant gene set, the potential senescence and immortality markers should be identified. Today, there is no strong diagnostic marker for cirrhosis that will help to monitor patients before HCC development, without biopsy. As senescent cells may represent cirrhosis, and immortal cells HCC; any cirrhosis and HCC markers should be searched. For this purpose, candidate molecules should be selected from the most dramatically changing genes and a large cohort of cirrhosis and HCC tissue and serum samples must be screened for the levels of these genes and their proteins.

We found that DNA damage response and repair genes were up-regulated in immortal cells. The possibility that DNA damage, which can not be repaired, may be one of the major causes of the senescence arrest should be tested. The role of DNA repair pathway in HCC should be investigated.

It is widely believed that tumor cells include a population of cells responsible for the initiation of the tumor that is called “cancer stem cell”. They have self-renewal capacity and potential for multidirectional differentiation. It is possible that in parental Huh7 cells, the cancer stem cell population may produce both highly tumorigenic immortal clones which may have the stem cell properties, and terminally differentiated cells which do not divide and become senescent. This hypothesis should be tested using some cancer stem cell markers.

It will be very useful to test some of the genes from SIGN signature on an independent cohort of liver samples. Especially, immunohistochemistry analysis with selected proteins on normal, dysplastic, cirrhotic and tumor liver samples and HCC samples with different subtypes should be performed.

DP-2 and senescence

We found that total DP-2 is over-expressed in senescence cells in mRNA and protein level. And, the expressed isoforms were changing between immortal and senescent cells. Over-expression and knock-down analysis of the two isoforms *in-vitro* should be carried out to examine their function in cell proliferation and growth. Although it will be challenging to raise specific antibodies against each isoform, target genes of each isoform will be useful to identify.

DP proteins are bound to E2F proteins before binding to the target promoter. It will be important to identify E2F partner(s) of DP-2 isoforms.

Surprisingly, we have observed extra bands in primary human liver cells. With mass spectrometry analysis, these bands should be tested whether they are DP-2 isoforms or not. DP proteins share high homology among each other and with E2F proteins also. The extra bands could be products of cross-reactivity or liver specific DP protein and its modified forms (ex. Phosphorylated forms).

To observe oscillations of DP-2 isoforms in different stages of cell cycle, the cell cycle phases should be determined with flow cytometry analysis after cell cycle synchronization of different HCC cell lines.

Epigenetic changes in immortality and senescence of liver *in vitro* and *in vivo*

The functional roles of the identified histone modifying enzymes in senescence and cell proliferation should be studied intensively with over-expression and silencing experiments *in-vitro.* Strong candidates obtained from *in-vitro* assays should be tested *in-vivo* using knock-out mice strains. Candidate proteins should be subjected to chromatin immunoprecipitation analysis to identify their targets in senescent and immortal conditions.

The histone methylation changes of senescent/immortal cells and non-tumor/tumor samples should be confirmed by mass spectrometry analysis. The expression targets of the changing residues should be determined by ChIP-Seq technology in these contexts. Also, methionine metabolism changes in these cells should be determined to test the possibility that global hypomethylation of histone residues could be result from aberrant methionine metabolism in HCC.

REFERENCES

1. Llovet JM, Burroughs A, Bruix J. Hepatocellular carcinoma. Lancet 2003;362:1907-1917.
2. Farazi PA, DePinho RA. Hepatocellular carcinoma pathogenesis: from genes to environment. Nat Rev Cancer 2006;6:674-687.
3. Schnater JM, Kohler SE, Lamers WH, von Schweinitz D, Aronson DC. Where do we stand with hepatoblastoma? A review. Cancer 2003;98:668-678.
4. Parkin DM, Pisani P, Ferlay J. Global cancer statistics. CA Cancer J Clin 1999;49:33-64, 31.
5. Thorgeirsson SS, Grisham JW. Molecular pathogenesis of human hepatocellular carcinoma. Nat Genet 2002;31:339-346.
6. Tannapfel A, Wittekind C. Genes involved in hepatocellular carcinoma: deregulation in cell cycling and apoptosis. Virchows Arch 2002;440:345-352.
7. Badvie S. Hepatocellular carcinoma. Postgrad Med J 2000;76:4-11.
8. Sherman M. Hepatocellular carcinoma: epidemiology, risk factors, and screening. Semin Liver Dis 2005;25:143-154.
9. Lavanchy D. Hepatitis B virus epidemiology, disease burden, treatment, and current and emerging prevention and control measures. J Viral Hepat 2004;11:97-107.
10. Chen CJ, Yang HI, Su J, Jen CL, You SL, Lu SN, Huang GT, et al. Risk of hepatocellular carcinoma across a biological gradient of serum hepatitis B virus DNA level. Jama 2006;295:65-73.
11. Chisari FV. Unscrambling hepatitis C virus-host interactions. Nature 2005;436:930-932.
12. Bowen DG, Walker CM. Adaptive immune responses in acute and chronic hepatitis C virus infection. Nature 2005;436:946-952.
13. Block TM, Mehta AS, Fimmel CJ, Jordan R. Molecular viral oncology of hepatocellular carcinoma. Oncogene 2003;22:5093-5107.
14. Tokino T, Tamura H, Hori N, Matsubara K. Chromosome deletions associated with hepatitis B virus integration. Virology 1991;185:879-882.
15. Murakami Y, Saigo K, Takashima H, Minami M, Okanoue T, Brechot C, Paterlini-Brechot P. Large scaled analysis of hepatitis B virus (HBV) DNA integration in HBV related hepatocellular carcinomas. Gut 2005;54:1162-1168.
16. Tarn C, Lee S, Hu Y, Ashendel C, Andrisani OM. Hepatitis B virus X protein differentially activates RAS-RAF-MAPK and JNK pathways in X-transforming versus non-transforming AML12 hepatocytes. J Biol Chem 2001;276:34671-34680.
17. Nijhara R, Jana SS, Goswami SK, Rana A, Majumdar SS, Kumar V, Sarkar DP. Sustained activation of mitogen-activated protein kinases and activator protein 1 by the hepatitis B virus X protein in mouse hepatocytes in vivo. J Virol 2001;75:10348-10358.
18. Feitelson MA, Sun B, Satiroglu Tufan NL, Liu J, Pan J, Lian Z. Genetic mechanisms of hepatocarcinogenesis. Oncogene 2002;21:2593-2604.
19. Ueda H, Ullrich SJ, Gangemi JD, Kappel CA, Ngo L, Feitelson MA, Jay G. Functional inactivation but not structural mutation of p53 causes liver cancer. Nat Genet 1995;9:41-47.
20. Kim CM, Koike K, Saito I, Miyamura T, Jay G. HBx gene of hepatitis B virus induces liver cancer in transgenic mice. Nature 1991;351:317-320.
21. Shimoda R, Nagashima M, Sakamoto M, Yamaguchi N, Hirohashi S, Yokota J, Kasai H. Increased formation of oxidative DNA damage, 8-hydroxydeoxyguanosine, in human livers with chronic hepatitis. Cancer Res 1994;54:3171-3172.

22. Galli A, Svegliati-Baroni G, Ceni E, Milani S, Ridolfi F, Salzano R, Tarocchi M, et al. Oxidative stress stimulates proliferation and invasiveness of hepatic stellate cells via a MMP2-mediated mechanism. Hepatology 2005;41:1074-1084.
23. Lindenbach BD, Evans MJ, Syder AJ, Wolk B, Tellinghuisen TL, Liu CC, Maruyama T, et al. Complete replication of hepatitis C virus in cell culture. Science 2005;309:623-626.
24. Lindenbach BD, Rice CM. Unravelling hepatitis C virus replication from genome to function. Nature 2005;436:933-938.
25. Rehermann B, Nascimbeni M. Immunology of hepatitis B virus and hepatitis C virus infection. Nat Rev Immunol 2005;5:215-229.
26. Pachiadakis I, Pollara G, Chain BM, Naoumov NV. Is hepatitis C virus infection of dendritic cells a mechanism facilitating viral persistence? Lancet Infect Dis 2005;5:296-304.
27. Hino O, Kajino K, Umeda T, Arakawa Y. Understanding the hypercarcinogenic state in chronic hepatitis: a clue to the prevention of human hepatocellular carcinoma. J Gastroenterol 2002;37:883-887.
28. Majumder M, Ghosh AK, Steele R, Ray R, Ray RB. Hepatitis C virus NS5A physically associates with p53 and regulates p21/waf1 gene expression in a p53-dependent manner. J Virol 2001;75:1401-1407.
29. McClain CJ, Hill DB, Song Z, Deaciuc I, Barve S. Monocyte activation in alcoholic liver disease. Alcohol 2002;27:53-61.
30. Hoek JB, Pastorino JG. Ethanol, oxidative stress, and cytokine-induced liver cell injury. Alcohol 2002;27:63-68.
31. Bressac B, Kew M, Wands J, Ozturk M. Selective G to T mutations of p53 gene in hepatocellular carcinoma from southern Africa. Nature 1991;350:429-431.
32. Minouchi K, Kaneko S, Kobayashi K. Mutation of p53 gene in regenerative nodules in cirrhotic liver. J Hepatol 2002;37:231-239.
33. Nishida N, Fukuda Y, Kokuryu H, Toguchida J, Yandell DW, Ikenega M, Imura H, et al. Role and mutational heterogeneity of the p53 gene in hepatocellular carcinoma. Cancer Res 1993;53:368-372.
34. Gregorieff A, Clevers H. Wnt signaling in the intestinal epithelium: from endoderm to cancer. Genes Dev 2005;19:877-890.
35. Ishizaki Y, Ikeda S, Fujimori M, Shimizu Y, Kurihara T, Itamoto T, Kikuchi A, et al. Immunohistochemical analysis and mutational analyses of beta-catenin, Axin family and APC genes in hepatocellular carcinomas. Int J Oncol 2004;24:1077-1083.
36. An FQ, Matsuda M, Fujii H, Tang RF, Amemiya H, Dai YM, Matsumoto Y. Tumor heterogeneity in small hepatocellular carcinoma: analysis of tumor cell proliferation, expression and mutation of p53 AND beta-catenin. Int J Cancer 2001;93:468-474.
37. Hsu HC, Jeng YM, Mao TL, Chu JS, Lai PL, Peng SY. Beta-catenin mutations are associated with a subset of low-stage hepatocellular carcinoma negative for hepatitis B virus and with favorable prognosis. Am J Pathol 2000;157:763-770.
38. Cagatay T, Ozturk M. P53 mutation as a source of aberrant beta-catenin accumulation in cancer cells. Oncogene 2002;21:7971-7980.
39. Kim YD, Park CH, Kim HS, Choi SK, Rew JS, Kim DY, Koh YS, et al. Genetic alterations of Wnt signaling pathway-associated genes in hepatocellular carcinoma. J Gastroenterol Hepatol 2008;23:110-118.
40. Taniguchi K, Roberts LR, Aderca IN, Dong X, Qian C, Murphy LM, Nagorney DM, et al. Mutational spectrum of beta-catenin, AXIN1, and AXIN2 in hepatocellular carcinomas and hepatoblastomas. Oncogene 2002;21:4863-4871.
41. Ito Y, Takeda T, Sakon M, Tsujimoto M, Higashiyama S, Noda K, Miyoshi E, et al. Expression and clinical significance of erb-B receptor family in hepatocellular carcinoma. Br J Cancer 2001;84:1377-1383.

42. Daveau M, Scotte M, Francois A, Coulouarn C, Ros G, Tallet Y, Hiron M, et al. Hepatocyte growth factor, transforming growth factor alpha, and their receptors as combined markers of prognosis in hepatocellular carcinoma. Mol Carcinog 2003;36:130-141.
43. Sakata H, Takayama H, Sharp R, Rubin JS, Merlino G, LaRochelle WJ. Hepatocyte growth factor/scatter factor overexpression induces growth, abnormal development, and tumor formation in transgenic mouse livers. Cell Growth Differ 1996;7:1513-1523.
44. Yu J, Zhang HY, Ma ZZ, Lu W, Wang YF, Zhu JD. Methylation profiling of twenty four genes and the concordant methylation behaviours of nineteen genes that may contribute to hepatocellular carcinogenesis. Cell Res 2003;13:319-333.
45. Lee S, Lee HJ, Kim JH, Lee HS, Jang JJ, Kang GH. Aberrant CpG island hypermethylation along multistep hepatocarcinogenesis. Am J Pathol 2003;163:1371-1378.
46. Herath NI, Leggett BA, MacDonald GA. Review of genetic and epigenetic alterations in hepatocarcinogenesis. J Gastroenterol Hepatol 2006;21:15-21.
47. Honda S, Haruta M, Sugawara W, Sasaki F, Ohira M, Matsunaga T, Yamaoka H, et al. The methylation status of RASSF1A promoter predicts responsiveness to chemotherapy and eventual cure in hepatoblastoma patients. Int J Cancer 2008;123:1117-1125.
48. Okochi O, Hibi K, Sakai M, Inoue S, Takeda S, Kaneko T, Nakao A. Methylation-mediated silencing of SOCS-1 gene in hepatocellular carcinoma derived from cirrhosis. Clin Cancer Res 2003;9:5295-5298.
49. Kaposi-Novak P, Libbrecht L, Woo HG, Lee YH, Sears NC, Coulouarn C, Conner EA, et al. Central role of c-Myc during malignant conversion in human hepatocarcinogenesis. Cancer Res 2009;69:2775-2782.
50. Hayflick L. The Limited in Vitro Lifetime of Human Diploid Cell Strains. Exp Cell Res 1965;37:614-636.
51. Campisi J, d'Adda di Fagagna F. Cellular senescence: when bad things happen to good cells. Nat Rev Mol Cell Biol 2007;8:729-740.
52. Ozturk M, Arslan-Ergul A, Bagislar S, Senturk S, Yuzugullu H. Senescence and immortality in hepatocellular carcinoma. Cancer Lett 2008.
53. De Lange T. Telomere-related genome instability in cancer. Cold Spring Harb Symp Quant Biol 2005;70:197-204.
54. Blackburn EH. Structure and function of telomeres. Nature 1991;350:569-573.
55. Cong YS, Wright WE, Shay JW. Human telomerase and its regulation. Microbiol Mol Biol Rev 2002;66:407-425, table of contents.
56. Karlseder J, Smogorzewska A, de Lange T. Senescence induced by altered telomere state, not telomere loss. Science 2002;295:2446-2449.
57. Di Micco R, Fumagalli M, d'Adda di Fagagna F. Breaking news: high-speed race ends in arrest--how oncogenes induce senescence. Trends Cell Biol 2007;17:529-536.
58. Lu T, Finkel T. Free radicals and senescence. Exp Cell Res 2008;314:1918-1922.
59. Xue W, Zender L, Miething C, Dickins RA, Hernando E, Krizhanovsky V, Cordon-Cardo C, et al. Senescence and tumour clearance is triggered by p53 restoration in murine liver carcinomas. Nature 2007;445:656-660.
60. Wu CH, van Riggelen J, Yetil A, Fan AC, Bachireddy P, Felsher DW. Cellular senescence is an important mechanism of tumor regression upon c-Myc inactivation. Proc Natl Acad Sci U S A 2007;104:13028-13033.
61. Ozturk N, Erdal E, Mumcuoglu M, Akcali KC, Yalcin O, Senturk S, Arslan-Ergul A, et al. Reprogramming of replicative senescence in hepatocellular carcinoma-derived cells. Proc Natl Acad Sci U S A 2006;103:2178-2183.
62. Gil J, Peters G. Regulation of the INK4b-ARF-INK4a tumour suppressor locus: all for one or one for all. Nat Rev Mol Cell Biol 2006;7:667-677.

63. el-Deiry WS, Tokino T, Velculescu VE, Levy DB, Parsons R, Trent JM, Lin D, et al. WAF1, a potential mediator of p53 tumor suppression. Cell 1993;75:817-825.
64. Deng Y, Chan SS, Chang S. Telomere dysfunction and tumour suppression: the senescence connection. Nat Rev Cancer 2008;8:450-458.
65. Fang L, Igarashi M, Leung J, Sugrue MM, Lee SW, Aaronson SA. p21Waf1/Cip1/Sdi1 induces permanent growth arrest with markers of replicative senescence in human tumor cells lacking functional p53. Oncogene 1999;18:2789-2797.
66. Auer H, Newsom DL, Kornacker K. Expression Profiling Using Affymetrix GeneChip Microarrays. Methods Mol Biol 2009;509:35-46.
67. Dufva M. Introduction to microarray technology. Methods Mol Biol 2009;529:1-22.
68. Weinberg RA. The retinoblastoma protein and cell cycle control. Cell 1995;81:323-330.
69. Trimarchi JM, Lees JA. Sibling rivalry in the E2F family. Nat Rev Mol Cell Biol 2002;3:11-20.
70. Iaquinta PJ, Lees JA. Life and death decisions by the E2F transcription factors. Curr Opin Cell Biol 2007;19:649-657.
71. Wu CL, Zukerberg LR, Ngwu C, Harlow E, Lees JA. In vivo association of E2F and DP family proteins. Mol Cell Biol 1995;15:2536-2546.
72. Milton A, Luoto K, Ingram L, Munro S, Logan N, Graham AL, Brummelkamp TR, et al. A functionally distinct member of the DP family of E2F subunits. Oncogene 2006;25:3212-3218.
73. Girling R, Partridge JF, Bandara LR, Burden N, Totty NF, Hsuan JJ, La Thangue NB. A new component of the transcription factor DRTF1/E2F. Nature 1993;365:468.
74. Rabbani F, Richon VM, Orlow I, Lu ML, Drobnjak M, Dudas M, Charytonowicz E, et al. Prognostic significance of transcription factor E2F-1 in bladder cancer: genotypic and phenotypic characterization. J Natl Cancer Inst 1999;91:874-881.
75. Han S, Park K, Bae BN, Kim KH, Kim HJ, Kim YD, Kim HY. E2F1 expression is related with the poor survival of lymph node-positive breast cancer patients treated with fluorouracil, doxorubicin and cyclophosphamide. Breast Cancer Res Treat 2003;82:11-16.
76. Gorgoulis VG, Zacharatos P, Mariatos G, Kotsinas A, Bouda M, Kletsas D, Asimacopoulos PJ, et al. Transcription factor E2F-1 acts as a growth-promoting factor and is associated with adverse prognosis in non-small cell lung carcinomas. J Pathol 2002;198:142-156.
77. Zacharatos P, Kotsinas A, Evangelou K, Karakaidos P, Vassiliou LV, Rezaei N, Kyroudi A, et al. Distinct expression patterns of the transcription factor E2F-1 in relation to tumour growth parameters in common human carcinomas. J Pathol 2004;203:744-753.
78. Johnson DG, Degregori J. Putting the Oncogenic and Tumor Suppressive Activities of E2F into Context. Curr Mol Med 2006;6:731-738.
79. Santoni-Rugiu E, Jensen MR, Thorgeirsson SS. Disruption of the pRb/E2F pathway and inhibition of apoptosis are major oncogenic events in liver constitutively expressing c-myc and transforming growth factor alpha. Cancer Res 1998;58:123-134.
80. Kwon JA, Rho HM. Transcriptional repression of the human p53 gene by hepatitis B viral core protein (HBc) in human liver cells. Biol Chem 2003;384:203-212.
81. Park YM, Choi JY, Bae SH, Byun BH, Ahn BM, Kim BS, Shin DY. Microsatellite instability and mutations of E2F-4 in hepatocellular carcinoma from Korea. Hepatol Res 2000;17:102-111.
82. Yasui K, Okamoto H, Arii S, Inazawa J. Association of over-expressed TFDP1 with progression of hepatocellular carcinomas. J Hum Genet 2003;48:609-613.

83. Rogers KT, Higgins PD, Milla MM, Phillips RS, Horowitz JM. DP-2, a heterodimeric partner of E2F: identification and characterization of DP-2 proteins expressed in vivo. Proc Natl Acad Sci U S A 1996;93:7594-7599.
84. Zhang Y, Chellappan SP. Cloning and characterization of human DP2, a novel dimerization partner of E2F. Oncogene 1995;10:2085-2093.
85. Liu LX, Jiang HC, Liu ZH, Zhu AL, Zhang WH, Wu LF, Zhou J, et al. Expression of cell cycle/growth regulator genes in human hepatocellular carcinoma and adjacent normal liver tissues. Oncol Rep 2003;10:1771-1775.
86. Vara D, Bicknell KA, Coxon CH, Brooks G. Inhibition of E2F abrogates the development of cardiac myocyte hypertrophy. J Biol Chem 2003;278:21388-21394.
87. Kusek JC, Greene RM, Pisano MM. Expression of the E2F and retinoblastoma families of proteins during neural differentiation. Brain Res Bull 2001;54:187-198.
88. Lam EW, Choi MS, van der Sman J, Burbidge SA, Klaus GG. Modulation of E2F activity via signaling through surface IgM and CD40 receptors in WEHI-231 B lymphoma cells. J Biol Chem 1998;273:10051-10057.
89. DeGregori J, Johnson DG. Distinct and Overlapping Roles for E2F Family Members in Transcription, Proliferation and Apoptosis. Curr Mol Med 2006;6:739-748.
90. Moss TJ, Wallrath LL. Connections between epigenetic gene silencing and human disease. Mutat Res 2007;618:163-174.
91. Li E. Chromatin modification and epigenetic reprogramming in mammalian development. Nat Rev Genet 2002;3:662-673.
92. Lund AH, van Lohuizen M. Epigenetics and cancer. Genes Dev 2004;18:2315-2335.
93. Yatabe Y, Mitsudomi T, Takahashi T. Maspin expression in normal lung and non-small-cell lung cancers: cellular property-associated expression under the control of promoter DNA methylation. Oncogene 2004;23:4041-4049.
94. Esteller M. Epigenetics in cancer. N Engl J Med 2008;358:1148-1159.
95. Moribe T, Iizuka N, Miura T, Kimura N, Tamatsukuri S, Ishitsuka H, Hamamoto Y, et al. Methylation of multiple genes as molecular markers for diagnosis of a small, well-differentiated hepatocellular carcinoma. Int J Cancer 2009;125:388-397.
96. Iliopoulos D, Satra M, Drakaki A, Poultsides GA, Tsezou A. Epigenetic regulation of hTERT promoter in hepatocellular carcinomas. Int J Oncol 2009;34:391-399.
97. Datta J, Kutay H, Nasser MW, Nuovo GJ, Wang B, Majumder S, Liu CG, et al. Methylation mediated silencing of MicroRNA-1 gene and its role in hepatocellular carcinogenesis. Cancer Res 2008;68:5049-5058.
98. Lu B, Ma Y, Wu G, Tong X, Guo H, Liang A, Cong W, et al. Methylation of Tip30 promoter is associated with poor prognosis in human hepatocellular carcinoma. Clin Cancer Res 2008;14:7405-7412.
99. Calvisi DF, Ladu S, Gorden A, Farina M, Lee JS, Conner EA, Schroeder I, et al. Mechanistic and prognostic significance of aberrant methylation in the molecular pathogenesis of human hepatocellular carcinoma. J Clin Invest 2007;117:2713-2722.
100. Kouzarides T. Histone methylation in transcriptional control. Curr Opin Genet Dev 2002;12:198-209.
101. Kouzarides T. Chromatin modifications and their function. Cell 2007;128:693-705.
102. Bernstein BE, Meissner A, Lander ES. The mammalian epigenome. Cell 2007;128:669-681.
103. Lee MG, Wynder C, Cooch N, Shiekhattar R. An essential role for CoREST in nucleosomal histone 3 lysine 4 demethylation. Nature 2005;437:432-435.
104. Metzger E, Wissmann M, Yin N, Muller JM, Schneider R, Peters AH, Gunther T, et al. LSD1 demethylates repressive histone marks to promote androgen-receptor-dependent transcription. Nature 2005;437:436-439.

105. Steward MM, Lee JS, O'Donovan A, Wyatt M, Bernstein BE, Shilatifard A. Molecular regulation of H3K4 trimethylation by ASH2L, a shared subunit of MLL complexes. Nat Struct Mol Biol 2006;13:852-854.
106. Chang B, Chen Y, Zhao Y, Bruick RK. JMJD6 is a histone arginine demethylase. Science 2007;318:444-447.
107. Fischle W, Tseng BS, Dormann HL, Ueberheide BM, Garcia BA, Shabanowitz J, Hunt DF, et al. Regulation of HP1-chromatin binding by histone H3 methylation and phosphorylation. Nature 2005;438:1116-1122.
108. Nelson CJ, Santos-Rosa H, Kouzarides T. Proline isomerization of histone H3 regulates lysine methylation and gene expression. Cell 2006;126:905-916.
109. Clements A, Poux AN, Lo WS, Pillus L, Berger SL, Marmorstein R. Structural basis for histone and phosphohistone binding by the GCN5 histone acetyltransferase. Mol Cell 2003;12:461-473.
110. Fraga MF, Ballestar E, Villar-Garea A, Boix-Chornet M, Espada J, Schotta G, Bonaldi T, et al. Loss of acetylation at Lys16 and trimethylation at Lys20 of histone H4 is a common hallmark of human cancer. Nat Genet 2005;37:391-400.
111. Tryndyak VP, Kovalchuk O, Pogribny IP. Loss of DNA methylation and histone H4 lysine 20 trimethylation in human breast cancer cells is associated with aberrant expression of DNA methyltransferase 1, Suv4-20h2 histone methyltransferase and methyl-binding proteins. Cancer Biol Ther 2006;5:65-70.
112. Pogribny IP, Ross SA, Tryndyak VP, Pogribna M, Poirier LA, Karpinets TV. Histone H3 lysine 9 and H4 lysine 20 trimethylation and the expression of Suv4-20h2 and Suv-39h1 histone methyltransferases in hepatocarcinogenesis induced by methyl deficiency in rats. Carcinogenesis 2006;27:1180-1186.
113. Esteller M. Epigenetics provides a new generation of oncogenes and tumour-suppressor genes. Br J Cancer 2006;94:179-183.
114. Sparmann A, van Lohuizen M. Polycomb silencers control cell fate, development and cancer. Nat Rev Cancer 2006;6:846-856.
115. Croonquist PA, Van Ness B. The polycomb group protein enhancer of zeste homolog 2 (EZH 2) is an oncogene that influences myeloma cell growth and the mutant ras phenotype. Oncogene 2005;24:6269-6280.
116. Su IH, Dobenecker MW, Dickinson E, Oser M, Basavaraj A, Marqueron R, Viale A, et al. Polycomb group protein ezh2 controls actin polymerization and cell signaling. Cell 2005;121:425-436.
117. van Lohuizen M, Verbeek S, Scheijen B, Wientjens E, van der Gulden H, Berns A. Identification of cooperating oncogenes in E mu-myc transgenic mice by provirus tagging. Cell 1991;65:737-752.
118. Jacobs JJ, Kieboom K, Marino S, DePinho RA, van Lohuizen M. The oncogene and Polycomb-group gene bmi-1 regulates cell proliferation and senescence through the ink4a locus. Nature 1999;397:164-168.
119. Norwood LE, Moss TJ, Margaryan NV, Cook SL, Wright L, Seftor EA, Hendrix MJ, et al. A requirement for dimerization of HP1Hsalpha in suppression of breast cancer invasion. J Biol Chem 2006;281:18668-18676.
120. Peters AH, O'Carroll D, Scherthan H, Mechtler K, Sauer S, Schofer C, Weipoltshammer K, et al. Loss of the Suv39h histone methyltransferases impairs mammalian heterochromatin and genome stability. Cell 2001;107:323-337.
121. Braig M, Lee S, Loddenkemper C, Rudolph C, Peters AH, Schlegelberger B, Stein H, et al. Oncogene-induced senescence as an initial barrier in lymphoma development. Nature 2005;436:660-665.

122. Kim KC, Geng L, Huang S. Inactivation of a histone methyltransferase by mutations in human cancers. Cancer Res 2003;63:7619-7623.
123. Cloos PA, Christensen J, Agger K, Maiolica A, Rappsilber J, Antal T, Hansen KH, et al. The putative oncogene GASC1 demethylates tri- and dimethylated lysine 9 on histone H3. Nature 2006;442:307-311.
124. Wang GG, Allis CD, Chi P. Chromatin remodeling and cancer, Part I: Covalent histone modifications. Trends Mol Med 2007;13:363-372.
125. Hamamoto R, Furukawa Y, Morita M, Iimura Y, Silva FP, Li M, Yagyu R, et al. SMYD3 encodes a histone methyltransferase involved in the proliferation of cancer cells. Nat Cell Biol 2004;6:731-740.
126. Shi X, Gozani O. The fellowships of the INGs. J Cell Biochem 2005;96:1127-1136.
127. Okada Y, Jiang Q, Lemieux M, Jeannotte L, Su L, Zhang Y. Leukaemic transformation by CALM-AF10 involves upregulation of Hoxa5 by hDOT1L. Nat Cell Biol 2006;8:1017-1024.
128. Iyer NG, Ozdag H, Caldas C. p300/CBP and cancer. Oncogene 2004;23:4225-4231.
129. Bolden JE, Peart MJ, Johnstone RW. Anticancer activities of histone deacetylase inhibitors. Nat Rev Drug Discov 2006;5:769-784.
130. Narita M, Nunez S, Heard E, Narita M, Lin AW, Hearn SA, Spector DL, et al. Rb-mediated heterochromatin formation and silencing of E2F target genes during cellular senescence. Cell 2003;113:703-716.
131. Beausejour CM, Krtolica A, Galimi F, Narita M, Lowe SW, Yaswen P, Campisi J. Reversal of human cellular senescence: roles of the p53 and p16 pathways. Embo J 2003;22:4212-4222.
132. Narita M. Cellular senescence and chromatin organisation. Br J Cancer 2007;96:686-691.
133. Brown DT. Histone variants: are they functionally heterogeneous? Genome Biol 2001;2:REVIEWS0006.
134. El-Serag HB, Rudolph KL. Hepatocellular carcinoma: epidemiology and molecular carcinogenesis. Gastroenterology 2007;132:2557-2576.
135. d'Adda di Fagagna F. Living on a break: cellular senescence as a DNA-damage response. Nat Rev Cancer 2008;8:512-522.
136. Plentz RR, Park YN, Lechel A, Kim H, Nellessen F, Langkopf BH, Wilkens L, et al. Telomere shortening and inactivation of cell cycle checkpoints characterize human hepatocarcinogenesis. Hepatology 2007;45:968-976.
137. Murakami Y, Hayashi K, Hirohashi S, Sekiya T. Aberrations of the tumor suppressor p53 and retinoblastoma genes in human hepatocellular carcinomas. Cancer Res 1991;51:5520-5525.
138. Wei W, Herbig U, Wei S, Dutriaux A, Sedivy JM. Loss of retinoblastoma but not p16 function allows bypass of replicative senescence in human fibroblasts. EMBO Rep 2003;4:1061-1066.
139. Baylin SB, Ohm JE. Epigenetic gene silencing in cancer - a mechanism for early oncogenic pathway addiction? Nat Rev Cancer 2006;6:107-116.
140. Gentleman RC, Carey VJ, Bates DM, Bolstad B, Dettling M, Dudoit S, Ellis B, et al. Bioconductor: open software development for computational biology and bioinformatics. Genome Biol 2004;5:R80.
141. de Hoon MJ, Imoto S, Nolan J, Miyano S. Open source clustering software. Bioinformatics 2004;20:1453-1454.
142. Eisen MB, Spellman PT, Brown PO, Botstein D. Cluster analysis and display of genome-wide expression patterns. Proc Natl Acad Sci U S A 1998;95:14863-14868.

143. Saldanha AJ. Java Treeview--extensible visualization of microarray data. Bioinformatics 2004;20:3246-3248.
144. Dennis G, Jr., Sherman BT, Hosack DA, Yang J, Gao W, Lane HC, Lempicki RA. DAVID: Database for Annotation, Visualization, and Integrated Discovery. Genome Biol 2003;4:P3.
145. Subramanian A, Tamayo P, Mootha VK, Mukherjee S, Ebert BL, Gillette MA, Paulovich A, et al. Gene set enrichment analysis: a knowledge-based approach for interpreting genome-wide expression profiles. Proc Natl Acad Sci U S A 2005;102:15545-15550.
146. Draghici S, Khatri P, Bhavsar P, Shah A, Krawetz SA, Tainsky MA. Onto-Tools, the toolkit of the modern biologist: Onto-Express, Onto-Compare, Onto-Design and Onto-Translate. Nucleic Acids Res 2003;31:3775-3781.
147. Schwarze SR, DePrimo SE, Grabert LM, Fu VX, Brooks JD, Jarrard DF. Novel pathways associated with bypassing cellular senescence in human prostate epithelial cells. J Biol Chem 2002;277:14877-14883.
148. Collado M, Gil J, Efeyan A, Guerra C, Schuhmacher AJ, Barradas M, Benguria A, et al. Tumour biology: senescence in premalignant tumours. Nature 2005;436:642.
149. Boyault S, Rickman DS, de Reynies A, Balabaud C, Rebouissou S, Jeannot E, Herault A, et al. Transcriptome classification of HCC is related to gene alterations and to new therapeutic targets. Hepatology 2007;45:42-52.
150. Pfaffl MW. A new mathematical model for relative quantification in real-time RT-PCR. Nucleic Acids Res 2001;29:e45.
151. Dimri GP, Lee X, Basile G, Acosta M, Scott G, Roskelley C, Medrano EE, et al. A biomarker that identifies senescent human cells in culture and in aging skin in vivo. Proc Natl Acad Sci U S A 1995;92:9363-9367.
152. Laurent-Puig P, Legoix P, Bluteau O, Belghiti J, Franco D, Binot F, Monges G, et al. Genetic alterations associated with hepatocellular carcinomas define distinct pathways of hepatocarcinogenesis. Gastroenterology 2001;120:1763-1773.
153. Watanuki A, Ohwada S, Fukusato T, Makita F, Yamada T, Kikuchi A, Morishita Y. Prognostic significance of DNA topoisomerase IIalpha expression in human hepatocellular carcinoma. Anticancer Res 2002;22:1113-1119.
154. Sancar A, Lindsey-Boltz LA, Unsal-Kacmaz K, Linn S. Molecular mechanisms of mammalian DNA repair and the DNA damage checkpoints. Annu Rev Biochem 2004;73:39-85.
155. Erdal E, Ozturk N, Cagatay T, Eksioglu-Demiralp E, Ozturk M. Lithium-mediated downregulation of PKB/Akt and cyclin E with growth inhibition in hepatocellular carcinoma cells. Int J Cancer 2005;115:903-910.
156. Wiemann SU, Satyanarayana A, Tsahuridu M, Tillmann HL, Zender L, Klempnauer J, Flemming P, et al. Hepatocyte telomere shortening and senescence are general markers of human liver cirrhosis. Faseb J 2002;16:935-942.
157. Villanueva A, Toffanin S, Llovet JM. Linking molecular classification of hepatocellular carcinoma and personalized medicine: preliminary steps. Curr Opin Oncol 2008;20:444-453.
158. Wang D, Russell J, Xu H, Johnson DG. Deregulated expression of DP1 induces epidermal proliferation and enhances skin carcinogenesis. Mol Carcinog 2001;31:90-100.
159. van der Sman J, Thomas NS, Lam EW. Modulation of E2F complexes during G0 to S phase transition in human primary B-lymphocytes. J Biol Chem 1999;274:12009-12016.
160. Jones RS. Epigenetics: reversing the 'irreversible'. Nature 2007;450:357-359.
161. Mato JM, Martinez-Chantar ML, Lu SC. Methionine metabolism and liver disease. Annu Rev Nutr 2008;28:273-293.

162. Gonzalo S, Blasco MA. Role of Rb family in the epigenetic definition of chromatin. Cell Cycle 2005;4:752-755.
163. Calvisi DF, Simile MM, Ladu S, Pellegrino R, De Murtas V, Pinna F, Tomasi ML, et al. Altered methionine metabolism and global DNA methylation in liver cancer: relationship with genomic instability and prognosis. Int J Cancer 2007;121:2410-2420.

Appendix A: Quality control of arrays using AffyPLM package of Bioconductor suite using R programme

%download AffyPLM

```
source("http://bioconductor.org/biocLite.R")
biocLite("affyPLM")
```

%load the package

```
library(affyPLM)
options(width = 60)
```

%load the dataset and fit probe-level models to all of the probesets

```
require(affydata)
data(DATA)
Dilution = updateObject(DATA)
Pset <- fitPLM(DATA)
```

%produce a chip pseudo image of the weights for the second array in the dataset

```
image(Pset, which = 2)
```

%produce the residual images for the second chip in the DATA dataset

```
image(Pset, which = 2, type = "resids")
image(Pset, which = 2, type = "pos.resids")
image(Pset, which = 2, type = "neg.resids")
```

%draw Relative Log Expression (RLE) box-plots

```
RLE(Pset, main = "RLE for DATA dataset")
```

%draw Normalized Unscaled Standard Errors (NUSE) box-plots

```
NUSE(Pset, main = "NUSE for Dilution dataset")
```

Appendix B: Normlization and significance analysis codes using R programme

B1. Code for normalization with RMA

```
library(affy)
setwd(system.file("data",package="DATA"))
dir()
getwd()
pd <-read.phenoData("PHENODATA.txt",header=TRUE,row.names=1,as.is=TRUE)
rawAffyData <- ReadAffy(filenames=pData(pd)$FileName,phenoData=pd)
rawAffyData
image(rawAffyData[,1])
image(rawAffyData[,2])
hist(log2(pm(rawAffyData[,1])), breaks=100, col="blue")
hist(log2(mm(rawAffyData[,1])), breaks=100, col="blue")
```

```
mva.pairs(pm(rawAffyData)[,c(1,3,5,7)])
eset <- rma(rawAffyData)
eset
```

%exame the effects of normalization using boxplots;

```
# Before RMA normalization:
boxplot(rawAffyData,col="red")

# After RMA normalization:
boxplot(data.frame(exprs(eset)),col="blue")
```

B2. Code for two-tailed, unpaired, unequal variance Welch's t-test

```
library(siggenes)
library(multtest)
library(genefilter)



callItSig<-function(normFile) {
#indices in R starts from 1!!!!!!!!!!!!!!!!!!!!
     explimit <- 4
     FDR <- 1.0
     for (i in 1:2) {
         for (j in (i+1):3) {
          print(c(i,j))
          getsiglistTtest(normFile,explimit,i,j,FDR)
         }
     }
     for (i in 4:5) {
         for (j in (i+1):6) {
          print(c(i,j))
          getsiglistTtest(normFile,explimit,i,j,FDR)
         }
     }
}

dene<-function(normFile) {
     explimit <- 4
```

```
        for (i in 5:5) {
        for (j in 6:6) {
         print(c(i,j))
         getsiglistTtest(normFile, explimit,i,j,FDR)
        }
     }
}


getsiglistTtest<-function(normFile, explimit,grp1,grp2,FDR) {
     getwd();
     Data <- read.csv(normFile)

     de = Data[, 2:19]
     de.gnames = Data[, 1:1]
     de.cl = c(1,1,1,2,2,2,3,3,3,4,4,4,5,5,5,6,6,6)
     dind1<-de.cl==grp1
     dind2<-de.cl==grp2
     dgr1<-de[,dind1]
     dgr2<-de[,dind2]
     de1<-cbind(dgr1,dgr2)

     #filter genes below explimit
     #At least 1 probe should be expressed above explimit
     #f1 <- kOverA(6, explimit);
     f1 <- kOverA(1, explimit);
     ffun <- filterfun(f1);
     which <- genefilter(de1, ffun);
     print('number of remaining genes after expfilter:')
     print(sum(which))
     def<-de1[which,]
     def.gnames<-data.matrix(Data[which,1])

     #t-test class labels should be either 0 or 1
```

```
     def.cl<-c(0,0,0,1,1,1)

     teststat <- mt.teststat(def, def.cl)

     qqnorm(teststat)
     qqline(teststat)
     print("qq plot for teststat plotted")

     #to get regulation information
     tmp <- mt.teststat.num.denum(def, def.cl, test = "t")
     num <- data.matrix(tmp$teststat.num)
     print ("num")
     print (dim(num))
     print (num[1:10,])

     #find raw p values
     rft    <-    rowFtests(data.matrix(def),    factor(def.cl),
var.equal= F)
     rawp0 <- rft$p.value

print (dim(data.matrix(rawp0)))

     procs <- c("BH")
     #adj_p is in its orijinal order -not in accending order
     res <- mt.rawp2adjp(rawp0, procs)
     adjp <- res$adjp[order(res$index), ]
print(dim(adjp))

     print(FDR)
     which  <-   mt.reject(cbind(adjp),  FDR  )$which[,2]  #there
are only one proc 'BH'
     result <-  mt.reject(cbind(adjp), seq(0,1.0,0.01) )$r

     #print significance into file
```

```
     fileName = paste(grp1,grp2,"sig.csv", sep = "")
     write.table(result, file = fileName, sep = "\t", col.names
= TRUE, quote = FALSE)

     print ("Number of significant genes")
     print(sum(which))
     gsignificant<-def[which,]

     probeLabels<-def.gnames[which] #first column of def.gnames
data matrix
     significantAdjPValues<-adjp[which,2]
     regulation<-num[which]
     #allSignificant           =           cbind(probeLabels,
significantAdjPValues, regulation)
     allSignificant = cbind(probeLabels, adjp, regulation)

     #TAGGING
     #grp1(3 digits-18 values,
     #grp2(3 digits-18) values

     reg = as.numeric(allSignificant[,3])

     #all significant genes
     print("all")
     print(dim(allSignificant))
     print(allSignificant[1:2,]);
     fileName = paste(grp1,grp2,"genes.csv", sep = "")

#write.table(tagValue, file = fileName, sep = "", col.names =
FALSE, row.names = FALSE)
     write.table(allSignificant, file = fileName, sep = "\t",
col.names = TRUE, row.names = FALSE, quote = FALSE) }
```

B3. For quantile and median center normalization, the below code was used in R;

```
d=read.table("DATA.txt",header=T)
dim(d)
d[1:5,1:5] # see a subset of the values in d
#Load the rfunctions using
source('rfunctions.txt')
#Make side-by-side boxplots of the log signals from each
channel.
#(The "[,-1]" removes column 1 which contains the geneID.)

boxplot(log(d[,-1]))
#Boxplot of unnormalized data after log transformation using
log.0 #function in which zeros are replaced by 1; the data in
logd is #indexed from column 2 to 17, instead of using d[,-1].

logd=log.0(d[,2:27])
boxplot(logd)

#List the objects that have been created during the R session
so far.

ls()
#Quantile normalize using quant.norm

qs<-quant.norm(logd)
dim(qs)
slide.medians<-apply(qs,2,median, na.rm=T)
qsm<-sweep(qs,2,slide.medians)  #1=row 2=column
plot(d[,2],d[,3]
```

Appendix C: Enriched gene sets (FDR<0.15) to immortal, pre-senescent and senescent phenotypes from GSEA analysis

Immortal Enriched Gene Sets

NAME	SIZE	ES	NES	NOM p-val	FDR q-val	FWER p-val
E2F1_TARGETS_CHIP	38	0.580218	1.66831	0.04	0.051051	0.24
CANCER_UNDIFFERENTIATED_META_UP	65	0.487906	1.4689	0.086957	0.113817	0.71
BRENTANI_REPAIR	36	0.621496	1.547644	0.058824	0.117194	0.59
MANALO_HYPOXIA_DOWN	80	0.563608	1.469109	0.106383	0.127927	0.71
NF90_DN	29	0.61834	1.479598	0	0.132696	0.7
CMV_IE86_UP	37	0.720344	1.519632	0.065217	0.139809	0.62
SERUM_FIBROBLAST_CELLCYCLE	114	0.581189	1.504461	0.083333	0.140873	0.68
PEART_HISTONE_DOWN	73	0.408196	1.433983	0.019231	0.144511	0.76
DOX_RESIST_GASTRIC_UP	47	0.614502	1.485551	0.130435	0.147354	0.7
SERUM_FIBROBLAST_CORE_UP	173	0.376459	1.401126	0.142857	0.154137	0.79

Pre-senescent Enriched Gene Sets

NAME	SIZE	ES	NES	NOM p-val	FDR q-val	FWER p-val
UV-CMV_UNIQUE_HCMV_6HRS_DN	92	0.527606	1.771172	0	0.033122	0.02
UVB_NHEK3_C8	68	0.442606	1.520431	0.033898	0.105614	0.62
IFNG_5ENDOTHELIAL_DOWN	68	0.44511	1.526414	0	0.106698	0.61
HYPOXIA_REVIEW	80	0.527992	1.522686	0	0.107922	0.61
BHATTACHARYA_ESC_UP	66	0.488177	1.53307	0	0.107988	0.59
ET743_HELA_UP	45	0.567194	1.681733	0	0.108232	0.2
TESTIS_EXPRESSED_GENES	61	0.402888	1.529274	0	0.108234	0.61
H2O2_CSBDIFF_C2	26	0.546498	1.612152	0.016949	0.109624	0.4
HPV31_DN	40	0.560783	1.517472	0.04	0.109773	0.63
HDACI_COLON_BUT12HRS_UP	34	0.476826	1.538593	0.016393	0.111217	0.59
TNFALPHA_30MIN_UP	38	0.388466	1.604211	0	0.111307	0.43
TNFALPHA_4HRS_UP	39	0.507071	1.542008	0.020408	0.111435	0.59
CHIARETTI_T_ALL	238	0.469172	1.542335	0	0.1137	0.58
OXSTRESS_BREASTCA_UP	27	0.519261	1.581281	0	0.114023	0.49
UV_UNIQUE_FIBRO_DN	28	0.613834	1.51406	0.043478	0.114061	0.64
UVB_NHEK3_C0	101	0.446388	1.665794	0.05	0.115345	0.25
CMV_24HRS_UP	58	0.521695	1.592209	0	0.116577	0.45
CROONQUIST_IL6_STROMA_UP	36	0.591776	1.615106	0.034483	0.11798	0.4
TNFA_5ENDOTHELIAL_DOWN	71	0.539296	1.588474	0	0.118261	0.48
UVB_NHEK1_UP	140	0.488482	1.542381	0.017857	0.118437	0.58
TNFA_5ENDOTHELIAL_UP	70	0.636198	1.505029	0	0.119345	0.66
HOX_GENES	52	0.626138	1.634224	0.033333	0.11986	0.36
AGUIRRE_PANCREAS_CHR1	28	0.444518	1.505444	0	0.122102	0.66
TSA_HEPATOMA_CANCER_UP	30	0.667311	1.543693	0	0.122257	0.57
BRCA1_OVEREXP_PROSTATE_UP	153	0.429095	1.548771	0	0.123862	0.55
UVB_NHEK3_C1	67	0.523373	1.50596	0.074074	0.123984	0.65
HINATA_NFKB_UP	107	0.495775	1.553349	0	0.124247	0.55
GNATENKO_PLATELET	42	0.497503	1.500949	0.019231	0.125204	0.67
MAGRANGEAS_LK_DOWN	27	0.566354	1.544468	0.018519	0.126184	0.57
CMV_HCMV_TIMECOURSE_14HRS_DN	47	0.545241	1.625472	0	0.127177	0.38
WERNERONLY_FIBRO_UP	30	0.516038	1.616954	0.017544	0.127732	0.4
DAVIES_MGUS_MM	35	0.582801	1.654868	0.017544	0.129001	0.29
CMV_ALL_UP	77	0.494515	1.553785	0	0.130787	0.55

CMV-UV_HCMV_6HRS_DN	122	0.440989	1.684124	0	0.133263	0.18
UVB_NHEK3_ALL	467	0.43419	1.635004	0	0.134843	0.36
TPA_RESIST_EARLY_DN	71	0.471609	1.706333	0	0.13683	0.13
VEGF_MMMEC_ALL_UP	81	0.470771	1.555033	0.070175	0.138053	0.55
TNFALPHA_ALL_UP	73	0.423217	1.638607	0.021277	0.144975	0.35
DSRNA_UP	37	0.615536	1.484818	0.050847	0.148374	0.72
TSA_HEPATOMA_UP	37	0.479156	1.473993	0.076923	0.148794	0.76

Senescence Enriched Gene Sets

NAME	SIZE	ES	NES	NOM p-val	FDR q-val	FWER p-val
UVB_NHEK3_C0	101	0.529704	1.795019	0	0.014449	0.01
JECHLINGER_EMT_DOWN	40	0.567248	1.632176	0	0.066461	0.31
ANDROGEN_GENES	52	0.674071	1.539559	0	0.066919	0.53
TPA_SENS_LATE_DN	215	0.438801	1.540199	0	0.06807	0.53
CMV_ALL_UP	77	0.526481	1.625971	0.016949	0.069499	0.32
CHAUHAN_2ME2	36	0.590136	1.540363	0	0.069772	0.53
GAMMA-UV_FIBRO_DN	39	0.602555	1.573477	0	0.069874	0.47
ET743_RESIST_DN	34	0.614287	1.536661	0	0.069904	0.53
WERNERONLY_FIBRO_UP	30	0.609646	1.543582	0	0.069974	0.51
HEARTFAILURE_ATRIA_DN	130	0.420789	1.516926	0	0.070258	0.57
TPA_RESIST_LATE_DN	57	0.396058	1.517356	0.032787	0.070383	0.57
BRENTANI_IMMUNE_FUNCTION	50	0.527649	1.51455	0	0.070526	0.58
ROSS_MLL_FUSION	77	0.548274	1.63458	0	0.07101	0.31
SMITH_HTERT_DOWN	61	0.530096	1.520991	0	0.071046	0.57
GNATENKO_PLATELET	42	0.560999	1.544467	0.038462	0.071057	0.51
CMV_HCMV_TIMECOURSE_6HRS_DN	55	0.499551	1.532718	0.087719	0.07112	0.54
CMV_HCMV_TIMECOURSE_ALL_DN	485	0.426087	1.517736	0	0.071663	0.57
VEGF_MMMEC_12HRS_UP	25	0.675701	1.515263	0	0.071742	0.58
TARTE_PC	75	0.498486	1.52461	0	0.071975	0.57
UV-CMV_UNIQUE_HCMV_6HRS_UP	132	0.507713	1.520013	0	0.072139	0.57
VEGF_MMMEC_3HRS_UP	55	0.565027	1.528134	0	0.072378	0.56
IFN_BETA_GLIOMA_UP	50	0.418442	1.521049	0	0.072413	0.57
POMEROY_CLASSIC_MD_UP	35	0.482009	1.574063	0	0.072561	0.47
UV_UNIQUE_FIBRO_DN	28	0.693883	1.509896	0.020408	0.072759	0.6
BRG1_ALAB_DN	32	0.637603	1.545172	0	0.072978	0.51
UVC_HIGH_D5_DN	30	0.509219	1.524963	0	0.073	0.57
TPA_SENS_EARLY_UP	43	0.506857	1.51335	0	0.073067	0.59
UVB_NHEK1_UP	140	0.531042	1.567796	0	0.073152	0.48
OLD_FIBRO_DN	144	0.473393	1.507356	0.017544	0.073555	0.6
CMV_HCMV_TIMECOURSE_24HRS_UP	78	0.409778	1.510753	0.032787	0.073605	0.6
TESTIS_EXPRESSED_GENES	61	0.420126	1.546217	0	0.073636	0.51
ZHAN_TONSIL_BONEMARROW	40	0.629071	1.587898	0	0.073705	0.43
MAGRANGEAS_LK_DOWN	27	0.592666	1.528387	0.02	0.073727	0.56
GAMMA-UV_FIBRO_UP	33	0.521609	1.50285	0	0.073809	0.64
UVC_TTD_8HR_DN	174	0.573355	1.503505	0.037736	0.07445	0.64
TPA_RESIST_MIDDLE_DN	95	0.526807	1.578068	0	0.074467	0.44
DAC_PANC_UP	402	0.492984	1.525007	0	0.07449	0.57
CMV_24HRS_UP	58	0.544419	1.525394	0.018519	0.0747	0.57
SHIPP_FL_UP	34	0.597953	1.510862	0	0.074812	0.6
UVB_NHEK3_ALL	467	0.482413	1.574972	0	0.075041	0.46
TSA_HEPATOMA_UP	37	0.579155	1.505651	0	0.075199	0.64
STRESS_TPA_SPECIFIC_UP	49	0.38809	1.528615	0	0.075366	0.56
DIAB_NEPH_DN	395	0.547135	1.54657	0	0.075378	0.51
HDACI_COLON_BUT12HRS_UP	34	0.581869	1.503598	0.036364	0.075561	0.64

H2O2_CSBDIFF_C2	26	0.520755	1.550485	0.032787	0.075762	0.51
UVB_SCC_UP	75	0.551089	1.589838	0.037736	0.076217	0.43
CMV_8HRS_UP	29	0.645522	1.504032	0.018182	0.076395	0.64
BRCA1_OVEREXP_UP	128	0.535055	1.552876	0	0.076798	0.5
BRCA1_OVEREXP_PROSTATE_UP	153	0.515546	1.581965	0	0.077091	0.43
CIS_XPC_DN	165	0.451638	1.498707	0.035714	0.077552	0.67
NELSON_ANDROGEN_UP	58	0.633904	1.564215	0.038462	0.078025	0.49
TPA_RESIST_EARLY_DN	71	0.559828	1.594541	0	0.078197	0.43
ESR_FIBROBLAST_UP	43	0.579866	1.635322	0	0.078899	0.31
ALZHEIMERS_INCIPIENT_DN	149	0.366612	1.552998	0.042553	0.079198	0.5
FRASOR_ER_DOWN	61	0.614683	1.497046	0.018868	0.079398	0.67
ELECTRON_TRANSPORTER_ACTIVITY	113	0.555891	1.591149	0	0.080027	0.43
PENG_RAPAMYCIN_UP	155	0.415837	1.495589	0	0.080085	0.67
TPA_SENS_EARLY_DN	275	0.436528	1.611422	0	0.080102	0.39
GAMMA_ESR_WS_UNREG	29	0.533182	1.557451	0.020833	0.080314	0.5
UVC_XPCS_8HR_DN	419	0.484027	1.494189	0.072727	0.0807	0.67
UV-CMV_UNIQUE_HCMV_6HRS_DN	92	0.560455	1.670083	0	0.08074	0.23
TPA_SENS_MIDDLE_DN	283	0.461157	1.553707	0	0.081753	0.5
TSADAC_HYPOMETH_OVCA_UP	46	0.568358	1.607481	0.04918	0.082456	0.39
4NQO_ESR_WS_UNREG	35	0.501657	1.595218	0	0.082541	0.43
OXSTRESS_RPE_HNETBH_DN	40	0.553098	1.489436	0	0.082673	0.67
HADDAD_10VS7	258	0.555508	1.491031	0	0.083298	0.67
BRENTANI_PROTEIN_MODIFICATION	144	0.482071	1.489966	0	0.083533	0.67
GAMMA_ESR_OLD_UNREG	27	0.555303	1.595654	0	0.083609	0.43
HADDAD_INTVSHI	78	0.591266	1.485886	0	0.083647	0.67
BRENTANI_SIGNALLING	179	0.480414	1.614325	0	0.083871	0.38
WELCSH_BRCA_UP	39	0.641943	1.640859	0	0.084011	0.3
UVC_HIGH_D2_DN	27	0.652063	1.485886	0	0.084733	0.67
CROONQUIST_IL6_STROMA_UP	36	0.668543	1.473661	0	0.084909	0.69
BRCA_BRCA1_NEG	126	0.507751	1.47201	0.017241	0.085109	0.72
AGEING_BRAIN_UP	235	0.499644	1.472514	0	0.085398	0.72
POMEROY_DESMO_MD_UP	43	0.66044	1.472946	0.02	0.085454	0.72
DIAB_NEPH_UP	79	0.518199	1.474644	0	0.085519	0.69
CMV_HCMV_TIMECOURSE_48HRS_DN	137	0.461609	1.475632	0	0.086275	0.69
BRENTANI_DEATH	70	0.499667	1.46901	0.019608	0.086309	0.74
UVC_TTD-XPCS_COMMON_DN	151	0.555435	1.47099	0.076923	0.086345	0.74
UVC_XPCS_ALL_DN	494	0.47413	1.47764	0.074074	0.086645	0.69
CIS_XPC_UP	127	0.475199	1.468085	0	0.087012	0.75
BAF57_BT549_DN	341	0.447133	1.4759	0	0.087017	0.69
FRASOR_ER_UP	30	0.487513	1.469477	0.018519	0.087128	0.74
BRCA_ER_POS	457	0.475909	1.478164	0.018182	0.087562	0.69
JISON_STRESS	30	0.519862	1.464754	0.058824	0.087565	0.75
CHIARETTI_T_ALL	238	0.482512	1.478452	0.019608	0.087858	0.69
DAVIES_MGUS_MM	35	0.645964	1.596943	0	0.088175	0.43
AGUIRRE_PANCREAS_CHR12	53	0.44193	1.465833	0.058824	0.088246	0.75
UV-4NQO_FIBRO_UP	26	0.504281	1.46477	0.017544	0.088458	0.75
HYPOXIA_RCC_NOVHL_UP	51	0.347478	1.480868	0	0.088775	0.69
HOX_GENES	52	0.524791	1.462452	0.068966	0.088914	0.77
ET743_SARCOMA_72HRS_UP	59	0.530077	1.478459	0.037736	0.088942	0.69
BAF57_BT549_UP	246	0.575868	1.480017	0	0.088972	0.69
WERNERONLY_FIBRO_DN	52	0.443119	1.464944	0.035714	0.089264	0.75
UVB_NHEK1_DN	207	0.47546	1.461989	0.072727	0.089756	0.78
JECHLINGER_EMT_UP	54	0.495615	1.456824	0	0.090063	0.78
TNFA_5ENDOTHELIAL_DOWN	71	0.547424	1.455563	0	0.090275	0.78
HYPOXIA_REVIEW	80	0.550173	1.460117	0.061224	0.090366	0.78
IL1_CORNEA_UP	49	0.51516	1.453653	0	0.090396	0.78

UVB_NHEK2_DN	71	0.501198	1.458573	0.018519	0.090462	0.78
PGC	345	0.358022	1.457049	0	0.090538	0.78
LVAD_HEARTFAILURE_DN	41	0.620823	1.455997	0.033333	0.090806	0.78
SMITH_HTERT_UP	102	0.364173	1.458991	0	0.090846	0.78
CMV-UV_HCMV_6HRS_UP	153	0.458724	1.453967	0	0.091035	0.78
LU_IL4BCELL	65	0.555422	1.449735	0.018868	0.092097	0.79
TARTE_MATURE_PC	369	0.481632	1.451684	0.019231	0.092127	0.78
ET743_HELA_UP	45	0.604097	1.450358	0.02	0.092689	0.79
HDACI_COLON_CLUSTER10	38	0.553578	1.449934	0.06383	0.092723	0.79
ALZHEIMERS_INCIPIENT_UP	363	0.474854	1.447433	0	0.093578	0.8
ROSS_CBF_MYH	48	0.559289	1.438206	0	0.093814	0.8
VEGF_MMMEC_ALL_UP	81	0.570704	1.439187	0	0.093995	0.8
SERUM_FIBROBLAST_CORE_DN	169	0.631641	1.441109	0	0.094016	0.8
WERNER_FIBRO_DN	145	0.430143	1.446245	0.019608	0.09412	0.8
UVB_NHEK3_C1	67	0.588784	1.43673	0.039216	0.094126	0.8
ELECTRON_TRANSPORT	74	0.525587	1.441727	0.018182	0.094717	0.8
UVB_NHEK3_C2	53	0.60958	1.44629	0.019231	0.094931	0.8
UVC_TTD_ALL_DN	372	0.489484	1.441936	0.076923	0.095513	0.8
VENTRICLES_UP	242	0.464334	1.641511	0	0.096013	0.3
CMV_HCMV_TIMECOURSE_24HRS_DN	46	0.578211	1.442004	0	0.096322	0.8
CMV-UV_HCMV_6HRS_DN	122	0.501885	1.670732	0	0.096888	0.23
AS3_FIBRO_DN	26	0.607452	1.432599	0.037037	0.097466	0.8
ASTON_DEPRESSION_DOWN	144	0.427018	1.4296	0.036364	0.097511	0.8
HDACI_COLON_CLUSTER9	46	0.638488	1.427057	0	0.097672	0.8
OLDWERNER_FIBRO_DN	94	0.4352	1.431258	0.054545	0.097845	0.8
UVC_HIGH_ALL_DN	228	0.404757	1.426302	0.055556	0.097872	0.8
EGF_HDMEC_UP	30	0.435594	1.425755	0	0.097924	0.8
PROLIF_GENES	364	0.41644	1.42977	0	0.098172	0.8
MYC_HUVEC_SAGE_ARRAY_UP	31	0.572238	1.427195	0.076923	0.098246	0.8
UVC_TTD_4HR_DN	311	0.474129	1.424411	0.074074	0.098356	0.8
HPV31_DN	40	0.595899	1.423133	0.02	0.098879	0.81
CMV_24HRS_DN	61	0.539501	1.420248	0	0.100492	0.81
KLEIN_PEL_DOWN	55	0.467475	1.418732	0.056604	0.101331	0.81
VANTVEER_POOR_OUTCOME_BREAST	26	0.515549	1.417785	0.032258	0.10204	0.81
UVC_HIGH_D7_DN	26	0.472073	1.413002	0.096154	0.10262	0.81
OLDONLY_FIBRO_DN	50	0.545787	1.415358	0.017544	0.102799	0.81
OKUMURA_MC_LPS	161	0.462536	1.41367	0.035088	0.103134	0.81
HDACI_COLON_SUL48HRS_UP	67	0.473486	1.415542	0.057692	0.103544	0.81
KANNAN_P53_UP	35	0.475635	1.411863	0.055556	0.103732	0.81
CMV_HCMV_TIMECOURSE_14HRS_DN	47	0.61967	1.727448	0	0.105336	0.07
BRG1_SW13_UP	42	0.557791	1.4068	0.019608	0.106262	0.82
CORDERO_KRAS_CONTROL_UP	55	0.43038	1.407318	0	0.106567	0.82
ROME_INSULIN_2F_UP	184	0.496577	1.674115	0	0.106804	0.21
BRG1_H1299_UP	27	0.677177	1.407374	0	0.107302	0.82
MUNSHI_MM_UP	65	0.421145	1.407426	0.036364	0.107853	0.82
HYPOXIA_NORMAL_UP	182	0.472328	1.407477	0.035714	0.108607	0.82
HDACI_COLON_SUL_UP	94	0.474511	1.401304	0.058824	0.110995	0.84
TSA_PANC50_UP	37	0.625755	1.400271	0.017857	0.111162	0.84
BROCKE_IL6	138	0.46826	1.396611	0.035088	0.112811	0.84
ROSS_AML1_ETO	71	0.429583	1.396838	0.034483	0.112897	0.84
GAMMA_UNIQUE_FIBRO_DN	57	0.565697	1.397869	0.055556	0.113286	0.84
CMV_HCMV_TIMECOURSE_16HRS_UP	61	0.434897	1.397183	0	0.11343	0.84
BRCA1_IRRADIATED_UP	67	0.374335	1.393639	0.103448	0.113904	0.84
SERUM_RESPONSE_QUIESCENT	124	0.616004	1.394092	0	0.114431	0.84
RETT_UP	34	0.646021	1.39102	0.056604	0.115319	0.86
BRENTANI_TRANSCRIPTION_FACTOR	64	0.477982	1.388916	0.037736	0.115321	0.86

IFNA_UV-CMV_COMMON_HCMV_6HRS_UP	37	0.591534	1.384813	0.038462	0.115437	0.87
DSRNA_UP	37	0.658925	1.386003	0.036364	0.115575	0.87
ADIP_HUMAN_DN	27	0.535716	1.385176	0.084746	0.115736	0.87
PENG_GLUCOSE_DOWN	134	0.372096	1.389107	0.038462	0.115879	0.86
UVC_XPCS_4HR_DN	256	0.456261	1.39117	0.075472	0.115992	0.86
KUROKAWA_5FU_IFN_RESISTANT	33	0.443834	1.386347	0.037736	0.11623	0.87
GOLDRATH_MEMORY	53	0.541729	1.387367	0	0.116415	0.87
TPA_RESIST_LATE_UP	35	0.439828	1.380128	0.074074	0.117864	0.87
ASTON_DEPRESSION_UP	42	0.548533	1.380537	0.105263	0.118125	0.87
VEGF_MMMEC_6HRS_UP	44	0.629904	1.378659	0.037736	0.11837	0.87
DER_IFNB_HT1080_UP	94	0.445926	1.379096	0.037736	0.118467	0.87
BRENTANI_CELL_ADHESION	92	0.480694	1.380578	0.054545	0.118718	0.87
NING_COPD_DOWN	118	0.451157	1.380803	0.074074	0.118991	0.87
IL1_CORNEA_DN	62	0.493998	1.376663	0.018868	0.120617	0.87
CMV_HCMV_TIMECOURSE_12HRS_UP	31	0.710426	1.37455	0.019608	0.121766	0.87
WERNER_FIBRO_UP	49	0.544032	1.68183	0	0.122409	0.16
TSA_HEPATOMA_CANCER_UP	30	0.674212	1.368497	0.019231	0.128198	0.88
PENG_RAPAMYCIN_DOWN	187	0.279038	1.369061	0.02	0.128297	0.88
BRCA_PROGNOSIS_POS	36	0.445108	1.366953	0.083333	0.128552	0.88
HPV31_UP	53	0.439527	1.364754	0.089286	0.130236	0.88
HEARTFAILURE_VENTRICLE_DN	91	0.40835	1.363438	0.078431	0.131722	0.88
TPA_RESIST_MIDDLE_UP	47	0.377921	1.362285	0.053571	0.132443	0.88
ZUCCHI_EPITHELIAL_DOWN	43	0.545408	1.359827	0.14	0.133983	0.89
UVC_TTD_8HR_UP	28	0.511491	1.36029	0.078431	0.134463	0.89
TNFALPHA_4HRS_UP	39	0.464211	1.357956	0.142857	0.134615	0.9
BLEO_HUMAN_LYMPH_HIGH_24HRS_UP	110	0.49081	1.358357	0.037736	0.134715	0.89
CMV_ALL_DN	85	0.481313	1.355426	0.018868	0.135342	0.9
HCV_HCC_MARKER	33	0.51848	1.358488	0.06	0.135403	0.89
PENG_GLUCOSE_UP	35	0.430133	1.356731	0.089286	0.135519	0.9
RCC_NL_UP	419	0.356098	1.356	0.092593	0.135557	0.9
HDACI_COLON_SUL16HRS_DN	60	0.412051	1.353572	0.050847	0.136727	0.9
BHATTACHARYA_ESC_UP	66	0.466258	1.350216	0.115385	0.137103	0.92
TARTE_BCELL	36	0.430114	1.349684	0.037736	0.137192	0.92
HDACI_COLON_BUT24HRS_UP	52	0.522272	1.35107	0.061224	0.137212	0.91
INSULIN_SIGNALLING	98	0.41471	1.350464	0.055556	0.137346	0.91
UVC_TTD-XPCS_COMMON_UP	30	0.410105	1.343498	0.086207	0.13743	0.93
ZUCCHI_EPITHELIAL_UP	42	0.414096	1.343823	0.056604	0.137729	0.93
MANALO_HYPOXIA_UP	94	0.510003	1.351183	0.092593	0.137771	0.91
UVB_NHEK3_C8	68	0.527932	1.342486	0.075472	0.137889	0.93
TGFBETA_EARLY_UP	35	0.575428	1.341942	0.037037	0.138104	0.93
TNFALPHA_ALL_UP	73	0.362589	1.35147	0.022222	0.138123	0.91
HDACI_COLON_TSA_DN	45	0.466434	1.343934	0.127273	0.138364	0.93
ET743PT650_COLONCA_DN	27	0.505724	1.340014	0.102041	0.138818	0.93
ATRIA_UP	237	0.439658	1.347618	0.018182	0.138855	0.93
DER_IFNA_HT1080_UP	68	0.46514	1.35149	0.056604	0.138857	0.91
HDACI_COLON_SUL24HRS_DN	106	0.371333	1.344118	0.018182	0.138936	0.93
HINATA_NFKB_UP	107	0.554817	1.344244	0	0.139634	0.93
CORDERO_KRAS_KNOCK_DOWN	73	0.539363	1.344624	0.058824	0.139851	0.93
UVB_NHEK1_C6	96	0.459619	1.337254	0.053571	0.140189	0.94
IL6_SCAR_FIBRO_UP	29	0.536438	1.344935	0.017544	0.140511	0.93
OXSTRESS_RPETWO_DN	90	0.40091	1.345197	0.018519	0.140513	0.93
IFNA_HCMV_6HRS_UP	63	0.535717	1.33742	0.072727	0.140664	0.94
CMV_HCMV_TIMECOURSE_8HRS_UP	25	0.53186	1.332702	0.06	0.144215	0.94
TGFBETA_ALL_UP	61	0.539831	1.331196	0.070175	0.144926	0.94

HDACI_COLON_SUL_DN	167	0.375718	1.32864	0.056604	0.145179	0.94
BRG1_ALAB_UP	38	0.598762	1.328125	0.111111	0.145449	0.94
IFNG_5ENDOTHELIAL_DOWN	68	0.431825	1.328703	0.09434	0.145813	0.94
OLD_FIBRO_UP	55	0.358771	1.329397	0.087719	0.146073	0.94
LVAD_HEARTFAILURE_UP	96	0.422225	1.327204	0.107143	0.146218	0.94
UVC_LOW_ALL_DN	39	0.590909	1.328879	0.078431	0.146395	0.94
RESISTANCE_XENOGRAFTS_UP	26	0.711607	1.323993	0.1	0.14662	0.94
OXSTRESS_BREASTCA_UP	27	0.477987	1.324023	0.125	0.14729	0.94
TENEDINI_MK	54	0.416251	1.324526	0.1	0.147439	0.94
TPA_RESIST_EARLY_UP	28	0.440015	1.324989	0.078431	0.147817	0.94

Appendix D: The list of probe sets obtained from binary tree analysis using SIGN probe-sets for distinct Boyault-HCC subclasses

Discriminative probe sets of 2a from 1a, 2b, and 1b (n=513)

Probe set	Gene symbol	1a,1b,2b/2a	IMM/SEN
200003_s_at	RPL28	0.73	1.15
200019_s_at	FAU	0.85	1.00
200043_at	ERH	0.79	1.01
200081_s_at	RPS6	0.75	1.54
200594_x_at	HNRNPU	0.68	1.23
200618_at	LASP1	0.73	0.75
200675_at	CD81	1.63	0.36
200708_at	GOT2	1.73	1.27
200770_s_at	LAMC1	0.65	0.68
200772_x_at	PTMA	0.70	2.12
200788_s_at	PEA15	0.74	0.77
200829_x_at	ZNF207	0.74	1.22
200843_s_at	EPRS	0.69	1.09
200847_s_at	TMEM66	1.38	0.93
200916_at	TAGLN2	0.71	1.06
200996_at	ACTR3	0.76	1.17
200998_s_at	CKAP4	0.49	0.95
201001_s_at	UBE2V1	0.77	1.57
201090_x_at	TUBA1B	0.67	1.11
201093_x_at	SDHA	1.43	1.66
201111_at	CSE1L	0.67	1.50
201128_s_at	ACLY	0.60	1.20
201135_at	ECHS1	1.66	1.28
201202_at	PCNA	0.69	1.92
201241_at	DDX1	0.82	1.27
201252_at	PSMC4	0.75	1.59
201254_x_at	RPS6	0.80	1.38
201291_s_at	TOP2A	0.52	2.26
201292_at	TOP2A	0.41	2.00
201353_s_at	BAZ2A	0.80	0.62
201414_s_at	NAP1L4	0.84	1.35
201425_at	ALDH2	1.94	1.15
201432_at	CAT	1.79	0.98
201458_s_at	BUB3	0.65	1.91
201477_s_at	RRM1	0.63	1.79
201485_s_at	RCN2	0.65	0.89
201488_x_at	KHDRBS1	0.70	1.36

201510_at	ELF3	0.62	0.41
201548_s_at	JARID1B	0.56	0.17
201555_at	MCM3	0.65	1.60
201584_s_at	DDX39	0.57	1.40
201594_s_at	PPP4R1	0.66	1.86
201608_s_at	PWP1	0.77	1.20
201697_s_at	DNMT1	0.61	1.88
201729_s_at	KIAA0100	0.67	1.33
201755_at	MCM5	0.69	2.23
201839_s_at	TACSTD1	0.28	0.26
201841_s_at	HSPB1	0.55	0.84
201853_s_at	CDC25B	0.70	1.71
201890_at	RRM2	0.40	1.83
201892_s_at	IMPDH2	0.67	1.51
201901_s_at	YY1	0.74	1.12
201968_s_at	PGM1	1.89	1.36
202003_s_at	ACAA2	2.40	1.48
202025_x_at	ACAA1	1.91	0.90
202029_x_at	RPL38	0.76	0.96
202041_s_at	FIBP	0.83	1.53
202094_at	BIRC5	0.83	1.44
202095_s_at	BIRC5	0.49	1.90
202153_s_at	NUP62	0.78	1.35
202187_s_at	PPP2R5A	0.67	0.61
202217_at	C21orf33	1.46	1.27
202220_at	KIAA0907	0.69	0.64
202240_at	PLK1	0.79	2.04
202246_s_at	CDK4	0.61	1.30
202261_at	VPS72	0.72	1.18
202309_at	MTHFD1	2.66	1.59
202324_s_at	ACBD3	0.61	0.60
202347_s_at	UBE2K	0.77	0.82
202372_at	RAB3GAP2	0.81	0.66
202396_at	TCERG1	0.65	1.54
202451_at	GTF2H1	0.73	1.29
202487_s_at	H2AFV	0.74	1.32
202503_s_at	KIAA0101	0.44	1.54
202556_s_at	MCRS1	0.77	1.28
202603_at	NA	0.61	0.77
202604_x_at	ADAM10	0.71	0.86
202651_at	LPGAT1	0.45	0.90
202656_s_at	SERTAD2	0.75	0.75
202679_at	NPC1	0.56	0.66
202691_at	SNRPD1	0.65	1.59
202705_at	CCNB2	0.57	1.46
202715_at	CAD	0.80	1.55
202726_at	LIG1	0.72	2.31
202758_s_at	RFXANK	0.78	1.16
202769_at	CCNG2	0.66	0.31
202779_s_at	UBE2S	0.54	2.09
202813_at	TARBP1	0.63	0.62
202846_s_at	PIGC	0.64	0.74
202852_s_at	FLJ11506	0.78	1.21
202862_at	FAH	1.69	1.24

202870_s_at	CDC20	0.51	1.69
202935_s_at	SOX9	0.33	0.87
202954_at	UBE2C	0.59	1.89
202971_s_at	DYRK2	0.76	0.49
202984_s_at	BAG5	0.83	1.08
203046_s_at	TIMELESS	0.76	1.85
203075_at	SMAD2	0.70	0.64
203103_s_at	PRPF19	0.81	1.34
203145_at	SPAG5	0.77	1.49
203213_at	CDC2	0.47	2.10
203214_x_at	CDC2	0.58	2.10
203228_at	PAFAH1B3	0.59	1.60
203276_at	LMNB1	0.76	2.86
203318_s_at	ZNF148	0.76	0.64
203319_s_at	ZNF148	0.68	0.69
203358_s_at	EZH2	0.67	3.52
203362_s_at	MAD2L1	0.65	1.86
203429_s_at	C1orf9	0.57	0.42
203436_at	RPP30	0.79	1.48
203564_at	FANCG	0.70	1.96
203630_s_at	COG5	0.72	0.86
203639_s_at	FGFR2	0.43	1.40
203682_s_at	IVD	1.46	1.55
203692_s_at	E2F3	0.79	0.86
203696_s_at	RFC2	0.74	1.47
203711_s_at	HIBCH	1.70	2.17
203725_at	GADD45A	2.12	0.54
203732_at	TRIP4	0.73	0.90
203755_at	BUB1B	0.54	1.62
203758_at	CTSO	1.86	0.35
203764_at	DLGAP5	0.55	2.12
203790_s_at	HRSP12	2.27	1.43
203832_at	SNRPF	0.68	1.29
203856_at	VRK1	0.68	1.81
203924_at	GSTA2	2.99	0.44
203963_at	CA12	0.48	0.57
203967_at	CDC6	0.58	1.86
203968_s_at	CDC6	0.59	2.24
204023_at	RFC4	0.50	2.42
204026_s_at	ZWINT	0.40	1.75
204107_at	NFYA	0.79	1.87
204108_at	NFYA	0.73	1.64
204167_at	BTD	1.44	0.45
204170_s_at	CKS2	0.51	1.20
204252_at	CDK2	0.77	2.27
204263_s_at	CPT2	1.65	1.42
204291_at	ZNF518A	0.73	1.47
204444_at	KIF11	0.70	1.94
204510_at	CDC7	0.69	2.10
204649_at	TROAP	0.82	1.26
204705_x_at	ALDOB	3.57	0.23
204744_s_at	IARS	0.69	1.25
204753_s_at	HLF	4.12	1.94
204755_x_at	HLF	3.50	2.33

204767_s_at	FEN1	0.60	1.45
204825_at	MELK	0.66	1.99
204867_at	GCHFR	1.64	1.32
204920_at	CPS1	5.36	0.64
204962_s_at	CENPA	0.57	1.85
205034_at	CCNE2	0.64	2.03
205042_at	GNE	2.31	1.97
205053_at	PRIM1	0.63	2.11
205141_at	ANG	1.92	0.57
205158_at	RNASE4	1.71	0.66
205167_s_at	CDC25C	0.74	2.41
205221_at	HGD	3.07	0.67
205235_s_at	KIF20B	0.90	1.75
205264_at	CD3EAP	0.82	1.45
205303_at	KCNJ8	1.85	0.27
205304_s_at	KCNJ8	2.34	0.27
205342_s_at	SULT1C2	0.38	0.81
205345_at	BARD1	0.61	1.93
205363_at	BBOX1	3.53	0.08
205364_at	ACOX2	2.29	1.45
205393_s_at	CHEK1	0.74	2.48
205394_at	CHEK1	0.75	2.34
205395_s_at	MRE11A	0.78	1.74
205436_s_at	H2AFX	0.53	1.53
205442_at	MFAP3L	3.04	0.46
205449_at	SAC3D1	0.54	1.55
205480_s_at	UGP2	1.61	0.91
205498_at	GHR	2.96	0.79
205530_at	ETFDH	2.43	0.68
205565_s_at	FXN	1.35	1.37
205614_x_at	MST1	1.98	1.73
205633_s_at	ALAS1	2.13	0.56
205650_s_at	FGA	1.64	0.69
205664_at	KIN	0.74	1.51
205690_s_at	BUD31	0.73	1.40
205768_s_at	SLC27A2	2.21	0.46
205769_at	SLC27A2	2.23	0.50
205807_s_at	TUFT1	0.59	0.51
205830_at	CLGN	0.32	1.08
205860_x_at	FOLH1	2.15	0.32
205865_at	ARID3A	0.64	1.16
205909_at	POLE2	0.65	2.51
205975_s_at	HOXD1	0.70	0.48
205999_x_at	CYP3A4	4.35	0.62
206036_s_at	REL	0.76	0.63
206052_s_at	SLBP	0.72	1.40
206074_s_at	HMGA1	0.59	1.76
206085_s_at	CTH	3.18	2.15
206102_at	GINS1	0.47	1.80
206208_at	CA4	1.28	0.21
206239_s_at	SPINK1	0.13	0.41
206262_at	ADH1C	6.15	0.16
206305_s_at	C8A	3.91	1.60
206316_s_at	KNTC1	0.71	1.60

206363_at	MAF	1.47	0.54
206424_at	CYP26A1	1.78	0.56
206445_s_at	PRMT1	0.74	2.61
206535_at	SLC2A2	2.39	1.99
206539_s_at	CYP4F12	1.72	1.78
206571_s_at	MAP4K4	0.65	1.34
206697_s_at	HP	2.52	0.83
206734_at	JRKL	0.83	0.58
206797_at	NAT2	3.39	0.31
207081_s_at	PI4KA	0.71	0.77
207098_s_at	MFN1	0.75	1.52
207168_s_at	H2AFY	0.62	0.71
207392_x_at	UGT2B15	2.91	0.08
207414_s_at	PCSK6	1.73	0.69
207426_s_at	TNFSF4	0.76	0.58
207544_s_at	ADH6	2.98	1.55
207808_s_at	PROS1	1.75	0.80
207819_s_at	ABCB4	4.97	1.98
207842_s_at	CASC3	0.77	1.16
208079_s_at	AURKA	0.54	1.98
208113_x_at	PABPC3	0.72	1.22
208228_s_at	FGFR2	0.31	1.44
208369_s_at	GCDH	1.88	1.47
208641_s_at	RAC1	0.75	0.97
208644_at	PARP1	0.71	1.34
208660_at	CS	0.75	1.14
208678_at	ATP6V1E1	0.81	0.62
208684_at	COPA	0.75	0.64
208693_s_at	GARS	0.69	1.53
208694_at	PRKDC	0.56	1.39
208753_s_at	NAP1L1	0.69	1.36
208754_s_at	NAP1L1	0.57	1.52
208777_s_at	PSMD11	0.76	1.22
208783_s_at	CD46	0.67	0.67
208795_s_at	MCM7	0.61	1.95
208821_at	SNRPB	0.57	1.46
208855_s_at	STK24	0.67	1.19
208869_s_at	GABARAPL1	1.88	0.47
208877_at	PAK2	0.71	1.71
208882_s_at	UBR5	0.61	1.54
208926_at	NEU1	0.62	0.35
208931_s_at	ILF3	0.70	3.04
209019_s_at	PINK1	1.51	0.44
209053_s_at	WHSC1	0.59	1.63
209054_s_at	WHSC1	0.76	1.40
209171_at	ITPA	0.83	1.62
209219_at	RDBP	0.64	0.86
209220_at	GPC3	0.13	0.62
209259_s_at	SMC3	0.55	1.50
209301_at	CA2	1.89	1.89
209302_at	POLR2H	0.78	1.40
209326_at	SLC35A2	0.79	0.48
209366_x_at	CYB5A	1.80	1.32
209368_at	EPHX2	2.64	1.33

209408_at	KIF2C	0.69	2.33
209421_at	MSH2	0.62	1.90
209460_at	ABAT	2.76	0.58
209464_at	AURKB	0.70	2.48
209484_s_at	NSL1	0.75	1.08
209642_at	BUB1	0.62	2.22
209646_x_at	ALDH1B1	1.41	1.62
209660_at	TTR	2.45	0.34
209678_s_at	PRKCI	0.56	1.19
209680_s_at	KIFC1	0.76	1.50
209699_x_at	AKR1C2	1.94	0.09
209713_s_at	SLC35D1	1.43	1.19
209735_at	ABCG2	3.59	0.57
209748_at	SPAST	0.75	1.25
209760_at	KIAA0922	1.58	1.02
209773_s_at	RRM2	0.50	2.33
209852_x_at	PSME3	0.71	1.34
209891_at	SPC25	0.81	2.96
209894_at	LEPR	3.94	1.26
209977_at	PLG	2.66	2.33
210049_at	SERPINC1	2.70	2.57
210052_s_at	TPX2	0.55	1.78
210053_at	TAF5	0.78	1.42
210059_s_at	MAPK13	0.55	0.22
210125_s_at	BANF1	0.78	1.17
210168_at	C6	5.53	0.25
210250_x_at	ADSL	0.74	1.59
210334_x_at	BIRC5	0.74	2.18
210473_s_at	GPR125	1.78	1.09
210652_s_at	TTC39A	0.58	0.47
210739_x_at	SLC4A4	1.26	1.65
210766_s_at	CSE1L	0.73	1.63
210891_s_at	GTF2I	0.73	0.94
210959_s_at	SRD5A1	2.26	2.03
211036_x_at	ANAPC5	0.81	1.15
211056_s_at	SRD5A1	1.76	1.37
211058_x_at	TUBA1B	0.65	1.08
211072_x_at	TUBA1B	0.66	1.10
211270_x_at	PTBP1	0.76	1.62
211303_x_at	PSMAL	2.06	0.36
211354_s_at	LEPR	4.60	1.06
211356_x_at	LEPR	4.63	1.17
211357_s_at	ALDOB	3.52	0.33
211401_s_at	FGFR2	0.60	1.51
211623_s_at	FBL	0.64	1.98
211682_x_at	UGT2B28	2.21	0.07
211761_s_at	CACYBP	0.62	1.21
211780_x_at	DCTN1	0.83	1.20
211814_s_at	CCNE2	0.70	2.45
211921_x_at	PTMA	0.72	1.91
211925_s_at	PLCB1	0.84	2.16
211928_at	DYNC1H1	0.73	0.74
211944_at	BAT2D1	0.73	0.80
211971_s_at	LRPPRC	0.76	1.25

211972_x_at	RPLP0	0.75	1.04
211977_at	GPR107	0.74	0.49
212020_s_at	MKI67	0.68	1.37
212021_s_at	MKI67	0.66	1.80
212022_s_at	MKI67	0.62	2.10
212073_at	CSNK2A1	0.78	1.38
212098_at	LOC151162	0.70	0.64
212110_at	SLC39A14	2.34	1.25
212141_at	MCM4	0.70	2.08
212160_at	XPOT	0.65	1.55
212185_x_at	MT2A	2.27	0.71
212247_at	NUP205	0.63	1.52
212365_at	MYO1B	1.79	0.75
212368_at	ZNF292	0.49	0.67
212371_at	FAM152A	0.66	1.48
212375_at	EP400	0.76	1.66
212403_at	UBE3B	0.82	0.71
212432_at	GRPEL1	1.34	1.27
212459_x_at	SUCLG2	1.63	1.33
212467_at	DNAJC13	0.80	0.59
212542_s_at	PHIP	0.68	0.89
212680_x_at	PPP1R14B	0.76	1.59
212688_at	PIK3CB	0.81	0.79
212742_at	RNF115	0.70	0.86
212836_at	POLD3	0.80	2.44
212840_at	UBXN7	0.72	0.85
212899_at	CDC2L6	0.54	0.73
212964_at	HIC2	0.63	0.77
212973_at	RPIA	0.70	1.29
212983_at	HRAS	0.75	1.34
213008_at	FANCI	0.64	2.00
213043_s_at	MED24	0.72	1.18
213054_at	KIAA0841	0.90	1.99
213073_at	ZFYVE26	0.76	0.50
213088_s_at	DNAJC9	0.62	2.24
213092_x_at	DNAJC9	0.63	2.75
213101_s_at	ACTR3	0.75	1.22
213119_at	SLC36A1	0.87	0.62
213165_at	CEP350	0.65	0.54
213179_at	RQCD1	0.78	1.30
213222_at	PLCB1	0.37	1.62
213226_at	CCNA2	0.67	2.73
213241_at	PLXNC1	0.60	0.46
213279_at	DHRS1	2.00	1.40
213374_x_at	HIBCH	1.70	1.93
213380_x_at	MSTP9	2.05	2.08
213390_at	ZC3H4	0.80	0.90
213397_x_at	ANG	1.58	0.61
213405_at	RAB22A	0.82	1.14
213485_s_at	ABCC10	0.64	0.59
213523_at	CCNE1	0.79	1.65
213599_at	OIP5	0.60	1.40
213626_at	CBR4	1.79	1.81
213632_at	DHODH	1.72	1.47

213646_x_at	TUBA1B	0.68	1.10
213671_s_at	MARS	0.64	1.44
213762_x_at	RBMX	0.76	1.54
213911_s_at	H2AFZ	0.64	1.32
213947_s_at	NUP210	0.71	1.89
213977_s_at	CIZ1	0.82	1.02
214004_s_at	VGLL4	0.75	0.66
214086_s_at	PARP2	0.81	1.38
214142_at	ZG16	2.16	1.86
214164_x_at	CA12	0.45	0.75
214198_s_at	DGCR2	0.75	0.69
214261_s_at	ADH6	2.87	2.58
214274_s_at	ACAA1	2.52	0.79
214306_at	OPA1	0.79	2.37
214308_s_at	HGD	2.56	0.71
214420_s_at	CYP2C9	1.58	0.51
214421_x_at	CYP2C9	3.27	0.24
214440_at	NAT1	1.63	0.50
214681_at	GK	1.34	0.99
214710_s_at	CCNB1	0.56	1.48
214719_at	SLC46A3	2.90	0.24
214734_at	EXPH5	2.09	0.21
214743_at	CUX1	0.65	0.89
214764_at	RRP15	0.78	2.59
214835_s_at	SUCLG2	1.57	1.25
214943_s_at	RBM34	0.79	1.14
215017_s_at	FNBP1L	0.64	0.70
215363_x_at	FOLH1	2.27	0.33
215380_s_at	GGCT	0.74	1.82
215772_x_at	SUCLG2	1.56	1.33
215773_x_at	PARP2	0.84	1.42
215867_x_at	CA12	0.47	0.70
216194_s_at	TBCB	0.74	1.52
216228_s_at	WDHD1	0.92	1.94
216237_s_at	MCM5	0.59	2.18
216271_x_at	SYDE1	1.13	1.32
216320_x_at	MST1	2.05	1.76
216381_x_at	AKR7A3	2.88	1.36
216559_x_at	LOC100128836	0.82	1.67
216661_x_at	CYP2C9	3.14	0.38
216687_x_at	UGT2B15	2.70	0.24
216952_s_at	LMNB2	0.79	1.42
217127_at	CTH	3.82	1.93
217238_s_at	ALDOB	4.45	0.28
217487_x_at	FOLH1	1.73	0.35
217564_s_at	CPS1	6.53	0.67
217640_x_at	C18orf24	0.88	1.76
217774_s_at	HSPC152	0.78	0.98
217815_at	SUPT16H	0.73	1.41
217829_s_at	USP39	0.77	1.34
217946_s_at	SAE1	0.66	1.77
217950_at	NOSIP	0.84	1.40
217973_at	DCXR	3.56	1.24
218021_at	DHRS4	1.44	1.32

218039_at	NUSAP1	0.47	1.65
218045_x_at	PTMS	1.39	1.77
218107_at	WDR26	0.63	0.55
218115_at	ASF1B	0.80	2.91
218125_s_at	CCDC25	1.42	1.92
218227_at	NUBP2	1.18	1.23
218308_at	TACC3	0.66	1.43
218329_at	PRDM4	0.83	0.92
218336_at	PFDN2	0.73	1.05
218349_s_at	ZWILCH	0.59	1.87
218355_at	KIF4A	0.61	1.84
218367_x_at	USP21	0.77	1.19
218399_s_at	CDCA4	0.72	2.49
218510_x_at	FAM134B	2.27	0.20
218532_s_at	FAM134B	2.16	0.15
218542_at	CEP55	0.67	2.02
218544_s_at	RCL1	1.65	1.53
218586_at	C20orf20	0.71	1.71
218593_at	RBM28	0.72	1.50
218594_at	HEATR1	0.66	1.32
218618_s_at	FNDC3B	0.55	0.75
218624_s_at	MGC2752	0.86	2.30
218662_s_at	NCAPG	0.62	2.49
218663_at	NCAPG	0.71	2.95
218670_at	PUS1	0.77	1.68
218699_at	RAB7L1	0.61	0.42
218700_s_at	RAB7L1	0.59	0.39
218726_at	HJURP	0.72	1.81
218728_s_at	DOCK5	0.45	0.59
218734_at	NAT11	0.76	1.51
218741_at	CENPM	0.69	1.83
218750_at	JOSD3	0.70	1.47
218755_at	KIF20A	0.66	2.46
218782_s_at	ATAD2	0.47	2.26
218788_s_at	SMYD3	0.53	1.68
218789_s_at	C11orf71	1.40	0.36
218853_s_at	MOSPD1	0.62	0.56
218869_at	MLYCD	1.82	1.00
218883_s_at	MLF1IP	0.55	2.53
218924_s_at	CTBS	1.47	0.59
218973_at	EFTUD1	0.83	1.06
218984_at	PUS7	0.67	1.91
219004_s_at	C21orf45	0.74	1.62
219060_at	C8orf32	0.66	2.06
219076_s_at	PXMP2	1.76	1.82
219238_at	PIGV	1.37	0.83
219281_at	MSRA	2.23	1.45
219306_at	KIF15	0.76	2.45
219481_at	TTC13	0.64	0.74
219512_at	DSN1	0.85	2.13
219526_at	C14orf169	0.84	1.10
219588_s_at	NCAPG2	0.75	2.82
219787_s_at	ECT2	0.54	1.99
219803_at	ANGPTL3	2.41	0.94

219848_s_at	ZNF432	0.69	0.48
219862_s_at	NARF	0.72	1.42
219874_at	SLC12A8	0.69	0.38
219954_s_at	GBA3	4.10	1.00
219997_s_at	COPS7B	0.85	1.80
220017_x_at	CYP2C9	3.55	0.22
220060_s_at	C12orf48	0.86	2.14
220085_at	HELLS	0.56	3.10
220108_at	GNA14	1.33	0.60
220239_at	KLHL7	0.63	2.00
220432_s_at	CYP39A1	2.94	0.42
220651_s_at	MCM10	0.74	3.41
220668_s_at	DNMT3B	0.78	1.52
220751_s_at	C5orf4	1.67	0.56
220964_s_at	RAB1B	0.86	0.86
221039_s_at	DDEF1	0.74	1.79
221142_s_at	PECR	1.52	2.39
221486_at	ENSA	0.70	0.72
221505_at	ANP32E	0.62	1.60
221520_s_at	CDCA8	0.76	2.03
221522_at	ANKRD27	0.57	0.90
221538_s_at	PLXNA1	0.65	0.63
221580_s_at	JOSD3	0.59	1.36
221637_s_at	C11orf48	0.78	1.06
221677_s_at	DONSON	0.70	1.86
221685_s_at	CCDC99	0.79	2.16
221708_s_at	UNC45A	0.87	0.78
221780_s_at	DDX27	0.78	1.16
221858_at	TBC1D12	0.81	1.93
221893_s_at	ADCK2	0.81	0.92
222036_s_at	MCM4	0.55	1.90
222037_at	MCM4	0.58	2.94
222039_at	KIF18B	0.72	1.51
222148_s_at	RHOT1	0.76	0.98
222155_s_at	GPR172A	0.67	1.29
222244_s_at	TUG1	0.71	0.54
33322_i_at	SFN	0.39	0.76
33323_r_at	SFN	0.37	0.68
33494_at	ETFDH	2.34	0.64
37943_at	ZFYVE26	0.86	0.61
41220_at	SEPT9	0.74	1.30
48031_r_at	C5orf4	1.35	0.69
49077_at	PPME1	0.85	0.87
57539_at	LIME1	2.14	1.29

Discriminative probe sets of 1b from 1a and 2b (n=164)

1a,2b/1b	Probe set	Gene symbol	IMM/SEN
1.31	177_at	PLD1	0.67
0.65	200770_s_at	LAMC1	0.68
0.64	200783_s_at	STMN1	1.62
0.70	201291_s_at	TOP2A	2.26
0.58	201292_at	TOP2A	2.00
0.73	201637_s_at	FXR1	1.64

1.59	201945_at	FURIN	1.25
0.59	201956_s_at	GNPAT	1.04
2.26	201983_s_at	EGFR	0.73
0.83	202240_at	PLK1	2.04
0.71	202338_at	TK1	1.58
1.70	202464_s_at	PFKFB3	1.81
0.54	202503_s_at	KIAA0101	1.54
0.66	202705_at	CCNB2	1.46
0.77	202715_at	CAD	1.55
0.63	202926_at	NAG	0.92
0.72	202954_at	UBE2C	1.89
0.62	203213_at	CDC2	2.10
0.67	203214_x_at	CDC2	2.10
0.80	203276_at	LMNB1	2.86
0.71	203362_s_at	MAD2L1	1.86
0.65	203418_at	CCNA2	2.68
1.32	203455_s_at	SAT1	0.61
0.77	203564_at	FANCG	1.96
2.32	203615_x_at	SULT1A1	1.41
0.61	203636_at	MID1	0.45
0.50	203637_s_at	MID1	0.41
0.69	203714_s_at	TBCE	1.02
0.27	203726_s_at	LAMA3	0.10
0.68	203755_at	BUB1B	1.62
0.69	203764_at	DLGAP5	2.12
1.96	203790_s_at	HRSP12	1.43
9.86	203914_x_at	HPGD	0.62
0.54	204026_s_at	ZWINT	1.75
0.77	204126_s_at	CDC45L	2.74
0.71	204127_at	RFC3	1.88
0.81	204444_at	KIF11	1.94
0.28	204602_at	DKK1	4.15
0.84	204603_at	EXO1	2.54
2.61	204646_at	DPYD	2.00
2.52	204705_x_at	ALDOB	0.23
0.45	204753_s_at	HLF	1.94
0.49	204755_x_at	HLF	2.33
0.83	204795_at	PRR3	1.45
0.72	204825_at	MELK	1.99
2.72	204836_at	GLDC	1.65
2.34	204846_at	CP	0.99
1.47	204934_s_at	HPN	0.32
3.83	204998_s_at	ATF5	1.53
3.61	204999_s_at	ATF5	1.96
2.20	205040_at	ORM1	2.03
0.80	205046_at	CENPE	2.54
0.66	205053_at	PRIM1	2.11
0.75	205167_s_at	CDC25C	2.41
1.34	205203_at	PLD1	0.73
1.34	205227_at	IL1RAP	2.09
4.43	205363_at	BBOX1	0.08
0.62	205436_s_at	H2AFX	1.53
1.68	205480_s_at	UGP2	0.91
3.60	205498_at	GHR	0.79

1.40	205614_x_at	MST1	1.73
2.47	205768_s_at	SLC27A2	0.46
2.52	205769_at	SLC27A2	0.50
0.55	205780_at	BIK	0.31
0.04	205815_at	REG3A	0.39
0.43	205862_at	GREB1	1.96
6.79	205943_at	TDO2	0.07
0.51	206110_at	HIST1H3H	0.23
1.90	206396_at	SLC1A1	1.25
0.82	206441_s_at	COMMD4	1.06
10.49	206643_at	HAL	0.18
0.84	207046_at	HIST2H4A	0.56
1.96	207122_x_at	SULT1A2	1.27
0.72	207156_at	HIST1H2AG	0.31
1.88	207254_at	SLC15A1	0.41
2.06	207574_s_at	GADD45B	0.74
1.28	207667_s_at	MAP2K3	1.29
0.76	207842_s_at	CASC3	1.16
2.90	208228_s_at	FGFR2	1.44
0.72	208583_x_at	HIST1H2AJ	0.60
0.47	208955_at	DUT	1.84
0.71	209053_s_at	WHSC1	1.63
1.60	209304_x_at	GADD45B	0.76
0.81	209680_s_at	KIFC1	1.50
1.42	209760_at	KIAA0922	1.02
0.49	209932_s_at	DUT	1.49
1.88	209980_s_at	SHMT1	2.95
0.61	210052_s_at	TPX2	1.78
1.90	210168_at	C6	0.25
1.28	210177_at	TRIM15	0.50
0.62	210387_at	HIST1H2BG	0.06
1.97	210473_s_at	GPR125	1.09
4.59	210587_at	INHBE	2.40
0.69	210766_s_at	CSE1L	1.63
1.25	210885_s_at	TRIM15	0.81
3.08	211026_s_at	MGLL	0.40
0.72	211165_x_at	EPHB2	0.63
2.67	211357_s_at	ALDOB	0.33
2.12	211385_x_at	SULT1A2	1.36
11.25	211548_s_at	HPGD	0.62
0.75	212020_s_at	MKI67	1.37
0.73	212021_s_at	MKI67	1.80
0.69	212022_s_at	MKI67	2.10
0.74	212115_at	HN1L	1.01
0.77	212145_at	MRPS27	1.92
0.80	212405_s_at	KIAA0859	0.83
0.43	212554_at	CAP2	0.93
0.76	212892_at	ZNF282	1.50
0.45	212922_s_at	SMYD2	1.20
0.79	213008_at	FANCI	2.00
0.74	213186_at	DZIP3	1.08
0.71	213226_at	CCNA2	2.73
1.37	213300_at	ATG2A	0.65
0.63	213301_x_at	TRIM24	1.20

0.80	213454_at	CORT	2.52
0.76	213599_at	OIP5	1.40
1.73	213632_at	DHODH	1.47
3.97	213664_at	SLC1A1	1.13
1.76	213695_at	PON3	0.30
0.87	214197_s_at	SETDB1	1.24
0.37	214290_s_at	HIST2H2AA3	0.17
0.43	214469_at	HIST1H2AE	0.10
0.70	214472_at	HIST1H3D	0.26
0.56	214710_s_at	CCNB1	1.48
0.59	215177_s_at	ITGA6	1.79
0.78	215195_at	PRKCA	0.52
2.35	215299_x_at	SULT1A1	1.33
1.26	215499_at	MAP2K3	1.14
1.82	215723_s_at	PLD1	0.66
0.74	215779_s_at	HIST1H2BG	0.13
2.98	217238_s_at	ALDOB	0.28
4.69	217521_at	NA	0.31
0.49	217678_at	SLC7A11	1.38
3.04	217739_s_at	NAMPT	0.91
0.75	217774_s_at	HSPC152	0.98
1.39	218045_x_at	PTMS	1.77
0.64	218257_s_at	UGCGL1	1.38
0.39	218280_x_at	HIST2H2AA3	0.17
0.62	218355_at	KIF4A	1.84
0.87	218399_s_at	CDCA4	2.49
0.71	218594_at	HEATR1	1.32
0.78	218619_s_at	SUV39H1	1.13
0.49	218638_s_at	SPON2	0.30
0.60	218662_s_at	NCAPG	2.49
0.74	218663_at	NCAPG	2.95
0.61	218755_at	KIF20A	2.46
1.68	218931_at	RAB17	0.35
0.69	218979_at	RMI1	1.62
1.51	219313_at	GRAMD1C	0.44
0.65	219345_at	BOLA1	0.77
6.34	219410_at	TMEM45A	0.58
1.56	219450_at	C4orf19	0.56
0.76	219502_at	NEIL3	3.27
3.06	219954_s_at	GBA3	1.00
0.85	220060_s_at	C12orf48	2.14
1.75	220528_at	VNN3	0.34
0.86	220668_s_at	DNMT3B	1.52
0.85	221064_s_at	UNKL	1.43
1.38	221614_s_at	RPH3AL	2.42
0.81	222039_at	KIF18B	1.51
0.59	33323_r_at	SFN	0.68
0.73	35820_at	GM2A	0.41
2.38	43427_at	ACACB	1.32
2.14	57539_at	LIME1	1.29

Discriminative probe sets of 2b from 1a (n=70)

1a/2b	Probe set	Gene symbol	IMM/SEN
0.70	200916_at	TAGLN2	1.06
0.53	200998_s_at	CKAP4	0.95
0.37	201266_at	TXNRD1	0.65
0.75	201353_s_at	BAZ2A	0.62
0.56	201377_at	UBAP2L	0.91
1.42	201432_at	CAT	0.98
1.48	201968_s_at	PGM1	1.36
1.98	202025_x_at	ACAA1	0.90
0.57	202220_at	KIAA0907	0.64
0.66	202244_at	PSMB4	1.07
0.72	202261_at	VPS72	1.18
2.10	202309_at	MTHFD1	1.59
0.68	202396_at	TCERG1	1.54
0.57	202779_s_at	UBE2S	2.09
0.73	202809_s_at	INTS3	0.84
0.62	202846_s_at	PIGC	0.74
0.76	202971_s_at	DYRK2	0.49
0.46	203429_s_at	C1orf9	0.42
0.32	204105_s_at	NRCAM	0.93
0.58	204744_s_at	IARS	1.25
2.39	204753_s_at	HLF	1.94
2.20	204755_x_at	HLF	2.33
1.72	204920_at	CPS1	0.64
1.83	205019_s_at	VIPR1	0.25
0.53	205807_s_at	TUFT1	0.51
0.25	205830_at	CLGN	1.08
0.70	206052_s_at	SLBP	1.40
0.02	206239_s_at	SPINK1	0.41
1.79	206535_at	SLC2A2	1.99
1.96	208369_s_at	GCDH	1.47
0.65	208684_at	COPA	0.64
0.65	208693_s_at	GARS	1.53
0.41	208700_s_at	TKT	2.25
0.62	209053_s_at	WHSC1	1.63
0.77	209054_s_at	WHSC1	1.40
0.05	209220_at	GPC3	0.62
0.75	209326_at	SLC35A2	0.48
0.61	209678_s_at	PRKCI	1.19
0.21	210519_s_at	NQO1	1.29
0.73	210927_x_at	JTB	0.92
0.64	211761_s_at	CACYBP	1.21
0.68	211944_at	BAT2D1	0.80
0.53	212160_at	XPOT	1.55
0.66	212296_at	PSMD14	1.56
0.67	212334_at	GNS	0.58
0.70	212556_at	SCRIB	1.38
0.63	213165_at	CEP350	0.54
0.24	213194_at	ROBO1	1.15
0.25	213222_at	PLCB1	1.62
0.72	213302_at	PFAS	1.58
0.62	213671_s_at	MARS	1.44
0.76	213947_s_at	NUP210	1.89
1.55	213988_s_at	SAT1	0.67

0.78	214061_at	WDR67	2.65
2.77	214142_at	ZG16	1.86
2.38	214274_s_at	ACAA1	0.79
2.04	216381_x_at	AKR7A3	1.36
0.72	217678_at	SLC7A11	1.38
0.65	218336_at	PFDN2	1.05
0.57	218361_at	GOLPH3L	0.62
1.85	218544_s_at	RCL1	1.53
0.75	218586_at	C20orf20	1.71
0.61	219060_at	C8orf32	2.06
0.64	219862_s_at	NARF	1.42
1.64	220108_at	GNA14	0.60
7.87	220432_s_at	CYP39A1	0.42
0.63	221486_at	ENSA	0.72
0.67	221884_at	EVI1	0.92
0.78	41220_at	SEPT9	1.30
3.29	57539_at	LIME1	1.29

Cancer Letters xxx (2008) xxx–xxx

Contents lists available at ScienceDirect

Cancer Letters

journal homepage: www.elsevier.com/locate/canlet

Mini-review

Senescence and immortality in hepatocellular carcinoma

Mehmet Ozturk [a,b,*], Ayca Arslan-Ergul [a], Sevgi Bagislar [a,b], Serif Senturk [a], Haluk Yuzugullu [a,b]

[a] Department of Molecular Biology and Genetics, Bilkent University, 06800 Ankara, Turkey
[b] Centre de Recherche INSERM-Université Joseph Fourrier U823, Institut Albert Bonniot, 38042 Grenoble, France

ARTICLE INFO

Article history:
Received 26 March 2008
Received in revised form 23 June 2008
Accepted 29 October 2008
Available online xxxx

Keywords:
Liver cancer
Senescence
Telomeres
DNA damage
p53
$p16^{INK4a}$
$p21^{Cip1}$
Retinoblastoma
Cirrhosis
Hepatocytes
Telomerase reverse transcriptase

ABSTRACT

Cellular senescence is a process leading to terminal growth arrest with characteristic morphological features. This process is mediated by telomere-dependent, oncogene-induced and ROS-induced pathways, but persistent DNA damage is the most common cause. Senescence arrest is mediated by $p16^{INK4a}$- and $p21^{Cip1}$-dependent pathways both leading to retinoblastoma protein (pRb) activation. p53 plays a relay role between DNA damage sensing and $p21^{Cip1}$ activation. pRb arrests the cell cycle by recruiting proliferation genes to facultative heterochromatin for permanent silencing. Replicative senescence that occurs in hepatocytes in culture and in liver cirrhosis is associated with lack of telomerase activity and results in telomere shortening. Hepatocellular carcinoma (HCC) cells display inactivating mutations of p53 and epigenetic silencing of $p16^{INK4a}$. Moreover, they re-express telomerase reverse transcriptase required for telomere maintenance. Thus, senescence bypass and cellular immortality is likely to contribute significantly to HCC development. Oncogene-induced senescence in premalignant lesions and reversible immortality of cancer cells including HCC offer new potentials for tumor prevention and treatment.

1. Introduction

Senescence is an evolutionary term meaning "the process of becoming old"; the phase from full maturity to death characterized by accumulation of metabolic products and decreased probability of reproduction or survival [1]. The term "cellular senescence" was initially used by Hayflick and colleagues to define cells that ceased to divide in culture [2]. Today, cellular senescence is recognized as a response of proliferating somatic cells to stress and damage from exogenous and endogenous sources. It is characterized by permanent cell cycle arrest. Senescent cells also display altered morphology and an altered pattern of gene expression, and can be recognized by the presence of senescence markers such as senescence-associated β-galactosidase (SABG), $p16^{INK4A}$, senescence-associated DNA-damage foci and senescence-associated heterochromatin foci (for a review see Ref. [3]). This cellular response has both beneficial (anti-cancer) and probably deleterious (such as tissue aging) effects on the organism. Most of our knowledge of cellular senescence is derived from in vitro studies performed with fibroblasts, and some epithelial cells such as mammary epithelial cells. Animal models are increasingly being used to study cellular senescence in vivo. Telomerase-deficient mouse models lacking RNA subunit (TERC−/−) have been very useful in demonstrating the critical role of telomeres in organ aging and tumor susceptibility [4]. Other mouse models including tumor suppressor gene-deficient and oncogene-expressing mice were also used extensively.

Compared to other tissues and cancer models, the role of senescence in liver cells and its implications in hepatocellular carcinogenesis have been less explored. One of

* Corresponding author. Address: Centre de Recherche INSERM-Université Joseph Fourrier U823, Institut Albert Bonniot, Grenoble 38000, France. Tel.: +33 (0) 4 76 54 94 10; fax: +33 (0) 4 76 54 94 54.
E-mail address: ozturkm@ujf-grenoble.fr (M. Ozturk).

0304-3835/$ - see front matter © 2008 Elsevier Ireland Ltd. All rights reserved.
doi:10.1016/j.canlet.2008.10.048

the main obstacles is the lack of adequate in vitro systems. As hepatocytes can not divide in cell culture, the study of their replicative senescence mechanisms is not easy. Nevertheless, these cells are able to quit their quiescent state in vivo and proliferate massively in response to partial hepatectomy or liver injury [5]. This capacity can be explored to study in vivo senescence of hepatocytes using rodent models. Studies with clinical samples indicate that hepatocyte senescence occurs in vivo in patients with chronic hepatitis, cirrhosis and HCC [6–8]. In contrast to the paucity of studies directly addressing cellular senescence, the critical role of telomere shortening (as a feature associated with replicative senescence) in cirrhosis and HCC development is well established [9]. Telomeres in normal liver show a consistent but slow shortening during aging. In contrast, hepatocyte DNA telomere shortening is accelerated in patients with chronic liver disease with shortest telomeres described in cirrhotic liver and HCC. Telomerase-deficient mice have also been used elegantly to demonstrate the critical roles of telomerase and telomeres in liver regeneration and experimentally induced cirrhosis [10,11]. A major accomplishment in recent years was the demonstration of critical role played by senescence for the clearance of ras-induced murine liver carcinomas following p53 restoration [12].

Despite a relatively important progress, the mechanisms of hepatocellular senescence and the role of cellular immortality in HCC remain ill-known issues. As one of the rare tissues with ample clinical data on senescence-related aberrations, liver may serve as an excellent model to further explore the relevance of cellular senescence in human biology. Moreover, a better understanding of senescence and immortality in hepatic tissues may help to develop new preventive and therapeutic approaches for severe liver diseases such as cirrhosis and HCC. Here we will review recent progress on senescence and immortality mechanisms with a specific emphasis on hepatocellular carcinogenesis.

2. Senescence pathways

Cellular senescence has long been considered as a mechanism that limits the number of cell divisions (or population doublings) in response to progressive telomere shortening. Most human somatic cells are telomerase-deficient because of the repression of telomerase reverse transcriptase (TERT) expression. Therefore, proliferating somatic cells undergo progressive telomere DNA erosion as a function of their number of cell divisions. This form of senescence is now called as replicative or telomere-dependent senescence (Fig. 1).

Human chromosome telomere ends are composed of TTAGGG repeats (5–20 kb) in a DNA-protein complex formed by six telomere-specific proteins, called "shelterin" [13]. Telomeric DNA has a structure called "t-loop" which is formed as a result of invasion of the single stranded G-rich sequence into the double-stranded telomeric tract. Since the 1930s, it has been known that telomeres, with telomere-binding proteins, prevent genomic instability and the loss of essential genetic information by "capping" chromosome ends. They are also indispensable for proper recombination and chromosomal segregation during cell division. Telomeres become shorter with every cell division in somatic cells, because of replication complex's inability to copy the ends of linear DNA, which also makes them a "cell cycle counter" for the cell [14]. Telomeres are added to the end of chromosomes with a complex containing the RNA template TERC and the reverse transcriptase TERT [15]. Most somatic cells lack telomerase activity because the expression of TERT is repressed, in contrast to TERC expression. The lack of sufficient TERT expression in somatic cells is the main cause of telomere shortening during cell replication. This telomerase activity also helps to maintain telomere integrity by telomere capping [15].

The loss of telomeres has long been considered to be the critical signal for senescence induction. It is now well known that telomere-dependent senescence is induced by a change in the protected status of shortened telomeres, whereby the loss of telomere DNA contributes to this change [16]. The loss of telomere protection or any other cause of telomere dysfunction results in inappropriate chromosomal end-to-end fusions through non-homologous end joining or homologous recombination DNA repair pathways [17]. These DNA repair pathways are used principally to repair double-strand DNA breaks (DSBs). Thus, it is highly likely that the open-ended telomere DNA is sensed as a DSB by the cell machinery when telomere structure becomes dysfunctional. Accordingly, dysfunctional telomeres elicit a potent DSB type DNA damage response by recruiting phosphorylated H2AX, 53BP1, NBS1 and MDC1 [18].

Telomere-dependent senescence is not the only form of senescence. At least two other forms of telomere-independent senescence are presently known: (1) oncogene-induced senescence; and (2) reactive oxygen species (ROS)-induced senescence (Fig. 1).

Oncogene-induced senescence had initially been identified as a response to expression of Ras oncogene in normal cells ([19], for a recent review see [20]). The expression of oncogenic Ras in primary human or rodent cells results in permanent G1 arrest. The arrest was accompanied by accumulation of p53 and $p16^{INK4a}$, and was phenotypically indistinguishable from cellular senescence. This landmark observation suggested that the onset of cellular senescence does not simply reflect the accumulation of cell divisions, but can be prematurely activated in response to an oncogenic stimulus [19]. In 10 years following this important discovery, telomere-independent forms of senescence have become a new focus of extensive research leading to the recognition of senescence as a common form of stress response. Moreover, oncogene-induced senescence is now recognized as a novel mechanism contributing to the cessation of growth of premalignant or benign neoplasms to prevent malignant cancer development [21]. In addition to Ras, other oncogenes including Raf, Mos, Mek, Myc and Cyclin E also induce senescence [20]. Conversely, the loss of PTEN tumor suppressor gene also leads to senescence [22]. Similar to telomere-dependent senescence, oncogene-induced senescence is also primarily a DNA damage response (Fig. 1). Experimental inactivation of DNA damage response abrogates Ras-induced senescence

Please cite this article in press as: M. Ozturk et al., Senescence and immortality in hepatocellular carcinoma, Cancer Lett. (2008), doi:10.1016/j.canlet.2008.10.048

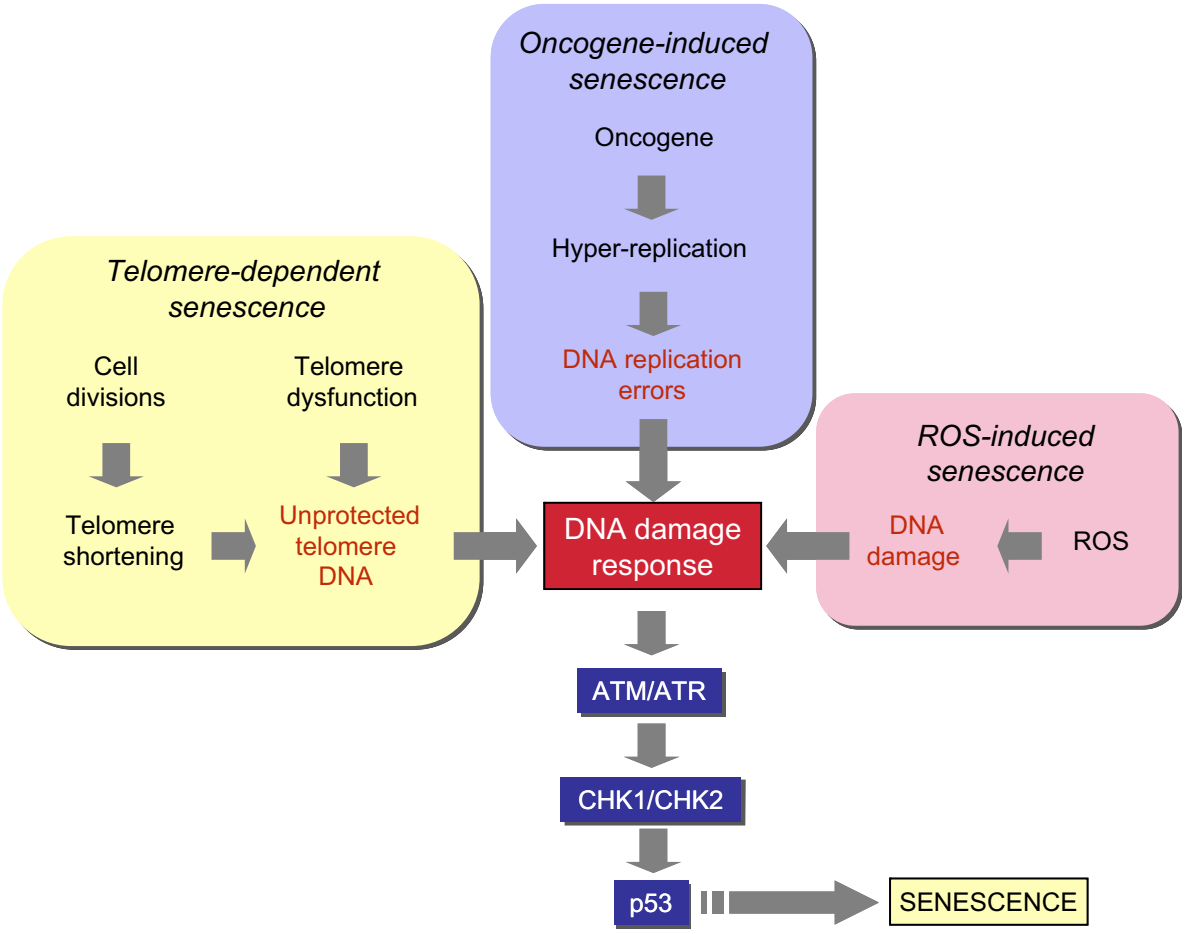

Fig. 1. DNA damage and p53 activation play a central role in different senescence pathways. DNA damage (often in the form of double-strand breaks) activate upstream kinases (ATM and ATR) leading to p53 phosphorylation by CHK1 and CHK2 kinases. Phosphoryated p53 is released from MDM, and stabilized in order to induce senescence arrest or apoptosis (not shown here).

and promotes cell transformation. DNA damage response and oncogene-induced senescence are established following DNA hyper-replication immediately after oncogene expression. Senescent cells arrest with partly replicated DNA, where DNA replication origins have fired multiple times, prematurely terminated DNA replication forks and DNA double-strand breaks are present [23,24].

ROS-induced senescence, the other telomere-independent senescence pathway is gaining importance (for a recent review see Ref. [25]). Mitochondria are the major intracellular sources of ROS which are mainly generated at the respiratory chain. Therefore, ROS have been suspected for many years as cellular metabolites involved in organismal aging [26]. ROS are also generated in the cytoplasm by the NOX family of enzymes [27]. Experimental induction of ROS accumulation in cells (for example by mild H2O2 treatment or glutathione depletion) induces senescence-like growth arrest in different cell types, whereas anti-oxidant treatment can inhibit senescence [25]. More importantly, ROS have been identified as critical mediators of both telomere-dependent and oncogene-induced senescence. Telomere-dependent senescence arrest is accelerated in cells grown under high O_2 conditions. Inversely, cells grown under low O_2 conditions display increased lifespan ([28], see Ref. [25]). ROS also play a critical role in Ras-induced senescence [29,30].

Currently, mechanisms of ROS-induced senescence are not fully understood. It is generally accepted that oxidative stress and ROS eventually cause DNA damage, whereby DNA damage response may contribute to senescence induction. The relationship between mitochondrial dysfunction, ROS, DNA damage and telomere-dependent senescence has recently been demonstrated [31]. However, ROS may also induce modifications in the cellular signaling pathways resulting in senescence arrest. For example, ROS induce senescence in hematopoietic stem cells by activating p38 MAPK [32].

Whether induced by telomere dysfunction, DNA replication stress following oncogene activation, or ROS accumulation, DNA damage is one of the common steps in the generation of senescence arrest via p53 activation (Fig. 1). Upstream checkpoint kinases, such as ATM or ATR are activated in response to DNA damage in the form of double-stand breaks. These kinases phosphorylate

Please cite this article in press as: M. Ozturk et al., Senescence and immortality in hepatocellular carcinoma, Cancer Lett. (2008), doi:10.1016/j.canlet.2008.10.048

downstream factors including CHK1 and CHK2 that in turn phosphorylate p53. Phosphorylation of p53 results in its activation by the displacement of the MDM2 protein. Critical involvement of this p53 activating pathway has been reported for both telomere-dependent [33], and oncogene-induced senescence [34].

Other mechanisms of senescence that are apparently not driven by DNA damage should also be discussed here. Of particular interest is the INK4 locus encoding two inhibitors of cyclin-dependent kinases ($p16^{INK4a}$, $p15^{INK4b}$), and ARF, a p53 regulatory protein (for a review see Ref. [35]). $p16^{INK4a}$ and $p15^{INK4b}$ connect some senescent initiating signals to the retinoblastoma (Rb) pathway, independent of p53 activation. These proteins are easily activated in cell culture and induce senescence arrest. Cells that escape senescence often display inactivation of $p16^{INK4a}$, and sometimes $p15^{INKb}$ and ARF either by homozygous deletion or by shutting-down gene expression. A prominent role for $p16^{INK4a}$ in senescence and tumor suppression in humans has emerged, despite some confusion due to the fact that a relatively small DNA segment encodes the 3 proteins of the INK4 locus. $p16^{INK4a}$ is activated during telomere-dependent and oncogene-induced senescence [19,36]. Moreover, its expression is induced in aging tissues [37]. The mechanisms of regulation of $p16^{INK4a}$ expression are not well known. Although individual components of INK4 locus can respond independently to positively – (for example to Ras) or negatively – (for example c-Myc) acting signals, the entire INK4 locus might be coordinately regulated by epigenetic mechanisms (reviewed in Ref. [35]).

A very recent addition to the list of senescence mechanisms is to be qualified as "senescence induced by secreted proteins". It was reported many years ago that TGF-β is a mediator of oncogene-induced senescence [38]. This mechanism of induction is of particular interest, because it suggests that not only intrinsic cellular factors, but also extracellular or secreted proteins can induce senescence. Recent discovery of several other secreted proteins, including IGFBP7 and IL6 as autocrine/paracrine mediators of oncogene-induced senescence arrest, provide strong support for an extracellularly induced form of senescence [39–41]. This new form of senescence regulation is reminiscent of the so called active apoptosis induction by death ligands. Thus, an active form of cellular senescence induced by "aging ligands" could be a major physiological regulator of tissue/organism aging.

3. Cyclin-dependent inhibitors as common mediators of senescence arrest

We have already stated that senescence and apoptosis share interesting similarities. Another similarity between these cellular processes is the convergence of different pathways in a common place to induce the same cell fate, independent of the initial signal. Similarly to caspase activation, prior to apoptosis induction by different stimuli, most if not all senescence pathways result in the activation of cyclin-dependent kinase inhibitors (CDKIs) in order to induce permanent cell cycle arrest. Senescent cells accumulate at G1 phase of the cell cycle due to an inability to enter into S phase in order to initiate DNA synthesis. The transition of proliferating cells from G1 to S phase requires the release of E2F factors from their inhibitory partner retinoblastoma protein (pRb) following phosphorylation by cyclin-dependent kinases (CDKs), in particular by CDK4/CDK6 and CDK2 at this stage of the cycle [35]. The senescence arrest is mediated by inhibition of pRb phosphorylation by CDK4 and CDK2. The activities of these enzymes are controlled by different mechanisms, but the major proteins involved in the control of senescence arrest are CDKIs. Almost all known CDKIs have been reported to be implicated in senescence arrest, but three of them are best characterized: $p16^{INK4a}$ and $p15^{INK4b}$ which inhibit CDK4/CDK6, and $p21^{Cip1}$ which inhibits CDK2 (Fig. 2).

$p21^{Cip1}$ is one of the main targets of p53 for the induction of cell cycle arrest following DNA damage [42]. Pathways that generate DNA damage response and p53 activation use $p21^{Cip1}$ as a major mediator of cellular senescence to control pRb protein [43]. Exceptionally, $p21^{Cip1}$ can be activated by p53-independent pathways to induce senescence [44].

The Rb protein plays two important and complementary roles that are necessary to initiate and to permanently maintain the cell cycle arrest in senescent cells. pRb proteins firstly contribute to the exit from the cell cycle by arresting cells at G1 phase, as expected [45]. In senescent cells, this exit is complemented with a dramatic remodeling of chromatin through the formation of domains of facultative heterochromatin called SAHF [46–48]. SAHF contain modifications and associated proteins characteristic of transcriptionally silent heterochromatin. Proliferation-promoting genes, such as E2F target genes are recruited into SAHF in a pRb protein-dependent manner. This recruitment is believed to contribute to irreversible silencing of these proliferation-promoting genes [49].

4. Senescence of hepatocytes and chronic liver disease

Hepatocytes in the adult liver are quiescent cells, they are renewed slowly, approximately once a year, as estimated by telomere loss which is 50–120 bp per year in healthy individuals [50,51]. However, the liver has an extremely powerful regenerative capacity, as demonstrated experimentally in rodents, and as observed in patients with chronic liver diseases [5]. This regenerative capacity is due mostly to the ability of mature hepatocytes to proliferate in response to a diminution of total liver mass either experimentally, or following exposure to viral and non viral hepatotoxic agents. In addition, the adult liver seems to harbor hepatocyte-progenitor cells (<0.10% of total hepatocyte mass) that are able to restore liver hepatocyte populations [52]. However, hepatocytes, like any other somatic cells, do not have unlimited replicative capacity, due to the lack of telomerase activity that is needed to avoid telomere shortening during successive cell divisions. This is best exemplified by decreased hepatocyte proliferation in liver cirrhosis stage of chronic liver diseases [53], providing in vivo evidence for the exhaustion of hepatocyte proliferation capacity. Senescence mechanisms in hepatocytes and in liver tissue are not well known. However, a limited

Please cite this article in press as: M. Ozturk et al., Senescence and immortality in hepatocellular carcinoma, Cancer Lett. (2008), doi:10.1016/j.canlet.2008.10.048

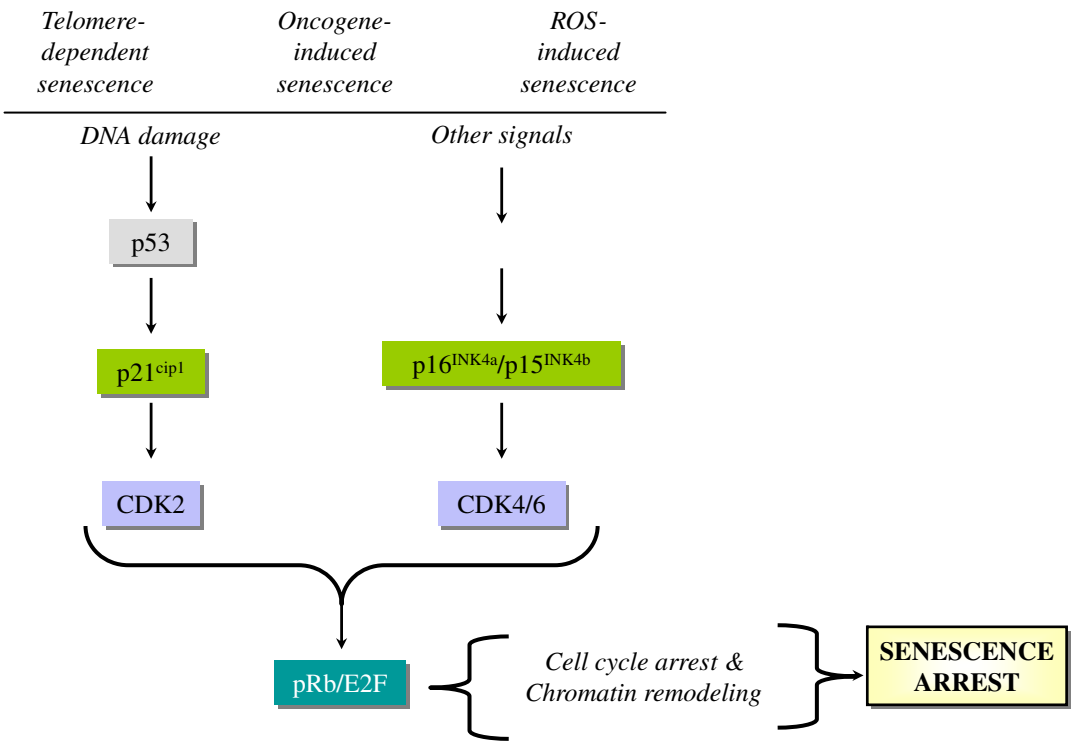

Fig. 2. All known senescence pathways converge at the level of activation of CDKIs ($p15^{INK4b}$, $p16^{INK4a}$ and $p21^{Cip1}$) that keep the pRb protein under the active form. The pRb protein inhibits E2F action and prevents the expression of growth-promoting genes for cell cycle exit. Furthermore, pRb recruits growth-promoting genes into a facultative chromatin structure for permanent silencing and growth arrest.

number of in vitro studies with hepatocytes, as well as numerous descriptive in vivo studies in liver tissue provide sufficient evidence that hepatocytes can undergo senescence type changes.

In vitro senescence in hepatocytes: as stated earlier, limited proliferative capacity of somatic cells is controlled by replicative senescence. The experimental study of replicative senescence is done traditionally by serial culture of primary cells. Initially observed in fibroblasts, this phenomenon has also been well understood in some epithelial cells, mammary epithelial cells in particular [54]. On the other hand, our knowledge of hepatocyte replicative senescence is highly limited. In contrast to in vivo conditions, mature hepatocytes are extremely resistant to cell proliferation in cell culture. Usually, more than 99.9% of adult liver hepatocytes do not divide and can only be maintained in culture for a few weeks at most. A small progenitor-type cell population (so called small hepatocytes) has been shown to proliferate in vitro, but they usually stop growing at passages 5–7, with an ill-defined senescence-like phenotype [55].

Fetal hepatocytes display better proliferation capacity in culture. A few studies have shown that these fetal cells enter replicative senescence, as shown by senescence-associated β-galactosidase assay (SABG) at population doubling (PD) 30–35 [55]. This is accompanied by progressive shortening of telomeres down to ~6 kbp, as these cells like adult hepatocytes lack telomerase activity. However, it was possible to immortalize these fetal hepatocytes by stable expression of TERT [55]. Such immortalized cells have been expanded beyond known senescence barriers (>300 PD).

In vivo senescence in liver tissue: in contrast to in vitro studies, in vivo senescence of human hepatocytes is better known. Indeed, the liver is one of the rare tissues where in vivo evidence for senescence has been convincingly and independently demonstrated by different investigators [6–9]. Replicative senescence (as tested by SABG assay) displayed a gradual increase from 10% in normal liver, to 84% in cirrhosis ([6,7]. It was also detected in 60% HCCs [6]. It has also been demonstrated that telomere shortening in cirrhosis is restricted to hepatocytes and this hepatocyte-specific shortening was correlated with SABG staining [7].

Potential mechanisms of senescence in hepatocytes and the liver: as presented in detail in the previous section, multiple pathways of senescence have been described in different experimental systems. Key molecules that are already involved in senescence arrest have also been summarized. The published data on different senescence pathways in the liver is fragmented and control mechanisms involved in hepatocyte senescence are not completely understood. Therefore, existing data on hepatocellular senescence together with potential mechanisms that may be involved in this process will be presented.

For reasons previously described, almost nothing is known about molecular mechanisms involved in replicative senescence and immortalization of hepatocytes in cul-

ture. There are only a few demonstrations of hepatocyte immortalization in vitro. Thus, ectopically expressed TERT may induce hepatocyte immortalization. However, as the published data using TERT immortalization is scarce, it is highly likely that the immortalization of hepatocytes is not an easy task even with a well-established protocol that works with other epithelial cell types such as mammary epithelial cells. The mechanisms of in vitro senescence induction in hepatocytes are also mostly unknown. Rapid induction of a senescence arrest in cultured hepatocytes suggests that these cells display robust telomere-independent senescence-inducing systems that are functional in vitro. However, they remain to be discovered. It is highly likely that, similar to other somatic cells, p53 and RB pathways in general, and some CDKIs in particular are also involved in hepatocyte senescence, but the evidence is lacking for the time being.

Telomere shortening during aging is slow (55–120 base pairs per year) and stabilizes at mid age in healthy liver, so that the loss of telomeric DNA does not reach a level to induce telomere dysfunction and DNA damage response [50,51]. Other forms of telomere-independent senescence such as ROS-induced senescence may also be rare under normal physiological conditions. On the other hand, telomere loss is accelerated in chronic liver disease to reach lowest levels in the cirrhotic liver [7,51]. Therefore, one plausible mechanism involved in cirrhosis is probably telomere-dependent senescence, or replicative senescence. The relevance of replicative senescence to liver tissue aging has been demonstrated experimentally using telomerase-deficient mice. Late generation telomerase-deficient mice display critically shortened telomeres and an impaired liver growth response to partial hepatectomy. A subpopulation of telomere-shortened hepatic cells displayed impaired proliferative capacity that is associated with SABG activity [11,56]. On the other hand, it has been reported that mouse liver cells are highly resistant to extensive telomere dysfunction. Conditional deletion of the telomeric protein TRF2 in hepatocytes resulted in telomeric accumulation of phospho-H2AX and frequent telomere fusions, indicating loss of telomere protection. However, there was no induction of p53 and liver function appeared unaffected. The loss of TRF2 did not compromise liver regeneration after partial hepatectomy. Liver regeneration occurred without cell division involving endoreduplication and cell growth, thereby circumventing the chromosome segregation problems associated with telomere fusions. Thus, it appears that hepatocytes display intrinsic resistance to telomere dysfunction, although they are apparently vulnerable to severe telomere loss [57].

Hepatocyte senescence that is observed in severe chronic liver diseases such as cirrhosis may also be induced by telomere-independent pathways. Chronic liver injury observed under such conditions is accompanied with inflammation, cell death, and oxidative stress [58–60]. Some of the etiological factors such as HCV and alcohol induce mitochondrial dysfunction may result in ROS accumulation [61,62]. Thus, ROS-induced senescence may also occur during cirrhosis, although this has not yet been reported. The status of DNA damage in chronic liver disease is less well-known. 8-Hydroxydeoxyguanosine, an indicator of DNA lesions produced by ROS, was reported to be increased in chronic liver disease [63]. On the other hand, the upregulation of DNA repair enzymes in cirrhosis has also been reported [64]. Increased DNA repair activity in cirrhosis which may reflect increased DNA damages as a consequence of chronic liver injury, but also inhibition of DNA damage responses such as senescence were observed. Taken together, these observations suggest that the primary cause of senescence in cirrhotic patients is telomere dysfunction and that ROS may also play additional roles.

Among senescence-related proteins, $p16^{INK4a}$ and $p21^{Cip1}$ expression was found to be high in cirrhosis, as compared to normal liver and tumor tissues [65], suggesting that these major senescence-inducing proteins accumulate in the cirrhotic liver. Promoter methylation of these CDKIs was also studied. Chronic liver disease samples displayed lower levels of methylation as compared to HCCs [66]. Thus, the progression of chronic liver disease towards cirrhosis is accompanied with a progressive activation of different CDKIs, as expected.

5. Senescence pathway aberrations and telomerase reactivation in hepatocellular carcinoma

As stated earlier, p53 and retinoblastoma (Rb) pathways play a critical role in senescence arrest as observed in different in vitro and in vivo models. Indirect evidence suggests that these pathways may also be important in hepatocellular senescence. The accumulation of p21 and p16 in cirrhotic liver tissues has been reported independently by different reports. On the other hand, HCC rarely develops in liver tissues absent of chronic liver disease. More than 80% of these cancers are observed in patients with cirrhosis [9]. As the appearance of proliferating malignant cells from this senescence stage requires the bypass of senescence, the status of both p53 and RB pathways in HCC is of great importance in terms of molecular aspects of hepatocellular carcinogenesis.

HCC is one of the major tumors displaying frequent p53 mutations [67,68]. The overall p53 mutation frequency in HCC is around 30%. Both the frequency and the spectrum of p53 mutations show great variations between tumors from different geographical areas of the World. A hotspot mutation (codon 249 AGG → AGT) has been linked to exposure to aflatoxins which are known to be potent DNA damaging agents (for a review see Ref. [67]). Although, it is unknown whether aflatoxins are able to generate a DNA damage-dependent senescence response in hepatocytes, their association with DNA damage and p53 mutation provides indirect evidence for such an ability. Other p53 mutations described in HCCs from low aflatoxin areas may similarly be correlated with other DNA damaging agents, such as ROS which are known to accumulate in the livers of patients with chronic liver diseases, including cirrhosis.

Another player of senescence arrest, the p16 gene is rarely mutated in HCC, but its epigenetic silencing by promoter methylation is highly frequent in this cancer. More than 50% of HCCs display de novo methylation of the promoter of CDKN2A gene, encoding p16 protein, resulting in

Please cite this article in press as: M. Ozturk et al., Senescence and immortality in hepatocellular carcinoma, Cancer Lett. (2008), doi:10.1016/j.canlet.2008.10.048

loss of gene expression [67]. Major components of p53 and Rb pathways in the same set of HCCs with different etiologies have been analyzed [69]. Retinoblastoma pathway alterations (p16 ^{INK4a}, p15^{INK4b} or RB1 genes) were present in 83% of HCCs, whereas p53 pathway alterations (p53 or ARF genes) were detected in only 31% of tumors. Alterations in both Rb and p53 pathways were present in 30% of HCCs. Thus, it appears that either the Rb and/or the p53 pathway are affected in the great majority of HCCs, and that both pathways are affected in at least one third of these tumors. Unfortunately, p53 and p16^{INK4a} aberrations observed in HCC have not yet been studied in relation to senescence aberrations. However, these observations provide supporting evidence on the critical role of senescence-controlling pathways in the development of HCC.

The lack of telomerase activity in normal and cirrhotic liver correlates with progressive loss of telomere sequences ending up with a senescence arrest. The emergence of malignant hepatocytes from this senescence-dominated cirrhotic milieu would require not only the bypass of senescence, but also a way of survival despite critically shortened telomeres. Additionally, the proliferative expansion of neoplastic cells in order to form sustained tumor masses would require telomeres at a minimal length required to maintain intact chromosomal structures.

Many studies showed that telomerase activity is a hallmark of all human cancers, including 80–90% of HCCs [70–72]. It is currently unclear how the TERT expression is repressed and released in normal hepatocytes and HCC cells, respectively. The integration of HBV DNA sequences into TERT gene provides evidence for a virus-induced deregulation of TERT expression, but this appears to rarely occur, as only four cases have been reported thus far [73–75]. Hbx and PreS2 proteins may upregulate TERT expression [76,77]. The molecular mechanisms involved in TERT suppression in somatic cells and its reactivation in cancer cells are ill-known. The TERT promoter displays binding sites for a dozen of transcriptional regulators: estrogen receptor, Sp1, Myc and ER81 acting positively, and vitamin D receptor, MZF-2, WT1, Mad, E2F1 and SMAD interacting protein-1 (SIP1, also called ZEB-2 or ZFHX1B) acting negatively [78]. Despite high telomerase activity, telomeres in HCC were repeatedly found to be highly shortened [65,79,80]. However, 3′ telomere overhangs were found to be increased in nearly 40% HCCs [80]. Moreover, the expression of several telomeric proteins is increased in HCC [80,81].

Another ill-known aspect of TERT activity in HCC cells is the cellular origin of these malignant cells. It is presently unclear whether HCC arises from mature hepatocytes which lack telomerase activity, or stem/progenitor cell-like cells that may already express TERT at sufficient levels to maintain telomere integrity. In the non-tumor area surrounding the cancer tissue, telomerase activity could not be detected, or was detected at very low levels.

The importance of telomerase activity in HCC development has been studied experimentally using telomerase-deficient mouse model. These mice show increased susceptibility to adenoma development (tumor initiation), but they are quite resistant to fully malignant tumor development [82]. Likewise, telomerase deletion limits the progression of p53-mutant HCCs with short telomeres [83]. These observations suggest that the aberrations affecting telomerase activity and senescence controlling genes such as p53 may cooperate during hepatocellular carcinogenesis.

In summary, HCC is characterized by mutational inactivation of p53, a major player in DNA damage-induced senescence. In addition, p15^{INK4b}, p16^{INK4a}, p21^{Cip1} CDKIs are often inactivated in this cancer mostly by epigenetic mechanisms involving promoter methylation. These changes may play a critical role in the bypass of senescence that is observed in most cirrhosis cases, allowing some initiated cells to escape senescence control and proliferate. In the absence of telomerase activity such cells would probably not survive due to telomere loss. However, since more than 80% of HCCs display telomerase activity, it is highly likely that the telomerase reactivation, together with the inactivation of major CDKIs, plays a critical role in HCC development by conferring premalignant or malignant cells the ability to proliferate indefinitely (Fig. 3). However, cellular immortality is not sufficient for full malignancy [84]. Thus, senescence-related aberrations that are observed in HCC cells, may confer a partial survival advantage that would need to be complemented by other genetic or epigenetic alterations.

6. Senescence as an anti-tumor mechanism in hepatocellular carcinoma

Senescence in normal somatic cells and tissues is expected. How about cancer cells and tumors? Initial studies using different cancer cell lines provided ample evidence for the induction of senescence by different genetic as well as chemical or biological treatments [85]. Thus, it appeared that cancer cells, immortalized by definition, do have a hidden senescence program that can be revealed by different senescence-inducing stimuli. These studies provided preliminary evidence for considering senescence induction as an anti-cancer therapy. The in vivo relevance of these observations and expectations became evident only very recently. Senescence was observed in tumors or pre-neoplastic lesions. SABG activity as well as several other senescence markers were detected in lung adenomas, but not in adenocarcinomas observed in oncogenic Ras ‘‘knock-in” mice [86]. Ras-driven mouse T-cell lymphomas entered senescence after drug therapy, when apoptosis was blocked [87]. The first direct evidence of cellular senescence in humans was reported for the melanocytic nevus [88].

Senescence response of HCC cells was not the subject of intensive study until very recently. Therefore the potential role of senescence in these tumors is less well understood. Treatment of HCC cell lines with 5-aza-2-deoxycytidine induced the expression of p16^{INK4a}, hypophosphorylation of pRb and G1 arrest associated with positive SABG staining [89]. Recent findings indicate that senescence induction is a powerful mechanism of HCC regression. Xue et al. expressed H-ras oncogene and suppressed endogenous p53 expression in mouse hepatoblasts which produced massive

Please cite this article in press as: M. Ozturk et al., Senescence and immortality in hepatocellular carcinoma, Cancer Lett. (2008), doi:10.1016/j.canlet.2008.10.048

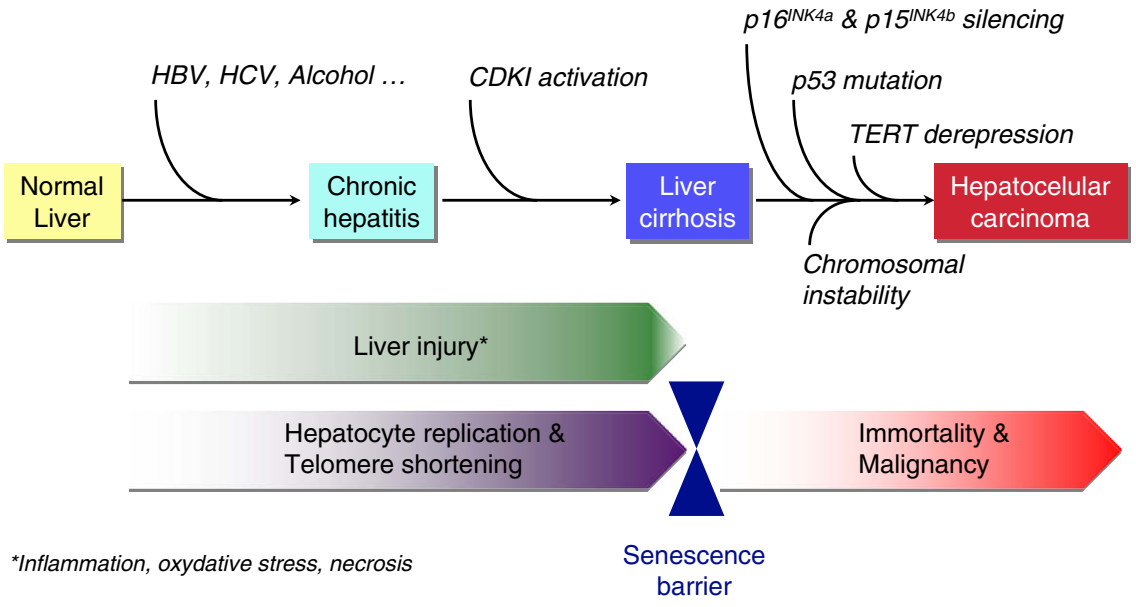

Fig. 3. Role of cellular senescence and immortalization in hepatocellular carcinogenesis. Chronic liver injury (triggered by major etiological factors HBV, HCV and alcohol) leading to cirrhosis is a common cause of HCC. Hepatocytes having no telomerase activity undergo progressive telomere shortening and DNA damage during this process. Consequently, CDKIs (primarily $p16^{INK4a}$ and $p21^{Cip1}$) are activated gradually to induce senescence in the preneoplastic cirrhosis stage. Mutation and expression analyses in HCC strongly suggest that neoplastic cells bypass the senescence barrier by inactivating major senescence-inducing genes (p53, $p16^{INK4a}$ and $p15^{INK4b}$). Moreover, they acquire the ability of unlimited proliferation (immortality) by re-expressing the TERT enzyme. Chromosomal instability that is generated by telomere erosion may contribute to additional mutations necessary for tumor progression.

HCCs upon implantation into livers of athymic mice [12]. However, these tumors regressed rapidly upon restoration of p53 expression. Tumor regression was due to differentiation and massive senescence induction, followed by immune-mediated clearance of senescent cells. These observations may indicate that oncogene-induced senescence is also involved in HCC. On the other hand, HCCs induced by tet-regulated c-Myc activation in mouse liver cells differentiate into mature hepatocytes and biliary cells or undergo senescence [90]. Thus, senescence induction may also be relevant to oncogene inactivation in HCC. In this regard, c-Myc down-regulation and senescence induction in several HCC cell lines as a response to TGF-β was observed (S. Senturk, M. Ozturk, unpublished data).

So far, all the reported examples of senescence induction in HCC cells are in the form of a telomere-independent permanent cell cycle arrest. Until recently, it was unknown whether replicative senescence could also be induced in immortal cancer cells. Ozturk et al. reported recently that immortal HCC cells can revert spontaneously to a replicative senescence phenotype [91]. Immortal HCC cells generated progeny that behaved, in vitro, similar to normal somatic cells. Such senescence-programmed progeny lacked telomerase activity due to TERT repression (probably mediated by SIP1 gene), and displayed progressive telomere shortening in cell culture, resulting in senescence arrest. It will be interesting to test whether such spontaneous reversal of replicative immortality is involved in well known tumor dormancy and/or spontaneous tumor regression.

7. Concluding remarks

Cellular senescence has gained great interest in recent years following the demonstration that it also occurs in vivo. It is also highly interesting that senescence can be mediated by a large number of pathways and molecules, as is the case for apoptosis. Recent findings that implicate secreted molecules in senescence induction strongly suggest that cellular senescence is not just a cellular event, but also a physiologically relevant process for the whole organism. In terms of tumor biology, oncogene-induced senescence that may serve as anti-tumor mechanism in pre-neoplastic lesions underlines its clinical relevance. On the other hand, induced or spontaneous senescence that is observed in cancer cells is promising to explore new approaches for tumor prevention and treatment. The role of senescence bypass and cellular immortality in hepatocellular carcinogenesis is not well defined. But, many findings (inactivation of senescence-mediator genes such as p53, $p16^{INK4a}$ and $p15^{INK4b}$, as well as reactivation of TERT) indicate that senescence mechanisms and their aberrations are critically involved in HCC. We may expect that this field will attract more attention in coming years for a better definition of senescence implications in hepatocellular carcinogenesis.

Please cite this article in press as: M. Ozturk et al., Senescence and immortality in hepatocellular carcinoma, Cancer Lett. (2008), doi:10.1016/j.canlet.2008.10.048

AcknowledgmentS

Authors' research is supported by grants from TUBITAK, DPT and TUBA (Turkey), and InCA (France). We thank D. Ozturk for language editing.

References

[1] D.E. Crew (Ed.), Human senescence-evolutionary and biocultural perspectives, Cambridge University Press, Cambridge, 2003.
[2] L. Hayflick, The limited in vitro lifetime of human diploid cell strains, Exp. Cell Res. 37 (1965) 614–636.
[3] J. Campisi, F. d'Adda di Fagagna, Cellular senescence: when bad things happen to good cells, Nat. Rev. Mol. Cell Biol. 8 (2007) 729–740.
[4] K.L. Rudolph, S. Chang, H.W. Lee, M. Blasco, G.J. Gottlieb, C. Greider, R.A. DePinho, Longevity, stress response, and cancer in aging telomerase-deficient mice, Cell 96 (1999) 701–712.
[5] G.K. Michalopoulos, Liver regeneration, J. Cell Physiol. 213 (2007) 286–300.
[6] V. Paradis, N. Youssef, D. Dargere, N. Ba, F. Bonvoust, J. Deschatrette, P. Bedossa, Replicative senescence in normal liver, chronic hepatitis C, and hepatocellular carcinomas, Hum. Pathol. 32 (2001) 327–332.
[7] S.U. Wiemann, A. Satyanarayana, M. Tsahuridu, H.L. Tillmann, L. Zender, J. Klempnauer, P. Flemming, S. Franco, M.A. Blasco, M.P. Manns, K.L. Rudolph, Hepatocyte telomere shortening and senescence are general markers of human liver cirrhosis, FASEB J. 16 (2002) 935–942.
[8] V. Trak-Smayra, J. Contreras, F. Dondero, F. Durand, S. Dubois, D. Sommacale, P. Marcellin, J. Belghiti, C. Degott, V. Paradis, Role of replicative senescence in the progression of fibrosis in hepatitis C virus (HCV) recurrence after liver transplantation, Transplantation 77 (2004) 1755–1760.
[9] H.B. El-Serag, K.L. Rudolph, Hepatocellular carcinoma: epidemiology and molecular carcinogenesis, Gastroenterology 132 (2007) 2557–2576.
[10] K.L. Rudolph, S. Chang, M. Millard, N. Schreiber-Agus, R.A. DePinho, Inhibition of experimental liver cirrhosis in mice by telomerase gene delivery, Science 287 (2000) 1253–1258.
[11] A. Satyanarayana, S.U. Wiemann, J. Buer, J. Lauber, K.E. Dittmar, T. Wüstefeld, M.A. Blasco, M.P. Manns, K.L. Rudolph, Telomere shortening impairs organ regeneration by inhibiting cell cycle re-entry of a subpopulation of cells, EMBO J. 22 (2003) 4003–4013.
[12] W. Xue, L. Zender, C. Miething, R.A. Dickins, E. Hernando, V. Krizhanovsky, C. Cordon-Cardo, S.W. Lowe, Senescence and tumour clearance is triggered by p53 restoration in murine liver carcinomas, Nature 445 (2007) 656–660.
[13] T. de Lange, Shelterin: the protein complex that shapes and safeguards human telomeres, Genes Dev. 19 (2005) 2100–2110.
[14] E.H. Blackburn, Structure and function of telomeres, Nature 350 (1991) 569–573.
[15] Y.S. Cong, W.E. Wright, J.W. Shay, Human telomerase and its regulation, Microbiol. Mol. Biol. Rev. 66 (2002) 407–425.
[16] J. Karlseder, A. Smogorzewska, T. de Lange, Senescence induced by altered telomere state, Not telomere loss, Science 295 (2002) 2446–2449.
[17] R.E. Verdun, J. Karlseder, Replication and protection of telomeres, Nature 447 (2007) 924–931.
[18] F. d'Adda di Fagagna, P.M. Reaper, L. Clay-Farrace, H. Fiegler, P. Carr, T. Von Zglinicki, G. Saretzki, N.P. Carter, S.P. Jackson, A DNA damage checkpoint response in telomere-initiated senescence, Nature 426 (2003) 194–198.
[19] M. Serrano, A.W. Lin, M.E. McCurrach, D. Beach, S.W. Lowe, Oncogenic ras provokes premature cell senescence associated with accumulation of p53 and p16INK4a, Cell 88 (1997) 593–602.
[20] R. Di Micco, M. Fumagalli, d'Adda F. di Fagagna, Breaking news: high-speed race ends in arrest-how oncogenes induce senescence, Trends Cell Biol. 17 (2007) 529–536.
[21] W.J. Mooi, D.S. Peeper, Oncogene-induced cell senescence-halting on the road to cancer, N. Engl. J. Med. 355 (2006) 1037–1046.
[22] Z. Chen, L.C. Trotman, D. Shaffer, H.K. Lin, Z.A. Dotan, M. Niki, J.A. Koutcher, H.I. Scher, T. Ludwig, W. Gerald, C. Cordon-Cardo, P.P. Pandolfi, Crucial role of p53-dependent cellular senescence in suppression of Pten-deficient tumorigenesis, Nature 436 (2005) 725–730.
[23] R. Di Micco, M. Fumagalli, A. Cicalese, S. Piccinin, P. Gasparini, C. Luise, C. Schurra, M. Garre', P.G. Nuciforo, A. Bensimon, R. Maestro, P.G. Pelicci, F. d'Adda di Fagagna, Oncogene-induced senescence is a DNA damage response triggered by DNA hyper-replication, Nature 444 (2006) 638–642.
[24] J. Bartkova, N. Rezaei, M. Liontos, P. Karakaidos, D. Kletsas, N. Issaeva, L.V. Vassiliou, E. Kolettas, K. Niforou, V.C. Zoumpourlis, M. Takaoka, H. Nakagawa, F. Tort, K. Fugger, F. Johansson, M. Sehested, C.L. Andersen, L. Dyrskjot, T. Ørntoft, J. Lukas, C. Kittas, T. Helleday, T.D. Halazonetis, J. Bartek, V.G. Gorgoulis, Oncogene-induced senescence is part of the tumorigenesis barrier imposed by DNA damage checkpoints, Nature 444 (2006) 633–637.
[25] T. Lu, T. Finkel, Free radicals and senescence, Exp. Cell Res. 314 (2008) 1918–1922.
[26] M. Giorgio, M. Trinei, E. Migliaccio, P.G. Pelicci, Hydrogen peroxide: a metabolic by-product or a common mediator of ageing signals?, Nat Rev. Mol. Cell Biol. 8 (2007) 722–728.
[27] C. Blanchetot, J. Boonstra, The ROS-NOX connection in cancer and angiogenesis, Crit. Rev. Eukaryot. Gene Expr. 18 (2008) 35–45.
[28] T. von Zglinicki, G. Saretzki, W. Döcke, C. Lotze, Mild hyperoxia shortens telomeres and inhibits proliferation of fibroblasts: a model for senescence?, Exp Cell Res. 220 (1995) 186–193.
[29] A.C. Lee, B.E. Fenster, H. Ito, K. Takeda, N.S. Bae, T. Hirai, Z.X. Yu, V.J. Ferrans, B.H. Howard, T. Finkel, Ras proteins induce senescence by altering the intracellular levels of reactive oxygen species, J. Biol. Chem. 274 (1999) 7936–7940.
[30] S. Courtois-Cox, S.L. Jones, K. Cichowski, Many roads lead to oncogene-induced senescence, Oncogene 27 (2008) 2801–2809.
[31] J.F. Passos, G. Saretzki, S. Ahmed, G. Nelson, T. Richter, H. Peters, I. Wappler, M.J. Birket, G. Harold, K. Schaeuble, M.A. Birch-Machin, T.B. Kirkwood, T. von Zglinicki, Mitochondrial dysfunction accounts for the stochastic heterogeneity in telomere-dependent senescence, PLoS Biol. 5 (2007) e110.
[32] K. Ito, A. Hirao, F. Arai, K. Takubo, S. Matsuoka, K. Miyamoto, M. Ohmura, K. Naka, K. Hosokawa, Y. Ikeda, T. Suda, Reactive oxygen species act through p38 MAPK to limit the lifespan of hematopoietic stem cells, Nat. Med. 12 (2006) 446–451.
[33] U. Herbig, W.A. Jobling, B.P. Chen, D.J. Chen, J.M. Sedivy, Telomere shortening triggers senescence of human cells through a pathway involving ATM, p53, and p21(CIP1), but not p16(INK4a) but not p16(INK4a), Mol. Cell. 14 (2004) 501–513.
[34] F.A. Mallette, M.F. Gaumont-Leclerc, G. Ferbeyre, The DNA damage signaling pathway is a critical mediator of oncogene-induced senescence, Genes Dev. 21 (2007) 43–48.
[35] J. Gil, G. Peters, Regulation of the INK4b-ARF-INK4a tumour suppressor locus: all for one or one for all, Nat. Rev. Mol. Cell Biol. 7 (2006) 667–677.
[36] D.A. Alcorta, Y. Xiong, D. Phelps, G. Hannon, D. Beach, J.C. Barrett, Involvement of the cyclin-dependent kinase inhibitor p16 (INK4a) in replicative senescence of normal human fibroblasts, Proc. Natl. Acad. Sci. U S A 93 (1996) 13742–13747.
[37] F. Zindy, D.E. Quelle, M.F. Roussel, C.J. Sherr, Expression of the p16INK4a tumor suppressor versus other INK4 family members during mouse development and aging, Oncogene 15 (1997) 203–211.
[38] R. Tremain, M. Marko, V. Kinnimulki, H. Ueno, E. Bottinger, A. Glick, Defects in TGF-beta signaling overcome senescence of mouse keratinocytes expressing v-Ha-ras, Oncogene 19 (2000) 1698–1709.
[39] N. Wajapeyee, R.W. Serra, X. Zhu, M. Mahalingam, M.R. Green, Oncogenic BRAF induces senescence and apoptosis through pathways mediated by the secreted protein IGFBP7, Cell 132 (2008) 363–374.
[40] J.C. Acosta, A. O'Loghlen, A. Banito, M.V. Guijarro, A. Augert, S. Raguz, M. Fumagalli, M. Da Costa, C. Brown, N. Popov, Y. Takatsu, J. Melamed, F. d'Adda di Fagagna, D. Bernard, E. Hernando, J. Gil, Chemokine signaling via the CXCR2 receptor reinforces senescence, Cell 133 (2008) 1006–1018.
[41] T. Kuilman, C. Michaloglou, L.C. Vredeveld, S. Douma, R. van Doorn, C.J. Desmet, L.A. Aarden, W.J. Mooi, D.S. Peeper, Oncogene-induced senescence relayed by an interleukin-dependent inflammatory network, Cell 133 (2008) 1019–1031.
[42] W.S. el-Deiry, T. Tokino, V.E. Velculescu, D.B. Levy, R. Parsons, J.M. Trent, D. Lin, W.E. Mercer, K.W. Kinzler, B. Vogelstein, WAF1, a potential mediator of p53 tumor suppression, Cell 75 (1993) 817–825.
[43] Y. Deng, S.S. Chan, S. Chang, Telomere dysfunction and tumor suppression: the senescence connection, Nat. Rev. Cancer 8 (2008) 450–458.
[44] L. Fang, M. Igarashi, J. Leung, M.M. Sugrue, S.W. Lee, S.A. Aaronson, p21Waf1/Cip1/Sdi1 induces permanent growth arrest with markers

of replicative senescence in human tumor cells lacking functional p53, Oncogene 18 (1999) 2789–2797.
[45] C. Giacinti, A. Giordano, RB and cell cycle progression, Oncogene 25 (2006) 5220–5227.
[46] M. Narita, S. Nunez, E. Heard, A.W. Lin, S.A. Hearn, D.L. Spector, G.J. Hannon, S.W. Lowe, Rb-mediated heterochromatin formation and silencing of E2F target genes during cellular senescence, Cell 113 (2003) 703–716.
[47] R. Zhang, M.V. Poustovoitov, X. Ye, H.A. Santos, W. Chen, S.M. Daganzo, J.P. Erzberger, I.G. Serebriiskii, A.A. Canutescu, R.L. Dunbrack, J.R. Pehrson, J.M. Berger, P.D. Kaufman, P.D. Adams, Formation of MacroH2A-containing senescence-associated heterochromatin foci and senescence driven by ASF1a and HIRA, Dev. Cell 8 (2005) 19–30.
[48] M. Narita, M. Narita, V. Krizhanovsky, S. Nunez, A. Chicas, S.A. Hearn, M.P. Myers, S.W. Lowe, A novel role for high-mobility group a proteins in cellular senescence and heterochromatin formation, Cell 126 (2006) 503–514.
[49] P.D. Adams, Remodeling of chromatin structure in senescent cells and its potential impact on tumor suppression and aging, Gene 397 (2007) 84–93.
[50] K. Takubo, N. Izumiyama-Shimomura, N. Honma, M. Sawabe, T. Arai, M. Kato, M. Oshimura, K. Nakamura, Telomere lengths are characteristic in each human individual, Exp. Gerontol. 37 (2002) 523–531.
[51] H. Aikata, H. Takaishi, Y. Kawakami, S. Takahashi, M. Kitamoto, T. Nakanishi, Y. Nakamura, F. Shimamoto, G. Kajiyama, T. Ide, Telomere reduction in human liver tissues with age and chronic inflammation, Exp. Cell Res. 256 (2000) 578–582.
[52] R. Utoh, C. Tateno, C. Yamasaki, N. Hiraga, M. Kataoka, T. Shimada, K. Chayama, K. Yoshizato, Susceptibility of chimeric mice with livers repopulated by serially subcultured human hepatocytes to hepatitis B virus, Hepatology 47 (2008) 435–446.
[53] M. Delhaye, H. Louis, C. Degraef, O. Le Moine, J. Devière, B. Gulbis, D. Jacobovitz, M. Adler, P. Galand, Relationship between hepatocyte proliferative activity and liver functional reserve in human cirrhosis, Hepatology 23 (1996) 1003–1011.
[54] M.R. Stampfer, P. Yaswen, Human epithelial cell immortalization as a step in carcinogenesis, Cancer Lett. 194 (2003) 199–208.
[55] H. Wege, H.T. Le, M.S. Chui, L. Lui, J. Wu, G. Giri, H. Malhi, B.S. Sappal, V. Kumaran, S. Gupta, M.A. Zern, Telomerase reconstitution immortalized human fetal hepatocytes without disrupting their differentiation potential, Gastroenterology 124 (2003) 432–444.
[56] A. Lechel, A. Satyanarayana, Z. Ju, R.R. Plentz, S. Schaetzlein, C. Rudolph, L. Wilkens, S.U. Wiemann, G. Saretzki, N.P. Malek, M.P. Manns, J. Buer, K.L. Rudolph, The cellular level of telomere dysfunction determines induction of senescence or apoptosis in vivo, EMBO Rep. 6 (2005) 275–281.
[57] E. Lazzerini Denchi, G. Celli, T. de Lange, Hepatocytes with extensive telomere deprotection and fusion remain viable and regenerate liver mass through endoreduplication, Genes Dev. 20 (2006) 2648–2653.
[58] G. Szabo, P. Mandrekar, A. Dolganiuc, Innate immune response and hepatic inflammation, Semin. Liver Dis. 27 (2007) 339–350.
[59] H. Malhi, G.J. Gores, Cellular and molecular mechanisms of liver injury, Gastroenterology 134 (2008) 1641–1654.
[60] D. Schuppan, N.H. Afdhal, Liver cirrhosis, Lancet 371 (2008) 838–851.
[61] F. Farinati, R. Cardin, M. Bortolami, P. Burra, F.P. Russo, M. Rugge, M. Guido, A. Sergio, R. Naccarato, Hepatitis C virus: from oxygen free radicals to hepatocellular carcinoma, J. Viral Hepat. 14 (2007) 821–829.
[62] A. Reuben, Alcohol and the liver, Curr. Opin. Gastroenterol. 24 (2008) 328–338.
[63] R. Shimoda, M. Nagashima, M. Sakamoto, N. Yamaguchi, S. Hirohashi, J. Yokota, H. Kasai, Increased formation of oxidative DNA damage, 8-hydroxydeoxyguanosine, in human livers with chronic hepatitis, Cancer Res. 54 (1994) 3171–3172.
[64] P. Zindy, L. Andrieux, D. Bonnier, O. Musso, S. Langouët, J.P. Campion, B. Turlin, B. Clément, N. Théret, Upregulation of DNA repair genes in active cirrhosis associated with hepatocellular carcinoma, FEBS Lett. 579 (2005) 95–99.
[65] R.R. Plentz, Y.N. Park, A. Lechel, H. Kim, F. Nellessen, B.H. Langkopf, L. Wilkens, A. Destro, B. Fiamengo, M.P. Manns, M. Roncalli, K.L. Rudolph, Telomere shortening and inactivation of cell cycle checkpoints characterize human hepatocarcinogenesis, Hepatology 45 (2007) 968–976.
[66] M. Roncalli, P. Bianchi, B. Bruni, L. Laghi, A. Destro, S. Di Gioia, L. Gennari, M. Tommasini, A. Malesci, G. Coggi, Methylation framework of cell cycle gene inhibitors in cirrhosis and associated hepatocellular carcinoma, Hepatology 36 (2002) 427–432.
[67] M. Ozturk, Genetic aspects of hepatocellular carcinogenesis, Semin. Liver Dis. 19 (1999) 235–242.
[68] T. Soussi, p53 alterations in human cancer: more questions than answers, Oncogene 26 (2007) 2145–2156.
[69] Y. Edamoto, A. Hara, W. Biernat, L. Terracciano, G. Cathamos, H.M. Riehle, M. Matsuda, H. Fuji, J.M. Scoazec, H. Ohgaki, Alterations of RB1, p53 and Wnt pathways in Hepatocellular carcinomas associated with HCV, HBV and alcoholic liver cirrhosis, Int. J. Cancer 106 (2003) 334–341.
[70] H. Tahara, T. Nakanishi, M. Kitamoto, R. Nakashio, J.W. Shay, E. Tahara, G. Kajiyama, T. Ide, Telomerase activity in human liver tissues: Comparison between chronic liver disease and hepatocellular carcinomas, Cancer Res. 55 (1995) 2734–2736.
[71] H. Kojima, O. Yokosuka, F. Imazeki, H. Saisho, M. Omata, Telomerase activity and telomere length in hepatocellular carcinoma and chronic liver disease, Gastroenterology 112 (1997) 493–500.
[72] J. Nakayama, H. Tahara, E. Tahara, M. Saito, K. Ito, H. Nakamura, T. Nakanishi, E. Tahara, T. Ide, F. Ishikawa, Telomerase activation by hTERT in human normal fibroblasts and hepatocellular carcinomas, Nat. Genet. 18 (1998) 65–68.
[73] D. Gozuacik, Y. Murakami, K. Saigo, M. Chami, C. Mugnier, D. Lagorce, T. Okanoue, T. Urashima, C. Bréchot, P. Paterlini-Bréchot, Identification of human cancer-related genes by naturally occurring Hepatitis B Virus DNA tagging, Oncogene 20 (2001) 6233–6240.
[74] I. Horikawa, JC. Barrett, Transcriptional regulation of the telomerase hTERT gene as a target for cellular and viral oncogenic mechanisms, Carcinogenesis 24 (2003) 1167–1176.
[75] Y. Murakami, K. Saigo, H. Takashima, M. Minami, T. Okanoue, C. Bréchot, P. Paterlini-Bréchot, Large scaled analysis of hepatitis B virus (HBV) DNA integration in HBV related hepatocellular carcinomas, Gut 54 (2005) 1162–1168.
[76] Z.L. Qu, S.Q. Zou, N.Q. Cui, X.Z. Wu, M.F. Qin, D. Kong, Z.L. Zhou, Upregulation of human telomerase reverse transcriptase mRNA expression by in vitro transfection of hepatitis B virus X gene into human hepatocarcinoma and cholangiocarcinoma cells, World J. Gastroenterol. 11 (2005) 5627–5632.
[77] H. Liu, F. Luan, Y. Ju, H. Shen, L. Gao, X. Wang, S. Liu, L. Zhang, W. Sun, C. Ma, In vitro transfection of the hepatitis B virus PreS2 gene into the human hepatocarcinoma cell line HepG2 induces upregulation of human telomerase reverse transcriptase, Biochem. Biophys. Res. Commun. 355 (2007) 379–384.
[78] R. Janknecht, On the road to immortality: hTERT upregulation in cancer cells, FEBS Lett. 564 (2004) 9–13.
[79] N. Miura, I. Horikawa, A. Nishimoto, H. Ohmura, H. Ito, S. Hirohashi, J.W. Shay, M. Oshimura, Progressive telomere shortening and telomerase reactivation during hepatocellular carcinogenesis, Cancer Genet. Cytogenet. 93 (1997) 56–62.
[80] J.E. Lee, B.K. Oh, J. Choi, Y.N. Park, Telomeric 3' overhangs in chronic HBV-related hepatitis and hepatocellular carcinoma, Int. J. Cancer 123 (2008) 264–272.
[81] B.K. Oh, Y.J. Kim, C. Park, Y.N. Park, Up-regulation of telomere-binding proteins, TRF1, TRF2, and TIN2 is related to telomere shortening during human multistep hepatocarcinogenesis, Am. J. Pathol. 166 (2005) 73–80.
[82] A. Satyanarayana, M.P. Manns, K.L. Rudolph, Telomeres and Telomerase: a Dual role in hepatocarcinogenesis, Hepatology 40 (2004) 276–283.
[83] A. Lechel, H. Holstege, Y. Begus, A. Schienke, K. Kamino, U. Lehmann, S. Kubicka, P. Schirmacher, J. Jonkers, K.L. Rudolph, Telomerase deletion limits progression of p53-mutant hepatocellular carcinoma with short telomeres in chronic liver disease, Gastroenterology 132 (2007) 1465–1475.
[84] W.C. Hahn, C.M. Counter, A.S. Lundberg, R.L. Beijersbergen, M.W. Brooks, R.A. Weinberg, Creation of human tumor cells with defined genetic elements, Nature 400 (1999) 464–468.
[85] J.W. Shay, I.B. Roninson, Hallmarks of senescence in carcinogenesis and cancer therapy, Oncogene 23 (2004) 2919–2933.
[86] M. Collado, J. Gil, A. Efeyan, C. Guerra, A.J. Schuhmacher, M. Barradas, A. Benguría, A. Zaballos, J.M. Flores, M. Barbacid, D. Beach, M. Serrano, Tumour biology: senescence in premalignant tumours, Nature 436 (2005) 642.
[87] M. Braig, S. Lee, C. Loddenkemper, C. Rudolph, A.H. Peters, B. Schlegelberger, H. Stein, B. Dörken, T. Jenuwein, C.A. Schmitt, Oncogene-induced senescence as an initial barrier in lymphoma development, Nature 436 (2005) 660–665.

Please cite this article in press as: M. Ozturk et al., Senescence and immortality in hepatocellular carcinoma, Cancer Lett. (2008), doi:10.1016/j.canlet.2008.10.048

[88] C. Michaloglou, L.C. Vredeveld, M.S. Soengas, C. Denoyelle, T. Kuilman, C.M. van der Horst, D.M. Majoor, J.W. Shay, W.J. Mooi, D.S. Peeper, BRAFE600-associated senescence-like cell cycle arrest of human naevi, Nature 436 (2005) 720–724.

[89] S.I. Suh, H.Y. Pyun, J.W. Cho, W.K. Baek, J.B. Park, T. Kwon, J.W. Park, M.H. Suh, D.A. Carson, 5-Aza-2'-deoxycytidine leads to down-regulation of aberrant p16 RNA transcripts and restores the functional retinoblastoma protein pathway in hepatocellular carcinoma cell lines, Cancer Lett. 160 (2000) 81–88.

[90] C.H. Wu, J. van Riggelen, A. Yetil, A.C. Fan, P. Bachireddy, D.W. Felsher, Cellular senescence is an important mechanism of tumor regression upon c-Myc inactivation, Proc. Natl. Acad. Sci. USA 104 (2007) 13028–13033.

[91] N. Ozturk, E. Erdal, M. Mumcuoglu, K.C. Akcali, O. Yalcin, S. Senturk, A. Arslan-Ergul, B. Gur, I. Yulug, R. Cetin-Atalay, C. Yakicier, T. Yagci, M. Tez, M. Ozturk, Reprogramming of replicative senescence in hepatocellular carcinoma-derived cells, Proc. Natl. Acad. Sci. USA 103 (2006) 2178–2183.

Please cite this article in press as: M. Ozturk et al., Senescence and immortality in hepatocellular carcinoma, Cancer Lett. (2008), doi:10.1016/j.canlet.2008.10.048